

THESE DE DOCTORAT

Présentée à
L'UNIVERSITE DE LILLE 1
Ecole Doctorale Régionale Sciences Pour l'Ingénieur Lille Nord-de-France



Pour obtenir le grade de
DOCTEUR EN SCIENCES
Dans la spécialité:
Micro et Nano Technologies, Acoustique et Télécommunications
Par

Amer Khudair Hussien Al-Nafiey

Reduced graphene oxide-based nanocomposites: Synthesis, characterization and applications

Soutenue le 20 Janvier 2016 devant le jury composé de :

Prof. Zineb MEKHALIF
Prof. Falah H.Hussien
Dr. Ayad Alkaim
Prof. Tuami LASRI
Dr. Rabah Boukherroub
Dr. Brigitte Sieber

Rapporteur
Rapporteur
Examineur
Examineur
Directeur de thèse
Co-directrice de thèse

Université de Namur
Université of Babylon
Université of Babylon
Université Lille 1
Université Lille 1
Université Lille 1



ABSTRACT

Since the first appearance in 2004, graphene and its derivatives have attracted considerable attention in different fields and created a revolution in materials science and condensed matter physics, owing to their amazing unique physical and chemical properties. These desirable properties have inspired the development of low-cost and high-yield preparation methods of chemically-derived graphene (reduced graphene oxide). The chemical reduction of graphene oxide (GO) is the most promising and effective method for the synthesis of reduced graphene oxide (rGO) because of its relatively large scale and low cost. Additionally, many investigations focused on the applications of graphene-based composites as catalysts for pollutants removal. Also, modified graphene can adsorb heavy metal ions with high efficiency and selectivity, and thus reduces them to metals for recycling.

The objective of my thesis is to develop simple, environmentally friendly, low cost, and controllable approaches for the chemical reduction of GO to rGO and its decoration with metal and metal oxide nanoparticles. These techniques use arginine and sodium borohydride as reducing agents, and silver nitrate, nickel chloride or cobalt chloride as a source for the metal/metal oxide nanoparticles.

The following nanocomposites: rGO/Arg-Ag NPs, rGO-Ni NPs and rGO-Co₃O₄NPs were successfully synthesized. The resulting rGO-based nanocomposites were characterized by a variety of different techniques, including , SEM, TEM, XPS, FTIR, Raman, XRD, UV-Vis and TGA. The analysis revealed that these graphene-based nanocomposites have excellent properties and stability.

We successfully applied the rGO-based nanocomposites as a catalyst for the reduction of 4-nitrophenol to 4-aminophenol, with a full reduction time in less than 1, 5 and 1 min at room temperature and remained active more than 4, 10, and 10 cycles for rGO/Arg-Ag NPs, rGO-Ni NPs and rGO-Co₃O₄NPs, respectively.

The Co₃O₄/rGO displayed high adsorption capacity for three organic dyes. The Co₃O₄/rGO nanocomposite removed 96%, 91% and 92% of RhB, MO and Rose Bengal after 2, 1 and 2 min, respectively. The maximum adsorption capacity of Cr (VI) was 222.2 mg. g⁻¹, which is very close to the experimental value of 208.8 mg.g⁻¹. These results were fast and highly-efficient compared with other reported data.

Key words: graphene oxide (GO), reduced graphene oxide (rGO), reduction, catalyst, adsorption, dyes, chromium, environmental applications.

RESUME

Nanocomposites à base d'oxyde de graphène réduit : Synthèse, caractérisation et application

Depuis la première apparition en 2004, le graphène et ses dérivés ont attiré une attention considérable dans différents domaines et créé une révolution dans la science des matériaux et la physique de la matière condensée, en raison de leurs propriétés physiques et chimiques uniques. Ces propriétés souhaitables ont inspiré le développement de faible coût et à haut rendement à partir de la méthode chimique de synthèse d'oxyde de graphène et de la (Oxide de graphène réduit). La réduction chimique de l'oxyde de graphène (GO) est la méthode la plus prometteuse et efficace pour la synthèse d'oxyde de graphène réduit (RGO) en raison de leur faible coût de synthèse et leur grande quantité de production. En outre, de nombreuses recherches ont été faites sur des applications des composites à base de graphène en tant que catalyseurs pour la dégradation des polluants. En outre, le graphène modifié peut absorber des ions de métaux lourds avec une grande efficacité et une sélectivité, et réduit ainsi les métaux à des fins de les recycler. L'objectif de ma thèse est de développer une méthode simple, pas chère, et les approches contrôlables pour la réduction chimique de GO à du rGO et le décorer avec des nanoparticules. Ces techniques utilisent le borohydrure de sodium et d'arginine comme agent réducteur, et le nitrate d'argent, le chlorure de nickel ou le chlorure de cobalt en tant que source pour les nanoparticules de métal / métal oxydé.

Les nanocomposites suivantes: rGO / Arg-Ag NP, rGO-Ni NPS et rGO-Co₃O₄NPs ont été synthétisés avec succès. Les nanocomposites à base de RGO résultants ont été caractérisés par une variété de techniques différentes, y compris, MEB, TEM, XPS, FTIR, Raman, XRD, UV-Vis et TGA. L'analyse a révélé que ces nanocomposites à base de graphène ont d'excellentes propriétés et la stabilité. Nous avons appliqué avec succès les nanocomposites à base de rGO en tant que catalyseur pour la réduction du 4-nitrophénol de 4-aminophénol, avec un temps de réduction complète en moins de 1, 5 et 1 min à une température ambiante et il a resté actif plus de 4, 10, et 10 cycles de rGO / Arg-Ag NP, rGO-Ni NPS et rGO-Co₃O₄NPs, respectivement. Le Co₃O₄ / rGO affiche une capacité d'adsorption élevée pour trois colorants organiques. Le nanocomposite Co₃O₄ / rGO retiré 96%, 91% et 92% des RhB, MO et Rose Bengale après 2, 1 et 2 min, respectivement. La capacité d'adsorption maximum de Cr (VI) était de 222,2 mg. g⁻¹, qui est très proche de la valeur expérimentale de 208,8 mg.g⁻¹. Ces résultats ont été rapides et très efficace par rapport à la bibliographie.

Mots clés: l'oxyde de graphène (GO), graphène oxide réduit (rGO), la réduction, le catalyseur, l'adsorption, de colorants, de chrome, les applications environnementales.

ACKNOWLEDGEMENTS

This research work was carried out in the Nanobiointerfaces group at Institut d'Electronique, de Microélectronique et de Nanotechnologie (IEMN). I would like to express my deepest gratitude to all those people who have helped and encouraged me in the successful completion of my doctoral study.

Primarily, I would like to give my most sincere thanks to my supervisors, Dr. Rabah Boukherroub and Dr. Brigitte Sieber, for their guidance, kindness, stimulating discussion, continued advice permanent support over past few years, as well as the time and patience they spent in reading and correcting the manuscript of this dissertation. With their enormous help and supervisions, I have obtained a lot of precious research experience such as scientific thinking, knowledge in chemistry and materials, as well as laboratory techniques. It was truly a great pleasure and privilege to study under their mentorships. It is my honor to have the chance to learn from them. My special thanks go to Prof. Sabine Szunerits from our group for her generous cooperation, helpful discussions and valuable suggestions.

I would like to express my thanks to Prof. Zineb Mekhalif and Prof. Falah H. Hussein for accepting to be the reviewers of the manuscript of my thesis and the committee members of my defense. I'm so grateful for their time and precious opinions. I would like to sincerely thank Dr. Ayad Alkaim and Prof. Tuami Lasri for accepting to be the committee members of my defense. I truly appreciate your time and your helpful comments.

My heartfelt thanks go to all my colleagues for all the help, discussions, and sharing. To Dr. Yannick Coffinier, Dr. Alexandre BARRAS, Dr. Ahmed Addad it's such a pleasure to work with you in the laboratory in past few years and for all the kind help and valuable advices. Also every member of my research group Lionel, Palan, Nadia, Manu, Stefka, Nazek, Roxana, Florina, Pawan, Faouzia, Hosam ... It is truly my honor to work with all of you. I would like also to thank my friends, Ahmed Al Mousawi, Alaa Al-Seraih, Ameen Al-ali, Ali Al-furajji , Dhia Ghibi ,Abass Al-Amiry, Mdlj Mayssam, Hussein Taher, Haider Al-Kinany....for their friendship and big supports.

In particular, I wish to thank the Iraqi Management Scholarships and Cultural Relations at the Ministry of Higher Education and Scientific Research in Iraq and the France government represented by CAMPUS FRANCE, which offered me the opportunity to pursue my PhD study in France.

Finally, to memory of my father, who is alive with me and to my mother, who always pray for me, and overwhelm me with love.

To my wife and my lovely kids, who supported me and give me the happiness at any time and my family for their support and motivation over the years. Their encouragements and warm words of advice have been very instrumental in my life.

Amer Khudair Hussien Al-Nafiey

Lille October 2015

Table of Contents

1. CHAPTER 1	11
INTRODUCTION.....	11
1.1. Introduction of graphene.....	12
1.2. Synthesis of graphene	13
1.2.1. Chemical vapor deposition (CVD)	15
1.2.2. Epitaxial growth.....	18
1.2.3. Mechanical exfoliation.....	19
1.2.4. Chemical reduction of graphene oxide (GO).....	20
1.2.5. Thermal reduction of GO.....	29
1.2.6. Photo-catalytic method	30
1.2.7. Electrochemical method	30
1.2.8. Other methods.....	31
1.3. Properties of graphene.....	33
1.3.1. Surface properties	33
1.3.2. Electronic properties	34
1.3.3. Optical properties	35
1.3.4. Mechanical properties	36
1.3.5. Thermal properties.....	37
1.3.6. Photo-catalytic properties	38
1.3.7. Magnetic properties	39
1.4. Characterizations of graphene.....	40
1.4.1. Morphology (SEM, TEM and AFM)	40
1.4.2. Raman spectroscopy	42
1.4.3. X-ray photoelectron spectroscopy (XPS).....	43
1.4.4. UV-Visible spectroscopy.....	44
1.4.5. X-ray diffraction (XRD)	45

1.4.6.	Thermogravimetric analysis (TGA).....	46
1.4.7.	FTIR spectroscopy	47
1.5.	Decoration of graphene with metal nanoparticles	48
1.5.1.	In situ decoration of nanoparticles onto graphene, GO and rGO.....	50
1.5.2.	Ex-situ decoration of nanoparticles on graphene, GO and rGO.....	53
1.6.	References	56
CHAPTER 2.....		76
Reduced graphene oxide decorated with silver nanoparticles.....		76
2.1	Introduction	76
2.2	Graphene decorated with silver nanoparticles.....	77
2.3	Reduction of graphene oxide by L-Arginine.....	80
2.4	Reduced graphene oxide decorated with silver nanoparticles (rGO-AgNPs) ...	85
2.5	Reduction of 4-nitrophenol to 4-aminophenol using graphene-based nanometals 92	
2.5.1	Introduction	92
2.5.2	Catalytic reduction of 4-nitrophenol by rGO/Ag NPs composite	99
2.6	Conclusion.....	104
2.7	References	106
CHAPTER 3.....		113
Reduced graphene oxide decorated with nickel nanoparticles.....		113
3.1.	Introduction	113
3.2.	Reduced graphene oxide decorated with nickel/nickel oxide nanoparticles	114
3.3.	Reduced graphene oxide decorated with Ni NPs (rGO/Ni NPs).....	122
3.4.	Catalytic reduction of 4-nitrophenol.....	132
3.4.1.	Reduction of 4-nitrophenol to 4-aminophenol by rGO-Ni NPs.....	132
3.5.	Conclusion	134
3.6.	References.....	136

CHAPTER 4	143
Preparation, characterizations and applications of reduced graphene oxide decorated with Co₃O₄ nanoparticles (rGO-Co₃O₄) nanocomposite	143
4.1. Introduction	143
4.2. Decoration of cobalt oxide on graphene sheets as a model to metal oxide/graphene nanocomposites	144
4.3. Reduced graphene oxide decorated with cobalt oxide nanoparticles (rGO-Co₃O₄ NPs).	146
4.4. Characterizations of rGO/Co₃O₄ nanocomposite	147
4.5. Applications	158
4.5.1. Catalytic reduction 4-nitrophenol	158
4.5.2. Treatment of wastewater using graphene/nanomaterials	161
4.5.3. Chromium Cr(VI) removal from aqueous solution by rGO-Co₃O₄ nanocomposite	171
4.5.4. Dye removal from aqueous solution	177
4.6. References	184
Chapter 5	191
CONCLUSION AND PERSPECTIVES	191
Appendix	194
EXPERIMENTAL PART	194
1. Chemicals	194
2. Preparation of graphene oxide (GO)	194
3. Instrumentation	195
3.1. X-ray photoelectron spectroscopy (XPS)	195
3.2. Fourier-transform infrared (FTIR) spectroscopy	196
3.3. Raman spectroscopy	196
3.4. UV-Vis measurements	197

General Introduction and Objective

Graphene a monolayer of carbon atoms densely packed in a honeycomb lattice was isolated for the first time in 2004. In recent years, the research on graphene and its derivative has been popular and extensive and generated tremendous interest in a wide range of research activities coming from its best properties like highest conductivity, high surface area and hardest materials. A facile and versatile pathway to obtain Graphene based nanocomposites is through the reduction of Graphene Oxide (GO). Several methods for reduced graphene oxide (rGO) that were developed include chemical, thermal, electrical, and optical process. Additionally, reduced graphene oxide (rGO)-based nanocomposites has been synthesized for potential applications in electronics, energy storage, catalysis, and gas sorption, storage, separation and sensing and so on. On the other hand, metal nanoparticles, have been exhibited remarkable in many applications but during synthesis, these nanoparticles tend to agglomerate resulting in loss of their nanoscale properties. Since reduce graphene oxide have high surface area can serve as nucleation sites for, it can be used as a substrate to deposit metal nanoparticles. This will reduce agglomeration of nanoparticles, and supported the metal nanoparticles properties as well as the graphene properties. Moreover, water pollution is world- wide environmental concern coming from heavy metal ions and organic dyes in wastewater that strongly threatens human, animals and plants. So, many effective strategies of water purification can be categorized into pollutants adsorption and conversion one of them, rGO-based nanocomposites typically show promising nanocomposites effective on reduced these pollutant species.

So, we will develop a simple, low cost, high quantity and controllable approaches for the chemical reduction of graphene oxide to rGO and decorate with nanometals and nanometals oxide. These techniques are based on use of arginine, nickel chloride, and sodium borohydride with cobalt chloride as reducing agents as well as a sources for the nanometals. We have successfully obtained these nanocomposites (rGO/Arg-Ag NPs, rGO-Ni NPs and rGO-Co₃O₄ NPs). This thesis content four chapters describe all the novel method that successfully reduced graphene oxide and decorated with nanometals and nanometals oxide.

Chapter 1, will be a general overview on graphene and graphene-based nanocomposite, preparation, characterization, and properties and their potential applications. In (**Chapter 2**), we will describe the bibliographer about rGO/Ag NPs preparation and developed environmentally friendly approaches method of preparation rGO/Arg-Ag NPs from GO, arginine and silver nitrate by novel chemical reduction and show there characterizations by

using different techniques. rGO/Arg-Ag NPs was used as a catalyst to reduction 4-nitrophenol to 4-aminophenol.

Chapter 3, we will show, it can be reduced graphene oxide and decorated with nickel nanoparticles by simple, novel chemical reduction method using only GO and nickel chloride. The characterizations doing by different techniques and show us that this method was able to reduce graphene oxide and decorated with nickel nanoparticles (rGO-Ni NPs). This nanocomposite also applied as catalyst to reduction 4-nitrophenol to 4-aminophenol.

In **Chapter 4**, we developed novel, quick, room temperature and simple method to reduce graphene oxide and decorated with cobalt oxide by using sodium borohydride with cobalt chloride as reducing agents as well as a sources for the nanometals (rGO-Co₃O₄ NPs). This rGO-Co₃O₄ NPs was characterized by different techniques and the result shown that the cobalt oxide anchored on the reduce graphene oxide successfully. We used this rGO-Co₃O₄ NPs as a catalyst to reduction 4-nitrophenol to 4-aminophenol and adsorbed dyes and Cr (VI) from wastewater.

CHAPTER 1

1. INTRODUCTION

Graphene has become an interesting nanomaterial from the time of its discovery due to its fascinating physical and chemical properties and for its promising applications [1, 2].

Graphene in simple terms is a thin layer of pure carbon; it is a single, tightly packed layer of carbon atoms that are bonded together in a hexagonal honeycomb lattice. In complex terms, it is an allotrope of carbon in the structure of a plane of sp^2 -bonded atoms (**Figure 1.1**) [3]. Before that, graphene had been investigated theoretically for over sixty years, although its existence as 2D crystals in free space was thought impossible [2]. In the last years, graphene has been the most studied material, attracting the attention of the entire scientific community for its exceptional physical and chemical properties [4].

Since the Geim and Novoselov's Nobel Prize in Physics for isolation of graphene by mechanical exfoliation of graphite in 2004 [5, 6], many researchers in the world searched in this field and investigated the different properties of graphene.

This chapter consists of a short review on the different synthetic routes of graphene and its derivatives. Graphene is the “thinnest” known material with a long range π -conjugation that exhibits a high specific surface area [7], extraordinary electronic properties and electron transport capabilities [8-10], strong mechanical strength [11], unprecedented pliability and impermeability [11, 12], remarkable optical transparency, as well as excellent thermal and electrical conductivities [13]. All these features have made graphene and graphene derivatives ideal candidates for diverse applications such as electronic devices [14], energy storage and conversion (supercapacitors [15, 16], batteries [17], fuel cells [18], solar cells [19]), sensors [20-23], and biomaterials [24, 25].

The wide range of useful physical and chemical properties of graphene attracted researchers interested in applications with an interdisciplinary approach spanning from applied physics, materials science, biology, mechanics, electronics and engineering [26]. The reported properties and applications of graphene have opened up new opportunities for future devices and systems [5].

1.1. Introduction of graphene

Carbon, one of the most common atoms on earth, occurs naturally in many forms. These are called allotropes of carbon. Two of these carbon allotropes have been collected from nature and used by humans for centuries: they are graphite and diamond.

Diamond is the most stable form of pure carbon. Formed at high temperatures and pressures under the earth's crust, diamond is a tetrahedral lattice with a carbon atom at each vertex. Each carbon atom forms four covalent bonds with four neighbouring atoms, completely filling its outer electron shell and resulting in one of the hardest and most valued materials in human history [27].

Three nanoscale forms of carbon have attracted widespread attention over the last years because of their novel properties. These carbon nanostructures are called fullerenes, carbon nanotubes, and graphene. These are the most common crystalline forms (allotropes) of carbon.

Fullerenes (called buckyballs when spherical) originate from the wrapping of graphene. It was discovered by Kroto *et al.* in (1985) while studying carbon clusters produced by vaporization of graphite upon laser heating [28]. Fullerenes are similar in structure to graphite, which is composed of stacked graphene sheets of linked hexagonal rings; but they may also contain pentagonal (or sometimes heptagonal) rings [27, 29, 30]. Fullerene is a super stable species, with its shape being that of a soccer ball. It is composed of sixty carbon atoms with 32 faces [31]. This discovery stimulated the scientific community to investigate other structures which can be formed from graphite. As a result, fullerene discovery was shortly followed by the observation of carbon nanotubes in 1991 by a Japanese scientist, Iijima [32].

Carbon nanotubes (CNT) have attracted great attention due to their exceptional electrical, mechanical, and thermal properties [30]. Iijima found CNTs in the solid deposit formed on the negative electrode after an electric discharge [33]. These carbon needles were later called carbon nanotubes, which are a single sheet of graphene rolled up to form a tube with one dimension. Iijima found that the solids consisted of tiny tubes made up of numerous concentric “graphene” cylinders, each cylinder wall consisting of a sheet of carbon atoms arranged in hexagonal rings. The cylinders usually have closed-off ends and range from 2 to 10 micrometres in length and 5 to 40 nanometres in diameter [34].

Graphite is a stack of graphene layers weakly bonded to each other [34]. While each sheet is tightly bound, only weak bonds (van der Waal bonds) exist between layers.

One method to massively produce graphene is to use graphite oxide (GO) as a precursor. GO consists of a single-layer of graphite oxide and is usually produced by chemical treatment of graphite through oxidation, with subsequent dispersion and exfoliation in water or suitable organic solvents.

As discussed above on carbon allotropes, a graphene sheet can be seen as the building block for graphitic materials of all other dimensionalities.

In this thesis, one attractive carbon allotrope, graphene, has been investigated and its composite materials have been applied for biosensing and environmental remediation.

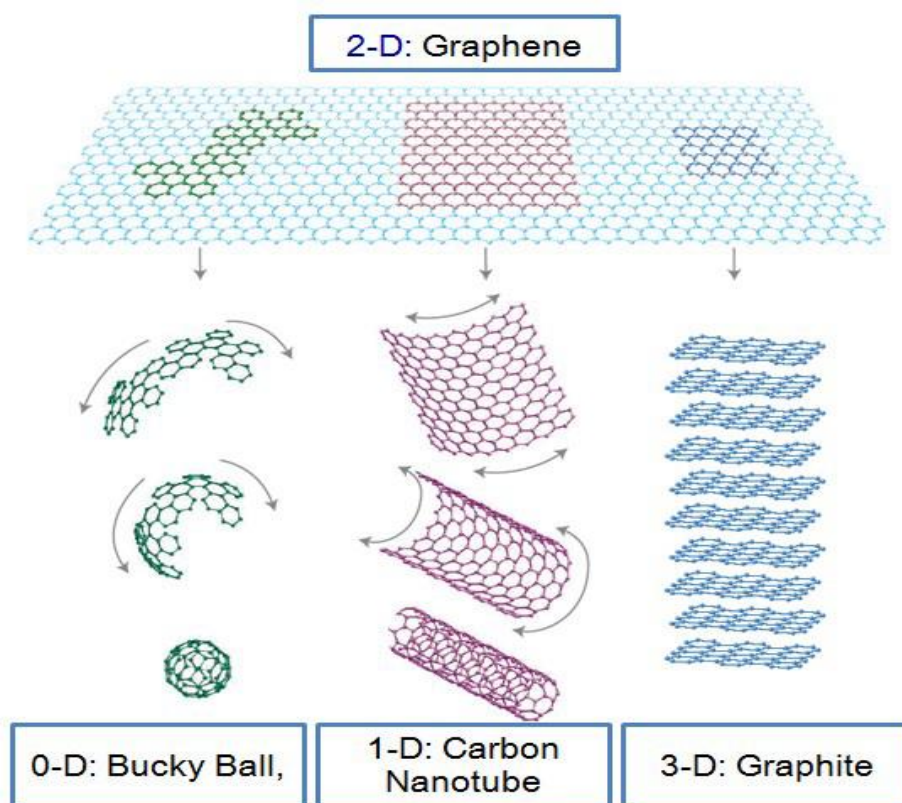


Figure 1.1: Graphene can be considered as the mother material of buckyballs, carbon-nanotubes and graphite [7].

1.2. Synthesis of graphene

To date, various synthetic methods have been developed for the preparation of graphene and its derivatives, not only to achieve high yield of production, but also for easy processing of the material [35]. Like carbon nanotubes and other nanomaterials, the vital challenge in synthesis and processing of bulk-quantity of graphene sheets is to prevent aggregation. Unless well

separated from each other, one-atom-thick planar sheets of graphene tend to form irreversible agglomerates, or even restack to form graphite through van der Waals interactions. The prevention of aggregation is essential because most of the unique properties of graphene sheets are only associated with individual sheets [36].

Synthetic methods have been developed in two possible directions: large-scale growth, or large-scale exfoliation [5, 37]. As a two-dimensional carbon nanomaterial, these methods for graphene synthesis can be divided into “bottom-up” and “top-down” approaches according to the classification of the synthesis method of nanomaterials (**Figure 1.2**) [35, 38].

The bottom-up approach involves the direct synthesis of graphene from carbon sources using chemical vapour-deposition (CVD) [1, 39, 40] or epitaxial growth on SiC [41], solvothermal reaction [42], and organic synthesis [43]. The advantage of the “bottom-up” is its ability to produce high quality pristine graphene for fundamental studies of transport physics and other properties. Its disadvantage is the limitation of large scale uniformity when up-scaling (for example, 100’s L of graphene solution or precise locations of interest on a chip) [44].

The “top-down” technique uses graphite as the starting material, and include mechanical exfoliation (the scotch tape method [39]), liquid-phase exfoliation [45, 46], chemical reduction of graphene oxide (GO) [47], thermal reduction of GO [48], photothermal reduction of GO [49] and electrochemical reduction of GO [50]. The latter features high yield, solution-based process ability and ease of implementation. The liquid phase exfoliation has been achieved by means of intercalation, chemical functionalization, and/or sonication of bulk graphite. The most common method adapted for large-scale production of graphene and GO is based on “top-down” approaches using physical and chemical exfoliation of graphite pioneered by Hummers *et al.* using strong acids and oxidants [51, 52]. This method requires extensive oxidation of aromatic structure in order to weaken van der Waals interactions between graphene sheets followed by their exfoliation and dispersion in solution [5]. The advantage of “top-down” is the ability to put the desired feature / entity in an exact location. The advantage is that it can utilise the existing silicon infrastructure and methodologies for precise feature placement and scalability. The disadvantages of the “top-down” approach is the resolution limitation due to the existing cutting tool technology (electron beam, ion-beam, etc.) [44].

We will discuss some methods for each approach, beginning with the “bottom-up” approaches (CVD and epitaxial growth) and ending with “top-down” ones (mechanical exfoliation, chemical reduction, thermal reduction and so on).

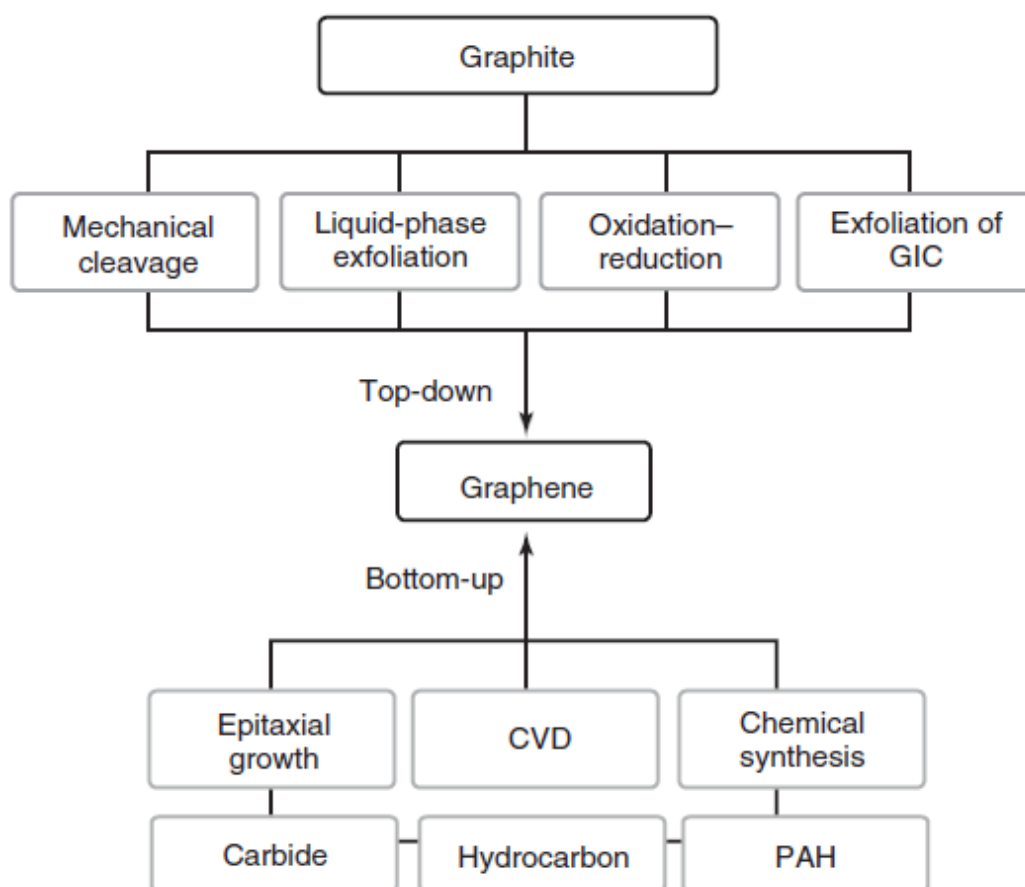


Figure 1.2: “Top-down” and “bottom-up” synthesis methods of graphene: GIC, CVD, and PAH correspond to graphite intercalation compounds, chemical vapour deposition, and polycyclic aromatic hydrocarbon, respectively [38].

1.2.1. Chemical vapor deposition (CVD)

The CVD technique is widely used for the production of semiconductor films in the industry, a metal crystal or film (copper or nickel) is used as a substrate and a hydrocarbon as the carbon source (methane, ethylene, etc.). By varying the experimental parameters (hydrocarbon, catalyst, gas flow, pressure, growth time, growth temperature, cooling rate, etc.), the thickness, size, and quality of graphene can be controlled [53, 54]. The CVD growth appears to be the most promising technique for large-scale production of mono- or few-layer graphene films. Although the formation of “monolayer graphite” was mentioned in early CVD studies on metal single crystals [55, 56], the first successful synthesis of few-layer graphene films using CVD was reported in 2006 by Somani and coworkers using camphor as the precursor on Ni foils [57].

Recently, Bae and co-workers reported a roll-to-roll production of 30-inch graphene films by using the CVD approach (**Figure 1.3**) [58]. The mechanism of graphene growth on substrates like Ni and Cu was investigated by Li et al. [59] by using carbon isotope labelling (**Figure 1.4**). It was reported that CVD growth of graphene on Ni occurs by a carbon segregation or precipitation process, whereas graphene on Cu grows by a surface adsorption process.

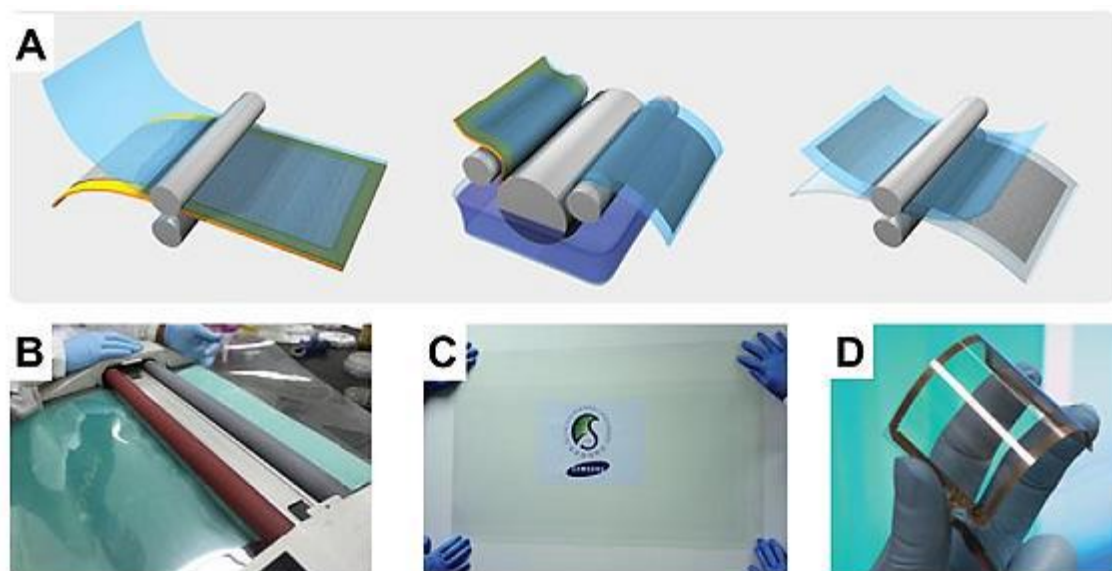


Figure 1.3: (A) Schematic of the roll-based production of graphene films grown on a copper foil. The process includes adhesion of polymer supports, copper etching (rinsing) and dry transfer-printing on a target substrate. (B) Roll-to-roll transfer of graphene films from a thermal release tape to a PET film at 120°C. (C) A transparent ultra-large area graphene film transferred on a 35 inch PET sheet. (D) An assembled graphene/PET touch panel showing outstanding flexibility [58].

The CVD process of substrates with medium-high carbon solubility (>0.1 atomic %) such as Ni and Co involves the dissolution of carbon and hydrocarbon decomposed onto the metal substrate, followed by carbon precipitation on the substrate by cooling down the metal [60, 61]. In contrast, graphene growth on low carbon solubility (<0.001 atomic %) substrate like Cu mainly happens on the surface through the following process [62, 63]: first, the catalytic decomposition of CH_4 occurs on Cu to form C_xH_y upon exposure of Cu to CH_4 and hydrogen. Then the nuclei start to form as a result of local super saturation of C_xH_y and grow to graphene islands until the graphene covers the full Cu surface. If $^{12}\text{CH}_4$ and $^{13}\text{CH}_4$ are both used as carbon source during the CVD process on Cu or Ni and are fed into the chamber sequentially, ^{12}C - and ^{13}C - are uniformly distributed on the Ni surface, while their spatial distribution on Cu follows

the precursor time sequence. This suggests that graphene growth on Ni is through dissolution-precipitation mechanism, while graphene growth on Cu is a surface process [63].

CVD graphene growth on a wide variety of other transition metal surfaces and even over dielectrics has been investigated. In particular, on Ru(0001), graphene grows epitaxially across the surface over large lateral distances [64]. The structure of graphene growth on Ir(111) exhibits a Moiré pattern due to the lattice mismatch between the Ir and graphene atomic distances [65].

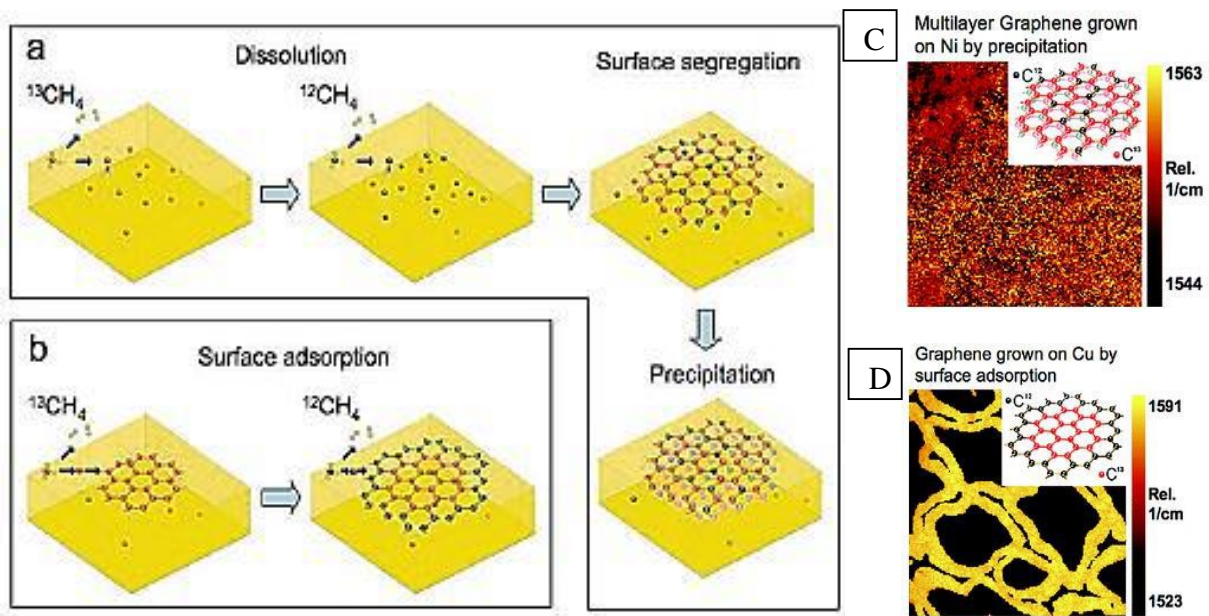


Figure 1.4: Schematic diagrams of the possible distribution of C isotopes in graphene films based on different growth mechanisms for sequential input of C isotopes. (a) Graphene with randomly mixed isotopes such as might occur from surface segregation and/or precipitation. The example (c) on Ni, (b) Graphene with separated isotopes such as might occur by surface adsorption. The example (d) on Cu [63].

The weak interaction between the metal substrate and the graphene for the Pt(111) system leads to the formation of many rotational domains [66]. Thermal CVD can also yield graphene over non-metallic catalysts. For example, sapphire was used as a substrate with propane as the carbon feedstock at 1350-1650°C [67]. Moreover, to fabricate a graphene device with an atomically uniform gate dielectric providing a uniform electric field, plasma enhanced CVD (PECVD) is a promising candidate. This technique is suitable for mass production of 2D graphene sheets, because of its simplicity (low-temperature manipulation) and compatibility with traditional semiconductor processes [68, 69].

1.2.2. Epitaxial growth

Graphene growth on silicon carbide (SiC) is generally meant for wafer-based applications, such as electronic devices or components, and generally it is not necessary to remove the graphene from the underlying substrate. The thermal decomposition of SiC consists of heating up SiC in ultra-high vacuum (UHV) to temperatures between 1000 and 1500°C usually in argon atmospheres [70]. The graphene produced is of relatively high quality, although the uniformity of graphene for single layer and bilayers is rather poor because of surface pits [71]. The number of layers depends on the decomposition temperature, and the demanding growth conditions are key challenges for growing graphene on SiC [38].

Emtsev et al. were able to achieve a significant improvement in the degree of homogeneity of the graphene films obtained by thermal decomposition of silicon carbide [72]. The authors showed that the growth of epitaxial graphene on SiC in an argon atmosphere close to atmospheric pressure provides morphologically superior graphene layers in comparison to vacuum graphitization [72].

Nowadays, hexagonal α -SiC (6H-SiC and 4H-SiC) is widely used to synthesize high-quality graphene with crystallites approaching hundreds of micrometers in size: Virojanadara et al. as well as Berger and co-workers produced few-layer graphene by thermal decomposition of SiC using 6H-SiC single crystal [73, 74]. The results showed thin graphene layers. Typically, between 1 and 3 layers were formed depending on the decomposition temperature. Using this method, devices were produced with mobilities of $1100 \text{ cm}^2 \text{ V}^{-1} \text{ s}^{-1}$ [74].

In addition to SiC substrate, graphene synthesis by epitaxy on transition metals has also been considered [64, 75, 76]. Sutter and co-workers used ruthenium as a substrate for graphene growth. The authors made use of the temperature-dependent solubility of interstitial carbon in transition metals to achieve the controlled layer-by-layer growth of large graphene domains on Ru [64]. The advantage of this approach is that the size of the synthesized sample can be comparable to the size of the original Ru crystal if the crystal is of a good quality. In addition to that, to study the electrical properties of graphene it should be placed on an insulating substrate, hence a considerable advantage of this method is that insulating SiC substrates can be used so that transfer to another insulator is not required in contrast to the situations when the sample is produced on a metallic substrate. However, the large-scale structural quality is limited by the lack of continuity and uniformity of the grown film [77, 78].

1.2.3. Mechanical exfoliation

Graphene has been the subject of intense widespread research for less than a decade. Most of the work used graphene created by a process of mechanical exfoliation called the “scotch tape method”. In this procedure, pure samples of bulk graphite are placed on the sticky side of common adhesive tape. The tape is pressed on a desired substrate and then peeled away. Flakes of graphene around 50 microns wide are left on the substrate, along with chunks of graphite and adhesive residue. The flakes can be discerned under an optical microscope due to thin-film interference, appearing as a region of slight discoloration [7]. The graphene left by the scotch tape method is pure and clean, which enables researchers to measure its electrical and mechanical properties exactly. However, a fair amount of time and luck are required to manually locate an appropriate flake on the region exposed to the tape (**Figure 1.5**). This difficulty is overcome if the graphene flake is positioned in a certain way above or around an existing feature on the substrate, as it is commonly desired for many nanoscale experiments. Lastly, when graphene is to be used as an electrode on a solar cell, it must cover the entire surface area of the cell, which is much larger than the area of a single flake [34].

Mechanical exfoliation of graphite can also be performed in liquid-phase with the target of reducing the agglomeration in graphite appreciably. Ultrasonication treatments are usually used for the graphite exposed to solvents. There are two approaches of ultrasonic exfoliation of graphite. One approach is to utilize the similar surface energy of some organic solvents (such as dimethylformamide (DMF), *N*-Methyl-2-pyrrolidone (NMP) or ethanol [45, 79, 80]) and graphene that facilitates the exfoliation. This route results in a monolayer graphene yield of around 1 wt. %, but can be as high as 12 wt. % [45, 81]. Another approach is based on the incorporation of small molecules between the layers of graphite or by non-covalently attaching molecules or polymers onto the sheets, forcing the graphene layers to split apart from each other. This is often done by introducing ultrasonic solvents (including sulphuric acid, nitric acid, acetic acid and hydrogen peroxide) [48, 82, 83] between the graphene layers and then quickly heating the samples in an air or formic gas at ~1000°C or microwave irradiation. The rapid evaporation of the intercalators yields exfoliated graphite flakes, which can be then separated into single graphene sheets via ultrasonication. This route can produce a suspension of which 90% are single layer graphene sheets [84].

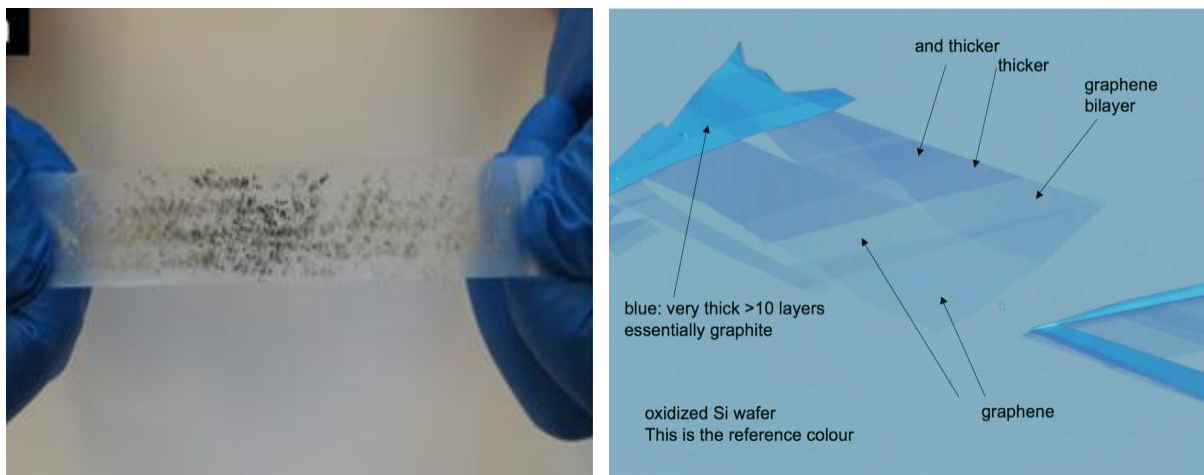


Figure 1.5: (A) Exfoliation of graphene using scotch tape; (B) Optical microscope image of graphene on SiO₂ substrate [7].

1.2.4. Chemical reduction of graphene oxide (GO)

While exfoliation produces very pure single-domain graphene with nearly ideal mechanical and electrical properties, it has one large disadvantage. That is, exfoliation results in graphene flakes scattered randomly on a substrate. Each flake is on the order of only microns in size, and much of the substrate remains uncovered. For many applications of graphene (including transparent conducting electrodes for an organic solar cell), a continuous covering of graphene is needed. To produce continuous graphene films, exfoliation cannot be used and chemical methods are needed instead to grow graphene from carbon atoms in another form.

The technique of reduced graphene oxide is really the intersection of exfoliation and chemical growth methods. Exfoliated graphene flakes are oxidized, enabling them to be suspended in aqueous solution.

Numerous methods of chemical reduction of graphite/graphene oxide have emerged or re-emerged in recent years. Despite the wide arrays of chemical reduction strategies, a number of reducing agents known to date may not be supported by mechanisms. These reducing agents are not widely applied in synthetic chemistry for the removal/reduction of oxygen functionalities. In fact, most of these are usually known to have non-specific antioxidant or oxygen scavenging properties.

1.2.4.1. Preparation of graphene oxide (GO)

The first reported synthesis of GO can be traced back to 1859, when Benjamin C. Brodie, a chemist from the University of Oxford, treated graphite with a mixture of fuming nitric acid and potassium chlorate [85]. The chemical formula of the product synthesized was $C_{11}H_4O_5$. Subsequently, chemist William S. Hummers and Richard E. Offeman devised a new method to synthesize GO that will take less than 2 h, as compared to the 3 days taken by the Brodie's method [51]. Their method involves the treatment of powdered graphite flakes with a mixture of concentrated sulphuric acid and sodium nitrate, kept at a reaction temperature of 0°C in an ice bath. Potassium permanganate is then added while the mixture is kept at a temperature below 20°C . The Hummer's method is a faster and safer method than Brodie's, and the synthesized GO has a higher degree of oxidation. Also reported by Jeong and co-workers [86] the oxidation reaction to synthesize GO requires at least 60 min under acid environment to complete. Oxygen atoms mainly exist on GO as hydroxyl, epoxy and carbonyl groups [35, 87]. Due to oxygen functional groups, layered-structure graphite is intercalated and becomes hydrophilic after Hummers' method [88]. The inter-layer distance of GO is approximately 1 nm, whereas for graphite it is 0.34 nm. Therefore, it is easier to exfoliate GO into single-atom-layer sheet *via* simple colloidal dispersion process [3, 34].

Several modifications of the Hummer's method have been developed recently to improve the quality of GO. GO synthesized by the Hummer's method was found to contain large quantity of GO sediments, which are made up of multi-layered graphite flakes that are oxidized at the outer layers, but are pristine or mildly oxidized at the inner layers [89]. The carbon atoms in GO becomes sp^3 hybridized, hence losing the high electrical conductivity of graphene. The electrical conductivity can be restored by the reduction of GO into reduced graphene oxide (rGO), albeit not to the same order of magnitude as the conductivity of graphene. This is due to the presence of defects and vacancies that cannot be completely eliminated during reduction [90, 91]. GO can be considered as a precursor for graphene synthesis by either chemical or thermal reduction processes.

1.2.4.2. Reduction of graphene oxide (GO)

For the reduction of GO using chemical methods, one of the most commonly used reducing agent is hydrazine monohydrate (N_2H_4) [92]. One major reason for its popularity is its inertness to water, which is present in GO as a dispersing solvent. Nevertheless, after careful studies of the products of the reduction process coupled with the knowledge of the reaction mechanisms of hydrazine with other organic species, it is suggested that the reduction of GO is similar to

that of the reduction of alkenes with hydrazine [93], which also leaves some functional groups intact. These functional groups, usually those with a C–N bond, cannot be easily removed by a single-step treatment [94]. The technique consists of the initial oxidation of graphite to graphite oxide, followed by the subsequent mechanical/chemical or thermal exfoliation of graphite oxide to graphene oxide (GO) sheets, and their reduction to graphene (**Figure 1.6**) [4, 87, 95, 96].

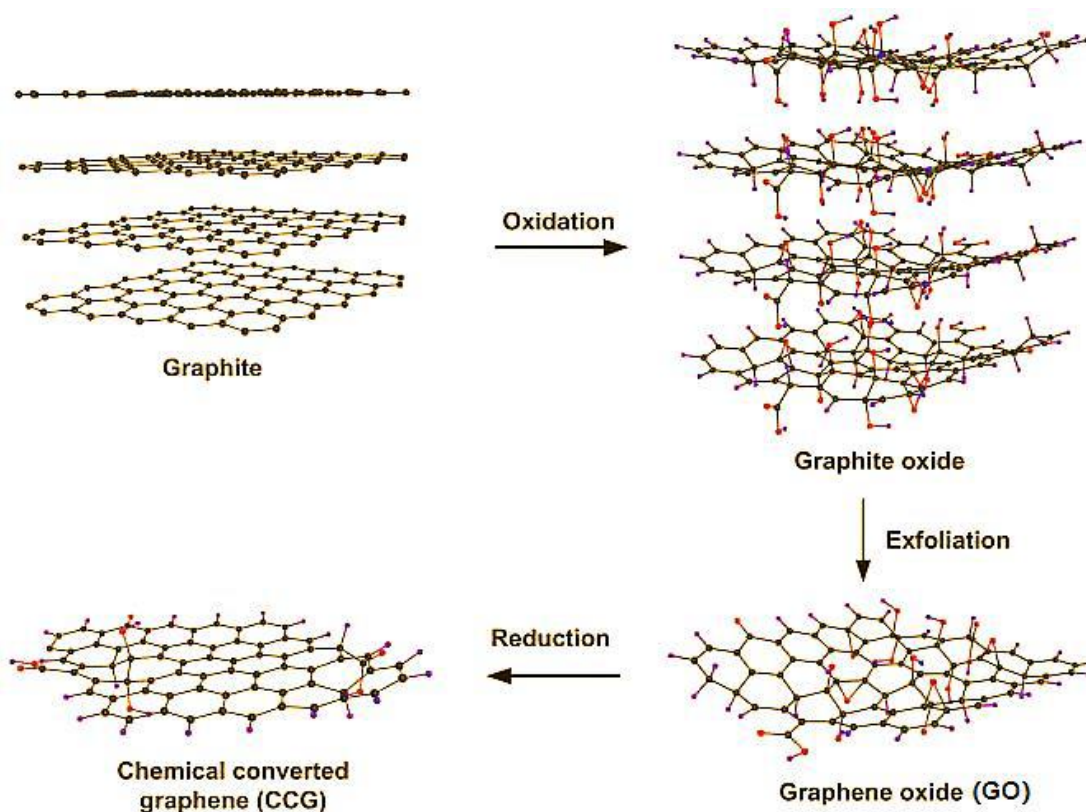


Figure 1.6: The oxidation-exfoliation-reduction process used to generate individual sheets of chemical converted graphene from graphite [97].

Sodium borohydride (NaBH_4) can also be used as a chemical reductant for graphene oxide. It is a salt containing a tetrahedral BH_4 anion, which readily solubilizes in aqueous and alcoholic media. In the presence of an electrophile such as a carbonyl functionality, the borohydride anion readily performs a hydride transfer reaction, which results in an oxyanion and an electron deficient BH_3 molecule. Subsequent stabilization of the BH_3 molecule with the oxyanion reinstates the borohydride as a hydride transfer agent. This is ideally the case until all the B–H bonds are consumed. However, the reaction is rarely as efficient in practice. The ability of BH_4 to reduce carbonyl groups is also limited by the types of carbonyl groups. Simple carbonyl

compounds such as aldehyde and ketone are reducible by NaBH_4 to alcohol groups, while less reactive carbonyl compounds like ester or amide are not reducible.

The usage of NaBH_4 as a reducing agent of GO was first reported by Kamat and co-workers to achieve the physisorption of gold nanoparticles on a graphene-octadecylamine material [98]. At about the same time, Si and Samulski performed the reduction of GO with NaBH_4 as the first of a three-step synthesis towards a total reduction effort to obtain a sulphonated graphene which dispersed well in aqueous and organic solvents [47]. A similar reduction method with NaBH_4 was also carried out by Ajayan and co-workers in their investigations related to the total reduction of GO [99]. Following that, Lee and co-workers conducted a study on the effect of NaBH_4 concentration on the electrical properties of the resulting graphene [100]. A C/O ratio of 8.6 was measured on the graphene prepared by dipping a strip of GO into a 150 mM solution of NaBH_4 . The electrical resistance of the NaBH_4 -reduced graphene oxide was measured to be lower than that of hydrazine reduced graphene oxide, possibly due to the absence of heteroatoms.

Due to the toxicity and explosive properties of some of the chemical reductants explored earlier, many environmentally friendly and highly-efficient reductants have been developed and used for the reduction of GO [97], including vitamin C [101, 102], amino acid [103], reducing sugar [104], alcohols [105], hydroiodic acid [106], reducing metal powder [107, 108], tea [109], and so on (**Table 1.1**).

Table 1.1. List of reducing agents of graphene oxide (GO) towards chemically reduced graphene oxide (rGO).

Reducing agent	C/O ratio	Doping	Conditions ^d	Ref.
Borohydrides				
NaBH ₄	4.8 ^a	—	80°C, 1 h	[47, 99, 100, 110]
	8.6 ^a	—	RT, 2 h	
	2.5 ^a	—	MeOH, 70 °C, 2 h	
NaBH ₃ (CN)	2.5 ^a	—	MeOH, 70°C, 2 h	[110]
NaBH(OAc) ₃	2.2 ^a	—	MeOH, 70°C, 2 h	[110]
NH ₃ BH ₃	14.2 ^a	B/N-doped	80°C, 12 h	[111]
	9.8 ^a	B/N-doped	THF, 66°C, 12 h	[111]
Aluminium hydride				
LiAlH ₄	12 ^a	—	THF, 70°C, 24 h	[112]
Hydrohalic acid				
HI/AcOH	11.5 ^b	—	40°C, 40 h	[106]
HI/TFA	12.5 ^b	—	-10°C, 40 h	[113]
HI	12 ^a	I-doped	100°C, 1 h	[114]
HBr	3.9 ^a	Br-doped	110°C, 24 h	[115]
HBr–KOTBu	7.1 ^a	—	THF, 66°C, 0.5 h	[116]
^a X-ray photoelectron spectroscopy. ^b Elemental analysis. ^c Energy dispersive spectroscopy. ^d Reduction carried out in aqueous medium or pure solution of the reducing agent unless stated otherwise.				

Reducing agent	C/O ratio	Doping	Conditions ^d	Ref.
Sulphur-containing reducing agents				
Thiourea dioxide/NaOH	14.5 ^a	—	EtOH/H ₂ O, 90°C, 1 h	[117]
Thiourea dioxide/NaOH/cholate Adsorbed	5.8 ^a	—	80°C, 0.5 h	[118]
Thiourea dioxide/NH	6.0 ^a	—	RT, 1 h	[119]
Ethanethiol/AlCl ₃	4.7 ^a	—	THF, 70°C, 5 h	[120]
Lawesson's reagent	—	S-doped	Toluene, 110°C, 24 h	[121]
NaHSO ₃	7.9 ^b	S- doped	95°C, 3 h	[122]
Na ₂ S ₂ O ₄ /NaOH	—	—	60°C, 15 min	[123]
Thiourea	5.6 ^a	Adsorbed	95°C, 8 h	[124]
Thiophene	10.9 ^a	Adsorbed	80°C, 24 h	[125]
Nitrogen-containing reducing agents				
Hydrazine	10.3 ^b	N-doped	100°C, 24 h	[92]
	11 ^b	N-doped	DMF/H ₂ O, 80°C, 12 h	[126]
Phenylhydrazine	9.5 ^b	N-doped	RT, 24 h	[127]
Hydroxylamine/NH ₃	9.7 ^a	—	90°C, 1 h	[128]
Hydroxylamine	1.5 ^a	N-doped	80°C, 30 h	[129]
Benzylamine	4.7 ^a	Adsorbed	90°C, 1.5 h	[130]
p-Phenylene diamine	7.4 ^a	Adsorbed	DMF/H ₂ O, 90°C, 24 h	[131]
Ethylenediamine	7.8 ^a	N-doped	DMF, 80°C, 8 h	[132]
^a X-ray photoelectron spectroscopy. ^b Elemental analysis. ^c Energy dispersive spectroscopy. ^d Reduction carried out in aqueous medium or pure solution of the reducing agent unless stated otherwise.				

Reducing agent	C/O ratio	Doping	Conditions ^d	Ref.
Nitrogen-containing reducing agents				
Urea/NH ₃	4.5 ^a	Adsorbed	95°C, 30 h	[133]
Dimethyl ketoxime/NH ₃	6.5 ^a	Adsorbed	100°C, 3 h	[134]
Hexamethylenetetramine	—	Adsorbed	100°C, 12 h	[135]
Polyelectrolyte		Adsorbed	90°C, 5 h	[136]
Poly(amido amine)	8.1 ^a	Covalent	90°C, 1 h	[137]
Oxygen-containing reducing agents				
Methanol	4.0 ^b	—	100°C, 5 days	[105]
Ethanol	6.0 ^b	—	100°C, 5 days	[105]
Isopropyl alcohol	6.9 ^b	—	100°C, 5 days	[105]
Benzyl alcohol	30 ^b	—	100°C, 5 days	[105]
Hydroquinone	—	—	RT, 20 h	[138]
L-Ascorbic acid/L-tryptohan/ NaOH	—	Adsorbed	80°C, 24 h	[101]
L-Ascorbic acid	—	Adsorbed	RT, 48 h	[139]
L-Ascorbic acid/NH ₃	12.5 ^a	—	95°C, 15 min	[102]
Glucose/NH ₃	—	Adsorbed	95°C, 1 h	[104]
Dextran/NH ₃	—	Adsorbed	95°C, 3 h	[140]
Gallic acid	5.3 ^a	Adsorbed	95°C, 6 h	[141]
^a X-ray photoelectron spectroscopy. ^b Elemental analysis. ^c Energy dispersive spectroscopy. ^d Reduction carried out in aqueous medium or pure solution of the reducing agent unless stated otherwise.				

Reducing agent	C/O ratio	Doping	Conditions ^d	Ref.
Metal–acid				
Al/HCl	18.6 ^a	—	RT, 30 min	[107]
Fe/HCl	7.9 ^a	Fe-doped	RT, 6 h	[142]
Zn/HCl	33.5 ^a	—	RT, 1 min	[143]
Zn/H ₂ SO ₄	21.2 ^a	—	RT, 2 h	[144]
Sn(II)/HCl	7.6 ^a	—	RT, 7 h	[145]
Al foil/HCl	21.1 ^b	—	RT, 20 min	[146]
Mg/HCl	3.9 ^c	—	RT, 5 min	[147]
Metal–alkaline				
Zn/NH ₃	8.6 ^a	—	RT, 10 min	[108]
Zn/NaOH	5.7 ^b	—	RT, 6 h	[148]
Al foil/NaOH	5.3 ^b	—	RT, 20 min	[146]
Na/NH ₃	16.6 ^a	N-doped	-78°C, 30 min	[149]
Amino acid				
L-Cysteine	—		RT, 72 h 9	[103]
L-Tyrosine	6.07 ^a	—	100°C, 24 h	[150]
Glycine	11.2 ^a	N-doped	95°C, 36 h	[151]
^a X-ray photoelectron spectroscopy. ^b Elemental analysis. ^c Energy dispersive spectroscopy. ^d Reduction carried out in aqueous medium or pure solution of the reducing agent unless stated otherwise.				

Reducing agent	C/O ratio	Doping	Conditions ^d	Ref.
Amino acid				
L-Lysine	8.5 ^a	N-doped	90°C, 9 h	[152]
L-Glutathione	—	Adsorbed	50°C, 6 h	[153]
Plant extracts				
Green tea	—	Adsorbed	90°C, 2.5 h	[109]
<i>C. esculenta</i> leaf	7.1 ^b	Adsorbed	RT	[154]
<i>M. ferrea</i> Linn. leaf	6.1 ^b	Adsorbed	RT	[154]
<i>C. sinensis</i> peel	6.0 ^b	Adsorbed	RT	[154]
<i>R. damascena</i>	—	—	95°C, 5.5 h	[155]
Microorganisms				
Shewanella	—	—	Anaerobic, 72 h	[156]
	3.1 ^a	—	Aerobic, 60 h	[157]
<i>E. coli</i> culture	—	—	37°C, 48 h	[158]
<i>E. coli</i> biomass	—	—	37°C, 72 h	[159]
Baker's yeast/NADPH	5.9 ^a	Adsorbed	35–40°C, 72 h	[160]
Wild carrot roots	11.9 ^a	Adsorbed	25°C, 72 h	[161]
Proteins				
Bovine serum albumin/NaOH	—	Adsorbed	55–90°C, 3–24 h	[162]
Hormones				
Melatonin/NH ₃	—	Adsorbed	80°C, 3 h	[163]
^a X-ray photoelectron spectroscopy. ^b Elemental analysis. ^c Energy dispersive spectroscopy. ^d Reduction carried out in aqueous medium or pure solution of the reducing agent unless stated otherwise.				

1.2.5. Thermal reduction of GO

Thermal and hydrothermal reduction of graphite oxide is also used by various researchers since it offers a nonchemical approach to obtain reduced graphite oxide, which may not contain residues of toxic reductants commonly found in the chemical approach. In the initial stages of graphene research, rapid heating ($>2000^{\circ}\text{C}/\text{min}$) was usually used to exfoliate graphite oxide to graphene [48, 164-166]. The mechanism of exfoliation is mainly the sudden expansion of CO or CO_2 gases that developed into the spaces between graphene sheets during the rapid heating of the graphite oxide. The rapid temperature increase makes the oxygen containing functional groups attached on carbon plane decompose into gases that create huge pressure between the stacked layers. Based on state equation, a pressure of 40 MPa is generated at 300°C , while 130 MPa is generated at 1000°C [48].

The exfoliated sheets can be directly named graphene (or chemically derived graphene) rather than GO, which means that the rapid heating process not only exfoliates graphite oxide but also reduces the functionalized graphene sheets by decomposing oxygen-containing groups at elevated temperature. This dual effect makes thermal expansion of graphite oxide a good strategy to produce bulk quantity graphene [167]. However, this procedure is found only to produce small size and wrinkled graphene sheets [48]. This is mainly because the decomposition of oxygen-containing groups also removes carbon atoms from the carbon plane, which splits the graphene sheets into small pieces, and results in the distortion of the carbon plane.

A notable effect of thermal exfoliation is the structural damage to graphene sheets caused by the release of carbon dioxide [168]. Approximately 30% of the mass of the graphite oxide is lost during the exfoliation process, leaving behind lattice defects throughout the sheet [48]. An alternative way is to exfoliate graphite oxide in the liquid phase, which enables the exfoliation of graphene sheets with large lateral sizes [169]. The reduction is carried out after the formation of macroscopic materials, e.g. films or powders, by annealing in inert or reducing atmospheres. In this strategy, the heating temperature significantly affects the effect of reduction on GO [48, 170-172]. Schniepp et al. [48] found that if the temperature was less than 500°C , the C/O ratio was no more than 7, while if the temperature reached 750°C , the C/O ratio could be higher than 13. Wang et al. [171] annealed GO thin films at different temperatures, and showed that the volume electrical conductivity of the reduced GO film obtained at 500°C was only 50 S/cm, while at 700°C and 1100°C it could be 100 S/cm and 550 S/cm, respectively. Wu et al. [172]

used arc-discharge treatment to exfoliate graphite oxide to graphene since the arc-discharge could provide temperatures above 2000°C in a short time.

Based on the above results, reduction of GO by high temperature annealing is highly effective. But the drawback of thermal annealing is also obvious. First, high temperature means large energy consumption and critical treatment conditions. Second, if the reduction is performed to an assembled GO structure, e.g. a GO film, heating must be slow enough to prevent the expansion of the structure, otherwise quick heating may explode the structure just like the exfoliation of graphite oxide. But slow heating makes the thermal reduction of GO a time-consuming process. Finally and importantly, some applications need to assemble GO on substrates, e.g. thin carbon films, but the high temperature means that this reduction method cannot be used for GO films on substrates with a low melting-point, such as glass and polymers.

1.2.6. Photo-catalytic method

GO can also be reduced by photo-chemical reactions with the assistance of a photocatalyst like TiO₂. Recently, Williams et al. reported the reduction of GO in a colloid state with the assistance of TiO₂ particles under ultraviolet (UV) irradiation [49]. As they showed, a change in colour from light brown to dark brown and finally to black can be seen as the reduction of GO. This colour change has previously been suggested to be due as partial restoration of the conjugated network in the carbon plane like that in chemical reduction processes [173]. Before reduction, the carboxyl groups in GO sheets can interact with the hydroxyl groups on the TiO₂ surface by charge transfer, producing a hybrid between the TiO₂ nanoparticles and the GO sheets, and this structure can be retained after reduction. The rGO sheets can work as a current collector to facilitate the separation of electron/hole pairs in some photovoltaic devices like a photocatalysis device [174] and a dye-sensitized solar cell [175]. Following the same idea, some other materials with photocatalytic activity, like ZnO [176] and BiVO₄ [177], have also been reported to achieve the reduction of GO.

1.2.7. Electrochemical method

Another method that shows promise for the reduction of GO relies on the electrochemical removal of oxygen functionalities [50, 178, 179]. Electrochemical reduction of GO sheets or films can be carried out in a normal electrochemical cell using an aqueous buffer solution at room temperature. The reduction usually needs no special chemical agent, and is mainly caused

by the electron exchange between GO and electrodes. In principle, this could avoid the use of dangerous reductants (e.g. hydrazine) and the need to dispose of the by-products.

After depositing a thin film of GO on a substrate (glass, plastic, ITO, etc.), an inert electrode is placed opposite to the film in an electrochemical cell; the reduction occurs during charging of the cell. By cyclic voltammetric scanning in the range of 0 to -0.1 V (respect to a saturated calomel electrode) to a GO-modified electrode in a 0.1 M KNO₃ solution, Ramesha and Sampath [180] found that the reduction of GO began at -0.6 V and reached a maximum at -0.87 V. The reduction can be achieved by only one scan and is an electrochemically irreversible process in this scanning voltage range. Zhou et al. [178] reported the best reduction effect using an electrochemical method. They found that the potential needed to realize the reduction is controlled by the pH value of the buffer solution. A low pH value is favourable to the reduction of GO, so the authors proposed that H⁺ ions participate in the reaction. An et al. [181] used electrophoretic deposition (EPD) to make GO films. They found that GO sheets can also be reduced on the anode surface during EPD, which seems counter-intuitive to the general belief that oxidation occurs at the anode in an electrolysis cell. Though the reduction mechanism is not clear, the simultaneous film assembly and reduction might be favourable to some electrochemical applications.

As with many of the aforementioned methods, the reduction mechanism remains unclear. Though this route appears to be extremely effective (and yet mild) at reducing the extant oxide functionality, and it precludes the need for hazardous chemical reactants and their by-products, electrochemical reduction has not been demonstrated on a large sample. The deposition of reduced graphene oxide onto the electrodes is likely to render bulk electrochemical reduction difficult on a preparative scale. Scalability is a fundamental requirement of a useful synthetic protocol if graphene is to be broadly utilized.

1.2.8. Other methods

In recent years, scientists have discovered methods for the reduction of GO based on photo-irradiation [182, 183], bacterial respiration [156-158] and un-zipping carbon nanotubes (CNTs).

The photo-irradiation methods are UV-induced photocatalytic reduction [183], photo-thermal reduction using a pulsed Xenon flash [184], selective reduction by direct laser writing [185] and laser converted graphene from GO [186]. The main advantage of photo-irradiating process

is that it does require neither chemicals nor high temperatures. Pulsed laser irradiation was demonstrated by Huang et al. [187] to reduce GO with removal of most of the oxygen functional groups. The reduced GO produced by this method showed a good electrical conductivity. Pulsed laser irradiation is simple, fast, consumes very less energy and is environmentally friendly compared to conventional chemical and thermal reduction methods. Femtosecond laser was also used for the reduction of GO in aqueous solution without any reducing agents [188]. The femtosecond laser has shorter laser pulse duration than the electron cooling time, and thus transfers minimum heat into the target materials. Several researchers used different techniques such as continuous wave diode laser [185], pulsed laser excitation [189] and picosecond pulsed laser irradiation [190] to reduce GO. These methods appeared to be a promising procedure for large-scale synthesis of graphene and open a new method to produce graphene composites for wide range of applications.

GO can be reduced to graphene in a normal aerobic setup under ambient conditions as mediated by microbial respiration of *Shewanella* cells and *E. coli* bacteria [156-158]. The reduction of the GO sheets by the bacterial suspension in the provided anaerobic condition can be assigned substantially to the metabolic activity of the bacteria (and partially to the glucose of the bacterial suspension). The promotion in the level of reduction of the GO sheets by increasing the contact time can be also assigned to increase in the number of the surviving bacteria contributing to the glycolysis process [158]. In addition to the *Shewanella* strains reported by Salas et al. [156, 191], GO was reduced by *Shewanella* bacterium through transferring metabolically-generated electrons from its cell interior to GO as an external electron acceptor.

A very recent method of graphene synthesis has used multi-walled carbon nanotubes (MWCNTs) as the starting material [192]. The process is popularly known as ‘unzipping of CNTs’. MWCNTs can be opened up longitudinally by using intercalation of Li and ammonia, followed by exfoliation in acid and abrupt heating [193]. The product, among nanoribbons and partially opened MWCNTs, also contained graphene flakes. In another study [194], graphene nanoribbons were produced by plasma etching of MWCNTs, partially embedded in a polymer film. The etching treatment basically opened up the MWCNTs to form graphene. In a different approach as shown in **Figure 1.7** [195], MWCNTs were unzipped by a multi-step chemical treatment, including exfoliation by concentrated H_2SO_4 , KMnO_4 and H_2O_2 , stepwise oxidation using KMnO_4 and finally reduction in NH_4OH and hydrazine monohydrate ($\text{N}_2\text{H}_4 \cdot \text{H}_2\text{O}$) solution. This new process of unzipping MWCNTs to produce graphene creates possibilities of synthesizing graphene in a substrate-free manner.

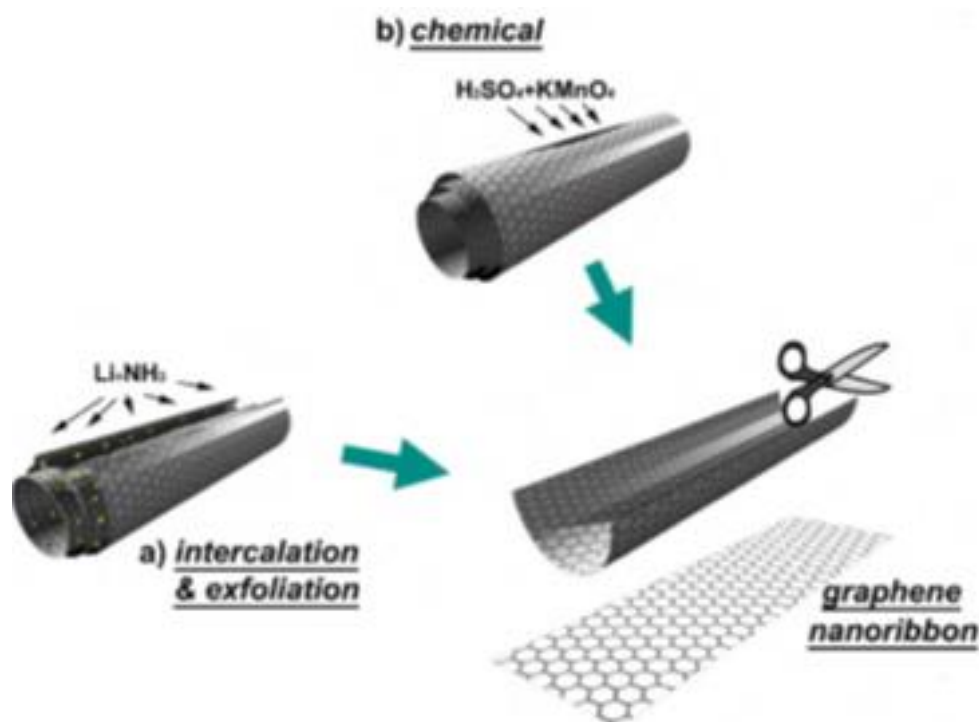


Figure 1.7: Sketch showing the different ways nanotubes could be unzipped to yield graphene nanoribbons (GNRs): (a) intercalation-exfoliation of MWCNTs, involving treatments in liquid NH_3 and Li, and subsequent exfoliation using HCl and heat treatments; (b) chemical route, involving acid reactions that start to break carbon-carbon bonds (e.g. H_2SO_4 and KMnO_4 as oxidizing agents) [196].

1.3. Properties of graphene

1.3.1. Surface properties

Single-layer graphene is theoretically predicted to have large surface area of $\sim 2630 \text{ m}^2 \text{ g}^{-1}$, surpassing that of graphite ($\sim 10 \text{ m}^2 \text{ g}^{-1}$), and being two times larger than that of single-walled carbon nanotubes (SWCNTs) ($\sim 1315 \text{ m}^2 \text{ g}^{-1}$) [1, 8]. Surface areas of different few layers graphene samples have been measured by the Brunauer-Emmett-Teller (BET) method and are in the range of $270\text{-}1550 \text{ m}^2 \text{ g}^{-1}$. Large surface area is an essential characteristic of an electrode material, particularly in sensing devices, and energy production and storage. For example, the high surface area of electrically conductive graphene sheets can give rise to fast electron transfer and high densities of attached analyte molecules. This in turn can facilitate high sensitivity and device miniaturization. Moreover, high surface area provides an excellent platform for the chemical functionalization.

1.3.2. Electronic properties

Isolated graphene crystallites exhibit exceptional electronic properties. The electrical conductivity of graphene has been calculated to be $\sim 64 \text{ mS cm}^{-1}$, which is approximately 60 times more than that of SWCNTs [197]. Its conductivity remains stable over a wide range of temperature and even in liquid-helium, a temperature which is essential for reliability within many applications [8].

One of the most interesting aspects of graphene is its highly unusual nature of charge carriers, which behave as massless relativistic particles (Dirac fermions). Dirac fermions behaviour is very abnormal compared to electrons when subjected to magnetic fields for example, the anomalous integer quantum Hall effect (QHE) [9, 198]. This effect was even observed at room temperature [10]. The band structure of single layer graphene exhibits two bands intersecting at two inequivalent points K and K' in the reciprocal space. Near these points electronic dispersion resembles that of the relativistic Dirac electrons. K and K' are referred as Dirac points where valence and conduction bands are degenerated, making graphene a zero band gap semiconductor (**Figure 1.8**).

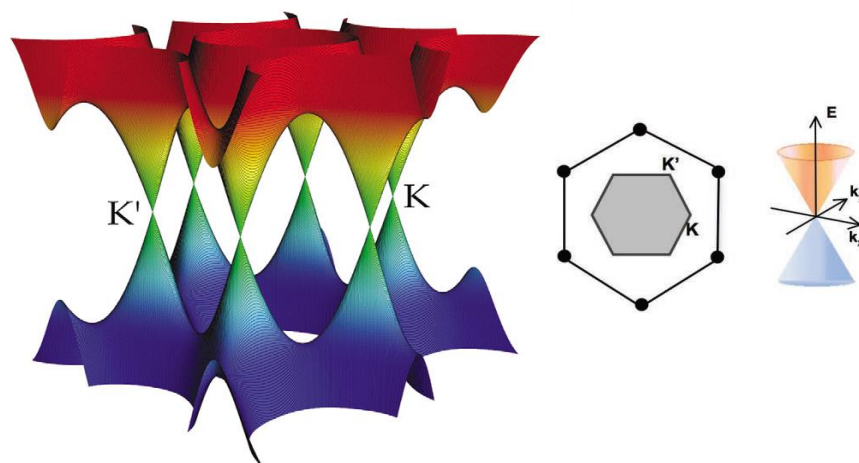


Figure 1.8: Band structure of graphene. The conduction band touches the valence band at the K and K' points [199].

It reveals itself in a pronounced ambipolar electric field effect at room temperature with the concentration of charge carriers up to 10^{13} cm^{-2} and mobilities of $\sim 10000 \text{ cm}^2 \text{V}^{-1} \text{s}^{-1}$, when a gate voltage is applied [39].

Besides, suspended graphene shows an ultra-high low-temperature mobility approaching 200 000 $\text{cm}^2\text{V}^{-1}\text{s}^{-1}$ for carrier densities below $5 \times 10^9 \text{ cm}^{-2}$ [200].

1.3.3. Optical properties

Graphene's unique optical properties produce an unexpectedly high opacity for an atomic monolayer suspended in vacuum, with a measured white light absorbance of 2.3% and a negligible reflectance ($<0.1\%$). Absorbance increases linearly with the layers number from 1 to 5 (**Figure 1.9**) [201, 202].

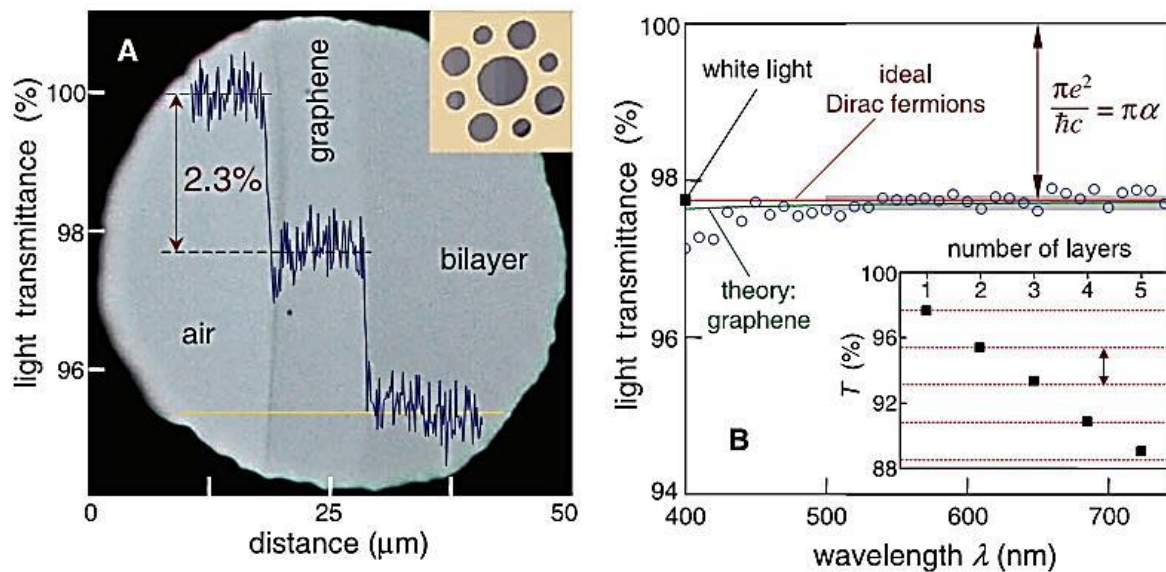


Figure 1.9: Looking through one-atom-thick crystal. (A) Photograph of a 50- μm aperture partially covered by graphene and its bilayer. The line scan profile shows the intensity of transmitted white light along the yellow line. (B) Transmittance spectrum of single-layer graphene (open circles). The red line is the transmittance $T = (1 + 0.5\pi\alpha)^{-2}$ expected for two dimensional Dirac fermions, whereas the green curve takes into account a nonlinearity and triangular warping of graphene's electronic spectrum. (Inset) Transmittance of white light as a function of the number of graphene layers (squares) [202].

In addition, the optical transition can be modified by changing the Fermi energy considerably through electrical gating [203]. Another property of graphene is its photoluminescence (PL). It is possible to make graphene luminescent by inducing a suitable band gap. Two routes have been proposed. The first method involves cutting graphene into nanoribbons and quantum dots.

The second one is a physical or chemical treatment with different gases to reduce the connectivity of the π electron network [4, 204]. For example it was shown that PL can be induced by oxygen plasma treatment of graphene single layer on silicon substrate covered with 100 nm SiO₂ [205]. This gives an opportunity of making hybrid structures by etching just the top layer, while keeping the underlying layer unaffected. Broad PL from solid GO and liquid GO suspension was also observed. The progressive chemical reduction of GO into rGO quenched the PL, whereas oxidation increases PL by producing a disruption of the π network and opening a direct electronic band gap [206].

Fluorescent organic compounds are very important for the development of low cost optoelectronic devices [207]. Particularly blue fluorescence from aromatic or olefin molecules and their derivatives are important for display and lighting applications [208]. Blue PL was observed for GO thin films deposited from thoroughly exfoliated suspensions [209]. The PL characteristic and its dependence on the reduction of GO originate from the recombination of electron-hole pairs localized within small sp² carbon clusters embedded within the GO sp³ matrix [209].

The exceptional electrical properties in conjunction with optical properties have fuelled lot of interests in novel photonic and optoelectronics devices [210-212]. Numerous promising applications using graphene have been suggested, including photodetectors, touch screens, light emitting devices, photovoltaics, transparent conductors, terahertz devices and optical limiters.

1.3.4. Mechanical properties

The mechanical properties of monolayer graphene membranes were measured based on nanoindentation using atomic force microscopy (AFM) [11]. Measurements have shown that graphene has a breaking strength of 42N m⁻¹ which is over 100 times greater than a hypothetical steel film of the same thickness [5, 213]. The tensile modulus (stiffness) is 1 TPa (150,000,000 psi).

The discussed experimental data on the Young modulus ($E = 1$ TPa) and the intrinsic strength ($\sigma = 130$ GPa) exhibited by pristine graphene are consistent with computer simulations [214], showing values of $E = 1.05$ TPa and $\sigma = 110$ GPa [215]. These values of E and σ are extremely large and make graphene to be very attractive for structural and other applications. This value

is one of the highest ever measured for real materials like diamond [216]. At the same time, graphene can be easily bent, and this specific behavioural feature can be exploited in practice.

These exceptional mechanical properties of graphene are of utmost importance for its applications, because they are highly needed (i) to exploit it as a superstrong structural material; (ii) to understand and control durability of graphene used in electronics and energy storage; (iii) to plastically form curved graphene specimens for electronics and structural applications; (iv) to exploit nanocomposites with graphene inclusions as structural and/or functional materials [215].

The strain on graphene may change electronic band structure, which indicates that the energy band gap can be tuned by introduction of controlled strain [217]. The elastic deformation of functionalized graphene sheets (FGSs), or chemically reduced graphene oxide has also been studied by AFM. After repeatedly folding and unfolding of the FGSs multiple times, the folding lines were found to appear at the same locations, which can be attributed to the pre-existing kinks or defect lines in the FGSs [201].

1.3.5. Thermal properties

The thermal conductivity (κ) of graphene is dominated by phonon transport, namely diffusive conduction at high temperature and ballistic conduction (transport without scattering) at sufficiently low temperature [218].

Thermal stability is one of the key factors for better performance and reliability of electronic devices. Considerable amount of heat generated during the device operation needs to be dissipated. Carbon allotropes such as graphite, diamond, and carbon nanotubes have shown a higher thermal conductivity due to strong C-C covalent bonds and phonon scattering [217]. Earlier, carbon nanotubes were known to have the highest thermal conductivity values at room temperature *i.e.* ~ 3000 W/mK for MWCNTs [219] and 3500 W/mK for single walled CNTs [220].

The thermal conductivity (κ) of single-layer suspended graphene at room temperature depends on the size of the measured graphene sheet [13]. Recently, the highest room temperature thermal conductivity up to 5000 W/mK for single-layer suspended graphene (defect-free) has been reported [13], whereas the thermal conductivity decreases to ~ 600 W/mK when graphene is supported on amorphous silica, a case similar to practical application. This reduction is

attributed to the leaking of phonons across the graphene–silica interface and strong interface-scattering [221]. Nevertheless, this value is still about twice and 50 times higher than copper and silicon, respectively, which are widely used in the electronics today.

Graphene is often thought to hold advantages over other materials because of its higher thermal conductivity. Thus, high thermal conductivity could suggest very good heat sinking and low temperature rise during device operation. However, under high-field and high-temperature (i.e., typical circuit) operating conditions, significant dissipation and temperature rise can nevertheless occur in graphene devices [222, 223].

1.3.6. Photo-catalytic properties

Recently, significant attention has been given to the application of graphene-based hybrid materials with semiconducting properties in photoelectrochemistry areas like electrochemical solar cells, photocatalytic degradation of organic pollutants, water splitting for hydrogen evolution, photocatalytic conversion of fuels, etc. An electron transition from valence band to conduction band in semiconductors upon excitation by a photon ($E \geq E_g$ – E_g is the band gap) generates an electron-hole pair (an electron in conduction band and a positive hole in the valence band) [41, 224].

The photoelectrochemical performance and the visible light absorption by the semiconductor materials have been improved by different metal-ion doping, anion doping, adding hole scavengers (electron donors), creating oxygen vacancies, adding co-catalyst, loading noble metal particles, dye sensitization and forming composite semiconductors. The excellent absorptivity, transparency, conductivity, nontoxicity, diverse functionalities and controllability of graphene led to its super photoelectrochemical performance by making its hybrids with semiconductors. The band gap and band potentials of the semiconductors are important for the particular type of photocatalytic process, as depicted in **Figure 1.6**. Graphene is considered to be an outstanding candidate for hybrid photocatalytic materials [225] with a work function around -4.4 eV, whereas important semiconductor have their conduction band position at around -3.5 eV (with respect to vacuum level, **Figure 1.10**). This helps in the photogenerated electron transfer process from conduction band of the semiconductor to graphene surface [226].

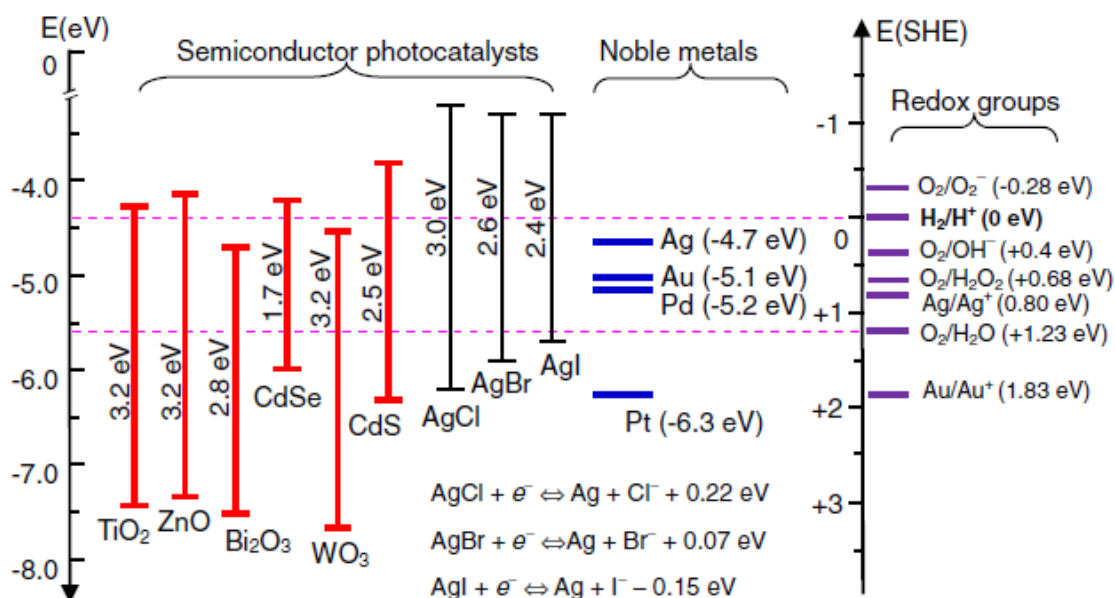


Figure 1.10: Electronic band gap and band potentials of different semiconductors and metals [227].

This delocalization of the photogenerated electron on graphene surface inhibits the recombination of electron hole pairs within the semiconductor, thus leading to an increase of the photocatalytic efficiency.

Graphene in nanocomposite photocatalytic materials also plays an important role by increasing the solar light absorption efficiency. Graphene also decreases the band gap of the semiconductors leading to an efficient solar light absorber. For example, TiO₂ (P25) nanoparticles are active in UV light [174]; however, they become effective visible light catalyst in conjugation with graphene [228]. ZnS nanoparticles extend their absorption edge towards the visible range in conjugation with graphene [229]. BiOBr nanoparticles conjugated to graphene have a smaller indirect band gap than that of pure BiOBr material [230]. In addition, graphene with its high surface area provides sufficient space for the adsorption of organic pollutants [231], which is one of the key factors for heterogeneous photocatalysis.

1.3.7. Magnetic properties

There has been considerable interest on the magnetism of nanographite particles for some time. Enoki et al. [232] pointed out that edge states as well as adsorbed or intercalated species play an important role in determining magnetic properties of these nanographite particles [87].

Room temperature ferromagnetism has been later observed in highly oriented pyrolytic graphite (HOPG) [233, 234]. Some reports have predicted that ferromagnetic ordering could exist among various defects on graphene structures, such as vacancy, topological defects or frustration, and hydrogen chemisorption or perhaps the edge. Graphene-like character [235] originates from the carbon π -electron system rather than from possible d-element impurities.

Similar observation has been carried out in carbon nanotubes (CNTs) under particular conditions [236]. Their growth inside alumina templates produces a high number of defects resulting from the elevated amount of hydrogen uptake during the annealing process. In this case ferromagnetism has been observed up to 1000K. Recently, magnetic properties of graphene samples prepared by thermal exfoliation of graphite oxide, conversion of nano-diamond, arc evaporation of graphite and partial chemical reduction of graphene oxide have been studied [237, 238]. Magnetic properties of graphene reveal that dominant ferromagnetic interactions coexist along with antiferromagnetic interactions in all of the samples.

It is not possible to exactly know the origin of magnetism in the graphene samples although defects and edge effects are playing a major role. We can also consider that the contamination of metal impurity detected in the samples (like Fe, Co, Ni) as sources of magnetism in the graphene [239, 240].

1.4. Characterizations of graphene

Usually graphene are characterized by microscopy (SEM, TEM, AFM), spectroscopic (UV-Vis, FT-IR, Raman, XPS) and thermal (TGA) techniques. Short accounts of these characterization techniques are discussed here.

1.4.1. Morphology (SEM, TEM and AFM)

Scanning Electron Microscopy (SEM) or field emission scanning electron microscopy (FESEM) allow to examine the topography, morphology, composition and crystallographic information of materials with sizes and shapes of the crystallites that constitute graphene sheets. [241, 242]. Electron beam is used to scan samples in a SEM or FESEM microscope. When the electron beam is moved across the surface of the sample, the charge will be accumulated on it that would affect the imaging if the sample is not conducting. **Figure 1.11** shows an example of SEM, TEM and AFM images of graphene.

Transmission electron microscopy (TEM) can also accurately identify the thickness of a graphene sheet. In TEM, a beam of electrons is transmitted through the sample and an image is formed onto a phosphor screen so that the image can be seen which is different with SEM [241].

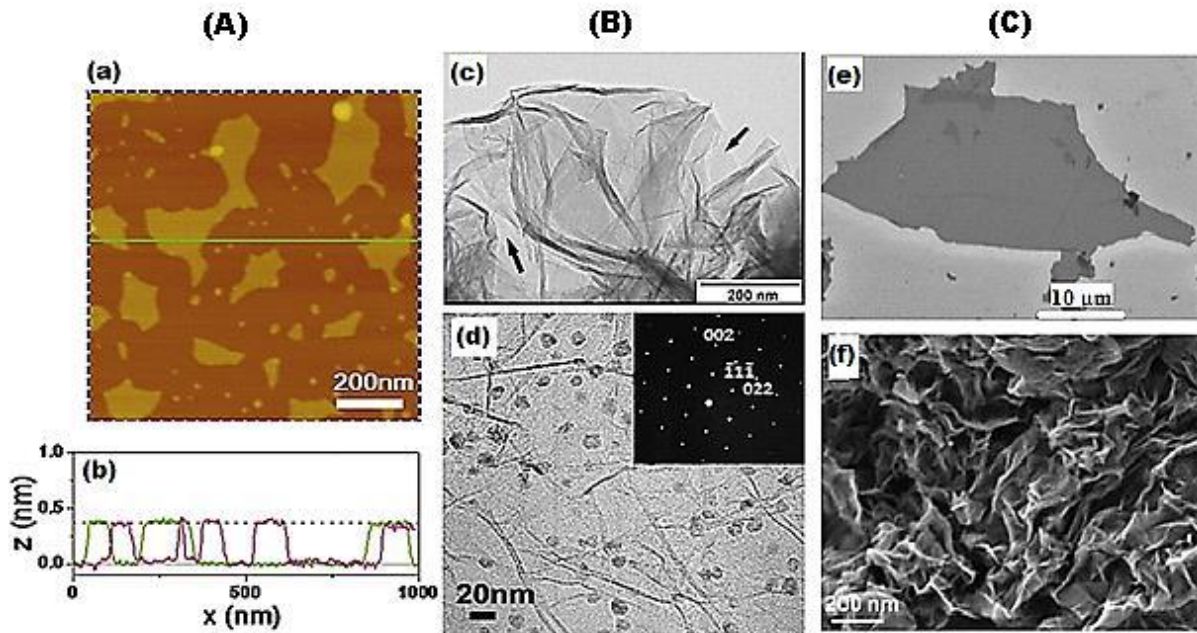


Figure 1.11: (A) AFM image (a) and the thickness (b) of a monolayer graphene sheet deposited on mica [243]. (B) TEM image (c) of graphene nanosheets, resembling crumpled silk. The featureless regions indicated by the arrows are monolayer graphene. High magnification TEM of Co_3O_4 /graphene composite (d) [138, 244]. (C) SEM image of a monolayer graphene sheet (e), and aggregated reduced GO sheets (f) [92, 245].

As reported by Hernandez *et al.* [45], the appearance of stable and transparent graphene sheets in the TEM analysis indicates the presence of single-layer graphene, and the edges of the suspended film always fold back, allowing a cross-sectional view of the film.

With high resolution TEM (HRTEM), the investigation of the edges provides a precise way to measure the number of layers at multiple locations on the film [61]. Additionally, TEM is a suitable tool to explore graphene/nanoparticles composites [98, 244, 246].

Another technique which is often used to study the sample thickness and morphology is Atomic Force Microscopy (AFM). This method uses the Van der Waals forces between a tip (a few nm long and tens of nm wide) and the sample surface. These interactions produce a deflection of

the cantilever which sustains the tip which can be measured and converted to obtain the sample profile. A pristine graphene and GO can be distinguished based on the different thickness using AFM imaging. This can be explained by the interaction forces between the AFM tip and the functional groups. Paredes et al. [247] demonstrated that chemically reduced and unreduced GO nanosheets can be distinguished using attractive regime of tapping-mode AFM. Besides thickness and imaging characterization, different AFM modes can be used to study the mechanical [11], frictional, electrical, magnetic and elastic properties of graphene nanosheets.

1.4.2. Raman spectroscopy

In Raman spectroscopy, the inelastic scattering of monochromatic light from a laser is used to study vibrational and rotational modes in a material. This allows the study of important physical and chemical phenomena in graphene, in a fast and non-destructive way. The first remarkable potential is the identification of single-layer graphene flakes and their distinction from 2-layer/few-layer graphene [248]. Other properties can be detected and studied by Raman such as disorder, doping [249], and strain [250]. Carbon allotropes possess their identity at D, G, and 2D peaks around 1350, 1580 and 2700 cm^{-1} , respectively under Raman spectroscopy investigation. The D-band of GO arising from the stretching of sp^3 carbons of graphene sheets occurs at 1350 cm^{-1} and a G-band due to the stretching of sp^2 carbon occurs at 1580 cm^{-1} ; this band is associated to the doubly degenerated E_{2g} phonon mode at the Brillouin zone centre [251, 252]. The D band appears due to the presence of disorder in atomic arrangement, e.g. impurities and edges which break the translational symmetry [59]. The most important band to study is the shape and intensity of 2D band of graphene and graphite. A single sharp peak can be observed for 2D band of monolayer graphene whereas, two peaks appear in graphite for this band [253]. The number of graphene layers increases proportionally with an increase in G band intensity as shown in **Figure 1.12** [253, 254].

The ratio of peak intensities I_D/I_G can be used to investigate the level of disorder in graphene [255, 256]. The ratio of the D to G intensities varied inversely with the crystallite size. When the disorder increases, I_D/I_G shows two different regimes: low defect density and high defect density. In low defect density regime, I_D/I_G will increase when higher defect density occurs and creates more elastic scattering. However, I_D/I_G will start to decrease when defect density increases which is attributed to more amorphous carbon structure in high defect density regime [257]. These two regimes are called nanocrystalline graphite and are mainly sp^2 amorphous carbon phases, respectively [257-259]. Comparison of Raman spectra between graphite, single and few layer graphene and GO, rGO are shown in **Figure 1.12**.

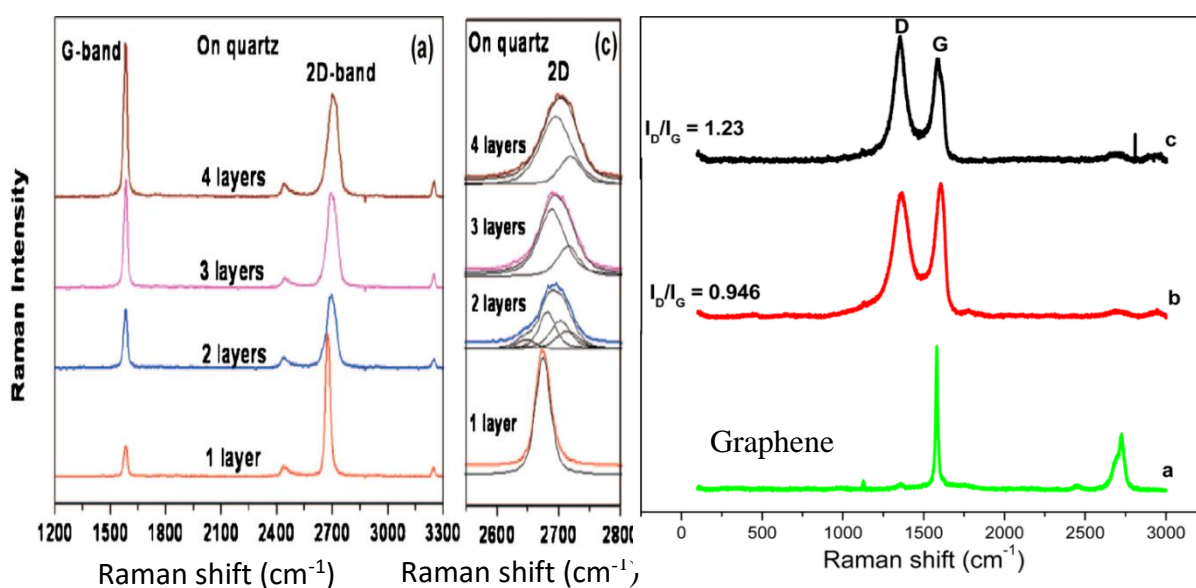


Figure 1.12: The Raman spectra of (a) monolayer, bilayer, tri-layer, and four-layer graphene on quartz; (b) graphene, GO and rGO; (c) The enlarged 2D-band regions with the curve fit are shown in panels [254].

1.4.3. X-ray photoelectron spectroscopy (XPS)

X-ray photoelectron spectroscopy (XPS) deals with the elemental composition, empirical formula, chemical state and electronic state of the elements that exist within a material [260]. XPS can be used to analyse the different oxidation states of carbon in both GO and rGO; thus GO and rGO can be differentiated [261, 262]. In the case of GO and the reduced exfoliated GO [92], the C_{1s} XPS spectrum of GO (**Figure 1.13**) clearly indicates a considerable degree of oxidation with four components that correspond to carbon atoms of different functional groups: the non-oxygenated ring C, the C in C–O bond, the carbonyl C=O, and the carboxylate carbon (O–C=O). Although the C_{1s} XPS spectrum of the reduced exfoliated GO also exhibits these same oxygen functionalities, their peak intensities are much smaller than those in GO, making the C–C peak predominant. The additional nitrogen bonded C (C–N) comes from the reduction process with hydrazine [261]. The comparison of XPS spectra between GO and rGO suggests that most of the oxygen functional groups in GO have been removed during the reduction process using hydrazine.

XPS also allows to characterize the defects in rGO/GO and provides a qualitative information of the defects. In XPS, the ratio of C_{1s} to O_{1s} peak can be related to the estimation of the defect

density in rGO sheets. A higher ratio values correspond to better reduction with lower defects [263].

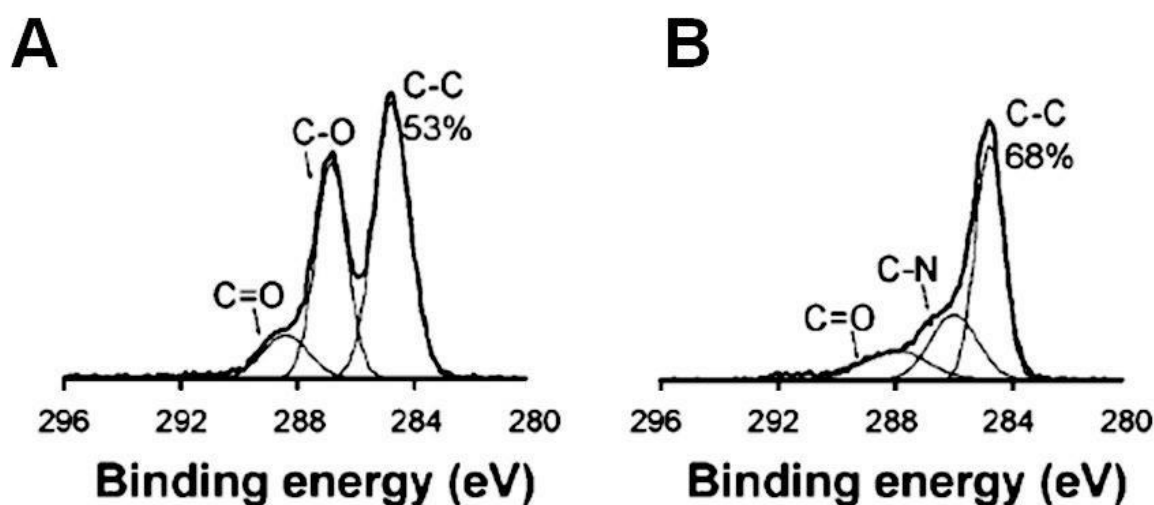


Figure 1.13: C1s XPS spectra of (A) GO and (B) rGO [261].

1.4.4. UV-Visible spectroscopy

UV-Vis spectroscopy (**Figure 1.14**) can provide a general information about graphene formation and the number of layers [264, 265]. The strictly two-dimensional graphene exhibits an absorption peak at around 262 nm, while a single-layer of GO shows absorption at around 228 nm in the UV-Vis spectrum [96]. This is attributed to the π - π^* transitions of aromatic C-C bonds. Also the transparency of GO is much higher than that of graphene, which originates from the recovery of sp^2 carbons from chemically derived graphene after reduction. This is an indication of the restoration of electronic conjugation in reduced graphene. In addition, the transparency of stacked graphene is much lower than that of the monolayer graphene. Sun et al. [266] have reported that monolayer graphene shows transmittance of 97.1% at a wavelength of 550 nm, while it is 94.3% for bilayer graphene, which shows a linear enhancement of the ultraviolet absorption [262].

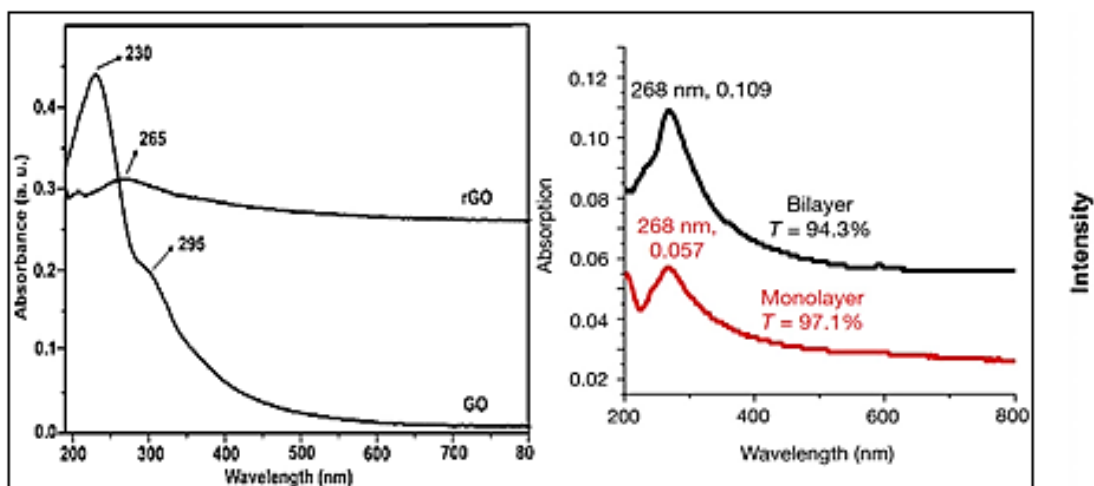


Figure 1.14: UV-Vis absorption spectra of GO and rGO suspensions (left); UV-Vis absorption spectra of monolayer graphene and bilayer graphene (right) (peaks are labelled with the wavelength of maximum absorption and the value of maximum absorption). The UV transmittance (T, %) is measured at 550 nm [148, 266].

1.4.5. X-ray diffraction (XRD)

X-ray diffraction (XRD) is a versatile, non-destructive analytical technique which provides the chemical composition and crystallographic structure of materials. It gives detailed information about the lattice parameter, lattice defects, lattice strain, crystallite size (in case of nanoparticles) and the type of molecular bond of crystalline phase.

Pristine graphite exhibits a basal reflection (002) peak at $2\theta=26.6^\circ$, indicating that the interlayer distance of graphite powder was 3.34 \AA in the XRD pattern. Upon oxidation of pristine graphite, the (002) reflection peak shifts to a lower angle at $2\theta=11.2^\circ$, which indicates that the graphite was fully oxidized into GO with an interlayer distance of 7.9 \AA . This increase in d spacing is due to the intercalation of water molecules and generation of oxygen functionality in the interlayer spacing of graphite. When graphite oxide is completely exfoliated to a single layer of rGO, it should be similar to graphene and a straight line with no apparent diffraction peak in the XRD pattern is obtained (**Figure 1.15**). On other hand, we can see the XRD pattern of the rGO yields only a new narrow peak at $2\theta=24.16^\circ$, suggesting that the rGO is fully reduced [267, 268]. The interlayer distance of rGO is 3.68 \AA , which is fairly close to that of graphite powder (3.34 \AA) [42, 269].

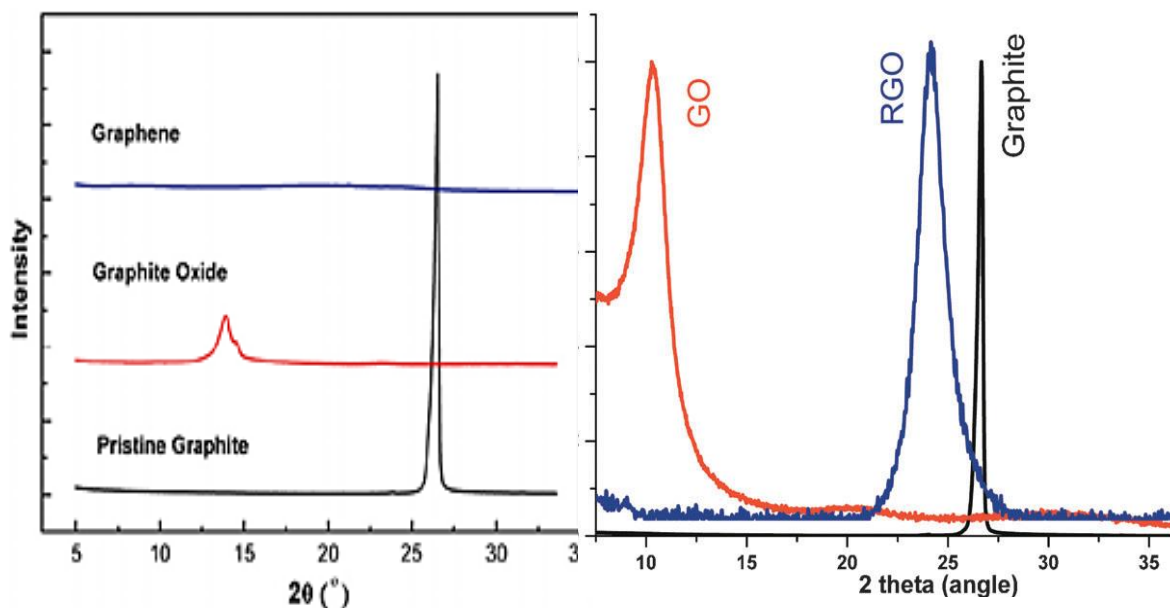


Figure 1.15: X-ray diffraction patterns of pristine graphite, graphite oxide, reduced graphene oxide and graphene [113, 270].

1.4.6. Thermogravimetric analysis (TGA)

TGA is an analytical technique used to determine thermal stability of a material and its fraction of volatile components by monitoring the change in weight that occurs as a specimen is heated [271]. The measurement is normally conducted in air or in an inert atmosphere, such as helium or argon, and the weight is recorded as a function of increasing temperature [92]. TGA is a tool to analysis and to quantify organic species between the graphene layers and probing the effectiveness of oxidation and reduction reactions [125].

TGA analysis was conducted to test the thermal stability of GO sheet and compare it with the rGO and the precursor graphite as shown in **Figure 1.16**. The TGA analysis of graphite shows its high thermal stability even at 1000°C. Since GO is thermally unstable, it starts losing mass from 100°C due to the evaporation of volatiles and adsorbed water molecules in the GO sheet layers. The major mass loss occurs at 200°C due to the removal of oxygen-containing functional groups such as -OH, epoxide and COOH etc. [272]. In case of rGO, already the oxygen-containing functional groups were removed during the reduction process, so the total weight loss is found within the temperature range of 300–900°C; it can be assigned to the

presence of some remaining organic species on the rGO sheets, yielding a better thermal stability than the GO [106].

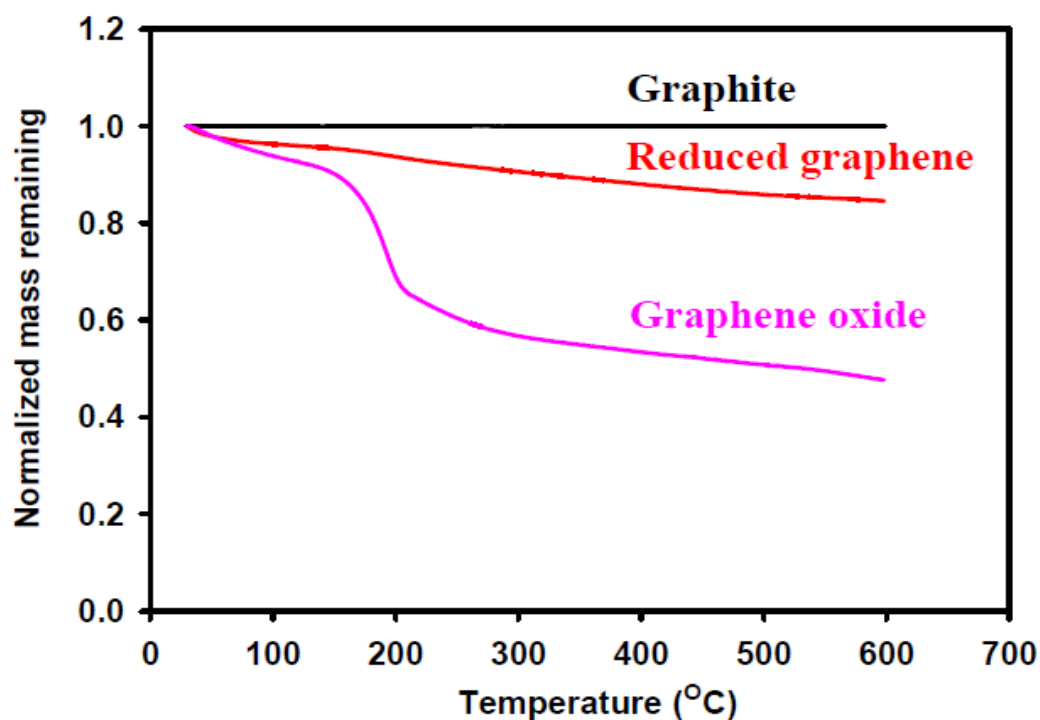


Figure 1.16: TGA plots of graphene, GO and rGO. rGO had better thermal stability than GO [273].

1.4.7. FTIR spectroscopy

The FTIR technique has been suitably modified to enable the study of nanoscale objects. It provides important information about chemical bonding in many newly developed nano materials. FTIR spectra analysis is performed to investigate the structure and functional groups of materials [274].

The GO sheets display various oxygen configurations *i.e.* hydroxyl (namely phenol, C–OH) ($3050\text{--}3800\text{ cm}^{-1}$ and 1070 cm^{-1}) with all C–OH vibrations from COOH and H₂O, carboxyl (ketonic species) (C=O) ($1600\text{--}1650\text{ cm}^{-1}$, $1750\text{--}1850\text{ cm}^{-1}$ including C–OH vibrations at 3530 and 1080 cm^{-1}), sp²-hybridized C=C ($1500\text{--}1600\text{ cm}^{-1}$, in-plane vibrations), and vibration modes of ether or epoxide (C–O–C) ($1000\text{--}1320\text{ cm}^{-1}$) groups [273, 275, 276]. After GO reduction, all the characteristic absorption bands of oxygen-containing groups (O–H, C=O, and C–O) are substantially weakened and almost eliminated [272, 277]. In the spectrum of graphene, the absorption bands near to 3432 cm^{-1} are known to be due to O–H stretching

vibrations; the peak located near 1614 cm^{-1} is attributed to the skeletal vibration of $\text{C}=\text{C}$ sp^2 bonds[278] (**Figure 1.17**).

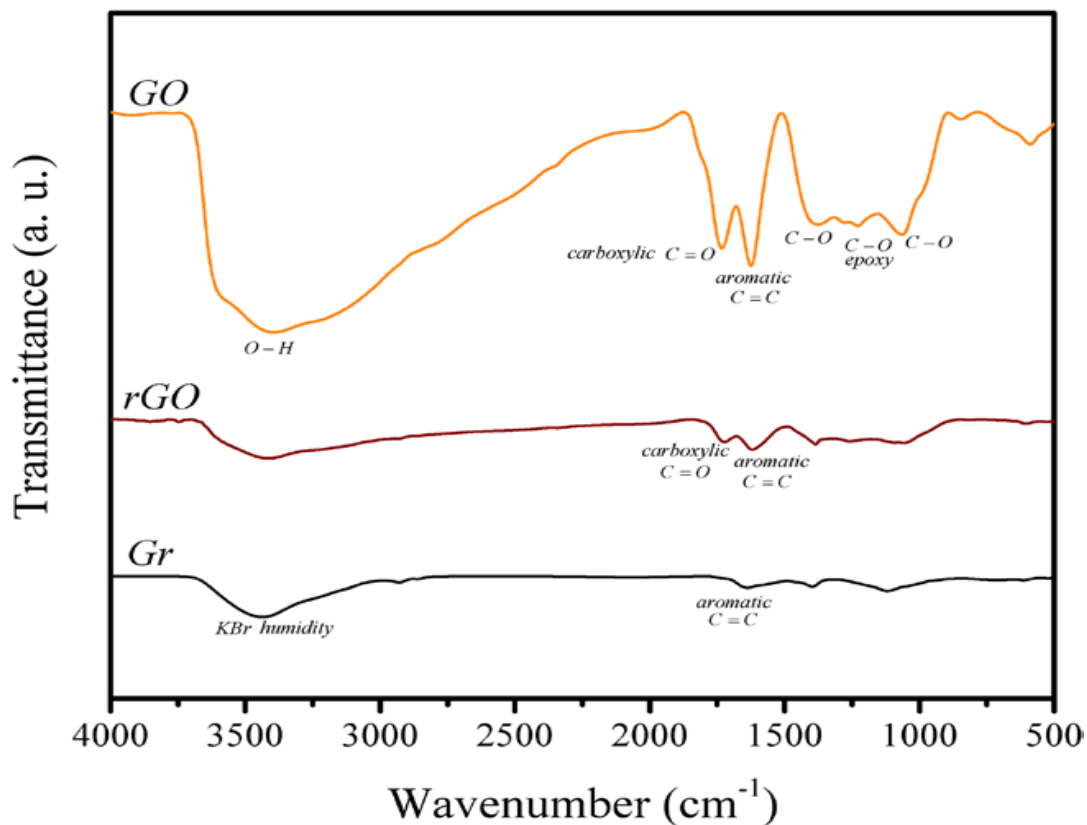


Figure 1.17: FTIR spectra of graphene, fresh graphene oxide and rGO [277].

1.5. Decoration of graphene with metal nanoparticles

Nanocomposites are hybrid materials, which make combination of the individual properties of the component materials resulting in synergistic and novel properties.

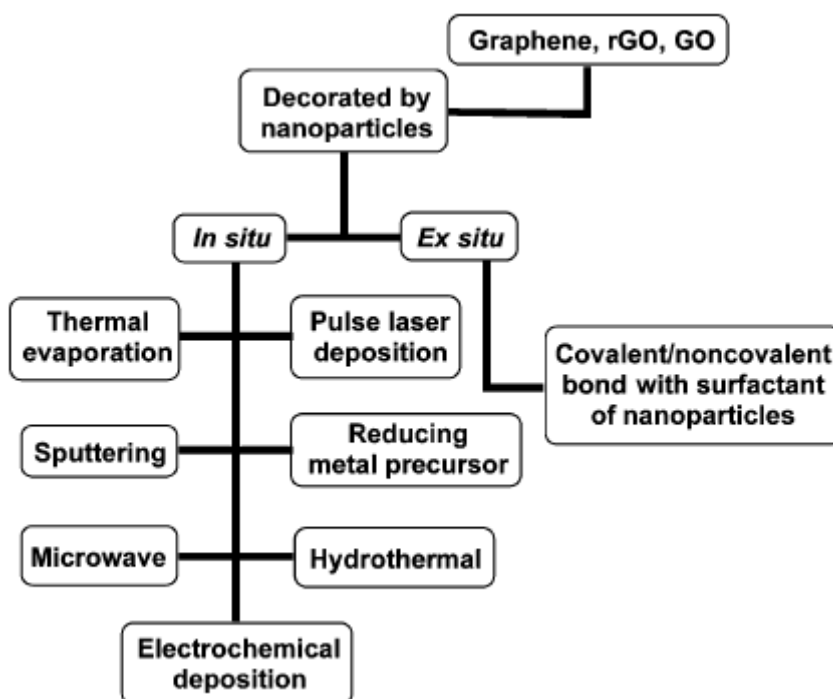
GO can be readily dispersed in water to yield stable dispersions by simple sonication. GO is known to be a good substrate for the dispersion of metal or semiconductor nanoparticles (NPs) because of functional groups such as hydroxyl, carbonyl, and epoxy moieties [279]. Moreover, these oxygen-containing functional groups can act as nucleation centres or anchoring sites for the attachment of nanoparticles [280, 281].

When the size of the metal/metal oxide nanoparticles is in the range of a few to about 100 nanometers, the metal/metal oxide nanoparticles are small and can be easily decorated onto the GO or rGO sheets.

There are many advantages associated with graphene as a substrate for the dispersion of nanoparticles (i) the limited growth of nanoparticles, and their improved stability and dispersion on GO or rGO; (ii) the attached nanoparticles are also useful for enlarging the interplanar spacing of the GO or rGO in the solid state, and for avoiding the aggregation of GO or rGO sheets into graphitic structure [282-284]; (iii) a high-specific surface area which could prevent the aggregation of nanoparticles; (iv) excellent properties of individual GO or rGO sheets such as thermal conductivity with an excellent thermal stability [13], high mobility of charge carriers, optical transmittance [285, 286], etc. .

Because of these above advantages, graphene-based nanocomposites have been intensively developed, and found to show a range of unique and excellent applications, which are attracting most attention in these days, like optoelectronic applications, fabricated into transparent conductive films, selectivity and efficiency of catalytic processes, photocatalytic applications, solar cells and so on [224, 287].

Such nanocomposites can be produced by anchoring various types of nanoparticles onto the surface of graphene sheets through both *in situ* (e.g., growing the nanoparticles on the graphene surface) and *ex situ* (e.g., attaching premade nanoparticles to the graphene surface) methods (Scheme 1.1).



Scheme 1.1: Summary of various synthetic techniques for two classes of hybrids: nanoparticles decorated on graphene or its derivatives.

1.5.1. *In situ* decoration of nanoparticles onto graphene, GO and rGO

Achieving uniform surface coverage of nanocrystals on rGO is very difficult in the *ex-situ* method of composite synthesis. In comparison, the *in-situ* technique gives uniform surface coverage by controlling the nucleation sites on rGO through surface modification. *In situ* reduction of metal salts followed by nucleation on graphene sheets is widely used to synthesize metal nanoparticle/rGO and metal nanoparticle/rGO hybrids [288, 289].

Out of several possibilities, chemical reduction method has been the most popular technique to grow metal nanostructures on graphene. The reductions of metal precursors, for example HAuCl_4 , AgNO_3 , K_2PtCl_4 , using reducing agents such as sodium hydroxide [290], sodium borohydride [98, 291], ascorbic acid [292] and ethylene glycol [293] were reported under facile and mild reaction conditions. More particularly, the negatively charged functional groups that exist on the surface of GO allow for the nucleation of positively charged metallic salts, resulting in the growth of metal nanoparticles on the GO surface. Moreover, by controlling the density of oxygen-containing groups on the GO and rGO surface, one can easily tune the density of nanoparticles formed on the resulting graphene-nanoparticle composites. The reaction mechanism is similar to conventional nanoparticle synthesis methods in solution and follows the steps of reduction, nucleation and particle growth. **Figure 1.18** shows GO-Au nanoparticles composite.

The functionalities that exist on the GO and rGO surface, such as alcohols, carbonyl groups, and acids, are responsible for the attachment of free metal ions through electrostatic interactions. Subsequently, the addition of a reducing agent promotes the reduction of the attached metal ions, thereby enabling the growth of metal nanoparticles on the GO and rGO surfaces [99].

Another method of deposition of nanoparticles on the inert surface of graphene is performed with the help of thermal evaporation [294], pulse laser deposition (PLD) [295, 296], or sputtering method [297]. By using these techniques, defect-free graphene is preserved and the high electron mobility is maintained. Therefore, these hybrids normally exhibit good performance in nanocapacitors [297] and counter electrodes [295, 296]. However, the requirements of high pressure (10^{-4} Pa) and high temperature (1260°C) associated with high cost and low synthesis efficiency have limited these techniques when applied in large-scale production.

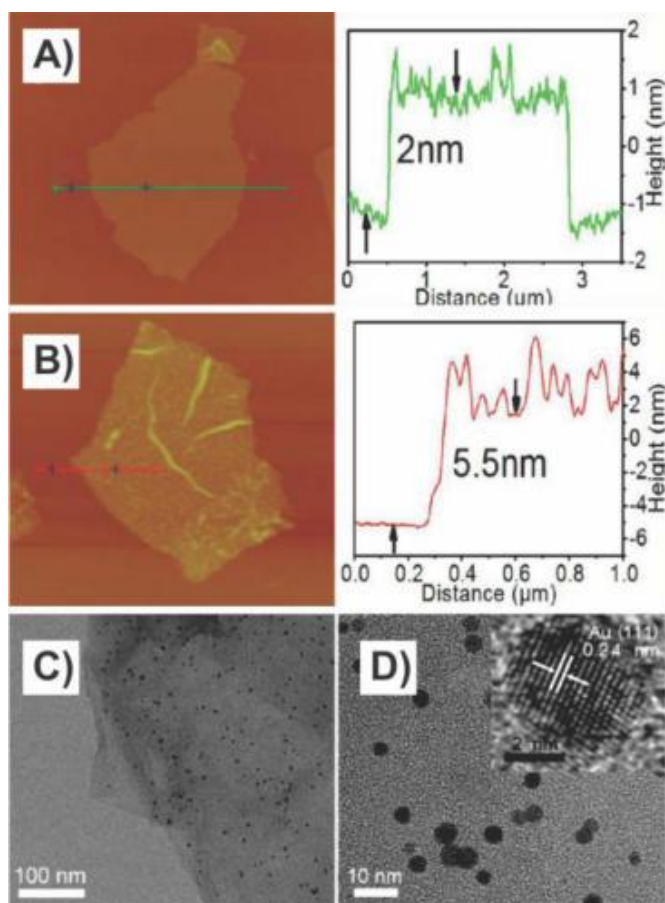


Figure 1.18: Graphene-nanoparticle composite composed of GO sheets decorated with AuNPs. (A) AFM image of a single GO sheet and (B) a GO sheet decorated with 3.5 nm AuNPs. The corresponding curves on the right side show the thicknesses of the GO sheet and the GO/AuNPs sheet (C and D). TEM images of the GO/AuNPs sheet with different magnifications. Inset of (D) shows a high-resolution TEM image of a single AuNP [291].

The hydrothermal method is another commonly used approach to synthesize nanoparticles with a high crystallinity on a single layer surface of carbon. To prepare graphene nanocomposites by hydrothermal or solvothermal processing, the precursor is mixed with graphene or GO in solution followed by hydrothermal or solvothermal deposition of the precursor on graphene in an autoclave. The process involves high temperature and high pressure, which induces the growth of nanocrystals and, at the same time, reduces GO to rGO. Graphene/metal oxide nanoparticle composites (e.g., ZnO [298], TiO₂ [299], Fe₃O₄ [300], SnO₂ [301], Co₃O₄ [302]) are the most common hybrids synthesized using the hydrothermal method. Also, graphene/metal nanoparticle composites have been synthesized (**Figure (1.19)**).

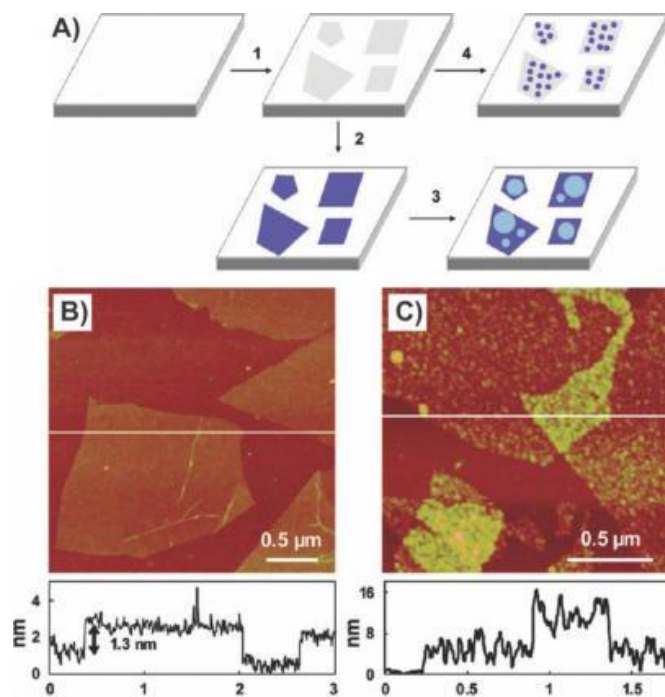


Figure 1.19: Hydrothermal method to synthesize graphene/AgNPs composites. (A) (1) GO is adsorbed on APTES-modified SiO_x substrate. (2) GO is reduced, and rGO is obtained. (3) Growth of Ag particles by heating the rGO substrate in 0.1 M AgNO_3 at 75°C for 30 min. (4) Growth of AgNPs by heating the GO substrate in 0.1 M AgNO_3 at 75°C for 30 min. (B) Tapping mode AFM topographic image and height profile of a single layer of GO adsorbed on an APTES-modified SiO_x substrate. (C) SEM image of Ag particles grown on an rGO surface [283].

Electrochemical deposition has been employed to directly deposit nanoparticles on graphene surfaces to form nanocomposites. This technique does not require a post-synthesis treatment including annealing and transferring and is very convenient to fabricate various graphene nanocomposites with metal, metal oxides, such as Pt, Au, Ag, Cu, TiO_2 , Fe_2O_3 , Mn_3O_4 and SnO_2 [283, 303-310]. This technique is illustrated in **Figure 1.20** in the case of Cu nanoparticles deposited on rGO.

As an alternative technique, the microwave method has been used as a source of energy to assist the reduction process. Metal nanoparticles (e.g. Au, Ag, Cu, Ru, and Rh) and metal oxide nanoparticles (e.g. Co_3O_4 and MnO_2) were decorated onto graphene and its derivatives in the presence or absence of reducing agents and stabilizing molecules, with the help of rapid microwave irradiation [311-314].

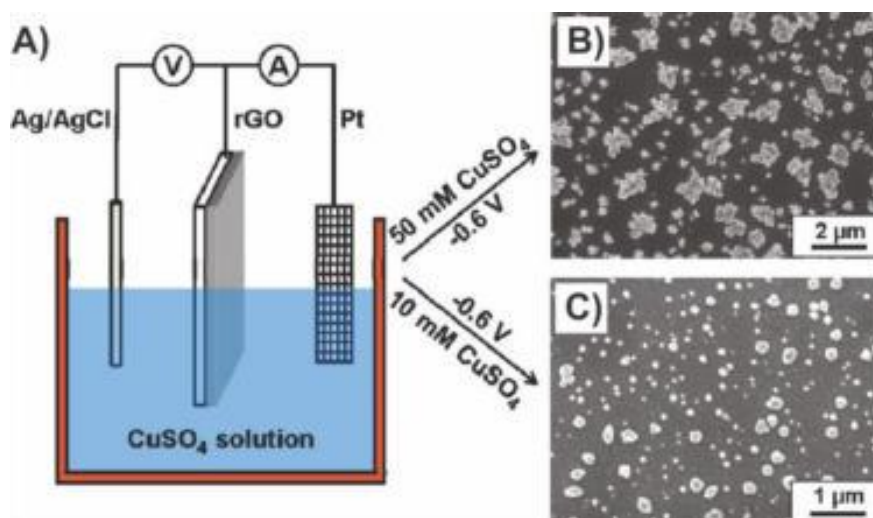


Figure 1.20: Electrochemical deposition of Cu nanoparticles on rGO. (A) Electrochemical experiments. The rGO electrode, a Pt mesh, and an Ag/AgCl (3M NaCl) electrode were used as the working, counter, and reference electrodes, respectively. (B) SEM image of Cu electrodeposited on an rGO electrode in 50 mM CuSO₄ solution at -0.6 V. (C) SEM image of Cu electrodeposited on an rGO electrode in 10 mM CuSO₄ solution at -0.6 V [315].

However, compared with the abovementioned techniques, the microwave-assisted method allows less control over the size and distribution of nanoparticles on the GO and rGO surface. The main advantage of microwave irradiation is the uniform and rapid heating of the reaction mixture, thereby reducing the barrier to reduction, nucleation, and ion incorporation [316].

1.5.2. *Ex-situ* decoration of nanoparticles on graphene, GO and rGO

Ex-situ technique is probably much more simplistic than the *in-situ* one. In general, the nanoparticles are synthesized separately and then later attached to the surface of graphene, rGO or GO sheets *via* linking agents that can utilize either covalent or noncovalent interactions, including van der Waals interactions, hydrogen bonding, π - π stacking, or electrostatic interactions. There are a number of advantages when compared to *in situ* method like good control over the size, shape, and functionality of the particles.

As we explained at the beginning of this chapter, GO and rGO have a large number of oxygen containing groups, which in turn can be used to link with other functional groups making

composites of graphene and inorganic nanoparticles through covalent interactions. A variety of nanoparticles have been attached to graphene using this method (Fe_3O_4 [317], CdSe [318], AuNPs [319]).

The π - π stacking and noncovalent bonding interactions between nanoparticles and the graphene surface are the main driving forces to anchor nanoparticles onto the 2D materials. For example, CdSe quantum dots (QDs) were encapsulated with conductive polymer polyaniline, and were decorated onto the graphene surface by π - π interactions between the polymer shell and graphene conjugated system to achieve the QD@PANI-G hybrid [320].

For π - π stacking, generally, aromatic compounds are attached to the nanoparticle surface, which enables their attachment to graphene via π - π stacking. For example, derivatives of the pyrene molecule as well as pyrene-functionalized block copolymers have provided an effective way for the noncovalent functionalization of carbon nanomaterials including graphene [321]. Specifically, pyrene groups have the ability to interact strongly with the basal plane of graphene via π - π stacking. For example, 1-pyrenebutyric acid (PBA) is one of the simplest pyrene containing molecules that are attached to a carboxyl group. Resultantly, graphene sheets functionalized with PBA become negatively charged allowing the attachment of positively charged nanoparticles *via* electrostatic interactions [322]. The use of pyrene-containing molecules has been reported for various nanoparticles. Examples include PBA, which was used to form graphene/AuNPs hybrids [323], and pyrene-grafted poly(acrylic acid), which was used to form graphene/CdSe nanoparticle hybrids [324].

GO and rGO have an inherent negative charge as a result of the ionization of the oxygen functional groups on their surface. As such, they can be decorated with positively charged inorganic nanoparticles through electrostatic interactions. For instance, graphene-metal oxide nanoparticle composites (e.g., rGO- Fe_3O_4 NPs [325] and GO- MnO_2 NPs [326]) have been formed by mixing positively charged metal oxide nanoparticles with negatively charged graphene nanosheets [325].

The GO and rGO surface was modified with “linker molecules” ending with thiol or amine groups or “adhesive polymers” to immobilize nanoparticles. Bovine serum albumin (BSA) was utilized for the fabrication of graphene-nanoparticle composites that could be composed of various types of nanoparticles (Au, Pt, Pd, Ag, and polystyrene beads) (**Figure 1.21**) [162]. In this study, the use of BSA not only effectively reduced GO to rGO, but also acted as a stabilizer to induce the attachment of nanoparticles onto the graphene surface.

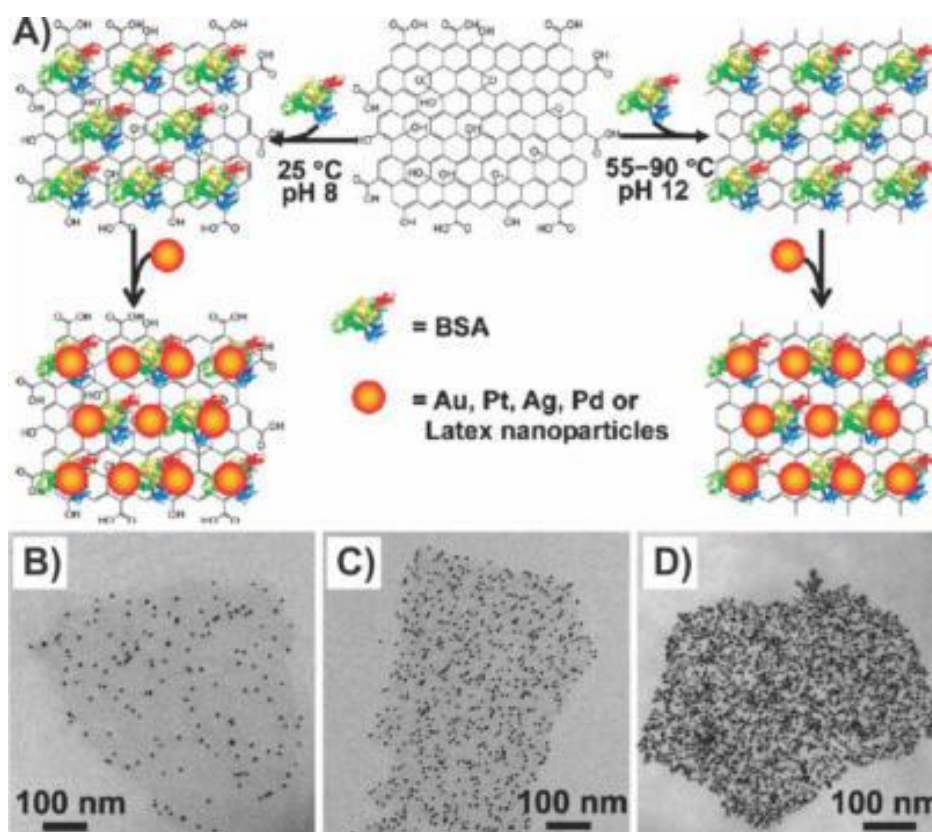


Figure 1.21: Protein-induced reduction and decoration of GO for the assembly of multiple nanoparticles. (A) General scheme depicting the BSA protein-based decoration and reduction of GO, leading to a general nanoplatform for nanoparticle assembly. (B) TEM image of AuNPs decorated BSA–GO with well-controlled densities of AuNPs. (B and C) AuNPs densities were varied by increasing the concentrations of BSA from 0.5 mg/mL (B) to 20 mg/mL (C) during the preparation of BSA–GO. NaCl was omitted for the samples in (B) and (C). (D) AuNP density was further increased (in comparison with (C)) by adding 0.1 M NaCl to the assembly system as in (C) [162].

1.6. References

- [1] Pati SK, Enoki T, Rao CNR. Graphene and Its Fascinating Attributes: World Scientific; 2011.
- [2] Dong L-X, Chen Q. Properties, synthesis, and characterization of graphene. *Front Mater Sci China*. 2010;4(1):45-51.
- [3] Vajtai R. Springer Handbook of Nanomaterials: Springer Science & Business Media; 2013.
- [4] Park S, Ruoff RS. Chemical methods for the production of graphenes. *Nature nanotechnology*. 2009;4(4):217-24.
- [5] Zhu Y, Murali S, Cai W, Li X, Suk JW, Potts JR, et al. Graphene and graphene oxide: synthesis, properties, and applications. *Advanced materials*. 2010;22(35):3906-24.
- [6] Novoselov KS, Fal'ko VI, Colombo L, Gellert PR, Schwab MG, Kim K. A roadmap for graphene. *Nature*. 2012;490(7419):192-200.
- [7] Geim AK, Novoselov KS. The rise of graphene. *Nature materials*. 2007;6(3):183-91.
- [8] Novoselov K, Geim AK, Morozov S, Jiang D, Katsnelson M, Grigorieva I, et al. Two-dimensional gas of massless Dirac fermions in graphene. *Nature*. 2005;438(7065):197-200.
- [9] Zhang Y, Tan Y-W, Stormer HL, Kim P. Experimental observation of the quantum Hall effect and Berry's phase in graphene. *Nature*. 2005;438(7065):201-4.
- [10] Novoselov KS, Jiang Z, Zhang Y, Morozov S, Stormer H, Zeitler U, et al. Room-temperature quantum Hall effect in graphene. *Science*. 2007;315(5817):1379-.
- [11] Lee C, Wei X, Kysar JW, Hone J. Measurement of the elastic properties and intrinsic strength of monolayer graphene. *science*. 2008;321(5887):385-8.
- [12] Bunch JS, Verbridge SS, Alden JS, van der Zande AM, Parpia JM, Craighead HG, et al. Impermeable atomic membranes from graphene sheets. *Nano letters*. 2008;8(8):2458-62.
- [13] Balandin AA, Ghosh S, Bao W, Calizo I, Teweldebrhan D, Miao F, et al. Superior thermal conductivity of single-layer graphene. *Nano letters*. 2008;8(3):902-7.
- [14] Hass J, De Heer W, Conrad E. The growth and morphology of epitaxial multilayer graphene. *Journal of Physics: Condensed Matter*. 2008;20(32):323202.
- [15] Stoller MD, Park S, Zhu Y, An J, Ruoff RS. Graphene-based ultracapacitors. *Nano letters*. 2008;8(10):3498-502.
- [16] Vivekchand S, Rout CS, Subrahmanyam K, Govindaraj A, Rao C. Graphene-based electrochemical supercapacitors. *Journal of Chemical Sciences*. 2008;120(1):9-13.
- [17] Yoo E, Kim J, Hosono E, Zhou H-s, Kudo T, Honma I. Large reversible Li storage of graphene nanosheet families for use in rechargeable lithium ion batteries. *Nano letters*. 2008;8(8):2277-82.
- [18] Yoo E, Okata T, Akita T, Kohyama M, Nakamura J, Honma I. Enhanced electrocatalytic activity of Pt subnanoclusters on graphene nanosheet surface. *Nano letters*. 2009;9(6):2255-9.

- [19] Wang X, Zhi L, Tsao N, Tomović Ž, Li J, Müllen K. Transparent carbon films as electrodes in organic solar cells. *Angewandte Chemie*. 2008;120(16):3032-4.
- [20] Lu CH, Yang HH, Zhu CL, Chen X, Chen GN. A graphene platform for sensing biomolecules. *Angewandte Chemie*. 2009;121(26):4879-81.
- [21] Ang PK, Chen W, Wee ATS, Loh KP. Solution-gated epitaxial graphene as pH sensor. *Journal of the American Chemical Society*. 2008;130(44):14392-3.
- [22] Arsat R, Breedon M, Shafiei M, Spizziri P, Gilje S, Kaner R, et al. Graphene-like nano-sheets for surface acoustic wave gas sensor applications. *Chemical Physics Letters*. 2009;467(4):344-7.
- [23] Kang X, Wang J, Wu H, Liu J, Aksay IA, Lin Y. A graphene-based electrochemical sensor for sensitive detection of paracetamol. *Talanta*. 2010;81(3):754-9.
- [24] Liu Z, Robinson JT, Sun X, Dai H. PEGylated nanographene oxide for delivery of water-insoluble cancer drugs. *Journal of the American Chemical Society*. 2008;130(33):10876-7.
- [25] Zhao X, Liu L, Li X, Zeng J, Jia X, Liu P. Biocompatible graphene oxide nanoparticle-based drug delivery platform for tumor microenvironment-responsive triggered release of doxorubicin. *Langmuir : the ACS journal of surfaces and colloids*. 2014;30(34):10419-29.
- [26] Schwierz F. Graphene transistors. *Nature nanotechnology*. 2010;5(7):487-96.
- [27] Pierson HO. *Handbook of carbon, graphite, diamonds and fullerenes: processing, properties and applications*: William Andrew; 2012.
- [28] Van Orden A, Saykally RJ. Small carbon clusters: spectroscopy, structure, and energetics. *Chemical reviews*. 1998;98(6):2313-58.
- [29] Shvartsburg AA, Hudgins RR, Gutierrez R, Jungnickel G, Frauenheim T, Jackson KA, et al. Ball-and-chain dimers from a hot fullerene plasma. *The Journal of Physical Chemistry A*. 1999;103(27):5275-84.
- [30] Nierengarten J-F, Bonifazi D. *Fullerenes and Other Carbon-Rich Nanostructures*: Springer; 2014.
- [31] Kroto HW, Petrukhina MA, Scott LT. *Fragments of fullerenes and carbon nanotubes: designed synthesis, unusual reactions, and coordination chemistry*: John Wiley & Sons; 2011.
- [32] Iijima S, Ichihashi T. Single-shell carbon nanotubes of 1-nm diameter. 1993.
- [33] Iijima S. Helical microtubules of graphitic carbon. *Nature*. 1991;354(6348):56-8.
- [34] Lazzeri M, Barreiro A. Carbon-Based Nanoscience. *Elements*. 2014;10(6):447-52.
- [35] Eigler S, Hirsch A. Chemistry with graphene and graphene oxide—challenges for synthetic chemists. *Angewandte Chemie International Edition*. 2014;53(30):7720-38.
- [36] Chabot V, Higgins D, Yu A, Xiao X, Chen Z, Zhang J. A review of graphene and graphene oxide sponge: material synthesis and applications to energy and the environment. *Energy & Environmental Science*. 2014;7(5):1564-96.
- [37] Allen MJ, Tung VC, Kaner RB. Honeycomb carbon: a review of graphene. *Chemical reviews*. 2009;110(1):132-45.

- [38] Yusoff ARbM. *Graphene Optoelectronics: Synthesis, Characterization, Properties, and Applications*: John Wiley & Sons; 2014.
- [39] Novoselov KS, Geim AK, Morozov S, Jiang D, Zhang Y, Dubonos S, et al. Electric field effect in atomically thin carbon films. *science*. 2004;306(5696):666-9.
- [40] Mas-Balleste R, Gomez-Navarro C, Gomez-Herrero J, Zamora F. 2D materials: to graphene and beyond. *Nanoscale*. 2011;3(1):20-30.
- [41] Yang J, Zeng X, Chen L, Yuan W. Photocatalytic water splitting to hydrogen production of reduced graphene oxide/SiC under visible light. *Applied Physics Letters*. 2013;102(8):083101.
- [42] Guo H-L, Wang X-F, Qian Q-Y, Wang F-B, Xia X-H. A green approach to the synthesis of graphene nanosheets. *ACS nano*. 2009;3(9):2653-9.
- [43] Paredes J, Villar-Rodil S, Martinez-Alonso A, Tascon J. Graphene oxide dispersions in organic solvents. *Langmuir : the ACS journal of surfaces and colloids*. 2008;24(19):10560-4.
- [44] Tour JM. Top-down versus bottom-up fabrication of graphene-based electronics. *Chemistry of Materials*. 2013;26(1):163-71.
- [45] Hernandez Y, Nicolosi V, Lotya M, Blighe FM, Sun Z, De S, et al. High-yield production of graphene by liquid-phase exfoliation of graphite. *Nature nanotechnology*. 2008;3(9):563-8.
- [46] Cui X, Zhang C, Hao R, Hou Y. Liquid-phase exfoliation, functionalization and applications of graphene. *Nanoscale*. 2011;3(5):2118-26.
- [47] Si Y, Samulski ET. Synthesis of Water Soluble Graphene. *Nano Letters*. 2008;8(6):1679-82.
- [48] Schniepp HC, Li J-L, McAllister MJ, Sai H, Herrera-Alonso M, Adamson DH, et al. Functionalized Single Graphene Sheets Derived from Splitting Graphite Oxide. *The Journal of Physical Chemistry B*. 2006;110(17):8535-9.
- [49] Williams G, Seger B, Kamat PV. TiO₂-graphene nanocomposites. UV-assisted photocatalytic reduction of graphene oxide. *ACS nano*. 2008;2(7):1487-91.
- [50] Wang Z, Zhou X, Zhang J, Boey F, Zhang H. Direct electrochemical reduction of single-layer graphene oxide and subsequent functionalization with glucose oxidase. *The Journal of Physical Chemistry C*. 2009;113(32):14071-5.
- [51] Hummers Jr WS, Offeman RE. Preparation of graphitic oxide. *Journal of the American Chemical Society*. 1958;80(6):1339-.
- [52] Pei S, Cheng H-M. The reduction of graphene oxide. *Carbon*. 2012;50(9):3210-28.
- [53] Wintterlin J, Bocquet M-L. Graphene on metal surfaces. *Surface Science*. 2009;603(10):1841-52.
- [54] Li X, Cai W, An J, Kim S, Nah J, Yang D, et al. Large-area synthesis of high-quality and uniform graphene films on copper foils. *Science*. 2009;324(5932):1312-4.
- [55] Shelton J, Patil H, Blakely J. Equilibrium segregation of carbon to a nickel (111) surface: A surface phase transition. *Surface Science*. 1974;43(2):493-520.
- [56] Eizenberg M, Blakely J. Carbon monolayer phase condensation on Ni (111). *Surface Science*. 1979;82(1):228-36.

- [57] Takagi D, Hibino H, Suzuki S, Kobayashi Y, Homma Y. Carbon nanotube growth from semiconductor nanoparticles. *Nano letters*. 2007;7(8):2272-5.
- [58] Bae S, Kim H, Lee Y, Xu X, Park J-S, Zheng Y, et al. Roll-to-roll production of 30-inch graphene films for transparent electrodes. *Nature nanotechnology*. 2010;5(8):574-8.
- [59] Liu W-W, Chai S-P, Mohamed AR, Hashim U. Synthesis and characterization of graphene and carbon nanotubes: A review on the past and recent developments. *Journal of Industrial and Engineering Chemistry*. 2014;20(4):1171-85.
- [60] Kim KS, Zhao Y, Jang H, Lee SY, Kim JM, Kim KS, et al. Large-scale pattern growth of graphene films for stretchable transparent electrodes. *Nature*. 2009;457(7230):706-10.
- [61] Reina A, Jia X, Ho J, Nezich D, Son H, Bulovic V, et al. Large area, few-layer graphene films on arbitrary substrates by chemical vapor deposition. *Nano letters*. 2008;9(1):30-5.
- [62] Yihong W, Zexiang S, Ting Y. *Two-Dimensional Carbon: Fundamental Properties, Synthesis, Characterization, and Applications*: Pan Stanford; 2014.
- [63] Li X, Cai W, Colombo L, Ruoff RS. Evolution of graphene growth on Ni and Cu by carbon isotope labeling. *Nano letters*. 2009;9(12):4268-72.
- [64] Sutter PW, Flege J-I, Sutter EA. Epitaxial graphene on ruthenium. *Nature materials*. 2008;7(5):406-11.
- [65] Coraux J, N'Diaye AT, Busse C, Michely T. Structural coherency of graphene on Ir (111). *Nano letters*. 2008;8(2):565-70.
- [66] Sutter P, Sadowski JT, Sutter E. Graphene on Pt (111): Growth and substrate interaction. *Physical Review B*. 2009;80(24):245411.
- [67] Hwang J, Shields VB, Thomas CI, Shivaraman S, Hao D, Kim M, et al. Epitaxial growth of graphitic carbon on C-face SiC and sapphire by chemical vapor deposition (CVD). *Journal of crystal growth*. 2010;312(21):3219-24.
- [68] Malesevic A, Vitchev R, Schouteden K, Volodin A, Zhang L, Van Tendeloo G, et al. Synthesis of few-layer graphene via microwave plasma-enhanced chemical vapour deposition. *Nanotechnology*. 2008;19(30):305604.
- [69] Qi J, Zheng W, Zheng X, Wang X, Tian H. Relatively low temperature synthesis of graphene by radio frequency plasma enhanced chemical vapor deposition. *Applied Surface Science*. 2011;257(15):6531-4.
- [70] Cooper DR, D'Anjou B, Ghattamaneni N, Harack B, Hilke M, Horth A, et al. Experimental review of graphene. *ISRN Condensed Matter Physics*. 2012;2012.
- [71] Sutter P. Epitaxial graphene: How silicon leaves the scene. *Nature materials*. 2009;8(3):171-2.
- [72] Emtsev KV, Bostwick A, Horn K, Jobst J, Kellogg GL, Ley L, et al. Towards wafer-size graphene layers by atmospheric pressure graphitization of silicon carbide. *Nature materials*. 2009;8(3):203-7.
- [73] Virojanadara C, Syväjarvi M, Yakimova R, Johansson L, Zakharov A, Balasubramanian T. Homogeneous large-area graphene layer growth on 6 H-SiC (0001). *Physical Review B*. 2008;78(24):245403.

- [74] Berger C, Song Z, Li T, Li X, Ogbazghi AY, Feng R, et al. Ultrathin epitaxial graphite: 2D electron gas properties and a route toward graphene-based nanoelectronics. *The Journal of Physical Chemistry B*. 2004;108(52):19912-6.
- [75] Bleikamp S, Feibelman PJ, Michely T. Two-dimensional Ir cluster lattice on a graphene moiré on Ir (111). *Physical Review Letters*. 2006;97(21):215501.
- [76] Juang Z-Y, Wu C-Y, Lo C-W, Chen W-Y, Huang C-F, Hwang J-C, et al. Synthesis of graphene on silicon carbide substrates at low temperature. *Carbon*. 2009;47(8):2026-31.
- [77] Hass J, Jeffrey C, Feng R, Li T, Li X, Song Z, et al. Highly-ordered graphene for two dimensional electronics. *arXiv preprint cond-mat/0604206*. 2006.
- [78] Hibino H, Kageshima H, Maeda F, Nagase M, Kobayashi Y, Yamaguchi H. Microscopic thickness determination of thin graphite films formed on SiC from quantized oscillation in reflectivity of low-energy electrons. *Physical Review B*. 2008;77(7):075413.
- [79] Chung D. Exfoliation of graphite. *Journal of materials science*. 1987;22(12):4190-8.
- [80] Zhao X, Zhang Q, Chen D, Lu P. Enhanced mechanical properties of graphene-based poly (vinyl alcohol) composites. *Macromolecules*. 2010;43(5):2357-63.
- [81] Hong W, Xu Y, Lu G, Li C, Shi G. Transparent graphene/PEDOT–PSS composite films as counter electrodes of dye-sensitized solar cells. *Electrochemistry Communications*. 2008;10(10):1555-8.
- [82] Zhu J. Graphene production: New solutions to a new problem. *Nature nanotechnology*. 2008;3(9):528-9.
- [83] Rafiee MA, Rafiee J, Wang Z, Song H, Yu Z-Z, Koratkar N. Enhanced mechanical properties of nanocomposites at low graphene content. *ACS nano*. 2009;3(12):3884-90.
- [84] Li X, Zhang G, Bai X, Sun X, Wang X, Wang E, et al. Highly conducting graphene sheets and Langmuir–Blodgett films. *Nature nanotechnology*. 2008;3(9):538-42.
- [85] Brodie BC. On the atomic weight of graphite. *Philosophical Transactions of the Royal Society of London*. 1859:249-59.
- [86] Jeong H, Jin M, So K, Lim S, Lee Y. Tailoring the characteristics of graphite oxides by different oxidation times. *Journal of Physics D: Applied Physics*. 2009;42(6):065418.
- [87] Dreyer DR, Park S, Bielawski CW, Ruoff RS. The chemistry of graphene oxide. *Chemical Society Reviews*. 2010;39(1):228-40.
- [88] Liao K-H, Mittal A, Bose S, Leighton C, Mkhoyan KA, Macosko CW. Aqueous only route toward graphene from graphite oxide. *ACS nano*. 2011;5(2):1253-8.
- [89] Marcano DC, Kosynkin DV, Berlin JM, Sinitskii A, Sun Z, Slesarev A, et al. Improved Synthesis of Graphene Oxide. *ACS Nano*. 2010;4(8):4806-14.
- [90] Hidalgo RS, López-Díaz D, Velázquez MM. Graphene Oxide Thin Films: Influence of Chemical Structure and Deposition Methodology. *Langmuir : the ACS journal of surfaces and colloids*. 2015;31(9):2697-705.
- [91] Chen D, Feng H, Li J. Graphene Oxide: Preparation, Functionalization, and Electrochemical Applications. *Chemical Reviews*. 2012;112(11):6027-53.

- [92] Stankovich S, Dikin DA, Piner RD, Kohlhaas KA, Kleinhammes A, Jia Y, et al. Synthesis of graphene-based nanosheets via chemical reduction of exfoliated graphite oxide. *Carbon*. 2007;45(7):1558-65.
- [93] Gao X, Jang J, Nagase S. Hydrazine and Thermal Reduction of Graphene Oxide: Reaction Mechanisms, Product Structures, and Reaction Design. *The Journal of Physical Chemistry C*. 2010;114(2):832-42.
- [94] Kim MC, Hwang GS, Ruoff RS. Epoxide reduction with hydrazine on graphene: a first principles study. *The Journal of chemical physics*. 2009;131(6):064704.
- [95] Stankovich S, Dikin DA, Dommett GH, Kohlhaas KM, Zimney EJ, Stach EA, et al. Graphene-based composite materials. *Nature*. 2006;442(7100):282-6.
- [96] Li D, Müller MB, Gilje S, Kaner RB, Wallace GG. Processable aqueous dispersions of graphene nanosheets. *Nature nanotechnology*. 2008;3(2):101-5.
- [97] Bai H, Li C, Shi G. Functional composite materials based on chemically converted graphene. *Advanced materials*. 2011;23(9):1089-115.
- [98] Muszynski R, Seger B, Kamat PV. Decorating graphene sheets with gold nanoparticles. *The Journal of Physical Chemistry C*. 2008;112(14):5263-6.
- [99] Gao W, Alemany LB, Ci L, Ajayan PM. New insights into the structure and reduction of graphite oxide. *Nature chemistry*. 2009;1(5):403-8.
- [100] Shin HJ, Kim KK, Benayad A, Yoon SM, Park HK, Jung IS, et al. Efficient reduction of graphite oxide by sodium borohydride and its effect on electrical conductance. *Advanced Functional Materials*. 2009;19(12):1987-92.
- [101] Gao J, Liu F, Liu Y, Ma N, Wang Z, Zhang X. Environment-friendly method to produce graphene that employs vitamin C and amino acid. *Chemistry of Materials*. 2010;22(7):2213-8.
- [102] Fernandez-Merino M, Guardia L, Paredes J, Villar-Rodil S, Solis-Fernandez P, Martinez-Alonso A, et al. Vitamin C is an ideal substitute for hydrazine in the reduction of graphene oxide suspensions. *The Journal of Physical Chemistry C*. 2010;114(14):6426-32.
- [103] Chen D, Li L, Guo L. An environment-friendly preparation of reduced graphene oxide nanosheets via amino acid. *Nanotechnology*. 2011;22(32):325601.
- [104] Zhu C, Guo S, Fang Y, Dong S. Reducing sugar: new functional molecules for the green synthesis of graphene nanosheets. *ACS nano*. 2010;4(4):2429-37.
- [105] Dreyer DR, Murali S, Zhu Y, Ruoff RS, Bielawski CW. Reduction of graphite oxide using alcohols. *Journal of Materials Chemistry*. 2011;21(10):3443-7.
- [106] Moon IK, Lee J, Ruoff RS, Lee H. Reduced graphene oxide by chemical graphitization. *Nature communications*. 2010;1:73.
- [107] Fan Z, Wang K, Wei T, Yan J, Song L, Shao B. An environmentally friendly and efficient route for the reduction of graphene oxide by aluminum powder. *Carbon*. 2010;48(5):1686-9.
- [108] Liu Y, Li Y, Zhong M, Yang Y, Yuefang W, Wang M. A green and ultrafast approach to the synthesis of scalable graphene nanosheets with Zn powder for electrochemical energy storage. *Journal of Materials Chemistry*. 2011;21(39):15449-55.

- [109] Wang Y, Shi Z, Yin J. Facile synthesis of soluble graphene via a green reduction of graphene oxide in tea solution and its biocomposites. *ACS applied materials & interfaces*. 2011;3(4):1127-33.
- [110] Chua CK, Pumera M. Reduction of graphene oxide with substituted borohydrides. *Journal of Materials Chemistry A*. 2013;1(5):1892-8.
- [111] Pham VH, Hur SH, Kim EJ, Kim BS, Chung JS. Highly efficient reduction of graphene oxide using ammonia borane. *Chemical communications*. 2013;49(59):6665-7.
- [112] Ambrosi A, Chua CK, Bonanni A, Pumera M. Lithium Aluminum Hydride as Reducing Agent for Chemically Reduced Graphene Oxides. *Chemistry of Materials*. 2012;24(12):2292-8.
- [113] Cui P, Lee J, Hwang E, Lee H. One-pot reduction of graphene oxide at subzero temperatures. *Chemical communications*. 2011;47(45):12370-2.
- [114] Pei S, Zhao J, Du J, Ren W, Cheng H-M. Direct reduction of graphene oxide films into highly conductive and flexible graphene films by hydrohalic acids. *Carbon*. 2010;48(15):4466-74.
- [115] Chen Y, Zhang X, Zhang D, Yu P, Ma Y. High performance supercapacitors based on reduced graphene oxide in aqueous and ionic liquid electrolytes. *Carbon*. 2011;49(2):573-80.
- [116] Chua CK, Pumera M. Renewal of sp² bonds in graphene oxides via dehydrobromination. *Journal of Materials Chemistry*. 2012;22(43):23227-31.
- [117] Chua CK, Ambrosi A, Pumera M. Graphene oxide reduction by standard industrial reducing agent: thiourea dioxide. *Journal of Materials Chemistry*. 2012;22(22):11054-61.
- [118] Wang Y, Sun L, Fugetsu B. Thiourea Dioxide as a Green Reductant for the Mass Production of Solution-Based Graphene. *Bulletin of the Chemical Society of Japan*. 2012;85(12):1339-44.
- [119] Ma Q, Song J, Jin C, Li Z, Liu J, Meng S, et al. A rapid and easy approach for the reduction of graphene oxide by formamidinesulfinic acid. *Carbon*. 2013;54:36-41.
- [120] Chua CK, Pumera M. Selective removal of hydroxyl groups from graphene oxide. *Chemistry-A European Journal*. 2013;19(6):2005-11.
- [121] Liu H, Zhang L, Guo Y, Cheng C, Yang L, Jiang L, et al. Reduction of graphene oxide to highly conductive graphene by Lawesson's reagent and its electrical applications. *Journal of Materials Chemistry C*. 2013;1(18):3104-9.
- [122] Chen W, Yan L, Bangal P. Chemical reduction of graphene oxide to graphene by sulfur-containing compounds. *The Journal of Physical Chemistry C*. 2010;114(47):19885-90.
- [123] Zhou T, Chen F, Liu K, Deng H, Zhang Q, Feng J, et al. A simple and efficient method to prepare graphene by reduction of graphite oxide with sodium hydrosulfite. *Nanotechnology*. 2011;22(4):045704.
- [124] Liu Y, Li Y, Yang Y, Wen Y, Wang M. Reduction of graphene oxide by thiourea. *Journal of nanoscience and nanotechnology*. 2011;11(11):10082-6.
- [125] Some S, Kim Y, Yoon Y, Yoo H, Lee S, Park Y, et al. High-Quality Reduced Graphene Oxide by a Dual-Function Chemical Reduction and Healing Process. *Sci Rep*. 2013;3.

- [126] Park S, An J, Jung I, Piner RD, An SJ, Li X, et al. Colloidal suspensions of highly reduced graphene oxide in a wide variety of organic solvents. *Nano letters*. 2009;9(4):1593-7.
- [127] Pham VH, Cuong TV, Nguyen-Phan T-D, Pham HD, Kim EJ, Hur SH, et al. One-step synthesis of superior dispersion of chemically converted graphene in organic solvents. *Chemical communications*. 2010;46(24):4375-7.
- [128] Zhou X, Zhang J, Wu H, Yang H, Zhang J, Guo S. Reducing graphene oxide via hydroxylamine: a simple and efficient route to graphene. *The Journal of Physical Chemistry C*. 2011;115(24):11957-61.
- [129] Mao S, Yu K, Cui S, Bo Z, Lu G, Chen J. A new reducing agent to prepare single-layer, high-quality reduced graphene oxide for device applications. *Nanoscale*. 2011;3(7):2849-53.
- [130] Liu S, Tian J, Wang L, Sun X. A method for the production of reduced graphene oxide using benzylamine as a reducing and stabilizing agent and its subsequent decoration with Ag nanoparticles for enzymeless hydrogen peroxide detection. *Carbon*. 2011;49(10):3158-64.
- [131] Chen Y, Zhang X, Yu P, Ma Y. Stable dispersions of graphene and highly conducting graphene films: a new approach to creating colloids of graphene monolayers. *Chemical communications*. 2009(30):4527-9.
- [132] Che J, Shen L, Xiao Y. A new approach to fabricate graphene nanosheets in organic medium: combination of reduction and dispersion. *Journal of Materials Chemistry*. 2010;20(9):1722-7.
- [133] Lei Z, Lu L, Zhao X. The electrocapacitive properties of graphene oxide reduced by urea. *Energy & Environmental Science*. 2012;5(4):6391-9.
- [134] Su P, Guo H-L, Tian L, Ning S-K. An efficient method of producing stable graphene suspensions with less toxicity using dimethyl ketoxime. *Carbon*. 2012;50(15):5351-8.
- [135] Shen X, Jiang L, Ji Z, Wu J, Zhou H, Zhu G. Stable aqueous dispersions of graphene prepared with hexamethylenetetramine as a reductant. *Journal of colloid and interface science*. 2011;354(2):493-7.
- [136] Zhang S, Shao Y, Liao H, Engelhard MH, Yin G, Lin Y. Polyelectrolyte-induced reduction of exfoliated graphite oxide: a facile route to synthesis of soluble graphene nanosheets. *ACS nano*. 2011;5(3):1785-91.
- [137] Wu T, Wang X, Qiu H, Gao J, Wang W, Liu Y. Graphene oxide reduced and modified by soft nanoparticles and its catalysis of the Knoevenagel condensation. *Journal of Materials Chemistry*. 2012;22(11):4772-9.
- [138] Wang G, Yang J, Park J, Gou X, Wang B, Liu H, et al. Facile synthesis and characterization of graphene nanosheets. *The Journal of Physical Chemistry C*. 2008;112(22):8192-5.
- [139] Zhang J, Yang H, Shen G, Cheng P, Zhang J, Guo S. Reduction of graphene oxide vial-ascorbic acid. *Chemical communications*. 2010;46(7):1112-4.
- [140] Kim Y-K, Kim M-H, Min D-H. Biocompatible reduced graphene oxide prepared by using dextran as a multifunctional reducing agent. *Chemical communications*. 2011;47(11):3195-7.

- [141] Li J, Xiao G, Chen C, Li R, Yan D. Superior dispersions of reduced graphene oxide synthesized by using gallic acid as a reductant and stabilizer. *Journal of Materials Chemistry A*. 2013;1(4):1481-7.
- [142] Fan Z-J, Kai W, Yan J, Wei T, Zhi L-J, Feng J, et al. Facile synthesis of graphene nanosheets via Fe reduction of exfoliated graphite oxide. *ACS nano*. 2010;5(1):191-8.
- [143] Mei X, Ouyang J. Ultrasonication-assisted ultrafast reduction of graphene oxide by zinc powder at room temperature. *Carbon*. 2011;49(15):5389-97.
- [144] Dey RS, Hajra S, Sahu RK, Raj CR, Panigrahi MK. A rapid room temperature chemical route for the synthesis of graphene: metal-mediated reduction of graphene oxide. *Chemical communications*. 2012;48(12):1787-9.
- [145] Kumar NA, Gambarelli S, Duclairoir F, Bidan G, Dubois L. Synthesis of high quality reduced graphene oxide nanosheets free of paramagnetic metallic impurities. *Journal of Materials Chemistry A*. 2013;1(8):2789-94.
- [146] Pham VH, Pham HD, Dang TT, Hur SH, Kim EJ, Kong BS, et al. Chemical reduction of an aqueous suspension of graphene oxide by nascent hydrogen. *Journal of Materials Chemistry*. 2012;22(21):10530-6.
- [147] Barman BK, Mahanandia P, Nanda KK. Instantaneous reduction of graphene oxide at room temperature. *RSC Advances*. 2013;3(31):12621-4.
- [148] Yang S, Yue W, Huang D, Chen C, Lin H, Yang X. A facile green strategy for rapid reduction of graphene oxide by metallic zinc. *RSC Advances*. 2012;2(23):8827-32.
- [149] Feng H, Cheng R, Zhao X, Duan X, Li J. A low-temperature method to produce highly reduced graphene oxide. *Nature communications*. 2013;4:1539.
- [150] Wang Q, Li M, Szunerits S, Boukherroub R. Environmentally Friendly Reduction of Graphene Oxide Using Tyrosine for Nonenzymatic Amperometric H₂O₂ Detection. *Electroanalysis*. 2014;26(1):156-63.
- [151] Bose S, Kuila T, Mishra AK, Kim NH, Lee JH. Dual role of glycine as a chemical functionalizer and a reducing agent in the preparation of graphene: an environmentally friendly method. *Journal of Materials Chemistry*. 2012;22(19):9696-703.
- [152] Ma J, Wang X, Liu Y, Wu T, Liu Y, Guo Y, et al. Reduction of graphene oxide with l-lysine to prepare reduced graphene oxide stabilized with polysaccharide polyelectrolyte. *Journal of Materials Chemistry A*. 2013;1(6):2192-201.
- [153] Pham TA, Kim JS, Kim JS, Jeong YT. One-step reduction of graphene oxide with L-glutathione. *Colloids and Surfaces A: Physicochemical and Engineering Aspects*. 2011;384(1):543-8.
- [154] Thakur S, Karak N. Green reduction of graphene oxide by aqueous phytoextracts. *Carbon*. 2012;50(14):5331-9.
- [155] Haghghi B, Tabrizi MA. Green-synthesis of reduced graphene oxide nanosheets using rose water and a survey on their characteristics and applications. *RSC Advances*. 2013;3(32):13365-71.
- [156] Salas EC, Sun Z, Luttge A, Tour JM. Reduction of graphene oxide via bacterial respiration. *ACS Nano*. 2010;4(8):4852-6.
- [157] Wang G, Qian F, Saltikov CW, Jiao Y, Li Y. Microbial reduction of graphene oxide by *Shewanella*. *Nano Research*. 2011;4(6):563-70.

- [158] Akhavan O, Ghaderi E. Escherichia coli bacteria reduce graphene oxide to bactericidal graphene in a self-limiting manner. *Carbon*. 2012;50(5):1853-60.
- [159] Gurunathan S, Han JW, Eppakayala V, Kim J-H. Microbial reduction of graphene oxide by Escherichia coli: a green chemistry approach. *Colloids and Surfaces B: Biointerfaces*. 2013;102:772-7.
- [160] Khanra P, Kuila T, Kim NH, Bae SH, Yu D-s, Lee JH. Simultaneous bio-functionalization and reduction of graphene oxide by baker's yeast. *Chemical Engineering Journal*. 2012;183:526-33.
- [161] Kuila T, Bose S, Khanra P, Mishra AK, Kim NH, Lee JH. A green approach for the reduction of graphene oxide by wild carrot root. *Carbon*. 2012;50(3):914-21.
- [162] Liu J, Fu S, Yuan B, Li Y, Deng Z. Toward a universal "adhesive nanosheet" for the assembly of multiple nanoparticles based on a protein-induced reduction/decoration of graphene oxide. *Journal of the American Chemical Society*. 2010;132(21):7279-81.
- [163] Esfandiari A, Akhavan O, Irajizad A. Melatonin as a powerful bio-antioxidant for reduction of graphene oxide. *Journal of Materials Chemistry*. 2011;21(29):10907-14.
- [164] Wu Z-S, Ren W, Gao L, Liu B, Jiang C, Cheng H-M. Synthesis of high-quality graphene with a pre-determined number of layers. *Carbon*. 2009;47(2):493-9.
- [165] McAllister MJ, Li J-L, Adamson DH, Schniepp HC, Abdala AA, Liu J, et al. Single sheet functionalized graphene by oxidation and thermal expansion of graphite. *Chemistry of Materials*. 2007;19(18):4396-404.
- [166] Wu Z-S, Ren W, Gao L, Zhao J, Chen Z, Liu B, et al. Synthesis of graphene sheets with high electrical conductivity and good thermal stability by hydrogen arc discharge exfoliation. *ACS Nano*. 2009;3(2):411-7.
- [167] Huh SH. Thermal reduction of graphene oxide: INTECH Open Access Publisher; 2011.
- [168] Kudin KN, Ozbas B, Schniepp HC, Prud'Homme RK, Aksay IA, Car R. Raman spectra of graphite oxide and functionalized graphene sheets. *Nano letters*. 2008;8(1):36-41.
- [169] Zhao J, Pei S, Ren W, Gao L, Cheng H-M. Efficient preparation of large-area graphene oxide sheets for transparent conductive films. *ACS Nano*. 2010;4(9):5245-52.
- [170] Yang D, Velamakanni A, Bozoklu G, Park S, Stoller M, Piner RD, et al. Chemical analysis of graphene oxide films after heat and chemical treatments by X-ray photoelectron and Micro-Raman spectroscopy. *Carbon*. 2009;47(1):145-52.
- [171] Wang X, Zhi L, Müllen K. Transparent, conductive graphene electrodes for dye-sensitized solar cells. *Nano letters*. 2008;8(1):323-7.
- [172] Pan D, Zhang J, Li Z, Wu M. Hydrothermal route for cutting graphene sheets into blue-luminescent graphene quantum dots. *Advanced materials*. 2010;22(6):734-8.
- [173] Akhavan O, Ghaderi E. Photocatalytic reduction of graphene oxide nanosheets on TiO₂ thin film for photoinactivation of bacteria in solar light irradiation. *The Journal of Physical Chemistry C*. 2009;113(47):20214-20.
- [174] Zhang H, Lv X, Li Y, Wang Y, Li J. P25-graphene composite as a high performance photocatalyst. *ACS nano*. 2009;4(1):380-6.
- [175] Kim SR, Parvez MK, Chhowalla M. UV-reduction of graphene oxide and its application as an interfacial layer to reduce the back-transport reactions in dye-sensitized solar cells. *Chemical Physics Letters*. 2009;483(1):124-7.

- [176] Williams G, Kamat PV. Graphene– Semiconductor Nanocomposites: Excited-State Interactions between ZnO Nanoparticles and Graphene Oxide†. *Langmuir : the ACS journal of surfaces and colloids*. 2009;25(24):13869-73.
- [177] Ng YH, Iwase A, Kudo A, Amal R. Reducing graphene oxide on a visible-light BiVO₄ photocatalyst for an enhanced photoelectrochemical water splitting. *The Journal of Physical Chemistry Letters*. 2010;1(17):2607-12.
- [178] Zhou M, Wang Y, Zhai Y, Zhai J, Ren W, Wang F, et al. Controlled Synthesis of Large-Area and Patterned Electrochemically Reduced Graphene Oxide Films. *Chemistry-A European Journal*. 2009;15(25):6116-20.
- [179] Shao Y, Wang J, Engelhard M, Wang C, Lin Y. Facile and controllable electrochemical reduction of graphene oxide and its applications. *Journal of Materials Chemistry*. 2010;20(4):743-8.
- [180] Ramesha GK, Sampath S. Electrochemical reduction of oriented graphene oxide films: an in situ Raman spectroelectrochemical study. *The Journal of Physical Chemistry C*. 2009;113(19):7985-9.
- [181] An SJ, Zhu Y, Lee SH, Stoller MD, Emilsson T, Park S, et al. Thin film fabrication and simultaneous anodic reduction of deposited graphene oxide platelets by electrophoretic deposition. *The Journal of Physical Chemistry Letters*. 2010;1(8):1259-63.
- [182] Ding Y, Zhang P, Zhuo Q, Ren H, Yang Z, Jiang Y. A green approach to the synthesis of reduced graphene oxide nanosheets under UV irradiation. *Nanotechnology*. 2011;22(21):215601.
- [183] Fellahi O, Das MR, Coffinier Y, Szunerits S, Hadjersi T, Maamache M, et al. Silicon nanowire arrays-induced graphene oxide reduction under UV irradiation. *Nanoscale*. 2011;3(11):4662-9.
- [184] Cote LJ, Cruz-Silva R, Huang J. Flash reduction and patterning of graphite oxide and its polymer composite. *Journal of the American Chemical Society*. 2009;131(31):11027-32.
- [185] Zhou Y, Bao Q, Varghese B, Tang LAL, Tan CK, Sow CH, et al. Microstructuring of graphene oxide nanosheets using direct laser writing. *Advanced materials*. 2010;22(1):67-71.
- [186] Abdelsayed V, Moussa S, Hassan HM, Aluri HS, Collinson MM, El-Shall MS. Photothermal deoxygenation of graphite oxide with laser excitation in solution and graphene-aided increase in water temperature. *The Journal of Physical Chemistry Letters*. 2010;1(19):2804-9.
- [187] Huang L, Liu Y, Ji L-C, Xie Y-Q, Wang T, Shi W-Z. Pulsed laser assisted reduction of graphene oxide. *Carbon*. 2011;49(7):2431-6.
- [188] Zhang Y, Guo L, Wei S, He Y, Xia H, Chen Q, et al. Direct imprinting of microcircuits on graphene oxides film by femtosecond laser reduction. *Nano Today*. 2010;5(1):15-20.
- [189] Sokolov DA, Shepperd KR, Orlando TM. Formation of graphene features from direct laser-induced reduction of graphite oxide. *The Journal of Physical Chemistry Letters*. 2010;1(18):2633-6.

- [190] Trusovas R, Ratautas K, Račiukaitis G, Barkauskas J, Stankevičienė I, Niaura G, et al. Reduction of graphite oxide to graphene with laser irradiation. *Carbon*. 2013;52:574-82.
- [191] Jiao Y, Qian F, Li Y, Wang G, Saltikov CW, Gralnick JA. Deciphering the electron transport pathway for graphene oxide reduction by *Shewanella oneidensis* MR-1. *Journal of bacteriology*. 2011;193(14):3662-5.
- [192] Choi W, Lahiri I, Seelaboyina R, Kang YS. Synthesis of graphene and its applications: a review. *Critical Reviews in Solid State and Materials Sciences*. 2010;35(1):52-71.
- [193] Cano-Márquez AG, Rodríguez-Macías FJ, Campos-Delgado J, Espinosa-González CG, Tristán-López F, Ramírez-González D, et al. Ex-MWNTs: graphene sheets and ribbons produced by lithium intercalation and exfoliation of carbon nanotubes. *Nano letters*. 2009;9(4):1527-33.
- [194] Jiao L, Zhang L, Wang X, Diankov G, Dai H. Narrow graphene nanoribbons from carbon nanotubes. *Nature*. 2009;458(7240):877-80.
- [195] Kosynkin DV, Higginbotham AL, Sinitskii A, Lomeda JR, Dimiev A, Price BK, et al. Longitudinal unzipping of carbon nanotubes to form graphene nanoribbons. *Nature*. 2009;458(7240):872-6.
- [196] Terrones M, Botello-Méndez AR, Campos-Delgado J, López-Urías F, Vega-Cantú YI, Rodríguez-Macías FJ, et al. Graphene and graphite nanoribbons: Morphology, properties, synthesis, defects and applications. *Nano Today*. 2010;5(4):351-72.
- [197] Chen X-m, Wu G-h, Jiang Y-q, Wang Y-r, Chen X. Graphene and graphene-based nanomaterials: the promising materials for bright future of electroanalytical chemistry. *Analyst*. 2011;136(22):4631-40.
- [198] Novoselov KS, Jiang D, Schedin F, Booth TJ, Khotkevich VV, Morozov SV, et al. Two-dimensional atomic crystals. *Proceedings of the National Academy of Sciences of the United States of America*. 2005;102(30):10451-3.
- [199] Katsnelson MI. Graphene: carbon in two dimensions. *Materials today*. 2007;10(1):20-7.
- [200] Du X, Skachko I, Barker A, Andrei EY. Approaching ballistic transport in suspended graphene. *Nature nanotechnology*. 2008;3(8):491-5.
- [201] Huang X, Qi X, Boey F, Zhang H. Graphene-based composites. *Chemical Society Reviews*. 2012;41(2):666-86.
- [202] Nair R, Blake P, Grigorenko A, Novoselov K, Booth T, Stauber T, et al. Fine structure constant defines visual transparency of graphene. *Science*. 2008;320(5881):1308-.
- [203] Wang F, Zhang Y, Tian C, Girit C, Zettl A, Crommie M, et al. Gate-variable optical transitions in graphene. *Science*. 2008;320(5873):206-9.
- [204] Elias D, Nair R, Mohiuddin T, Morozov S, Blake P, Halsall M, et al. Control of graphene's properties by reversible hydrogenation: evidence for graphane. *Science*. 2009;323(5914):610-3.
- [205] Gokus T, Nair R, Bonetti A, Bohmler M, Lombardo A, Novoselov K, et al. Making graphene luminescent by oxygen plasma treatment. *ACS nano*. 2009;3(12):3963-8.
- [206] Luo Z, Vora PM, Mele EJ, Johnson AC, Kikkawa JM. Photoluminescence and band gap modulation in graphene oxide. *Applied physics letters*. 2009;94(11):111909.

- [207] Sheats JR, Antoniadis H, Hueschen M, Leonard W, Miller J, Moon R, et al. Organic electroluminescent devices. *Science*. 1996;273(5277):884-8.
- [208] Rothberg LJ, Lovinger AJ. Status of and prospects for organic electroluminescence. *Journal of materials research*. 1996;11(12):3174-87.
- [209] Eda G, Lin YY, Mattevi C, Yamaguchi H, Chen HA, Chen I, et al. Blue photoluminescence from chemically derived graphene oxide. *Advanced materials*. 2010;22(4):505-9.
- [210] Xia F, Mueller T, Golizadeh-Mojarad R, Freitag M, Lin Y-m, Tsang J, et al. Photocurrent imaging and efficient photon detection in a graphene transistor. *Nano letters*. 2009;9(3):1039-44.
- [211] Eda G, Fanchini G, Chhowalla M. Large-area ultrathin films of reduced graphene oxide as a transparent and flexible electronic material. *Nature nanotechnology*. 2008;3(5):270-4.
- [212] Bonaccorso F, Sun Z, Hasan T, Ferrari A. Graphene photonics and optoelectronics. *Nature photonics*. 2010;4(9):611-22.
- [213] Liu L, Zhang J, Zhao J, Liu F. Mechanical properties of graphene oxides. *Nanoscale*. 2012;4(19):5910-6.
- [214] Liu F, Ming P, Li J. Ab initio calculation of ideal strength and phonon instability of graphene under tension. *Physical Review B*. 2007;76(6):064120.
- [215] Ovid'ko I. Mechanical properties of graphene. *Reviews on Advanced Materials Science*. 2013;34:1-11.
- [216] Zhang P, Ma L, Fan F, Zeng Z, Peng C, Loya PE, et al. Fracture toughness of graphene. *Nature communications*. 2014;5.
- [217] Singh V, Joung D, Zhai L, Das S, Khondaker SI, Seal S. Graphene based materials: Past, present and future. *Progress in Materials Science*. 2011;56(8):1178-271.
- [218] Yu C, Shi L, Yao Z, Li D, Majumdar A. Thermal conductance and thermopower of an individual single-wall carbon nanotube. *Nano letters*. 2005;5(9):1842-6.
- [219] Kim P, Shi L, Majumdar A, McEuen P. Thermal transport measurements of individual multiwalled nanotubes. *Physical review letters*. 2001;87(21):215502.
- [220] Pop E, Mann D, Wang Q, Goodson K, Dai H. Thermal conductance of an individual single-wall carbon nanotube above room temperature. *Nano letters*. 2006;6(1):96-100.
- [221] Seol JH, Jo I, Moore AL, Lindsay L, Aitken ZH, Pettes MT, et al. Two-dimensional phonon transport in supported graphene. *Science*. 2010;328(5975):213-6.
- [222] Liao AD, Wu JZ, Wang X, Tahy K, Jena D, Dai H, et al. Thermally limited current carrying ability of graphene nanoribbons. *Physical review letters*. 2011;106(25):256801.
- [223] Bae M-H, Islam S, Dorgan VE, Pop E. Scaling of high-field transport and localized heating in graphene transistors. *ACS nano*. 2011;5(10):7936-44.
- [224] Ojha K, Anjaneyulu O, Ganguli AK. Graphene-based hybrid materials: synthetic approaches and properties. *CURRENT SCIENCE*. 2014;107(3):397.

- [225] Wang HX, Wang Q, Zhou KG, Zhang HL. Graphene in Light: Design, Synthesis and Applications of Photo-active Graphene and Graphene-Like Materials. *Small*. 2013;9(8):1266-83.
- [226] Tu W, Zhou Y, Zou Z. Versatile Graphene-Promoting Photocatalytic Performance of Semiconductors: Basic Principles, Synthesis, Solar Energy Conversion, and Environmental Applications. *Advanced Functional Materials*. 2013;23(40):4996-5008.
- [227] Zhang X, Chen YL, Liu R-S, Tsai DP. Plasmonic photocatalysis. *Reports on Progress in Physics*. 2013;76(4):046401.
- [228] Yang N, Liu Y, Wen H, Tang Z, Zhao H, Li Y, et al. Photocatalytic properties of graphdiyne and graphene modified TiO₂: from theory to experiment. *ACS nano*. 2013;7(2):1504-12.
- [229] Chen F-J, Cao Y-L, Jia D-Z. A room-temperature solid-state route for the synthesis of graphene oxide–metal sulfide composites with excellent photocatalytic activity. *CrystEngComm*. 2013;15(23):4747-54.
- [230] Tu X, Luo S, Chen G, Li J. One-Pot Synthesis, Characterization, and Enhanced Photocatalytic Activity of a BiOBr–Graphene Composite. *Chemistry-A European Journal*. 2012;18(45):14359-66.
- [231] Ramesha G, Kumara AV, Muralidhara H, Sampath S. Graphene and graphene oxide as effective adsorbents toward anionic and cationic dyes. *Journal of colloid and interface science*. 2011;361(1):270-7.
- [232] Enoki T, Kobayashi Y. Magnetic nanographite: an approach to molecular magnetism. *J Mater Chem*. 2005;15(37):3999-4002.
- [233] Červenka J, Katsnelson M, Flipse C. Room-temperature ferromagnetism in graphite driven by two-dimensional networks of point defects. *Nature Physics*. 2009;5(11):840-4.
- [234] Esquinazi P, Setzer A, Höhne R, Semmelhack C, Kopelevich Y, Spemann D, et al. Ferromagnetism in oriented graphite samples. *Physical Review B*. 2002;66(2):024429.
- [235] Barzola-Quiquia J, Esquinazi P, Rothermel M, Spemann D, Butz T, Garcia N. Experimental evidence for two-dimensional magnetic order in proton bombarded graphite. *Physical Review B*. 2007;76(16):161403.
- [236] Friedman AL, Chun H, Jung YJ, Heiman D, Glaser ER, Menon L. Possible room-temperature ferromagnetism in hydrogenated carbon nanotubes. *Physical Review B*. 2010;81(11):115461.
- [237] Matte HR, Subrahmanyam K, Rao C. Novel magnetic properties of graphene: presence of both ferromagnetic and antiferromagnetic features and other aspects. *The Journal of Physical Chemistry C*. 2009;113(23):9982-5.
- [238] Wang Y, Huang Y, Song Y, Zhang X, Ma Y, Liang J, et al. Room-temperature ferromagnetism of graphene. *Nano Letters*. 2008;9(1):220-4.
- [239] Jain SL, Panwar V, Al-Nafiey A, Addad A, Sieber B, Roussel P, et al. Magnetic Co₃O₄/reduced graphene oxide nanocomposite as superior heterogeneous catalyst for one-pot oxidative esterification of aldehydes to methyl esters. *RSC Advances*. 2015.

- [240] Xiong R, Wang Y, Zhang X, Lu C, Lan L. In situ growth of gold nanoparticles on magnetic $\gamma\text{-Fe}_2\text{O}_3$ @ cellulose nanocomposites: a highly active and recyclable catalyst for reduction of 4-nitrophenol. *RSC Advances*. 2014;4(13):6454-62.
- [241] Williams DB, Carter CB. *The transmission electron microscope*: Springer; 1996.
- [242] Newbury DE, Joy DC, Echlin P, Fiori CE, Goldstein JI. *Scanning electron microscopy and X-ray microanalysis*: Springer; 2003.
- [243] Xu K, Cao P, Heath JR. Graphene visualizes the first water adlayers on mica at ambient conditions. *Science*. 2010;329(5996):1188-91.
- [244] Wu Z-S, Ren W, Wen L, Gao L, Zhao J, Chen Z, et al. Graphene anchored with Co_3O_4 nanoparticles as anode of lithium ion batteries with enhanced reversible capacity and cyclic performance. *ACS nano*. 2010;4(6):3187-94.
- [245] Tung VC, Allen MJ, Yang Y, Kaner RB. High-throughput solution processing of large-scale graphene. *Nature nanotechnology*. 2009;4(1):25-9.
- [246] Skákalová V, Kaiser AB. *Graphene: Properties, Preparation, Characterisation and Devices*: Elsevier; 2014.
- [247] Paredes JI, Villar-Rodil S, Solís-Fernández P, Martínez-Alonso A, Tascón JMD. Atomic Force and Scanning Tunneling Microscopy Imaging of Graphene Nanosheets Derived from Graphite Oxide. *Langmuir : the ACS journal of surfaces and colloids*. 2009;25(10):5957-68.
- [248] Ferrari A, Meyer J, Scardaci V, Casiraghi C, Lazzeri M, Mauri F, et al. Raman spectrum of graphene and graphene layers. *Physical review letters*. 2006;97(18):187401.
- [249] Das A, Pisana S, Chakraborty B, Piscanec S, Saha S, Waghmare U, et al. Monitoring dopants by Raman scattering in an electrochemically top-gated graphene transistor. *Nature nanotechnology*. 2008;3(4):210-5.
- [250] Mohiuddin T, Lombardo A, Nair R, Bonetti A, Savini G, Jalil R, et al. Uniaxial strain in graphene by Raman spectroscopy: G peak splitting, Grüneisen parameters, and sample orientation. *Physical Review B*. 2009;79(20):205433.
- [251] Beams R, Cançado LG, Novotny L. Raman characterization of defects and dopants in graphene. *Journal of Physics: Condensed Matter*. 2015;27(8):083002.
- [252] Childres I, Jauregui LA, Park W, Cao H, Chen YP. *Raman spectroscopy of graphene and related materials. Developments in photon and materials research*. 2013.
- [253] Ni Z, Wang Y, Yu T, Shen Z. Raman spectroscopy and imaging of graphene. *Nano Research*. 2008;1(4):273-91.
- [254] Wang Yy, Ni Zh, Yu T, Shen ZX, Wang Hm, Wu Yh, et al. Raman Studies of Monolayer Graphene: The Substrate Effect. *The Journal of Physical Chemistry C*. 2008;112(29):10637-40.
- [255] Ferrari AC. Raman spectroscopy of graphene and graphite: disorder, electron-phonon coupling, doping and nonadiabatic effects. *Solid state communications*. 2007;143(1):47-57.
- [256] Tuinstra F, Koenig JL. Raman spectrum of graphite. *The Journal of Chemical Physics*. 1970;53(3):1126-30.

- [257] Lucchese MM, Stavale F, Ferreira EM, Vilani C, Moutinho M, Capaz RB, et al. Quantifying ion-induced defects and Raman relaxation length in graphene. *Carbon*. 2010;48(5):1592-7.
- [258] Campos-Delgado J, Cançado LG, Achete CA, Jorio A, Raskin J-P. Raman scattering study of the phonon dispersion in twisted bilayer graphene. *Nano Research*. 2013;6(4):269-74.
- [259] Ferreira EM, Moutinho MV, Stavale F, Lucchese M, Capaz RB, Achete C, et al. Evolution of the Raman spectra from single-, few-, and many-layer graphene with increasing disorder. *Physical Review B*. 2010;82(12):125429.
- [260] Waltman R, Pacansky J, Bates Jr C. X-ray photoelectron spectroscopic studies on organic photoconductors: evaluation of atomic charges on chlorodiane blue and p-(diethylamino) benzaldehyde diphenylhydrazone. *Chemistry of materials*. 1993;5(12):1799-804.
- [261] Becerril HA, Mao J, Liu Z, Stoltenberg RM, Bao Z, Chen Y. Evaluation of solution-processed reduced graphene oxide films as transparent conductors. *ACS nano*. 2008;2(3):463-70.
- [262] Song J, Wang X, Chang C-T. Preparation and Characterization of Graphene Oxide. *Journal of Nanomaterials*. 2014;2014:1-6.
- [263] Mattevi C, Eda G, Agnoli S, Miller S, Mkhoyan KA, Celik O, et al. Evolution of electrical, chemical, and structural properties of transparent and conducting chemically derived graphene thin films. *Advanced Functional Materials*. 2009;19(16):2577-83.
- [264] Shukla S, Saxena S. Spectroscopic investigation of confinement effects on optical properties of graphene oxide. *Applied Physics Letters*. 2011;98(7):073104.
- [265] Kuila T, Bose S, Mishra AK, Khanra P, Kim NH, Lee JH. Chemical functionalization of graphene and its applications. *Progress in Materials Science*. 2012;57(7):1061-105.
- [266] Sun Z, Yan Z, Yao J, Beitler E, Zhu Y, Tour JM. Growth of graphene from solid carbon sources. *Nature*. 2010;468(7323):549-52.
- [267] Gao W, Alemany LB, Ci L, Ajayan PM. New insights into the structure and reduction of graphite oxide. *Nature chemistry*. 2009;1(5):403-8.
- [268] Ding J, Yan W, Xie W, Sun S, Bao J, Gao C. Highly efficient photocatalytic hydrogen evolution of graphene/YInO₃ nanocomposites under visible light irradiation. *Nanoscale*. 2014;6(4):2299-306.
- [269] Chen H, Müller MB, Gilmore KJ, Wallace GG, Li D. Mechanically strong, electrically conductive, and biocompatible graphene paper. *Advanced materials*. 2008;20(18):3557-61.
- [270] Zhang H-B, Zheng W-G, Yan Q, Yang Y, Wang J-W, Lu Z-H, et al. Electrically conductive polyethylene terephthalate/graphene nanocomposites prepared by melt compounding. *Polymer*. 2010;51(5):1191-6.
- [271] Krishnamoorthy K, Veerapandian M, Mohan R, Kim S-J. Investigation of Raman and photoluminescence studies of reduced graphene oxide sheets. *Applied Physics A*. 2012;106(3):501-6.
- [272] Durmus Z, Durmus A, Kavas H. Synthesis and characterization of structural and magnetic properties of graphene/hard ferrite nanocomposites as microwave-absorbing material. *Journal of Materials Science*. 2015;50(3):1201-13.

- [273] Choi E-Y, Han TH, Hong J, Kim JE, Lee SH, Kim HW, et al. Noncovalent functionalization of graphene with end-functional polymers. *Journal of Materials Chemistry*. 2010;20(10):1907-12.
- [274] Singh SC, Zeng H, Guo C, Cai W. *Nanomaterials: processing and characterization with lasers*: John Wiley & Sons; 2012.
- [275] Yang T, Liu L-h, Liu J-w, Chen M-L, Wang J-H. Cyanobacterium metallothionein decorated graphene oxide nanosheets for highly selective adsorption of ultra-trace cadmium. *Journal of Materials Chemistry*. 2012;22(41):21909-16.
- [276] Peng S, Fan X, Li S, Zhang J. GREEN SYNTHESIS AND CHARACTERIZATION OF GRAPHITE OXIDE BY ORTHOGONAL EXPERIMENT. *Journal of the Chilean Chemical Society*. 2013;58(4):2213-7.
- [277] Karimzadeh R, Arandian A. Unusual nonlinear absorption response of graphene oxide in the presence of a reduction process. *Laser Physics Letters*. 2015;12(2):025401.
- [278] Peng X, Li Y, Zhang G, Zhang F, Fan X. Functionalization of graphene with nitrile groups by cycloaddition of tetracyanoethylene oxide. *Journal of Nanomaterials*. 2013;2013:11.
- [279] Buchsteiner A, Lerf A, Pieper J. Water dynamics in graphite oxide investigated with neutron scattering. *The Journal of Physical Chemistry B*. 2006;110(45):22328-38.
- [280] Jasuja K, Berry V. Implantation and growth of dendritic gold nanostructures on graphene derivatives: electrical property tailoring and Raman enhancement. *Acs Nano*. 2009;3(8):2358-66.
- [281] Xu C, Wang X, Zhu J. Graphene– metal particle nanocomposites. *The Journal of Physical Chemistry C*. 2008;112(50):19841-5.
- [282] Ji Z, Shen X, Zhu G, Zhou H, Yuan A. Reduced graphene oxide/nickel nanocomposites: facile synthesis, magnetic and catalytic properties. *Journal of Materials Chemistry*. 2012;22(8):3471.
- [283] Zhou X, Huang X, Qi X, Wu S, Xue C, Boey FY, et al. In situ synthesis of metal nanoparticles on single-layer graphene oxide and reduced graphene oxide surfaces. *The Journal of Physical Chemistry C*. 2009;113(25):10842-6.
- [284] Huang X, Zhou X, Wu S, Wei Y, Qi X, Zhang J, et al. Reduced Graphene Oxide-Templated Photochemical Synthesis and in situ Assembly of Au Nanodots to Orderly Patterned Au Nanodot Chains. *Small*. 2010;6(4):513-6.
- [285] Hong T-K, Lee DW, Choi HJ, Shin HS, Kim B-S. Transparent, flexible conducting hybrid multilayer thin films of multiwalled carbon nanotubes with graphene nanosheets. *Acs Nano*. 2010;4(7):3861-8.
- [286] Tung VC, Chen L-M, Allen MJ, Wassei JK, Nelson K, Kaner RB, et al. Low-temperature solution processing of graphene– carbon nanotube hybrid materials for high-performance transparent conductors. *Nano Letters*. 2009;9(5):1949-55.
- [287] Zahed B, Hosseini-Monfared H. A comparative study of silver-graphene oxide nanocomposites as a recyclable catalyst for the aerobic oxidation of benzyl alcohol: Support effect. *Applied Surface Science*. 2015;328:536-47.
- [288] Yin PT, Shah S, Chhowalla M, Lee K-B. Design, Synthesis, and Characterization of Graphene–Nanoparticle Hybrid Materials for Bioapplications. *Chemical reviews*. 2015;115(7):2483-531.

- [289] Nguyen KT, Zhao Y. Integrated graphene/nanoparticle hybrids for biological and electronic applications. *Nanoscale*. 2014;6(12):6245-66.
- [290] Qin X, Li Q, Asiri AM, Al-Youbi AO, Sun X. One-pot synthesis of Au nanoparticles/reduced graphene oxide nanocomposites and their application for electrochemical H₂O₂, glucose, and hydrazine sensing. *Gold Bulletin*. 2013;47(1-2):3-8.
- [291] Zhuo Q, Ma Y, Gao J, Zhang P, Xia Y, Tian Y, et al. Facile Synthesis of Graphene/Metal Nanoparticle Composites via Self-Catalysis Reduction at Room Temperature. *Inorganic chemistry*. 2013;52(6):3141-7.
- [292] Kim Y-G, Akbar ZA, Kim DY, Jo SM, Jang S-Y. Aqueous Dispersible Graphene/Pt Nanohybrids by Green Chemistry: Application as Cathodes for Dye-Sensitized Solar Cells. *ACS applied materials & interfaces*. 2013;5(6):2053-61.
- [293] Fu X, Bei F, Wang X, O'Brien S, Lombardi JR. Excitation profile of surface-enhanced Raman scattering in graphene-metal nanoparticle based derivatives. *Nanoscale*. 2010;2(8):1461-6.
- [294] Zhou H, Qiu C, Liu Z, Yang H, Hu L, Liu J, et al. Thickness-Dependent Morphologies of Gold on N-Layer Graphenes. *Journal of the American Chemical Society*. 2010;132(3):944-6.
- [295] Bajpai R, Roy S, Kumar P, Bajpai P, Kulshrestha N, Rafiee J, et al. Graphene Supported Platinum Nanoparticle Counter-Electrode for Enhanced Performance of Dye-Sensitized Solar Cells. *ACS applied materials & interfaces*. 2011;3(10):3884-9.
- [296] Bajpai R, Roy S, kulshrestha N, Rafiee J, Koratkar N, Misra DS. Graphene supported nickel nanoparticle as a viable replacement for platinum in dye sensitized solar cells. *Nanoscale*. 2012;4(3):926-30.
- [297] Son JY, Shin Y-H, Kim H, Jang HM. NiO Resistive Random Access Memory Nanocapacitor Array on Graphene. *ACS Nano*. 2010;4(5):2655-8.
- [298] Zou W, Zhu J, Sun Y, Wang X. Depositing ZnO nanoparticles onto graphene in a polyol system. *Materials Chemistry and Physics*. 2011;125(3):617-20.
- [299] Perera SD, Mariano RG, Vu K, Nour N, Seitz O, Chabal Y, et al. Hydrothermal synthesis of graphene-TiO₂ nanotube composites with enhanced photocatalytic activity. *Acs Catalysis*. 2012;2(6):949-56.
- [300] Castrillon M, Mayoral A, Urtizbera A, Marquina C, Irusta S, Meier J, et al. Synthesis and magnetic behavior of ultra-small bimetallic FeCo/graphite nanoparticles. *Nanotechnology*. 2013;24(50):505702.
- [301] Park S-K, Yu S-H, Pinna N, Woo S, Jang B, Chung Y-H, et al. A facile hydrazine-assisted hydrothermal method for the deposition of monodisperse SnO₂ nanoparticles onto graphene for lithium ion batteries. *Journal of Materials Chemistry*. 2012;22(6):2520-5.
- [302] Wang B, Wang Y, Park J, Ahn H, Wang G. In situ synthesis of Co₃O₄/graphene nanocomposite material for lithium-ion batteries and supercapacitors with high capacity and supercapacitance. *Journal of Alloys and Compounds*. 2011;509(29):7778-83.
- [303] Li Y, Tang L, Li J. Preparation and electrochemical performance for methanol oxidation of Pt/graphene nanocomposites. *Electrochemistry Communications*. 2009;11(4):846-9.

- [304] Guo S, Dong S, Wang E. Three-Dimensional Pt-on-Pd Bimetallic Nanodendrites Supported on Graphene Nanosheet: Facile Synthesis and Used as an Advanced Nanoelectrocatalyst for Methanol Oxidation. *ACS Nano*. 2010;4(1):547-55.
- [305] Xu C, Wang X. Fabrication of Flexible Metal-Nanoparticle Films Using Graphene Oxide Sheets as Substrates. *Small*. 2009;5(19):2212-7.
- [306] Shen J, Shi M, Li N, Yan B, Ma H, Hu Y, et al. Facile synthesis and application of Ag-chemically converted graphene nanocomposite. *Nano research*. 2010;3(5):339-49.
- [307] Chen Q, Zhang L, Chen G. Facile preparation of graphene-copper nanoparticle composite by in situ chemical reduction for electrochemical sensing of carbohydrates. *Analytical chemistry*. 2012;84(1):171-8.
- [308] Tang Y-B, Lee C-S, Xu J, Liu Z-T, Chen Z-H, He Z, et al. Incorporation of Graphenes in Nanostructured TiO₂ Films via Molecular Grafting for Dye-Sensitized Solar Cell Application. *ACS Nano*. 2010;4(6):3482-8.
- [309] Mao S, Wen Z, Kim H, Lu G, Hurley P, Chen J. A General Approach to One-Pot Fabrication of Crumpled Graphene-Based Nanohybrids for Energy Applications. *ACS Nano*. 2012;6(8):7505-13.
- [310] Zou R, Zhang Z, Yu L, Tian Q, Chen Z, Hu J. A general approach for the growth of metal oxide nanorod arrays on graphene sheets and their applications. *Chemistry-A European Journal*. 2011;17(49):13912-7.
- [311] Marquardt D, Vollmer C, Thomann R, Steurer P, Mülhaupt R, Redel E, et al. The use of microwave irradiation for the easy synthesis of graphene-supported transition metal nanoparticles in ionic liquids. *Carbon*. 2011;49(4):1326-32.
- [312] Yan J, Wei T, Qiao W, Shao B, Zhao Q, Zhang L, et al. Rapid microwave-assisted synthesis of graphene nanosheet/Co₃O₄ composite for supercapacitors. *Electrochimica Acta*. 2010;55(23):6973-8.
- [313] Yan J, Fan Z, Wei T, Qian W, Zhang M, Wei F. Fast and reversible surface redox reaction of graphene-MnO₂ composites as supercapacitor electrodes. *Carbon*. 2010;48(13):3825-33.
- [314] Jasuja K, Linn J, Melton S, Berry V. Microwave-Reduced Uncapped Metal Nanoparticles on Graphene: Tuning Catalytic, Electrical, and Raman Properties. *The Journal of Physical Chemistry Letters*. 2010;1(12):1853-60.
- [315] Wu S, Yin Z, He Q, Lu G, Yan Q, Zhang H. Nucleation mechanism of electrochemical deposition of Cu on reduced graphene oxide electrodes. *The Journal of Physical Chemistry C*. 2011;115(32):15973-9.
- [316] Tsuji M, Hashimoto M, Nishizawa Y, Kubokawa M, Tsuji T. Microwave-Assisted Synthesis of Metallic Nanostructures in Solution. *Chemistry-A European Journal*. 2005;11(2):440-52.
- [317] He F, Fan J, Ma D, Zhang L, Leung C, Chan HL. The attachment of Fe₃O₄ nanoparticles to graphene oxide by covalent bonding. *Carbon*. 2010;48(11):3139-44.
- [318] Pham TA, Choi BC, Jeong YT. Facile covalent immobilization of cadmium sulfide quantum dots on graphene oxide nanosheets: preparation, characterization, and optical properties. *Nanotechnology*. 2010;21(46):465603.

- [319] Ismaili H, Geng D, Sun AX, Kantzas TT, Workentin MS. Light-activated covalent formation of gold nanoparticle–graphene and gold nanoparticle–glass composites. *Langmuir : the ACS journal of surfaces and colloids*. 2011;27(21):13261-8.
- [320] Nguyen KT, Li D, Borah P, Ma X, Liu Z, Zhu L, et al. Photoinduced Charge Transfer within Polyaniline-Encapsulated Quantum Dots Decorated on Graphene. *ACS applied materials & interfaces*. 2013;5(16):8105-10.
- [321] Björk J, Hanke F, Palma C-A, Samori P, Cecchini M, Persson M. Adsorption of aromatic and anti-aromatic systems on graphene through π - π stacking. *The Journal of Physical Chemistry Letters*. 2010;1(23):3407-12.
- [322] Wang W, Guo S, Penchev M, Zhong J, Lin J, Bao D, et al. Hybrid low resistance ultracapacitor electrodes based on 1-pyrenebutyric acid functionalized centimeter-scale graphene sheets. *Journal of nanoscience and nanotechnology*. 2012;12(9):6913-20.
- [323] Hong W, Bai H, Xu Y, Yao Z, Gu Z, Shi G. Preparation of gold nanoparticle/graphene composites with controlled weight contents and their application in biosensors. *The Journal of Physical Chemistry C*. 2010;114(4):1822-6.
- [324] Zhang X, Li S, Jin X, Zhang S. A new photoelectrochemical aptasensor for the detection of thrombin based on functionalized graphene and CdSe nanoparticles multilayers. *Chemical communications*. 2011;47(17):4929-31.
- [325] Zhu G, Liu Y, Xu Z, Jiang T, Zhang C, Li X, et al. Flexible Magnetic Nanoparticles–Reduced Graphene Oxide Composite Membranes Formed by Self-Assembly in Solution. *Chemphyschem : a European journal of chemical physics and physical chemistry*. 2010;11(11):2432-7.
- [326] Zhai D, Li B, Du H, Gao G, Gan L, He Y, et al. The preparation of graphene decorated with manganese dioxide nanoparticles by electrostatic adsorption for use in supercapacitors. *Carbon*. 2012;50(14):5034-43.

CHAPTER 2

Reduced graphene oxide decorated with silver nanoparticles

2.1 Introduction

There are many methods to synthesize graphene and the most common method adapted for large-scale production of graphene oxide (GO) and reduced graphene oxide (rGO) is based on “top-down” approaches using physical and chemical exfoliation of graphite, pioneered by Hummers et al. using strong acids and oxidants [1, 2]. In the reduction of GO using chemical methods, one of the most commonly used reducing agent is hydrazine monohydrate [3]. Due to the toxicity and explosive properties of some of the chemical reductants explored earlier, many environmentally friendly and highly-efficient reductants have been developed and used for the reduction of GO [4], including vitamin C [5], amino acid [6], reducing sugar [7], tea [8] and so on.

In this thesis, we have used an easy and environmentally friendly L-Arginine (Arg) ($C_6H_{14}N_4O_2$) as an efficient chemical agent for GO reduction. L-Arginine is an amino acid that is obtained from the diet and plays a role in protein synthesis as a substrate for the urea cycle and nitric oxide production and as a secretagogue for growth hormone, prolactin, and insulin [9]. The L-Arginine chain consists of a 3-carbon aliphatic straight chain, the distal end of which is capped by a complex guanidinium group (**Figure 2.1**). The guanidinium group is positively charged in neutral, acidic, and even most basic environments, and thus imparts basic chemical properties to arginine. Because of the conjugation between the double bond and the nitrogen lone pairs, the positive charge is delocalized, enabling the formation of multiple bonds [10].

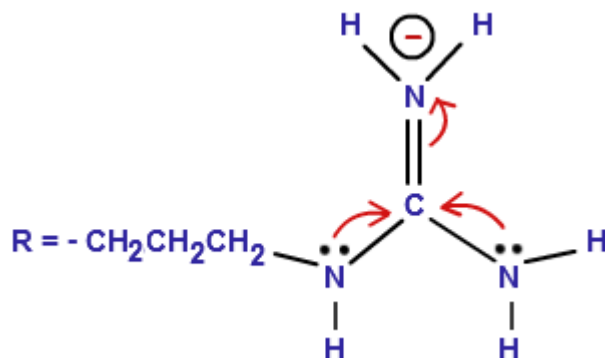


Figure 2.1: Side chain of Arginine.

L-Arginine has been used successfully for the green synthesis of some metal and metal oxide nanoparticles because it plays the role of reducing agent but also it acts as a capping agent [11-15]. Recently, L-Arginine has been used as an agent for the reduction of GO and its decoration with metal/metal oxide [16-20] .

In this chapter, we will describe some reports on graphene decorated with silver nanoparticles. We will also discuss the use of L-Arginine as an agent to reduce GO into rGO and its decoration with silver nanoparticles (AgNPs). The developed AgNPs/rGO has been successfully applied as efficient catalyst for the reduction of 4-nitrophenol to 4-aminophenol.

2.2 Graphene decorated with silver nanoparticles

Silver nanoparticles were chosen because they are cheaper as compared to other noble metal catalysts such as Au, Pt, and Pd [21-24]. Ag NPs can be immobilized on various organic/inorganic support materials [25, 26]; this confirms to be an effective strategy in protecting these metal NPs against agglomeration because of strong van der Waals force between Ag NPs [27]. This results in an increase of available electrochemical activity and detection sensitivity. Recently, Ag NPs-decorated graphene has received considerable attention [28] due to the enhancement of unusual properties of Ag NPs by graphene, such as surface enhanced Raman spectroscopy (SERS) effect [29, 30], antibacterial activity [31, 32], catalytic activity [33, 34], gas interaction [35, 36], and photocurrent generation [37].

Until now, a large number of methods for the synthesis of Ag NPs/rGO have been developed. On the other hand, there are reports of separate synthesis of metal nanoparticles followed by subsequent deposition on GO.

Herein, we review the literature on the thermal, photo-reduction, chemical reduction and electrochemical techniques used to deposit Ag NPs on rGO.

The thermal method (thermal decomposition, sometimes called pyrolysis) of metal salts has been used extensively for the preparation of metal-containing nanoparticles and nanorods. To obtain particles in nanometer size, salt decomposition was often performed at a slow heating rate and/or in a solvent. Researchers usually manually mixed metal salts of silver acetate with SWNTs (single-walled nanotubes), MWNTs (multi-walled nanotubes), expanded graphite and carbon black as the carbon source as shown in **Table 2.1**.

Table 2.1: Thermal method for the deposition of silver nanoparticles on graphene sheets

Composite	Conditions	Size of Ag NPs	Application	Ref.
Thermal Method				
CH ₃ COOAg/MWCNT	300 or 350°C for 1 h and held isothermally for 3 h.	39 nm / 47 nm	SERS	[38]
G/Ag NPs	Deposited on the graphene at a rate of 0.5 Å/min by thermal evaporator	4 nm	SERS	[39]
G/Ag NPs	60–90°C for 10–20 min. By citrate reduction method	---	Effect of deposited Ag on graphene (interlayer doped graphene film is better than that of surface doped graphene sheets)	[40]

Photochemical-assisted for metal decoration of carbon substrates have been reported by several research groups over the years [41-46], as shown in **Table 2.2**.

Table 2.2: Photochemical method to deposit silver nanoparticles on graphene sheets

Composite	Conditions	Size of Ag NPs	Application	Ref.
Photochemical method				
GO/Ag NPs	Illuminated by rows of LEDs, excitation wavelength of 465 nm for 240 min.	5 -70 nm	Study of SERS , fluorescence of rhodamine 6G	[41]
G/ZnO@Ag NPs	ZnO nanorods as photocatalytic, UV irradiation.	12 -34 nm	Electrocatalysis	[42]
Mg-ZnO/rGO-Ag NPs	Irradiate under the UV lamp	15-20 nm	Degradation of methylene blue (MB)	[43]

In the electrochemical method, several types of nanoparticles are electrodeposited on graphene. This method is easy, fast, one-step, cost-effective and environmentally-friendly for the synthesis of Ag NPs decorated graphene nanosheets as shown in **Table 2.3**.

Table 2.3: Electrochemical method to deposit silver nanoparticles on graphene sheets

Composite	Conditions	Size of Ag NPs	Application	Ref.
Electrochemical method				
rGO/ Ag NPs on ITO	Silver-ammonia [Ag(NH ₃) ₂ OH], GO	20-48 nm	Enzyme-less hydrogen peroxide detection	[47]
rGO/Ag nanodendrites	AgNO ₃ , GO	-----	Photoelectrical conversion, H ₂ O ₂ detection	[48]
rGO/MnO ₂ /Ag	KMnO ₄ , AgNO ₃ , GO	-----	Oxygen reduction reaction (ORR) in alkaline fuel cells	[49]

Chemical reduction method of nanoparticles is an attractive wet chemistry method which can be utilized for one-pot synthesis of metal nanoparticles and subsequent decoration of substrates. This technique has been applied for simultaneous reduction of GO into rGO and silver nanoparticles deposition on the graphene sheets [30, 50-52], as shown in **Table 2.4**.

Table 2.4: Chemical reduction method to deposit AgNPs on graphene sheets

Composite	Conditions	Size of Ag NPs	Application	Ref.
Chemical reduction				
Ag/GO	Sodium borohydride as reducing agent; Cetrimonium bromide as transfer agent; Silver nitrate as source of Ag.	10 nm	Reduction of 4-nitrophenol to 4-aminophenol	[34]
G/Ag NPs	Dimethylacetamide (DMAc/H ₂ O) as reducing agent. Silver nitrate as source of Ag. 150°C for 10 h.	16–20 nm	Understanding the growth of Ag NPs on graphene	[51]
AgNPs/rGO	(3-aminopropyl)-triethoxysilane (APS). Silver nitrate as source of Ag at 100°C for 12 h.	10–30 nm	Trace detection of organic dyes.	[30]

On the other hand, to avoid using harmful or toxic agents many researchers investigated environmentally friendly agents [32, 37, 53, 54], see **Table 2.5**.

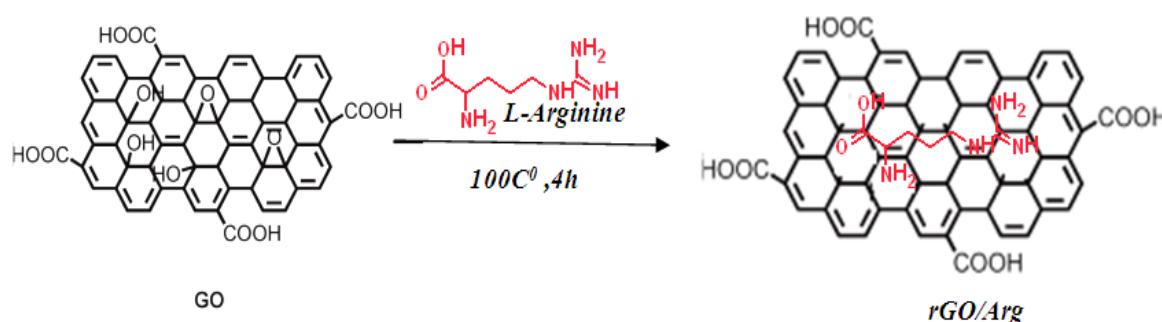
Table 2.5: Environmentally-friendly agents to deposit silver nanoparticles on graphene sheets

Composite	Conditions	Size of Ag NPs	Application	Ref.
Environmentally-friendly agents				
AgNPs/rGO	Gallic acid as reducing agent, AgNO ₃ , 190°C for 5h	average size 12.29 nm	Nonenzymatic sensor of H ₂ O ₂	[53]
GO–Ag	AgNO ₃ , sodium citrate as a stabilizing/reducing agent	average size 7.5 nm	Antibacterial activity against Gram-negative bacteria.	[32]
AgNPs/N-G	Urea as the N-dopant, vitamin C as the reducing agent, AgNO ₃ , 60°C for 24h.	average size of 12 nm	Electrochemical sensor for H ₂ O ₂ detection	[54]
Ag NPs/rGO	AgNO ₃ , sodium hydroxide at 80°C for 10 min	15 - 30 nm	Photocurrent generation in the visible spectral region	[37]

In our work we have used an environmentally friendly reagent, L-Arginine (Arg), to reduce graphene oxide and its subsequent decoration with silver nanoparticles.

2.3 Reduction of graphene oxide by L-Arginine

Because most of the methods to reduce GO use toxic agents or expensive materials, we have developed a method which uses L-Arginine (Arg), an environmentally friendly agent, which has the following advantages: (1) non-toxic, (2) water soluble, (3) scalable in production, (4) stable, (5) the reaction condition is easily attainable, (6) cost effective.

**Figure 2.2:** Schematic illustration of the reduction of GO using L-Arginine.

A mixture of GO (0.5 mg/mL) and L-Arginine (10 mM) heated at 100°C for 4 h produces a black precipitate that can be easily separated from the supernatant *via* centrifugation. After

washing with Milli-Q water, the rGO/Arg is obtained. The success of the reaction is confirmed by UV-Vis absorption spectra (**Figure 2.3**).

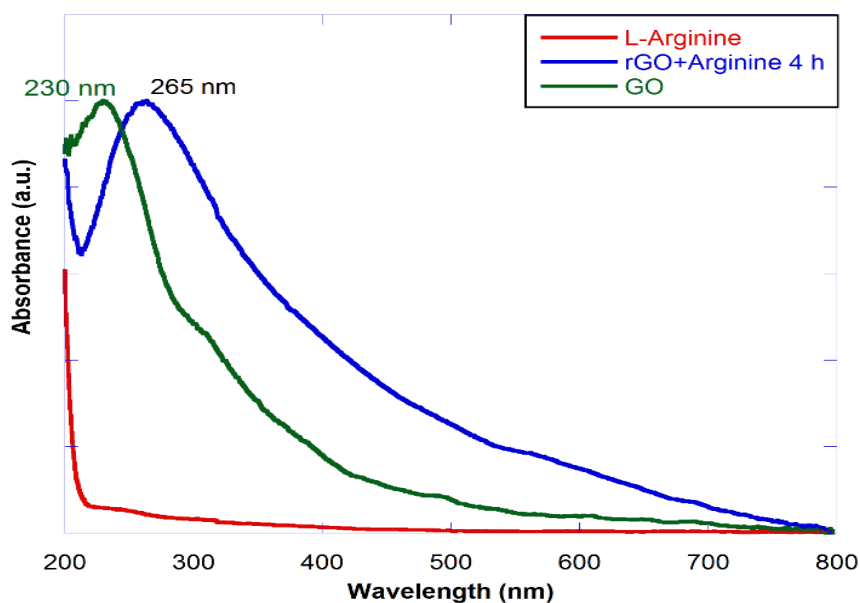


Figure 2.3: UV-Vis absorption spectra of GO before (green) and after (blue) reduction with L-Arginine at 100°C for 4 h and (red) L- Arginine.

The UV–Vis spectra clearly show that the absorption peak red-shifts from 230 to 265 nm upon reaction with L-arginine at 100°C for 4 h; the 230 nm absorption band is due to the $\pi \rightarrow \pi^*$ transition of C=C bonds in sp^2 region. For comparison, we have recorded the UV-vis spectrum of free arginine. As seen in **Figure 2.3** (red curve), arginine exhibits a weak absorption peak at 223 nm [55]. In addition, the intensity of the absorption of product has significantly increased. The result suggests that the GO nanosheets have been reduced and the electronic conjugation within the GO nanosheets restored upon reaction with L-Arginine (**Figure 2.3**).

X-ray photoelectron spectroscopy (XPS) analysis offers further information on the chemical transformations between GO and arginine. **Figure 2.4A** depicts the major element peaks namely C_{1s} , O_{1s} and N_{1s} , respectively. The weight percentage of each element was analyzed by CasaXPS software, as shown in **Table 2.6**.

Table 2.6: The atomic concentration of each element in GO and rGO/Arg

Material	At. %	Ratio C/O
GO	C _{1s} =71.31 O _{1s} =28.69	2.4
rGO	C _{1s} =74.22 O _{1s} =12.85 N _{1s} =12.93	5.85

The weight percentage of C_{1s} increases and O_{1s} decreases after reaction with arginine for 4 h at 100°C. Also a new peak which corresponds to nitrogen (N_{1s}) appears in rGO/Arg (**Figure 2.4B**), indicating the incorporation of arginine (or its oxidized components) on the rGO sheets.

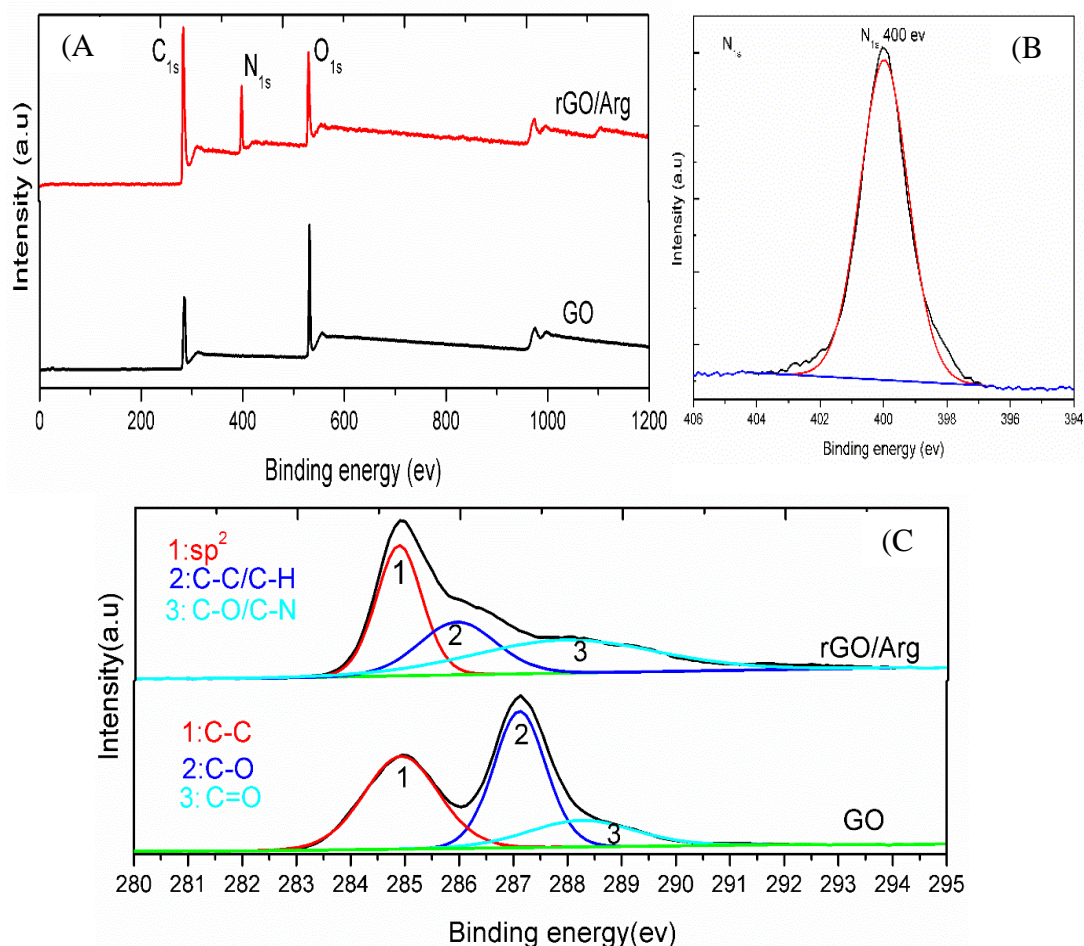


Figure 2.4: XPS survey spectra of GO and rGO/Arg (A), (B) corresponds to N_{1s} core level spectrum of rGO/Arg, and (C) C_{1s} of GO and rGO/Arg.

The C_{1s} core level XPS spectrum of GO nanosheets is displayed in **Figure 2.4C**. It can be deconvoluted into three components with binding energies at about 284.9, 287 and 288.8 eV

assigned to C-C, C-O and C=O species, respectively. The C/O ratio of GO is 2.4 comparable to reported data in the literature [56]. After reaction of GO with arginine, analysis of the resulting composite indicates significant changes in the C_{1s} core level spectrum of rGO/Arg. C_{1s} exhibits bands at 284 eV (sp^2 -hybridized carbon), 285.3 eV (C-C/C-H), and 287.6 eV (C=O/C-N) [30, 37, 51]. The intensity of the band at 284 eV increases and shifts significantly compared to GO, suggesting that the sp^2 network has been restored during the process. The ratio of carbon to oxygen (C/O) increased from 2.4 in GO to 5.85 for rGO/Arg (**Table 2.6**). Indeed, GO is a good electron acceptor that can be easily reduced in the presence of electron donors. Arginine seems to act as a good reducing agent for GO. This might be due to the L-arginine or its derivatives capped on the surface of rGO/Arg as further confirmed by the presence of nitrogen (N_{1s}) in the XPS spectrum at ~ 400 eV belong to C-N (**Figure 2.4B**).

Figure 2.5 depicts the Raman spectra of GO and rGO/Arg. They present the main features of graphene-based materials with a D-band at 1350 cm^{-1} assigned to the breathing mode of κ -point phonons [41], a G band at 1600 cm^{-1} attributed to the tangential stretching mode of the E_{2g} phonon of sp^2 atoms and a 2D-band at $\approx 2930\text{ cm}^{-1}$. The G band is related to the graphitic hexagon-pinch mode, while the D band corresponds to defects in GO.

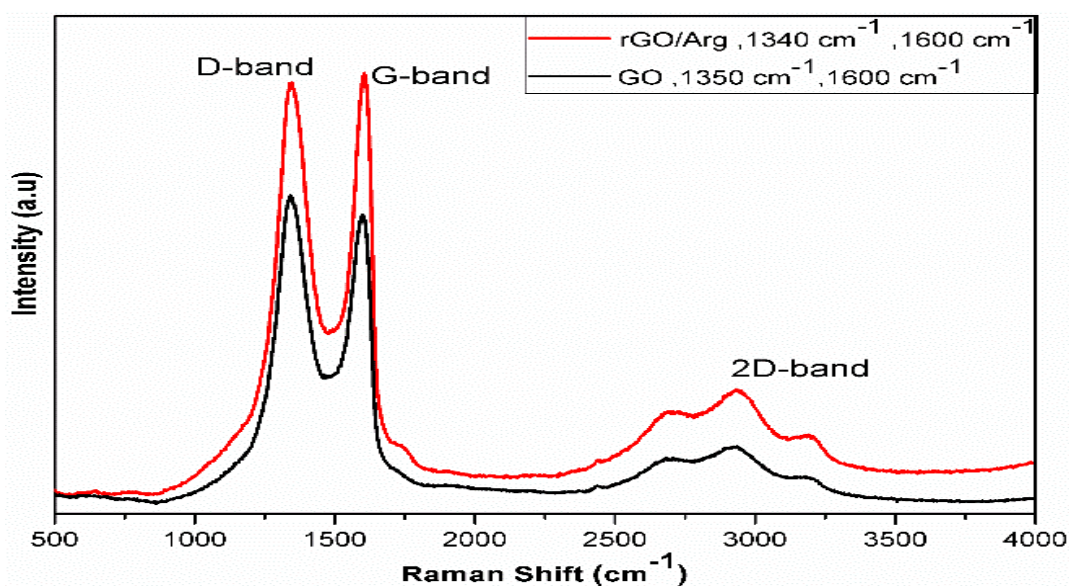


Figure 2.5: Raman spectra of GO (black) and rGO/Arg (red). The spectra were recorded at a wavelength of 532 nm.

The ratio of the intensities of the D and G bands (I_D/I_G) is found to be 0.72 for GO and 0.98 for rGO/Arg, comparable to the literature [37]. This ratio obviously increases in comparison with that of the original GO under the same conditions, indicating the reduction of GO [53, 57].

FTIR analysis was performed in order to identify the functional groups present in the GO. Transmission FTIR spectra of exfoliated GO and rGO/Arg are depicted in **Figure 2.6**. The spectrum of GO shows both water and O-H stretching vibrations at 3400 cm^{-1} , the presence of C=O in carboxylic acid and carbonyl moieties (1732 cm^{-1}), C=C bonds (1623 cm^{-1}), C-OH of carboxyl groups (1415 cm^{-1}), C-O-C bonds (1223 cm^{-1}) and C-O of epoxy or alkoxy groups (1051 cm^{-1}). After reaction of GO with arginine, the intensity of the OH, C-OH, C-O-C and C-O bands strongly decrease and C=O band disappears. The band of C=C at 1623 cm^{-1} shifts to 1561 cm^{-1} , which again confirms that GO was reduced.

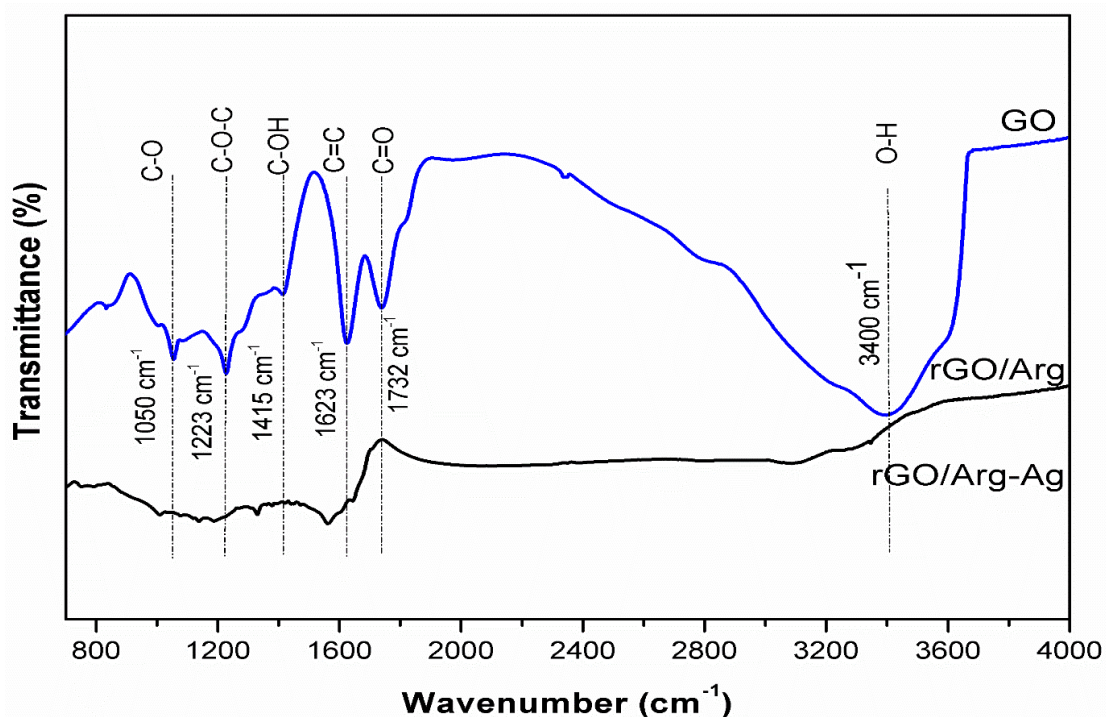


Figure 2.6: Transmission FTIR spectra of GO and rGO/Arg.

The morphology and microstructure of GO and rGO/Arg were examined by SEM and TEM. The SEM images in **Figure 2.7** exhibit the sheet layer of GO before and after reduction with arginine. Both SEM images look quite similar in the sense that only the GO sheets are visible. In fact this is not surprising since the presence of oxygen groups cannot be detected by SEM.

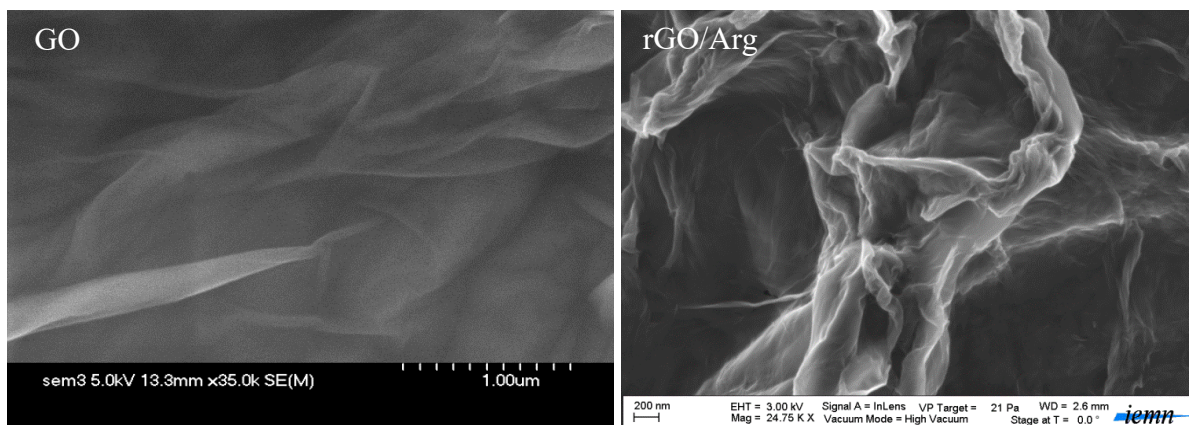


Figure 2.7: SEM images of GO and rGO/Arg.

All the characterizations confirm that GO was successfully reduced using a mild reducing agent, arginine.

2.4 Reduced graphene oxide decorated with silver nanoparticles (rGO-AgNPs)

As shown on the previous section, we have successfully reduced GO using L-arginine under mild conditions. Our next target was to exploit this mild technique to prepare reduced graphene oxide decorated silver nanoparticles (rGO- Ag NPs). The rGO/Arg-Ag NPs was synthesized as follows: silver nitrate (AgNO_3) as a source of Ag NPs at four different concentrations (0.04, 0.004, 0.0004 and 0.00004 M), was mixed with rGO/Arg aqueous solution and kept under stirring for 10 min at 100°C . The resulting black precipitate was separated from the aqueous supernatant by centrifugation. After washing with Milli-Q water, the precipitate was dispersed in Milli-Q water or in DMF. This method is schematically illustrated in **Figure 2.8B**.

The UV-Vis absorption spectra of rGO/Arg-Ag NPs nanocomposites are displayed in **Figure 2.9**; two characteristic peaks can be observed at 420 nm due to Ag NPs[30], and at 265 nm which belong to reduced graphene oxide (rGO). This indicates that the Ag nanoparticles are successfully deposited on rGO nanosheets when the concentration of silver nitrate in the aqueous solution is higher than 0.004 M. This is comparable to data reported in the literature [30, 48].

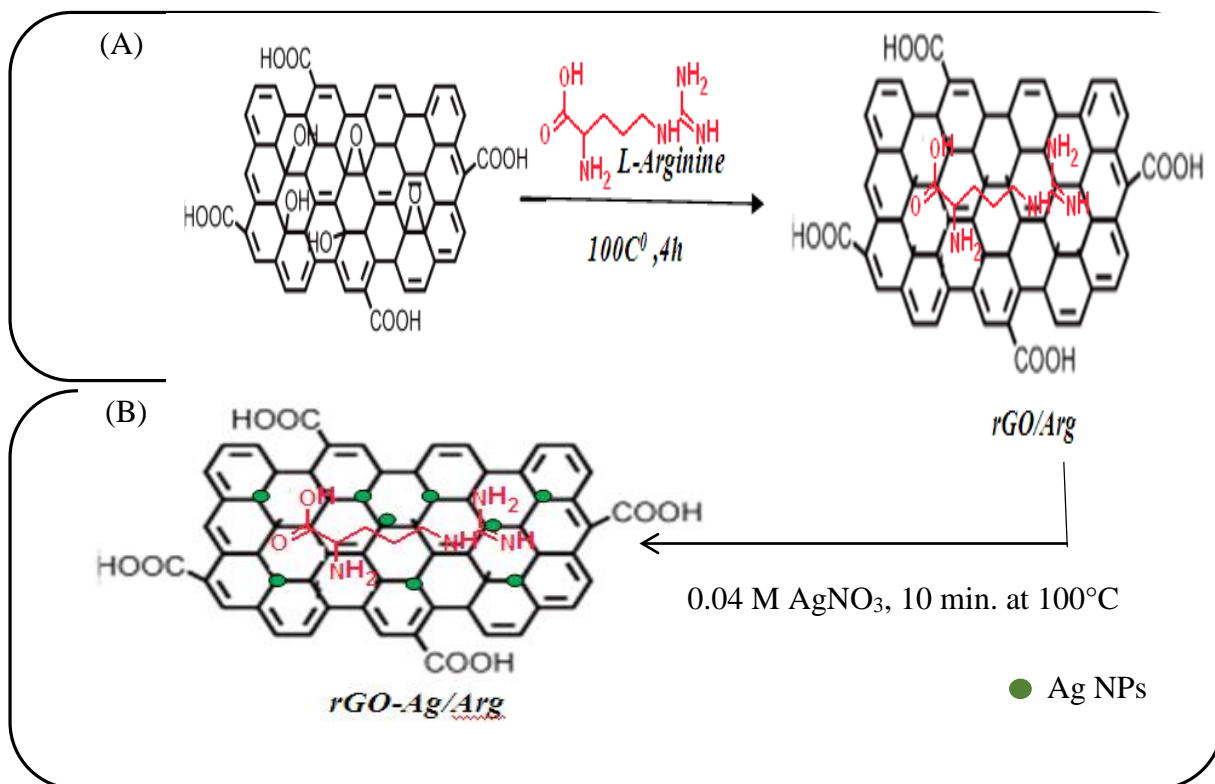


Figure 2.8: Schematic illustration of the reduction of GO using L-Arginine (A) and subsequent decoration of rGO/Arg with silver nanoparticles (rGO/Arg-Ag NPs) (B).

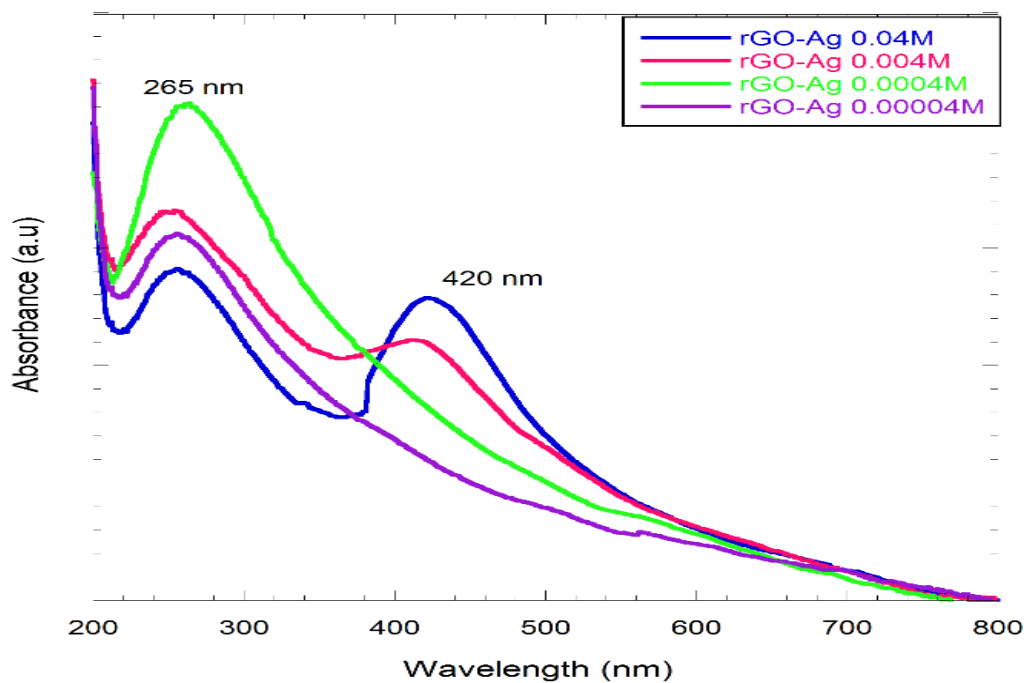


Figure 2.9: UV-Vis absorption spectra of rGO/Arg-Ag NPs at different Ag NO₃ concentrations.

XPS was also used to further characterize the rGO/Arg-Ag; for comparison the data of GO and rGO/Arg are also included. The survey XPS spectrum of rGO/Ag NPs in **Figure 2.10A** shows the major elements peaks present in the sample, namely C_{1s}, O_{1s}, N_{1s} and Ag_{3d}. The C_{1s} of rGO/Ag NPs clearly indicates the presence of three main types of carbon bonds: 284 eV (sp²-hybridized carbon), 285.3 eV (C-C/C-H), and 287.6 eV (C=O/C-N) which are consistent with the earlier reports on rGO/Arg (**Figure 2.10B**).

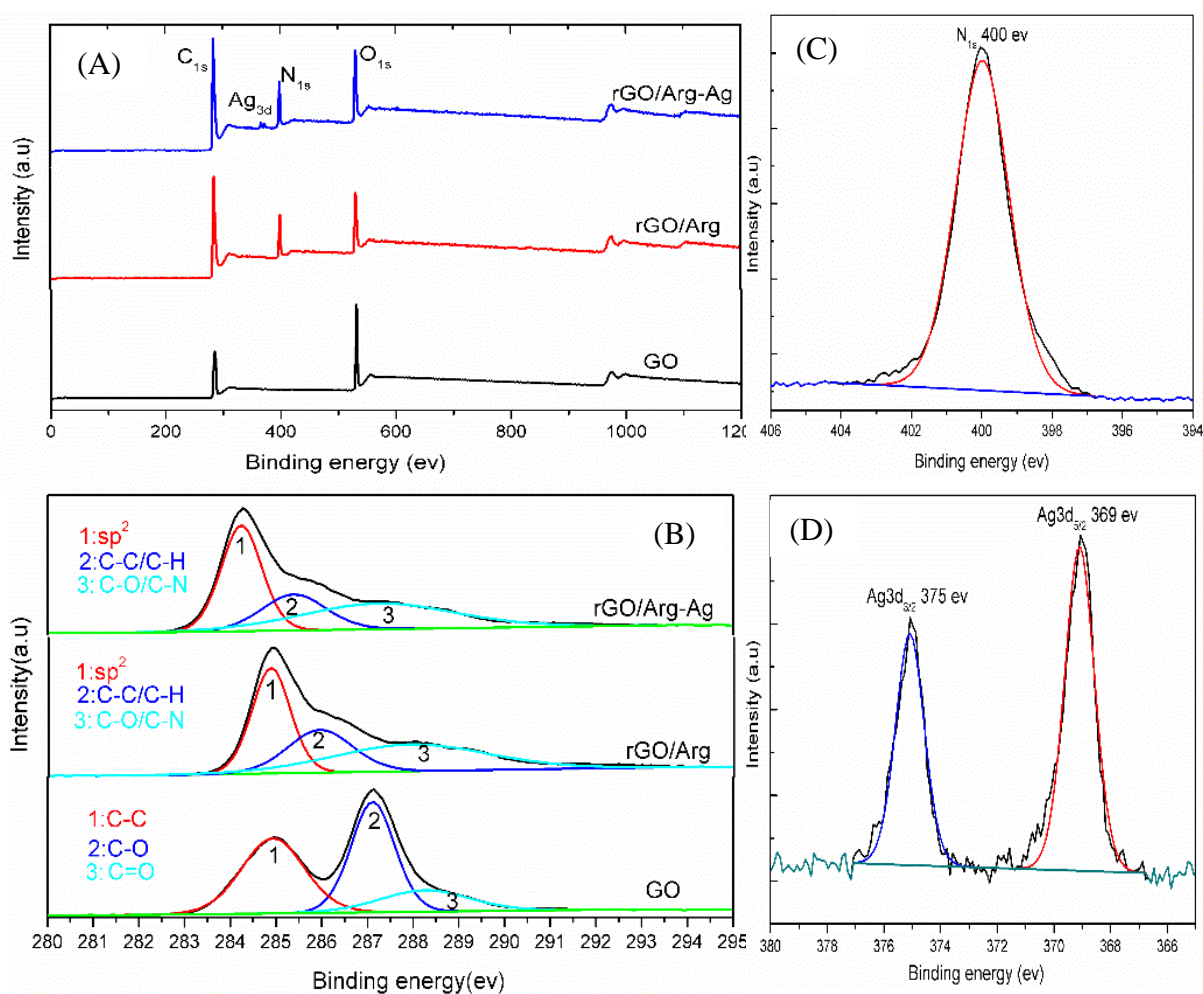


Figure 2.10: (A) XPS survey spectra of GO, rGO/Arg and rGO/Ag NPs, (B) high resolution spectra of C_{1s} of GO, rGO/Arg and rGO/Ag NPs, (C) corresponds to N_{1s} core level spectrum of rGO/Arg composite and (D) corresponds to Ag_{3d} core level spectrum of rGO/Ag NPs composite.

The XPS spectrum of Ag_{3d} in **Figure 2.10D** exhibits two major peaks with binding energies at 369 and 375 eV, corresponding to Ag_{3d_{5/2}} and Ag_{3d_{3/2}}, respectively, with a spin energy separation of 6 eV, suggesting the formation of metallic silver [30, 33, 53].

The atomic percentage of each element in different materials is reported in **Table 2.7**. As expected both rGO/Arg and rGO/Ag NPs display comparable chemical composition with additional silver for rGO/Ag NPs. This is not surprising since rGO/Ag NPs was prepared from rGO/Arg. The ratio of carbon to oxygen (C/O) increases from 2.4 for GO to 5.85 and 5.30 for rGO/Arg and rGO/Arg-Ag, respectively.

Table 2.7: Atomic percentage of each element in GO, rGO/Arg and rGO/Ag NPs.

Material	%At	Ratio C/O
GO	C _{1s} =71.31 O _{1s} =28.69	2.4
rGO/Arg	C _{1s} =74.22 O _{1s} =12.85 N _{1s} =12.93	5.85
rGO-Ag NPs	C _{1s} =74.58 O _{1s} =14.05 N _{1s} =11.22 Ag _{3d} =0.15	5.30

The Raman spectra of rGO/Arg before and after the deposition of Ag NPs on its surface are seen in **Figure 2.11**: three characteristic bands are observed in both Raman spectra, namely the D, G and 2D bands.

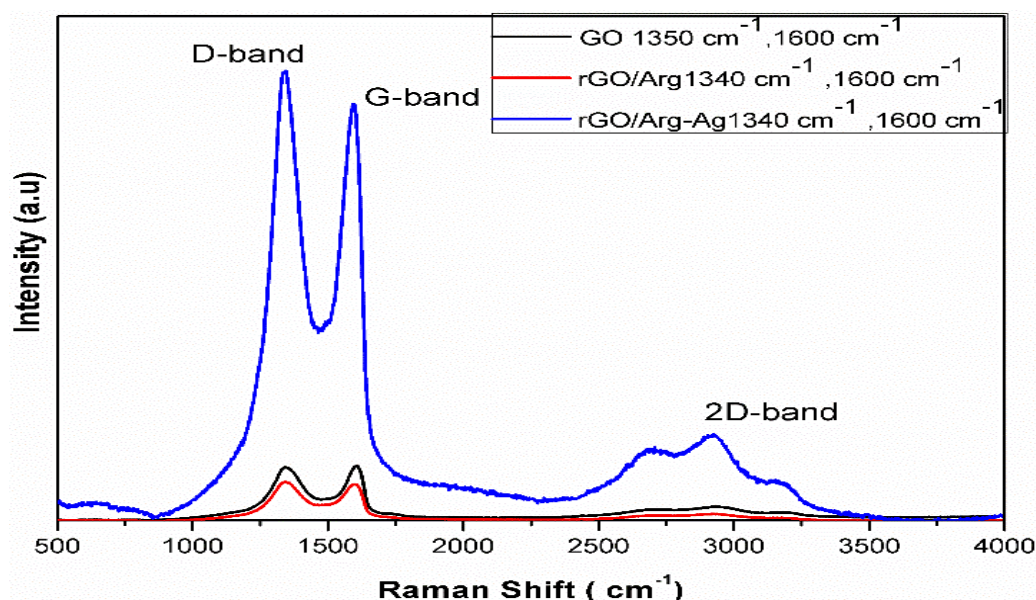


Figure 2.11: Raman spectra of GO (red), rGO/Arg (black) and rGO/Ag NPs (blue). The spectra were recorded at a wavelength of 532 nm.

The (I_D/I_G) ratios for GO, rGO/Arg and rGO/Ag NPs are 0.72, 0.98, and 1.07, respectively. This suggests that the conjugated graphene network (sp^2 carbon) has been re-established after the chemical reduction of GO [33]. Thus, silver ions and GO were reduced simultaneously by L-Arginine. Also, the (I_D/I_G) ratio of rGO/Ag NPs is slightly larger than that of rGO/Arg. This might be due to the increase of the number of defects in rGO after the deposition of Ag NPs on rGO/Arg. In addition, it has to be noticed that the intensities of these three bands are enhanced about eight times after the decoration of Ag NPs on the surface of rGO/Arg. This is due to the Ag NPs deposited on rGO/Arg which enhance the Raman signal *via* the Surface-Enhanced Raman Spectroscopy (SERS) effect [17, 30].

The FTIR spectrum of rGO/Ag NPs is similar to that of rGO/Arg, with a weaker intensity and a small shift toward low wavenumbers, which is due to the presence of large amounts of Ag NPs [58]. The intensity of the OH, C-OH and C-O bands strongly decrease and the C=O bond disappears. This means that many oxygen groups were removed during the transformation of GO to rGO (**Figure 2.12**). The C=C band at 1623 cm^{-1} in GO is shifted to 1571 cm^{-1} . No peak characteristic of an Ag compound can be detected, may be because FTIR is not sensitive enough to detect it.

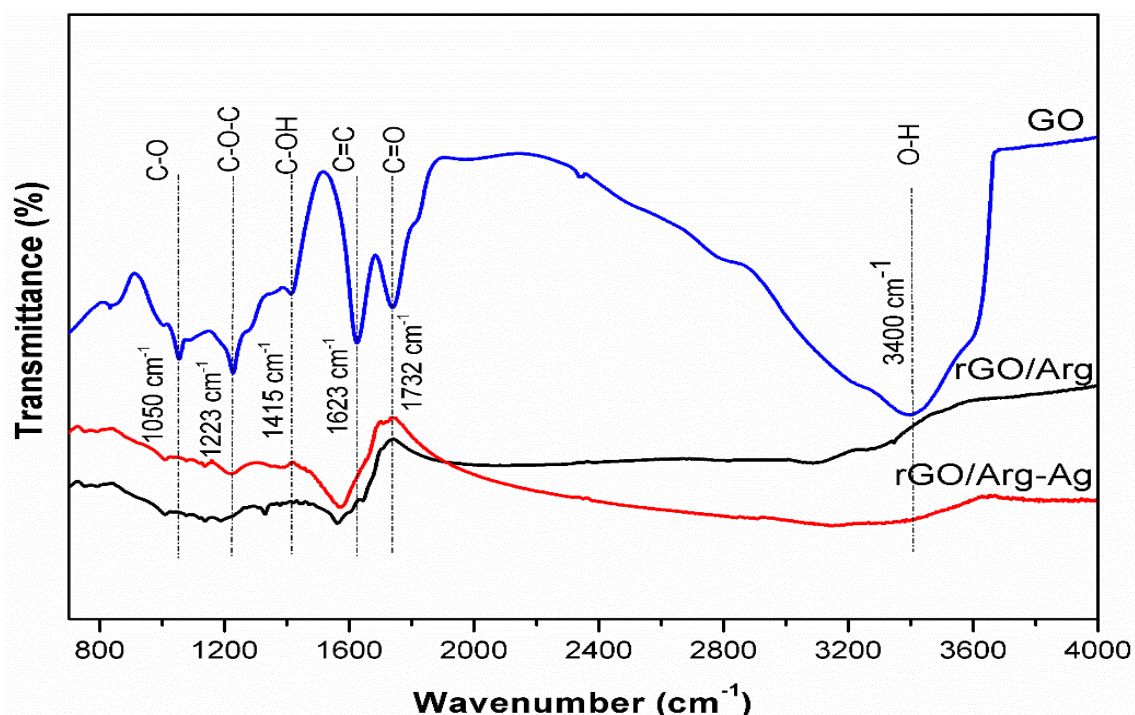


Figure 2.12: FTIR spectra of GO, rGO/Arg and rGO/Ag NPs.

In the SEM images of rGO/Ag NPs, the uniform distribution of Ag NPs on the rGO/Arg sheets is clearly seen, as well as the different sizes of these particles that depend on the concentration of silver nitrate used in the reaction. The Ag NPs appear as white spots on the rGO/Arg black sheet (**Figure 2.13**).

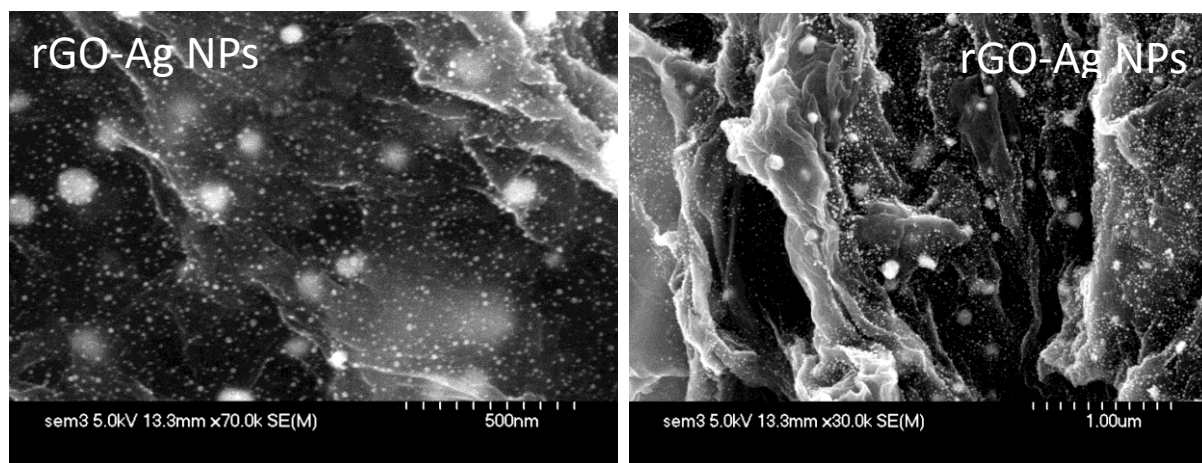


Figure 2.13: SEM images of rGO/Ag NPs after reaction of rGO/Arg with silver nitrate for 10 min at 100°C.

TEM analysis was performed to determine the morphology of stacked graphitic sheets and the size distribution of Ag NPs. **Figure 2.14** exhibits a representative TEM image of rGO/Ag NPs sheet. TEM images of rGO/AgNPs illustrate that Ag NPs have different sizes when the concentration changes. For a concentration of 0.004 M, it can be observed that the rGO/Arg sheet have three different distributions of Ag NPs (20-40 nm, 11-17 nm, 4.5- 8 nm) as in **Figure 2.14A**. The lattice spacing, equal to 0.23 nm, corresponds to (111) planes of Ag NPs as in **Figure 2.14B**. The two first rings of the selected area diffraction pattern (SAED) obtained on Ag NPs correspond to the (111) and (200) planes of silver (**Figure 2.13C**) [59, 60].

When the concentration increases to 0.04 M, the distribution of Ag NPs becomes a little more uniform and the Ag NPs become larger. This means that the increase of silver nitrate concentration causes the increase of the size of Ag NPs on the rGO/Arg sheet.

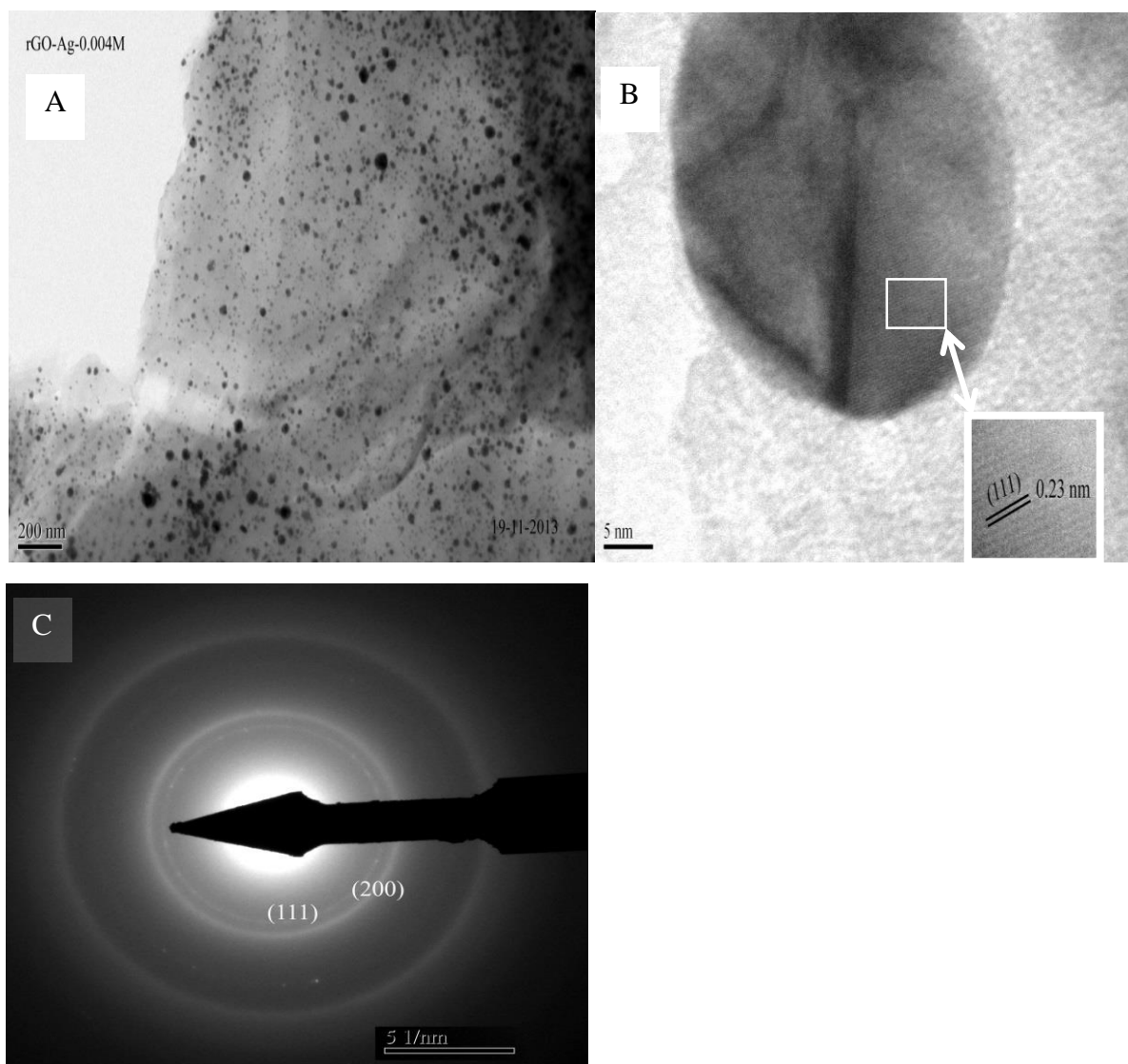


Figure 2.14: TEM images for rGO/Ag NPs using AgNO_3 concentration of 0.004 M (A), (B) one Ag NP with lattice space area and (C) selected area diffraction pattern recorded on the Ag NPs.

For AgNO_3 concentration of 0.04 M two different distributions of Ag NPs (85-400 nm, 11-25 nm) were observed (**Figure 2.15A**). The lattice spacing of 0.23 nm corresponds to the (111) planes of Ag NPs (**Figure 2.15 B**).

All these characterizations of rGO/Ag NPs provided that the Ag NPs were uniformly distributed the surface of rGO/Arg with different sizes. Almost no aggregation of Ag NPs was observed.

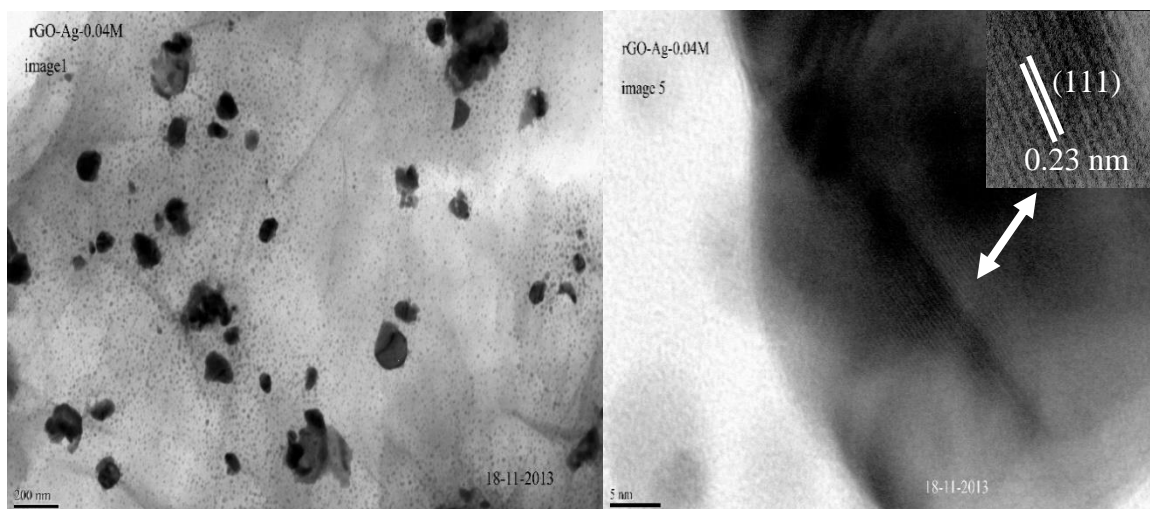


Figure 2.15: TEM images of rGO/Ag NPs at AgNO_3 concentration of 0.04 M (A), (B) one Ag NP with lattice space area.

2.5 Reduction of 4-nitrophenol to 4-aminophenol using graphene-based nanometals

2.5.1 Introduction

4-Nitrophenol (4-NP) is considered to be one of the most prevalent organic pollutants in wastewaters generated from agricultural and industrial sources [61]. 4-NP is also a common precursor of 4-aminophenol (4-AP), which is a potent intermediate for the manufacture of many analgesic/antipyretic drugs, such as paracetamol, phenacetin and can be used as the photographic developer, corrosion inhibitor, anti-corrosion lubricant, and hair-dyeing agent [62].

4-NP removal by many processes have been developed, including adsorption [63], microbial degradation [64], photocatalytic degradation [65], electro-Fenton method [66], electrocoagulation [67], electrochemical treatment [68] and so on.

In this work, we will focus on the catalytic reduction of 4-NP to 4-AP with an excess amount of NaBH_4 . The catalytic reduction of 4-NP to 4-AP with an excess amount of NaBH_4 has been extensively used as a benchmark system to evaluate the catalytic activity of metal NPs or graphene-metal NPs composites [69, 70]. Graphene-metal NPs composites can effectively catalyze the reduction of nitro compounds by acting as an electronic relay system, wherein the

electron transfer takes place from donor BH_4^- (donor) to 4-NP (acceptor) through the nanocatalysts [71, 72].

This reaction was first reported by Pal et al. in 2002 who used Ag NPs as the catalyst [73]. Nitro compounds like 2-nitrophenol (2-NP), 4-nitrophenol (4-NP) and 4-nitroaniline (4-NA) were tested with NaBH_4 using Ag NPs; they observed that the rate of reduction was following the sequence 4-NP>2-NP>4-NA. It has been suggested that a strong interaction between the catalyst surface and the substrate is essential for an effective catalytic process. But in turn, this type of interaction may cause poisoning of the catalyst surface if it is vulnerable to oxidation.

As we know, graphene has the highest surface area. If it is decorated with nanoparticles, it will have the highest reaction surface area, thus making reduction of 4-NP to 4-AP fast and effective. On the other hand, graphene facilitates the reaction because it has a high affinity for the adsorption of 4-NP via π - π stacking interactions [74]. This increases the concentration of 4-NP near the catalyst which speeds up the reaction because the electron transfer from the graphene to metals nanoparticles increases the local electron concentration, facilitating the uptake of electrons by 4-NP molecules [71]. The results which use the composites of different nanoparticles-graphene, GO or rGO as a catalyst are displayed in **Table 2.8**.

Table 2.8: Types and conditions for the catalytic transformation of p-nitrophenol to p-aminophenol.

Catalyst	Catalyst loading	Time of conversion	NaBH ₄ Conc.	4-nitrophenol Conc.	Ref.
rGO-Au NPs	0.03 mg.ml ⁻¹	2 min	0.09 M	0.09 mM	[75]
Au NPs-bohemite film	Film	32 min	10 mM	1 mM	[76]
Au/Ls/PPyNTs hybrid (PPyNTs): polypyrrole nanotubes	0.1 mM	14 min	13 mM	0.17 mM	[77]
PANI-Au NPs PANI: polyaniline	Composite membrane	110 min	0.1 M	0.1 mM	[78]
Pd NPs-rGO-CNT	5 mg. ml ⁻¹	20 s	0.3 M	0.1 mM	[79]
Fe ₃ O ₄ /Gr/ M (M=Pt, Pd, PtPd)	2 mg. ml ⁻¹	Pd/40 s Pt/2 min PdPt/60 s	2.4 M	7.4 mM	[80]
Au-Ag/GO	6.99 mg.ml ⁻¹	60 sec	0.88 M	1.5 mM	[81]
Pt/Ni-Gr	0.1 mg.ml ⁻¹	2.5 min	0.1 mM	0.1 mM	[82]
Au/PMMA PMMA [Poly(methyl methacrylate)].	0.43 mg.ml ⁻¹	10 min	0.65 M	0.09 mM	[83]
Ag/CA Au/CA CA(Alginate)	1.2 g.L ⁻¹	8 min 45min	0.1 M	0.1 mM	[62]

Catalyst	Catalyst loading	Time of conversion	NaBH ₄ Conc.	4-nitrophenol Conc.	Ref.
Au/graphene hydrogel 1.08 cm in diameter and 1.28 cm in height	9.2 wt%	720 s	0.1 M	0.1 mM	[74]
Ag@Co/rGO	5 mg.ml ⁻¹	45 s	0.35 M	1.2 mM	[69]
Ni-Ag@rGO	6.6 mg.ml ⁻¹	45 s	0.88 M	1.54 mM	[84]
rGO/Pt/CeO ₂	6.2 mg.ml ⁻¹	14 min	2.5 M	5 mM	[85]
SiO ₂ @rGO@Ag NPs	0.5 µg.ml ⁻¹	9 min	10 mM	0.1 mM	[86]
rGO/Ag/CeO ₂	0.1 mg.ml ⁻¹	10 min	1.5 M	10 mM	[70]
GO/Ag-Fe ₃ O ₄	0.1 mg.ml ⁻¹	140 s	0.1 M	10 mM	[58]
Ag-Fe ₃ O ₄ /rGO	1.2 g.L ⁻¹	200 s	0.15 M	0.1 mM	[87]
ICC@Au _{0.2} ICC (iron oxide@carboxylated cellulose)	3.10 ⁻⁷ M	10 min	0.128 M	0.1 mM	[88]
Au _{0.3} Pt _{0.7} @BGNs/Fe ₃ O ₄ (BGNs/Fe ₃ O ₄) poly- (ethylenimine) (BPEI) functionalized graphene/iron oxide	0.8 mg.ml ⁻¹	21 s	3 M	10 mM	[89]

As shown in **Table 2.8** there are many catalytic nanocomposites using different metals, these metals being anchored on different surfaces like [PMMA (poly(methyl methacrylate)), carboxylated cellulose, poly(ethylenimine) (BPEI), polypyrrole nanotubes (PPyNTs), polyaniline (PANI), CNT and graphene]. Graphene having become one of the most widely

used support materials, we will detail some literature reports which can be taken as examples and then compared with our material.

Li et al. [80] developed a method to selectively deposit noble metal (Pt, Pd, or PtPd) nanoparticles 3–5 nm in size on magnetite/graphene composites. They used L-lysine, which was chosen as a bridge to link the metal NPs and magnetite/graphene, and then deposited M (M=Pt, Pd, or PtPd NPs) on the surface of Fe₃O₄/graphene. After having successfully prepared the nanocomposite, they used it for the reduction of 4-nitrophenol (4-NP) by NaBH₄. With only the Fe₃O₄/graphene as a catalyst, the reduction did not proceed even with a large excess of NaBH₄. On the opposite, the Fe₃O₄/graphene/M composites showed high catalytic activities, and even with a trace amount of the catalysts the reduction quickly went to completion. For instance, when Fe₃O₄/graphene/M (2 mg.mL⁻¹) catalyst was added, the reaction could be completed in 40 s, 2 min and 1 min for Pd, Pt and PdPt, respectively. The bright yellow solution faded to completely colourless, and no characteristic absorption of 4-NP could be detected at 400 nm [80].

Adhikari and co-workers [75], have used amino acid (2,4-dihydroxy phenyl alanine, Dopa) to reduce simultaneously GO to rGO and noble metal salts (AuCl₃/AgNO₃) to produce the corresponding rGO/metal NPs nanohybrid systems. A freshly prepared aqueous solution of NaBH₄ (0.3 mL, 0.1 M) added to the 3 mL aqueous solution of p-nitrophenol (0.1 mM) at room temperature changed the colour from light yellow to yellowish green. Then 0.1 mg of rGO/Au NPs composite was added into the mixture with stirring. These catalytic reductions were monitored by UV-Vis absorption spectroscopy (**Figure 2.16**). A decrease in the UV-Vis absorption peak at 400 nm was observed with the concomitant appearance of a new peak at 298 nm, because of the formation of p-aminophenol. Adhikari and co-workers noted that in absence of rGO-Au NPs catalyst, no change in UV-vis absorption spectrum is observed and also graphene alone does not show any catalytic property [75].

Wu et al. [81] fabricated Au–Ag nanoparticle/graphene oxide nanocomposites (Au–Ag/GO) by using simultaneous redox reactions between AgNO₃, HAuCl₄ and GO. For the reaction conditions, 2.5 ml aliquot of 1.54×10⁻³ M 4-NP solution and 0.5 ml of 0.88 M NaBH₄ solution were mixed in a 3 ml standard quartz cuvette and then a UV–vis spectroscopy was used to monitor the absorption maximum of 4-NP at 400 nm.

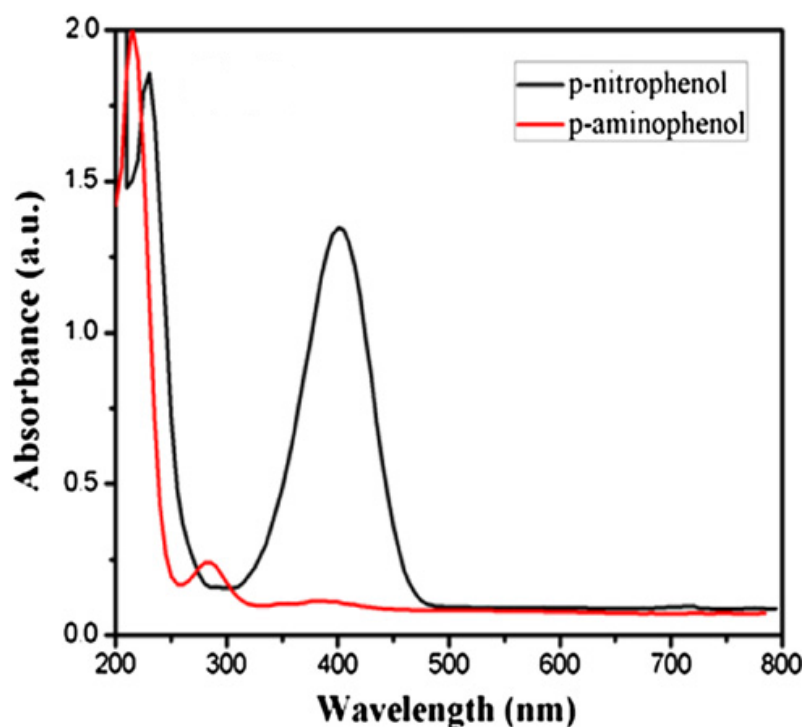


Figure 2.16: UV-Vis spectroscopy to monitor the reduction of (i) p-nitrophenol to p-aminophenol catalyzed by rGO/Au NPs [75].

When Au–Ag/GO was added to the mixture, the reaction was complete in less than 60 s. These results indicate that the Au–Ag/GO catalyst is highly active and has excellent recyclability. The interfacial regions between the nanoparticles and the GO may contribute to the origin of the catalytic activity of Au–Ag/GO [81].

Mahesh and co-workers [87] have grown Ag and Fe₃O₄ NPs on the surface of reduced graphene oxide (rGO) sheets using one-pot hydrothermal process. The catalytic activity of the as-prepared Ag-Fe₃O₄/rGO (1.2 g.L⁻¹) was demonstrated through the reduction of 4-NP (0.1 mM) in presence of NaBH₄ (1.5 M) as a reductant. An aqueous solution of 4-NP displays maximum absorbance at 317 nm. After immediate addition of freshly prepared NaBH₄, the maximum absorption peak shifted from 317 to 400 nm which corresponds to a colour change of light yellow to yellow green. However, addition of a small quantity of as-prepared nanocomposite causes the fading and ultimate bleaching of the yellow colour of the reaction mixture, with the appearance of a new peak at 302 nm, confirming that the reduction was mainly catalyzed by Ag-Fe₃O₄/rGO (**Figure 2.17**) [87]. The authors reported that the time of reaction generally decreases linearly with increased amount of catalyst. The recyclability of Ag-Fe₃O₄/RGO catalyst was evaluated and reveals that the catalytic reduction efficiency of as-synthesized

composite is almost the same even after 7th successive reaction. They showed that magnetically recoverable Ag-Fe₃O₄/rGO catalyst was not deactivated or poisoned during catalytic and separation process [87].

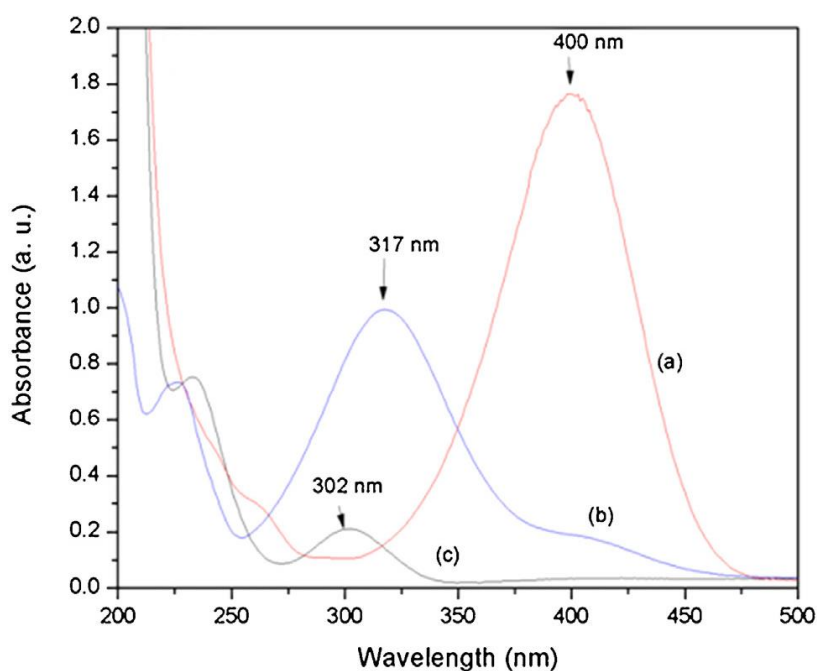


Figure 2.17: UV–visible spectra of 4-NP (a), nitrophenolate ion (b) and 4-AP (c) [87].

Zhang et al. [84] used hydrazine hydrate as a reducing agent to reduce simultaneously graphene oxide, Ni²⁺ and Ag⁺ to form Ni-Ag@rGO hybrid. The prepared material exhibited good magnetic properties, which were determined by vibrating sample magnetometer. In addition, the Ni-Ag@rGO hybrid displayed excellent catalytic activity for the reduction of 4-NP. In a general procedure, 4-NP solution (2.5 mL, 1.54×10^{-3} mol.L⁻¹) was mixed with 0.5 mL of freshly prepared aqueous NaBH₄ solution (0.88 mol.L⁻¹) to form a deep yellow solution. Then, 20 mg of catalyst was added to the solution. The peak intensity of 4-NP at about 400 nm rapidly decreased and the peak disappeared in 45 s. The reaction of 4-NP with Ni@rGO, Ag@rGO, Ni–Ag bimetallic, Ni monometallic, Ag monometallic and rGO were also investigated under the same conditions and the reaction times were 6, 1.5, 10, 15, 12 and 240 min, respectively. Since the Ni-Ag@RGO hybrid is magnetic, it is easy to recycle. The hybrid can be separated from the reaction solution under a magnet field. The reaction time slowly increased for the first five cycles, and then it increased greatly to 1.5 min for the tenth cycle (**Figure 2.18**) [84].

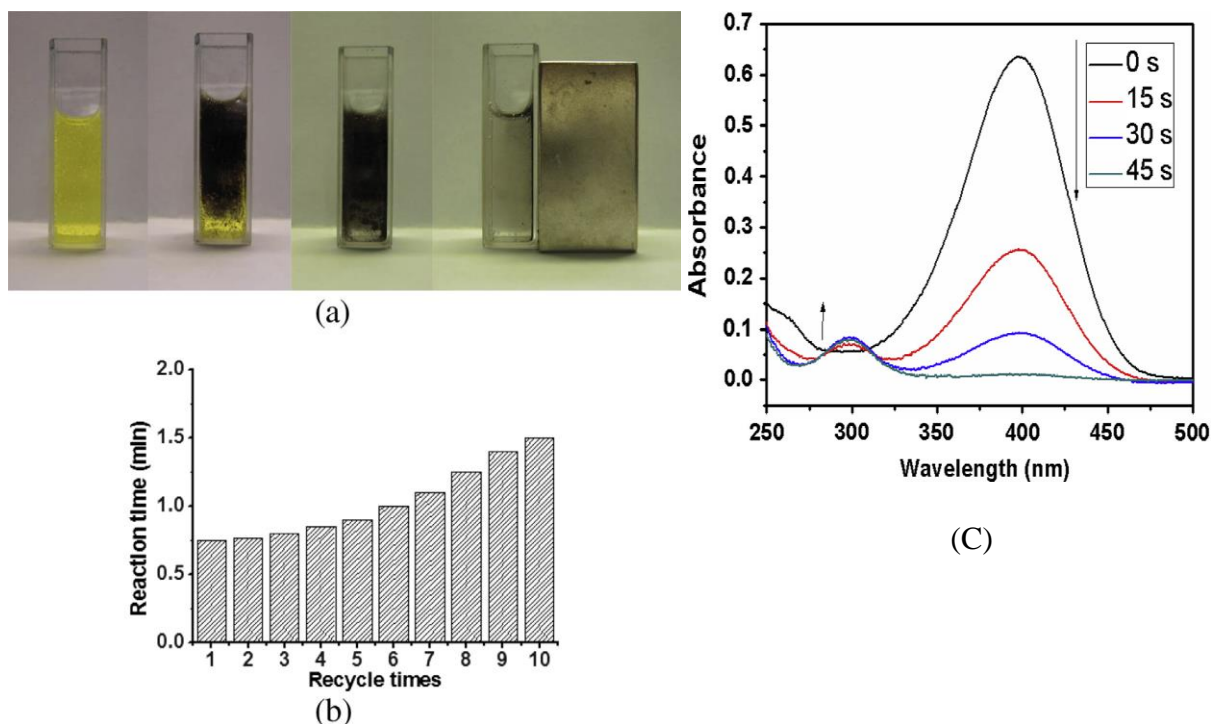


Figure 2.18: Digital photographs of the reaction solution process (a), recyclability of the Ni-Ag@rGO hybrid for the reduction of 4-NP by NaBH₄ (b), and UV-vis spectra for the reduction of 4-NP by NaBH₄ with Ni-Ag@rGO (c) [84].

2.5.2 Catalytic reduction of 4-nitrophenol by rGO/Ag NPs composite

We have investigated the catalytic ability of our rGO/Ag NPs nanocomposite at room temperature for the reduction of 4-NP with NaBH₄ as a model. Typically, after having prepared 0.1 mM 4-NP solution and 0.1 M NaBH₄, a mixture of 3 ml of 4-NP with 0.5 ml NaBH₄ was prepared. The color changed from light yellow to yellow-green because 4-NP was converted to nitrophenolate anion by NaBH₄. Upon addition of 100 μ l of our catalyst rGO/Ag NPs (0.5 mg.ml⁻¹) to the mixture, the yellow-green color disappeared; this means that the 4-NP was reduced to 4-AM. We have performed experiments with different rGO/Ag NPs synthesized using different Ag concentrations (0.04, 0.004, 0.0004 and 0.00004 M). The course of the reaction was monitored by UV-Vis spectroscopy.

We have also conducted recycling catalysis experiments in order to study the catalytic stability and activity. Similar to the above reduction process, a given amount of the as-prepared rGO/Ag NPs (0.5 mg.ml⁻¹) was used to catalyze the reduction of 0.1 mM of 4-NP mixture with 0.1 M NaBH₄. When the reaction was completed, the catalyst was separated by centrifugation at 4000 rpm for 5 min, and the supernatant was analyzed using UV-vis spectroscopy. The same

procedures were repeated at least ten times in order to explore the reusability and activity of the nanocatalyst.

The catalytic performance of the rGO/Ag NPs was monitored by UV-Vis spectroscopy (**Figure 2.19**).

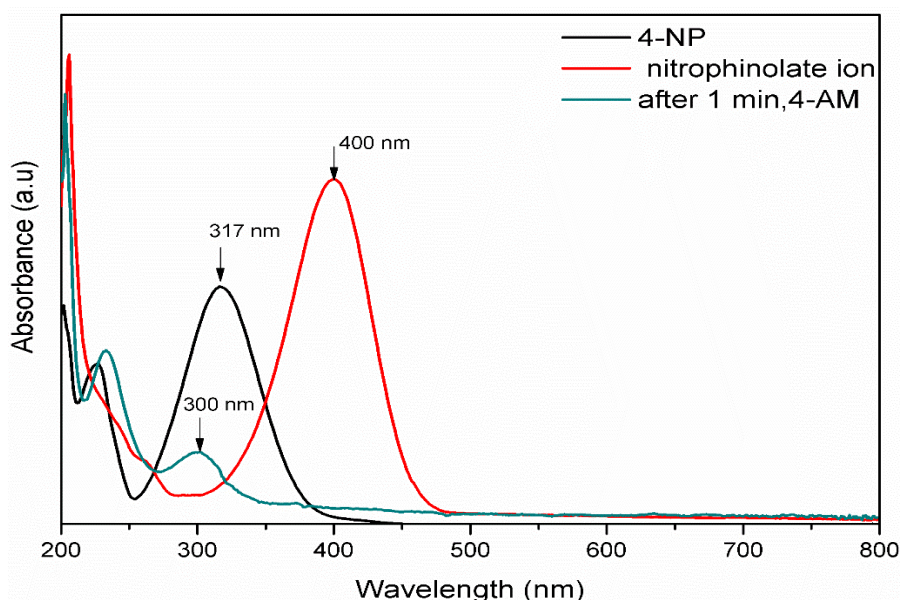


Figure 2.19: UV–visible spectra of 4-NP (a), nitrophenolate ion (b) and 4-AP (c) after addition of 100 μl of rGO/Ag NPs ($0.5 \text{ mg}\cdot\text{ml}^{-1}$); the concentration of AgNO_3 used for the preparation of the composite is 0.04 M.

The original absorption peak of 4-NP at 317 nm shifts to 400 nm immediately upon the addition of freshly prepared NaBH_4 solution, corresponding to a colour change from light yellow to yellow-green due to the formation of p-nitrophenolate ions (**Figure 2.20**) [70, 89, 90].

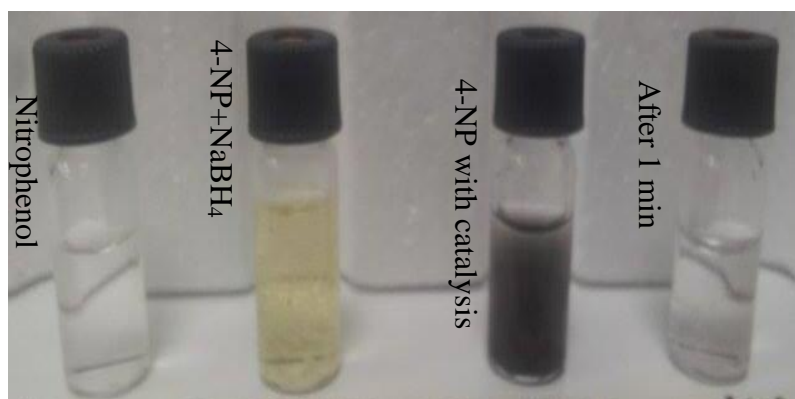


Figure 2.20: Photographs of 4-NP reduction process.

In absence of rGO/Ag NPs catalyst, the peak due to 4-nitrophenolate ion at 400 nm remains unaltered even after a couple of days, as reported in the literature [87]. Addition of the nanocatalyst in small quantity (100 μ l, rGO/Ag NPs (0.5 mg.ml⁻¹)) causes the fading and ultimate bleaching of the yellow colour of the reaction mixture, with the appearance of a new peak at 300 nm which confirms that the reduction was mainly catalyzed by rGO/Ag NPs.

The intensity of the absorption peak at 400 nm gradually decreases as the reaction proceeds, indicating the reduction of the -NO₂ group of 4-NP to the -NH₂ group (**Figure 2.21**) [87], and finally disappears at its completion. The reaction was completed within 1 min for a rGO/Ag NPs catalyst prepared using AgNO₃ concentration of 0.04 M. Meanwhile, a new peak appears at 300 nm and gradually increases, revealing the reduction of 4-NP to 4-AP. This phenomenon indicates that the reduction of 4-NP to 4-aminophenol (4-AP) is successfully catalysed by the nanocatalyst.

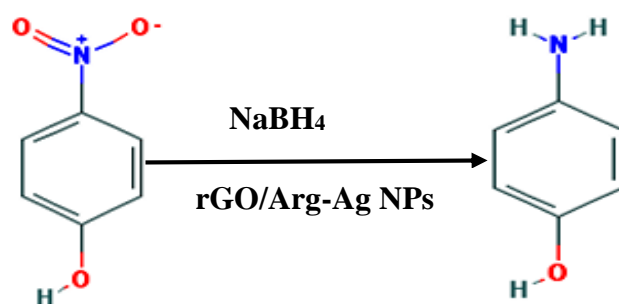


Figure 2.21: Schematic illustration of the reduction of p-nitrophenol by NaBH₄ with rGO/Ag NPs nanocomposite as catalyst.

It was found that the increase of the Ag content within a certain range enhances the catalytic efficiency. This is mainly because the more Ag nanoparticles are deposited, the more reaction sites are provided in the composite materials, which lead to a higher reaction rate (**Table 2.9**) [58].

Table 2.9: The experimental details, time for the reduction reaction of p-nitrophenol and the concentration of Ag in the rGO/Ag NPs catalyst

Sample	Ag concentration	Time /min
rGO/Arg-Ag 1	0.04 M	1
rGO/Arg-Ag 2	0.004 M	5
rGO/Arg-Ag 3	0.0004 M	10
rGO/Arg-Ag 4	0.00004 M	20

Figure 2.22 shows that the time of reduction reaction of 4-NP to 4-AM decreases by increasing the concentration of Ag nanoparticles in the rGO/Ag NPs catalyst. The result points out the important effect of the Ag nanoparticles on the catalytic activity. The catalytic reduction could be considered to be attributable to the following factors: 1- rGO sheets have high adsorption ability toward p-nitrophenol via π - π stacking interactions. This provides a high concentration of p-nitrophenol near the Ag nanoparticles on rGO, leading to an efficient contact between them [74]; 2- the electron transfer from graphene to Ag NPs increases the local electron concentration, facilitating the uptake of electrons by 4-NP molecules. A higher Ag concentration leads to a higher density of Ag nanoparticles of medium size *i.e.* between 11 and 25 nm and large size (85-400 nm) (**Figures 2.14 and 2.15**).

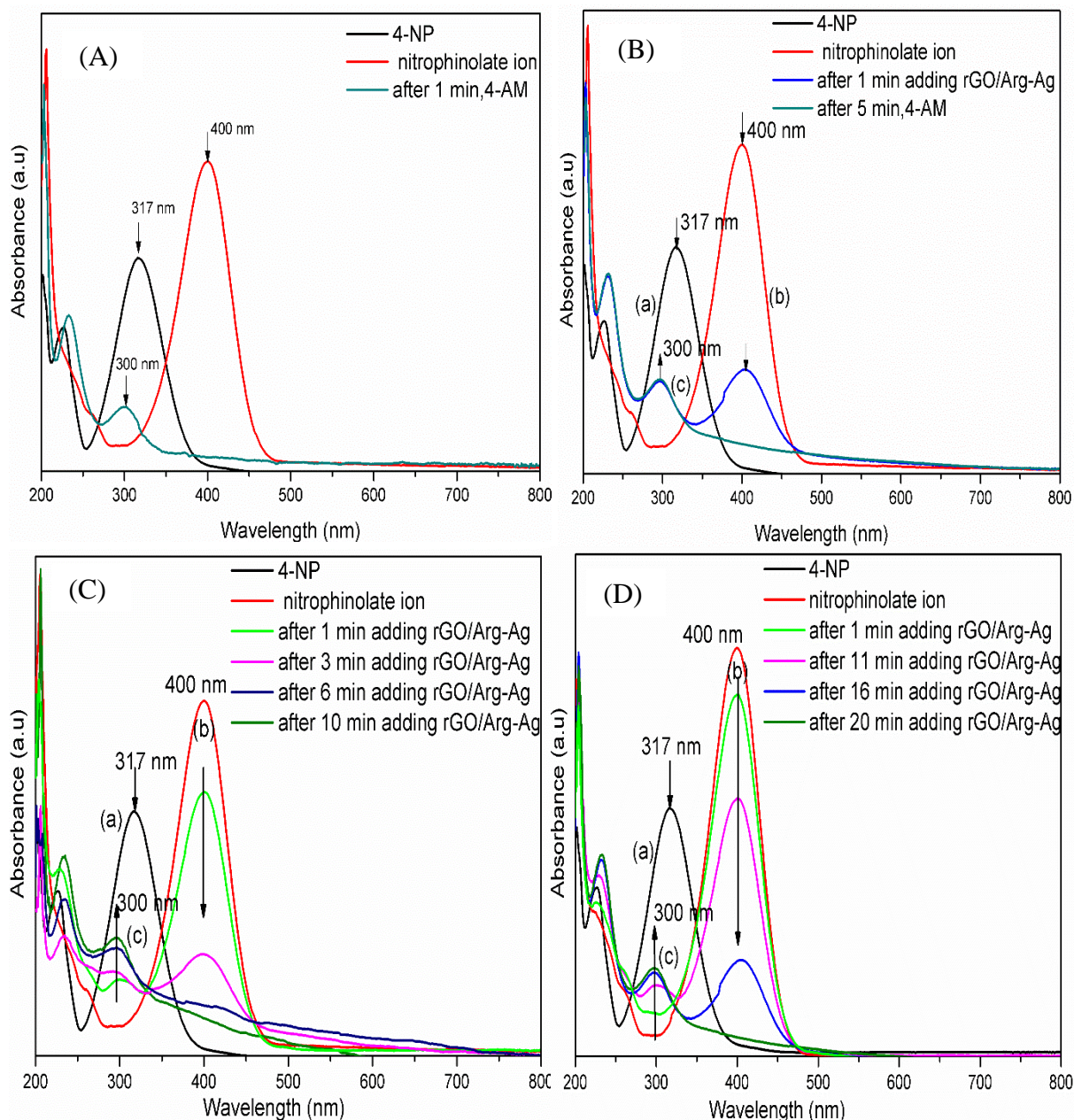


Figure 2.22: UV–visible spectra of 4-NP (black) (a), nitrophenolate ion (red) (b) and 4-aminophenol (green) (c) after addition of 100 μl of rGO/Ag NPs ($0.5 \text{ mg}\cdot\text{ml}^{-1}$); the concentration of AgNO_3 used for the preparation of rGO/Ag NPs catalyst: 0.04 M (A), 0.004 M (B), 0.0004 M (C) and 0.00004 M (D).

The reusability of the rGO/Ag NPs nanocatalyst was also studied (**Figure 2.23**). The catalytic activity of the nanocatalyst slightly maintains a high performance for the first four cycles for the concentration 0.04 M. This means that the catalysis of rGO/Arg-Ag has a good stability and activity until the fourth cycle; then the completion time increases greatly (60 min) for the

eight cycle. The reaction time increases may because of the surface of the silver particles become vulnerable to oxidation and resulting a coating of silver oxide layer onto the silver surface [73, 91]. Also, BH_4^- again reduces the oxide layer and regenerates the fresh surface of the silver cluster. In this process, the particle size of silver is also affected [12]. Additionally, nitrophenolate ion adsorbed from reduced graphene oxide at the first four cycle and after that it's not able to adsorb more nitrophenolate ion to be near to active surface.

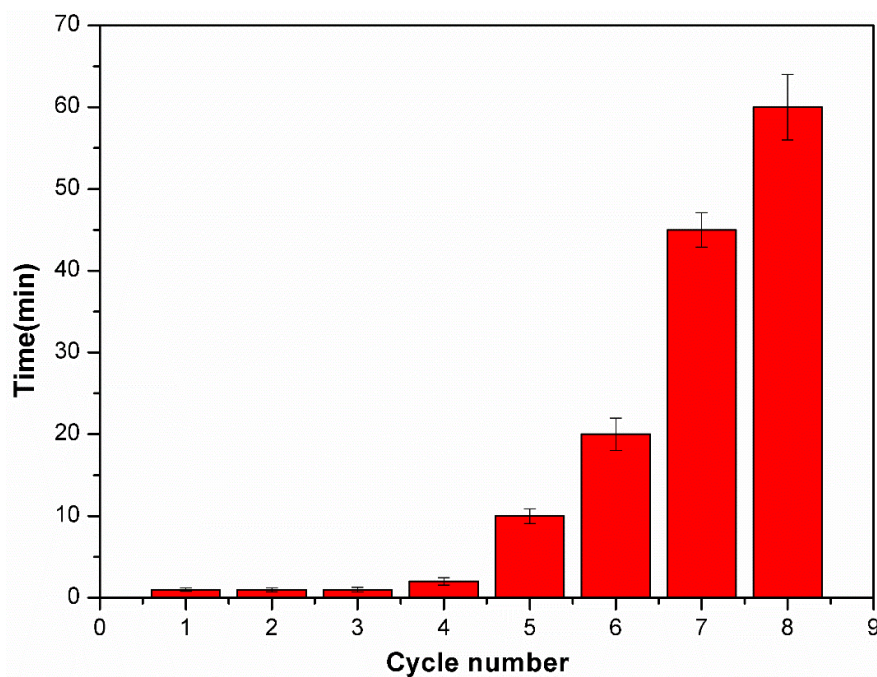


Figure 2.23: The catalytic performance of rGO/Ag NPs catalyst, prepared using AgNO_3 concentration of 0.04 M.

2.6 Conclusion

In summary, a facile method to synthesize a novel nanocomposite rGO/Ag NPs was developed by using a green and facile hydrothermal technique in a two-step process. The amino acid L-Arginine has been successfully used as an agent for the reduction of graphene oxide. FTIR, XPS and UV-vis indicated that the conjugated graphene network (sp^2 carbon) is re-established after the chemical reduction of GO, and that most of the oxygen-containing groups is removed. In the second step, the Ag NPs were well dispersed by an easy hydrothermal method on the surface of rGO/Arg. The rGO/Arg possesses a large surface area per volume, a high density of interfacial chemical groups and semiconducting properties, allowing effective contact with the

reactants and making the catalytic reactivity of the nanomaterial to be highly enhanced. Moreover, the Ag nanoparticles are uniformly deposited on the surface of rGO/Arg sheets with different sizes depending on the initial concentration of AgNO₃.

Moreover, the reduction of 4-NP to 4-AP by NaBH₄ was used as a model reaction to investigate the catalytic property of the rGO/Ag NPs. The experimental results indicated that the incorporation rGO/Arg with Ag NPs nanocomposites can significantly enhance the catalytic activity and stability of the composite catalysts. We have also obtained the relationship between the catalytic activity and the Ag NPs concentration: that is, the given information about the best Ag concentration on the surface of rGO to complete the 4-NP reduction in a short time (1 min). This value is small and efficient compared with other reports, maybe because other authors used metal complexes (Ni-Ag, Co-Ag, Au-Ag, SiO₂-Ag, Fe₃O₄-Ag) with graphene. Moreover, we have demonstrated that the nanocomposite catalyst can be reused for about four cycles where it is still very active (completion of the reduction in about 1 min). After 8 cycles, the completion time increased to 60 min. The presented composite nanocatalyst synthesis protocol is simple, fast, efficient, non-toxic, and low-cost to produce unique nanocomposite. Finally, we believe that this promising hybrid nanocomposite will have potential applications in many other fields especially in environmental control and biomedical applications.

2.7 References

- [1] Wang Z, Zhou X, Zhang J, Boey F, Zhang H. Direct electrochemical reduction of single-layer graphene oxide and subsequent functionalization with glucose oxidase. *The Journal of Physical Chemistry C*. 2009;113(32):14071-5.
- [2] Pei S, Cheng H-M. The reduction of graphene oxide. *Carbon*. 2012;50(9):3210-28.
- [3] Stankovich S, Dikin DA, Piner RD, Kohlhaas KA, Kleinhammes A, Jia Y, et al. Synthesis of graphene-based nanosheets via chemical reduction of exfoliated graphite oxide. *Carbon*. 2007;45(7):1558-65.
- [4] Bai H, Li C, Shi G. Functional composite materials based on chemically converted graphene. *Advanced materials*. 2011;23(9):1089-115.
- [5] Fernandez-Merino M, Guardia L, Paredes J, Villar-Rodil S, Solis-Fernandez P, Martinez-Alonso A, et al. Vitamin C is an ideal substitute for hydrazine in the reduction of graphene oxide suspensions. *The Journal of Physical Chemistry C*. 2010;114(14):6426-32.
- [6] Gao J, Liu F, Liu Y, Ma N, Wang Z, Zhang X. Environment-friendly method to produce graphene that employs vitamin C and amino acid. *Chemistry of Materials*. 2010;22(7):2213-8.
- [7] Zhu C, Guo S, Fang Y, Dong S. Reducing sugar: new functional molecules for the green synthesis of graphene nanosheets. *ACS nano*. 2010;4(4):2429-37.
- [8] Wang Y, Shi Z, Yin J. Facile synthesis of soluble graphene via a green reduction of graphene oxide in tea solution and its biocomposites. *ACS applied materials & interfaces*. 2011;3(4):1127-33.
- [9] Stechmiller JK, Childress B, Cowan L. Arginine supplementation and wound healing. *Nutrition in Clinical Practice*. 2005;20(1):52-61.
- [10] Tapiero H, Mathe G, Couvreur P, Tew K. I. Arginine. *Biomedicine & pharmacotherapy*. 2002;56(9):439-45.
- [11] Hu B, Wang S-B, Wang K, Zhang M, Yu S-H. Microwave-assisted rapid facile “green” synthesis of uniform silver nanoparticles: self-assembly into multilayered films and their optical properties. *The Journal of Physical Chemistry C*. 2008;112(30):11169-74.
- [12] Chiou J-R, Lai B-H, Hsu K-C, Chen D-H. One-pot green synthesis of silver/iron oxide composite nanoparticles for 4-nitrophenol reduction. *Journal of hazardous materials*. 2013;248:394-400.
- [13] Fernández-Merino M, Villar-Rodil S, Paredes J, Solís-Fernández P, Guardia L, García R, et al. Identifying efficient natural bioreductants for the preparation of graphene and graphene-metal nanoparticle hybrids with enhanced catalytic activity from graphite oxide. *Carbon*. 2013;63:30-44.
- [14] Lai Y, Yin W, Liu J, Xi R, Zhan J. One-pot green synthesis and bioapplication of L-arginine-capped superparamagnetic Fe₃O₄ nanoparticles. *Nanoscale research letters*. 2010;5(2):302-7.
- [15] Wang Z, Zhu H, Wang X, Yang F, Yang X. One-pot green synthesis of biocompatible arginine-stabilized magnetic nanoparticles. *Nanotechnology*. 2009;20(46):465606.

- [16] Wang T, Wang L, Wu D, Xia W, Zhao H, Jia D. Hydrothermal synthesis of nitrogen-doped graphene hydrogels using amino acids with different acidities as doping agents. *Journal of Materials Chemistry A*. 2014;2(22):8352-61.
- [17] Hsu K-C, Chen D-H. Microwave-assisted green synthesis of Ag/reduced graphene oxide nanocomposite as a surface-enhanced Raman scattering substrate with high uniformity. *Nanoscale research letters*. 2014;9(1):1-9.
- [18] Lin T-Y, Chen D-H. One-step green synthesis of arginine-capped iron oxide/reduced graphene oxide nanocomposite and its use for acid dye removal. *RSC Advances*. 2014;4(56):29357-64.
- [19] Zhang H, Zhou L, Yu C. Highly crystallized Fe₂O₃ nanocrystals on graphene: a lithium ion battery anode material with enhanced cycling. *RSC Advances*. 2014;4(1):495-9.
- [20] Zhang F, Wang Z, Zhang Y, Zheng Z, Wang C, Du Y, et al. Simultaneous electrochemical determination of uric acid, xanthine and hypoxanthine based on poly (l-arginine)/graphene composite film modified electrode. *Talanta*. 2012;93:320-5.
- [21] Li C, Yamauchi Y. Facile solution synthesis of Ag@ Pt core-shell nanoparticles with dendritic Pt shells. *Physical Chemistry Chemical Physics*. 2013;15(10):3490-6.
- [22] Ataee-Esfahani H, Liu J, Hu M, Miyamoto N, Tominaka S, Wu KC, et al. Mesoporous metallic cells: design of uniformly sized hollow mesoporous Pt-Ru particles with tunable shell thicknesses. *Small*. 2013;9(7):1047-51.
- [23] Rong L-Q, Yang C, Qian Q-Y, Xia X-H. Study of the nonenzymatic glucose sensor based on highly dispersed Pt nanoparticles supported on carbon nanotubes. *Talanta*. 2007;72(2):819-24.
- [24] Si Y, Samulski ET. Exfoliated graphene separated by platinum nanoparticles. *Chemistry of Materials*. 2008;20(21):6792-7.
- [25] Nemes CT, Vijapurapu DK, Petoukhoff CE, Cheung GZ, O'Carroll DM. Absorption and scattering effects by silver nanoparticles near the interface of organic/inorganic semiconductor tandem films. *Journal of nanoparticle research*. 2013;15(8):1-13.
- [26] Liu S, Tian J, Wang L, Sun X. A method for the production of reduced graphene oxide using benzylamine as a reducing and stabilizing agent and its subsequent decoration with Ag nanoparticles for enzymeless hydrogen peroxide detection. *Carbon*. 2011;49(10):3158-64.
- [27] Chang Q, Wang Z, Wang J, Yan Y, Ma Z, Zhu J, et al. Graphene nanosheets inserted by silver nanoparticles as zero-dimensional nanopacers for dye sensitized solar cells. *Nanoscale*. 2014;6(10):5410-5.
- [28] Zhou X, Huang X, Qi X, Wu S, Xue C, Boey FY, et al. In situ synthesis of metal nanoparticles on single-layer graphene oxide and reduced graphene oxide surfaces. *The Journal of Physical Chemistry C*. 2009;113(25):10842-6.
- [29] Qian Z, Cheng Y, Zhou X, Wu J, Xu G. Fabrication of graphene oxide/Ag hybrids and their surface-enhanced Raman scattering characteristics. *Journal of colloid and interface science*. 2013;397:103-7.
- [30] Huang Q, Wang J, Wei W, Yan Q, Wu C, Zhu X. A facile and green method for synthesis of reduced graphene oxide/Ag hybrids as efficient surface enhanced Raman scattering platforms. *Journal of hazardous materials*. 2015;283:123-30.

- [31] Liu L, Liu J, Wang Y, Yan X, Sun DD. Facile synthesis of monodispersed silver nanoparticles on graphene oxide sheets with enhanced antibacterial activity. *New Journal of Chemistry*. 2011;35(7):1418-23.
- [32] de Faria AF, Martinez DST, Meira SMM, de Moraes ACM, Brandelli A, Souza Filho AG, et al. Anti-adhesion and antibacterial activity of silver nanoparticles supported on graphene oxide sheets. *Colloids and Surfaces B: Biointerfaces*. 2014;113:115-24.
- [33] Hsu KC, Chen DH. Green synthesis and synergistic catalytic effect of Ag/reduced graphene oxide nanocomposite. *Nanoscale research letters*. 2014;9(1):484.
- [34] Mao A, Zhang D, Jin X, Gu X, Wei X, Yang G, et al. Synthesis of graphene oxide sheets decorated by silver nanoparticles in organic phase and their catalytic activity. *Journal of Physics and Chemistry of Solids*. 2012;73(8):982-6.
- [35] Tjoa V, Jun W, Dravid V, Mhaisalkar S, Mathews N. Hybrid graphene-metal nanoparticle systems: electronic properties and gas interaction. *Journal of Materials Chemistry*. 2011;21(39):15593-9.
- [36] Zhang R, Alecrim V, Hummelgård M, Andres B, Forsberg S, Andersson M, et al. Thermally reduced kaolin-graphene oxide nanocomposites for gas sensing. *Scientific reports*. 2015;5.
- [37] Tian J, Liu S, Zhang Y, Li H, Wang L, Luo Y, et al. Environmentally friendly, one-pot synthesis of Ag nanoparticle-decorated reduced graphene oxide composites and their application to photocurrent generation. *Inorganic chemistry*. 2012;51(8):4742-6.
- [38] Lin Y, Watson KA, Fallbach MJ, Ghose S, Smith Jr JG, Delozier DM, et al. Rapid, solventless, bulk preparation of metal nanoparticle-decorated carbon nanotubes. *ACS nano*. 2009;3(4):871-84.
- [39] Lee J, Novoselov KS, Shin HS. Interaction between metal and graphene: dependence on the layer number of graphene. *ACS nano*. 2010;5(1):608-12.
- [40] Wu T, Shen H, Sun L, Cheng B, Liu B, Shen J. Facile synthesis of Ag interlayer doped graphene by chemical vapor deposition using polystyrene as solid carbon source. *ACS applied materials & interfaces*. 2012;4(4):2041-7.
- [41] Chen J, Zheng X, Wang H, Zheng W. Graphene oxide-Ag nanocomposite: In situ photochemical synthesis and application as a surface-enhanced Raman scattering substrate. *Thin Solid Films*. 2011;520(1):179-85.
- [42] Gu H, Yang Y, Tian J, Shi G. Photochemical synthesis of noble metal (Ag, Pd, Au, Pt) on graphene/ZnO multihybrid nanoarchitectures as electrocatalysis for H₂O₂ reduction. *ACS applied materials & interfaces*. 2013;5(14):6762-8.
- [43] Wang LQ, Wu Y, Yang X. Enhanced Photocatalytic Properties of Ag-Modified Mg-Doped ZnO Nanocrystals Hybridized with Reduced Graphene Oxide Sheets. *Materials Science Forum: Trans Tech Publ*; p. 161-6.
- [44] Andryushina N, Stroyuk A, Ustavytska O, Kurys YI, Kuchmy SY, Koshechko V, et al. Graphene Oxide Composites with Silver Nanoparticles: Photochemical Formation and Electrocatalytic Activity in the Oxidation of Methanol and Formaldehyde. *Theoretical and Experimental Chemistry*. 2014;50(3):155-61.
- [45] Wu T, Liu S, Luo Y, Lu W, Wang L, Sun X. Surface plasmon resonance-induced visible light photocatalytic reduction of graphene oxide: using Ag nanoparticles as a plasmonic photocatalyst. *Nanoscale*. 2011;3(5):2142-4.

- [46] Li B, Zhang X, Chen P, Li X, Wang L, Zhang C, et al. Waveband-dependent photochemical processing of graphene oxide in fabricating reduced graphene oxide film and graphene oxide–Ag nanoparticles film. *RSC Advances*. 2014;4(5):2404-8.
- [47] Golsheikh AM, Huang NM, Lim HN, Zakaria R, Yin C-Y. One-step electrodeposition synthesis of silver-nanoparticle-decorated graphene on indium-tin-oxide for enzymeless hydrogen peroxide detection. *Carbon*. 2013;62:405-12.
- [48] Zhang X, Wang A, Ke R, Zhang S, Niu H, Mao C, et al. Electrochemical synthesis and photoelectrochemical properties of a novel RGO/AgNDs composite. *RSC Advances*. 2015;5(42):32994-3000.
- [49] Lee K, Ahmed MS, Jeon S. Electrochemical deposition of silver on manganese dioxide coated reduced graphene oxide for enhanced oxygen reduction reaction. *Journal of Power Sources*. 2015;288:261-9.
- [50] Mao S, Yu K, Cui S, Bo Z, Lu G, Chen J. A new reducing agent to prepare single-layer, high-quality reduced graphene oxide for device applications. *Nanoscale*. 2011;3(7):2849-53.
- [51] Gao W, Ran C, Wang M, Yao X, He D, Bai J. Understanding the growth mechanism of stabilizer-free Ag nanoparticles on reduced graphene oxide: the role of CO. *Journal of Nanoparticle Research*. 2013;15(6).
- [52] Zahed B, Hosseini-Monfared H. A comparative study of silver-graphene oxide nanocomposites as a recyclable catalyst for the aerobic oxidation of benzyl alcohol: Support effect. *Applied Surface Science*. 2015;328:536-47.
- [53] Wang MY, Shen T, Wang M, Zhang D, Chen J. One-pot green synthesis of Ag nanoparticles-decorated reduced graphene oxide for efficient nonenzymatic H₂O₂ biosensor. *Materials Letters*. 2013;107:311-4.
- [54] Tian Y, Wang F, Liu Y, Pang F, Zhang X. Green synthesis of silver nanoparticles on nitrogen-doped graphene for hydrogen peroxide detection. *Electrochimica Acta*. 2014;146:646-53.
- [55] Kumar S, Rai S. Spectroscopic studies of L-arginine molecule. *Indian J Pure Appl Phys*. 2010;48:251-5.
- [56] Fellahi O, Das MR, Coffinier Y, Szunerits S, Hadjersi T, Maamache M, et al. Silicon nanowire arrays-induced graphene oxide reduction under UV irradiation. *Nanoscale*. 2011;3(11):4662-9.
- [57] Zhang Y, Liu S, Wang L, Qin X, Tian J, Lu W, et al. One-pot green synthesis of Ag nanoparticles-graphene nanocomposites and their applications in SERS, H₂O₂, and glucose sensing. *Rsc Advances*. 2012;2(2):538-45.
- [58] Qu J-c, Ren C-l, Dong Y-l, Chang Y-p, Zhou M, Chen X-g. Facile synthesis of multifunctional graphene oxide/AgNPs-Fe₃O₄ nanocomposite: a highly integrated catalysts. *Chemical Engineering Journal*. 2012;211:412-20.
- [59] Theivasanthi T, Alagar M. Electrolytic synthesis and characterizations of silver nanopowder. *arXiv preprint arXiv:11110260*. 2011.
- [60] Dinh NX, Quy NV, Huy TQ, Le A-T. Decoration of Silver Nanoparticles on Multiwalled Carbon Nanotubes: Antibacterial Mechanism and Ultrastructural Analysis. *Journal of Nanomaterials*. 2015;2015.

- [61] Anpo M, Kamat PV. Environmentally benign photocatalysts: applications of titanium oxide-based materials: Springer Science & Business Media; 2010.
- [62] Saha S, Pal A, Kundu S, Basu S, Pal T. Photochemical green synthesis of calcium-alginate-stabilized Ag and Au nanoparticles and their catalytic application to 4-nitrophenol reduction. *Langmuir : the ACS journal of surfaces and colloids*. 2009;26(4):2885-93.
- [63] Marais E, Nyokong T. Adsorption of 4-nitrophenol onto Amberlite® IRA-900 modified with metallophthalocyanines. *Journal of hazardous materials*. 2008;152(1):293-301.
- [64] O'Connor OA, Young L. Toxicity and anaerobic biodegradability of substituted phenols under methanogenic conditions. *Environmental toxicology and chemistry*. 1989;8(10):853-62.
- [65] Dieckmann MS, Gray KA. A comparison of the degradation of 4-nitrophenol via direct and sensitized photocatalysis in TiO₂ slurries. *Water Research*. 1996;30(5):1169-83.
- [66] Oturan MA, Peiroten J, Chartrin P, Acher AJ. Complete destruction of p-nitrophenol in aqueous medium by electro-Fenton method. *Environmental Science & Technology*. 2000;34(16):3474-9.
- [67] Modirshahla N, Behnajady M, Mohammadi-Aghdam S. Investigation of the effect of different electrodes and their connections on the removal efficiency of 4-nitrophenol from aqueous solution by electrocoagulation. *Journal of hazardous materials*. 2008;154(1):778-86.
- [68] Canizares P, Saez C, Lobato J, Rodrigo M. Electrochemical treatment of 4-nitrophenol-containing aqueous wastes using boron-doped diamond anodes. *Industrial & engineering chemistry research*. 2004;43(9):1944-51.
- [69] Krishna R, Fernandes DM, Dias C, Ventura J, Ramana EV, Freire C, et al. Novel synthesis of Ag@Co/RGO nanocomposite and its high catalytic activity towards hydrogenation of 4-nitrophenol to 4-aminophenol. *International Journal of Hydrogen Energy*. 2015;40(14):4996-5005.
- [70] Ji Z, Shen X, Yang J, Zhu G, Chen K. A novel reduced graphene oxide/Ag/CeO₂ ternary nanocomposite: green synthesis and catalytic properties. *Applied Catalysis B: Environmental*. 2014;144:454-61.
- [71] Yang Y, Ren Y, Sun C, Hao S. Facile route fabrication of nickel based mesoporous carbons with high catalytic performance towards 4-nitrophenol reduction. *Green Chemistry*. 2014;16(4):2273-80.
- [72] Sahoo PK, Panigrahy B, Bahadur D. Facile synthesis of reduced graphene oxide/Pt-Ni nanocatalysts: their magnetic and catalytic properties. *RSC Advances*. 2014;4(89):48563-71.
- [73] Pradhan N, Pal A, Pal T. Silver nanoparticle catalyzed reduction of aromatic nitro compounds. *Colloids and Surfaces A: Physicochemical and Engineering Aspects*. 2002;196(2):247-57.
- [74] Li J, Liu C-y, Liu Y. Au/graphene hydrogel: synthesis, characterization and its use for catalytic reduction of 4-nitrophenol. *Journal of Materials Chemistry*. 2012;22(17):8426-30.

- [75] Adhikari B, Banerjee A. Catalytic properties of graphene–metal nanoparticle hybrid prepared using an aromatic amino acid as the reducing agent. *Materials Chemistry and Physics*. 2013;139(2):450-8.
- [76] Jana D, Dandapat A, De G. Anisotropic gold nanoparticle doped mesoporous boehmite films and their use as reusable catalysts in electron transfer reactions. *Langmuir : the ACS journal of surfaces and colloids*. 2010;26(14):12177-84.
- [77] Qiu L, Peng Y, Liu B, Lin B, Peng Y, Malik MJ, et al. Polypyrrole nanotube-supported gold nanoparticles: An efficient electrocatalyst for oxygen reduction and catalytic reduction of 4-nitrophenol. *Applied Catalysis A: General*. 2012;413:230-7.
- [78] Shi Z, Zhou H, Lu Y. Poly (tetrafluoroethylene)@ polyaniline/gold composite membranes: Preparation, characterization and application. *Colloids and Surfaces A: Physicochemical and Engineering Aspects*. 2012;393:153-9.
- [79] Sun T, Zhang Z, Xiao J, Chen C, Xiao F, Wang S, et al. Facile and green synthesis of palladium nanoparticles-graphene-carbon nanotube material with high catalytic activity. *Scientific reports*. 2013;3.
- [80] Li X, Wang X, Song S, Liu D, Zhang H. Selectively deposited noble metal nanoparticles on Fe₃O₄/graphene composites: stable, recyclable, and magnetically separable catalysts. *Chemistry*. 2012;18(24):7601-7.
- [81] Wu T, Ma J, Wang X, Liu Y, Xu H, Gao J, et al. Graphene oxide supported Au–Ag alloy nanoparticles with different shapes and their high catalytic activities. *Nanotechnology*. 2013;24(12):125301.
- [82] Liu R, Zhao Q, Li Y, Zhang G, Zhang F, Fan X. Graphene supported Pt/Ni nanoparticles as magnetically separable nanocatalysts. *Journal of Nanomaterials*. 2013;2013.
- [83] Kuroda K, Ishida T, Haruta M. Reduction of 4-nitrophenol to 4-aminophenol over Au nanoparticles deposited on PMMA. *Journal of Molecular Catalysis A: Chemical*. 2009;298(1):7-11.
- [84] Zhang L, Wu T, Xu X, Xia F, Na H, Liu Y, et al. Magnetic bimetallic nanoparticles supported reduced graphene oxide nanocomposite: Fabrication, characterization and catalytic capability. *Journal of Alloys and Compounds*. 2015;628:364-71.
- [85] Ji Z, Shen X, Xu Y, Zhu G, Chen K. Anchoring noble metal nanoparticles on CeO₂ modified reduced graphene oxide nanosheets and their enhanced catalytic properties. *Journal of colloid and interface science*. 2014;432:57-64.
- [86] Xiao W, Zhang Y, Liu B. Raspberry-like SiO₂@ Reduced Graphene Oxide@ AgNP Composite Microspheres with High Aqueous Dispersity and Excellent Catalytic Activity. *ACS applied materials & interfaces*. 2015;7(11):6041-6.
- [87] Joshi MK, Pant HR, Kim HJ, Kim JH, Kim CS. One-pot synthesis of Ag-iron oxide/reduced graphene oxide nanocomposite via hydrothermal treatment. *Colloids and Surfaces A: Physicochemical and Engineering Aspects*. 2014;446:102-8.
- [88] Xiong R, Wang Y, Zhang X, Lu C, Lan L. In situ growth of gold nanoparticles on magnetic γ -Fe₂O₃@ cellulose nanocomposites: a highly active and recyclable catalyst for reduction of 4-nitrophenol. *RSC Advances*. 2014;4(13):6454-62.

- [89] Gu W, Deng X, Jia X, Li J, Wang E. Functionalized graphene/Fe₃O₄ supported AuPt alloy as a magnetic, stable and recyclable catalyst for a catalytic reduction reaction. *Journal of Materials Chemistry A*. 2015;3(16):8793-9.
- [90] Zeng J, Zhang Q, Chen J, Xia Y. A comparison study of the catalytic properties of Au-based nanocages, nanoboxes, and nanoparticles. *Nano letters*. 2009;10(1):30-5.
- [91] Pal T, Sau TK, Jana NR. Reversible formation and dissolution of silver nanoparticles in aqueous surfactant media. *Langmuir : the ACS journal of surfaces and colloids*. 1997;13(6):1481-5.

CHAPTER 3

Reduced graphene oxide decorated with nickel nanoparticles

3.1. Introduction

Graphene, one of the important materials in recent years, has attracted the attention of many scientists. This exciting material shows outstanding thermal, mechanical and electrical properties, which make it a potential material for possible applications in various fields [1]. The attention towards graphene has expanded to many areas of chemical applications, including adsorption and photocatalysis [2], heterogeneous catalysis [3], and biosensors [4]. Properties such as high surface area and an absence of mass transfer barriers make this material extremely suitable in catalysis as a new form of carbon material [5,6]. Up to now, numerous methods have been developed for the production of graphene sheets including micromechanical exfoliation, thermal expansion of graphite, [7, 8] chemical vapour deposition [9, 10] and solution-based chemical reduction of exfoliated graphite oxide to reduced graphene oxide (rGO) [11, 12]. Among these methods, the solution-based chemical reduction of exfoliated graphite oxide is the most suitable approach for the efficient production of graphene sheets owing to its low-cost and massive scalability [13] and an affordable technique for the large-scale production of graphene sheets.

The presence of oxygen functional groups in graphene oxide (GO) can act as nucleation centres or anchoring sites for the landing of nanoparticles [7, 14], limiting the nanoparticles growth and improving the stability and dispersion of nanoparticles on rGO. At the same time, these nanoparticles can help to enlarge the interplanar spacing of the rGO, avoid them aggregating on the graphene structure, and maintain the excellent properties of individual rGO nanosheets [8, 15]. Some of the current studies on graphene-based nanocomposites have shown that a synergistic combination of metal/metal oxide nanoparticles with graphene sheets enhances their properties and performances, which make them utilizable in various fields of promising applications [16, 17].

In this chapter, we will describe a simple chemical method for decorating rGO sheets with nickel nanoparticles (rGO/Ni NPs). The rGO/Ni NPs is prepared by simultaneous reduction of GO and NiCl₂ salt in water at room temperature. To examine the catalytic activity of the Ni NPs, the resulting nanocomposite was applied for the reduction of 4-nitrophenol to 4-aminophenol using NaBH₄ as a reducing agent.

3.2. Reduced graphene oxide decorated with nickel/nickel oxide nanoparticles

Nickel nanoparticles (Ni NPs) have received considerable attention recently because of their low cost and remarkable catalytic performances in hydrogenation of nitrobenzene and nitrophenol, reduction of oxygen and oxidation of olefins [18-20], magnetic devices [21], batteries [22], catalysts [23], capacitors [24], etc. Regarding electrochemical applications, nickel-based nanomaterials are mainly employed in alkaline medium leading to $\text{Ni}(\text{OH})_2$ and NiOOH species. To facilitate catalyst recovery and limit nanoparticles aggregation, Ni NPs are commonly dispersed onto solid matrices to prepare heterogeneous nickel catalysts. The conversion of metallic nickel to those electroactive species is directly related to the morphological characteristics of the nickel nanomaterial. Thus, control and knowledge of the characteristics of the nickel nanoparticles are key-factors for their further application [25-27].

Many reports, however, relate a loss of performance during some applications [28, 29]. This deleterious effect can be minimized by combining metal nanoparticles with graphene, which avoid significant changes in the nickel morphology during the reduction process [28-30]. Besides enhanced stability, the use of graphene to prepare nanocomposites leads to higher conductivity and surface area, increasing its performance in many applications [31, 32]. Nickel nanoparticles/graphene nanocomposites, have many applications like sensors [30], electrodes for batteries [33], catalyst [34], and materials for hydrogen storage [30].

The physical properties of graphene are significantly altered when decorated with nickel nanoparticles because of the chemical interaction between graphene and nickel is due to hybridization of the metal d-electrons with the π -orbitals of graphene [31]. This interaction causes a smaller separation between the nickel surface and graphene (0.21 nm) than the typical van der Waals gap-distance between graphitic layers (0.33 nm). This chemical interaction is stronger than for other group of metals as shown in **Figure 3.1** [35].

Therefore, a lot of works reported recently deals with the synthesis of nickel nanoparticles/graphene nanocomposites. The most common experimental route to produce these nanocomposites is based on the direct reduction of both nickel salt and graphene oxide [32] or the reduction of nickel salt in the presence of graphene. Thermal decomposition of precursors [36] and electrochemical deposition [37] have also been commonly employed. It is

well known that different synthetic approaches to nanocomposite materials lead to important modifications in their structure, morphology and properties.

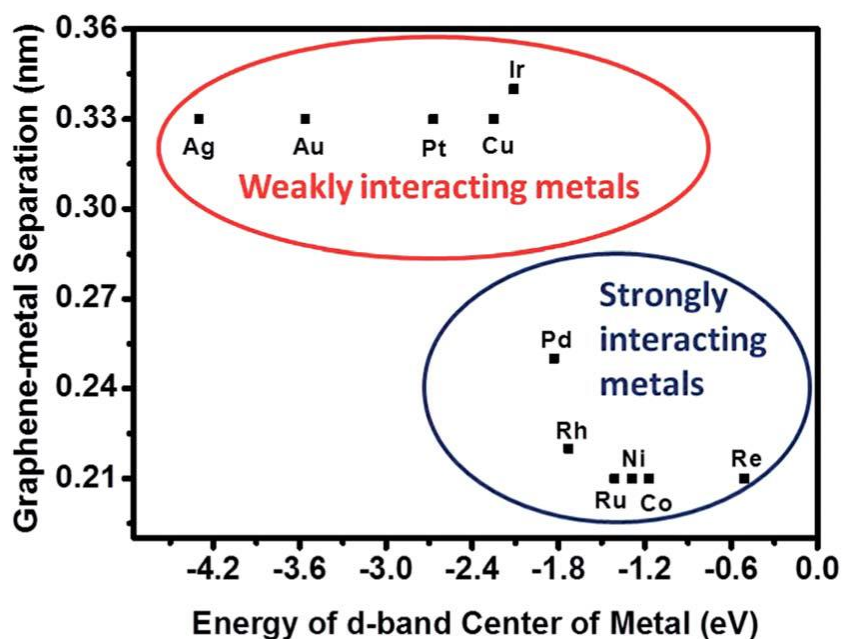


Figure 3.1: Illustration of the correlation of graphene–metal separation with the energy of the d-band centre of the transition metal. A transition from ‘weak’ to ‘strong’ interaction occurs at a d-band centre position ~ 2 eV below the Fermi-level [35].

However, these synthetic routes usually use a considerable quantity of organic solvents such as ethylene glycol [38], *N,N*-dimethylformamide [39] and *N*-methylpyrrolidone [28], or surfactant templates such as benzenesulfonate [40], which inevitably leads to the difficulty in the removal of organic solvents or surfactant templates, a rise in cost, and potential environmental pollution, and consequently, infeasibility of the large-scale production.

Therefore, we have developed a suitable synthetic approach, which can be performed in the absence of organic solvents for the reduction of both nickel salt and graphene oxide without using sophisticated equipments, long preparation time, and high temperature treatment, is fundamental to produce nickel/graphene composites.

Previous methods developed for the deposition of nickel/nickel oxide on GO, rGO or graphene are summarized in **Table 3.1**.

Table 3.1: Graphene/Ni NPs or Ni(OH)₂ composites, conditions and applications

Composite	Method	Source of Ni NPs	Conditions	Applications	Ref.
Graphene/NiO	Hydrothermal	C ₄ H ₁₄ NiO ₈	160°C, 16h	Anode in Li-ion batteries	[33]
Membrane Graphene/NiO	Thermal treatment	Ni (NO ₃) ₂	500°C, 5 h	Electrochemical energy storage	[41]
rGO/Ni	Hydrothermal	NiCl ₂ .6H ₂ O	100°C, 3 h	Reduction of 4-NP	[34]
rGO–NiO	Solvothermal	Ni(NO ₃) ₂	180°C, 12 h	Supercapacitors	[42]
rGO- Ni(OH) ₂	Hydrothermal	Ni(NO ₃) ₂	180°C, 12 h.	Electrochemical energy storage	[28]
rGO–NiO	Solvothermal	NiCl ₂ .6H ₂ O	100°C, 24 h	Supercapacitors	[43]
rGO–NiO	Solvothermal	NiCl ₂ .6H ₂ O	100°C, 24 h	Anode in Li-ion batteries	[44]
GO-NiAc	Photothermal	C ₄ H ₁₄ NiO ₈	exposure to focused sunlight	Nonenzymatic glucose sensor	[45]
RGO-Ni NPs	Hydrothermal	NiCl ₂ .6H ₂ O	100°C, 22 h	Bio-separation	[46]
GO-NiFe ₂ O ₄	Hydrothermal	NiSO ₄ .6H ₂ O	180°C, 10 h	Degradation of organic dyes	[47]
Ni/graphene aerogel	Hydrothermal	NiSO ₄ .6H ₂ O	180°C ,12 h	Electrocatalysis	[48]
rGO-Ni(OH) ₂	Hydrothermal	nickel foam	180°C ,12 h	Supercapacitors	[49]
rGO/Co.Ni NPs	Solvothermal	NiCl ₂ .6H ₂ O	RT, ammonia borane	Hydrogen generation	[50]

Composite	Method	Source of Ni NPs	Conditions	Applications	Ref.
rGO-Ni(OH) ₂	Hydrothermal	Ni(NO ₃) ₂ ·6H ₂ O	180°C, 10 h	Supercapacitors	[51]
Ni(OH) ₂ /G sheets	Hydrothermal	NiSO ₄ ·7H ₂ O	95°C, 16 h.	Supercapacitors	[52]
NiCo ₂ S ₄ -rGO	Hydrothermal	Ni(OAc) ₂ ·6H ₂ O	180°C, 12 h	Oxygen reduction reaction (ORR)	[53]
rGO/Pt-Ni	Chemical reduction	Ni(NO ₃) ₂ ·6H ₂ O	110°C, 3 h	Reduction of p-nitrophenol	[54]
Graphene/NiO	Electrochemical	Ni(NO ₃) ₂ ·6H ₂ O	-1.2, 0 V, scan rate 50 mVs ⁻¹ , 20 cycles	Nonenzymatic glucose sensors	[55]
Ni(OH) ₂ -rGO-MWCNT	Electrochemical	NiCl ₂ ·6H ₂ O	-1.1 V for 15 s	Nonenzymatic glucose sensing, H ₂ O ₂ sensing	[37]
Ni-rGO	Hydrothermal	NiCl ₂ ·6H ₂ O	380°C, 1 h	Reduction of Cr(VI)	[56]
Pt/Ni-G	Chemical reduction	NiSO ₄	N ₂ H ₄ ·H ₂ O, KOH	Reduction of p-nitrophenol	[57]
Ni(OH) ₂ /CoO/rGO	Solvothermal	Ni(CH ₃ COO) ₂ ·4H ₂ O	160°C, 6 h.	Supercapacitors	[58]
Ni-rGO	Microwave-assisted method	Ni(NO ₃) ₂ ·6H ₂ O	microwave irradiation (300 W) for 20 min	Nonenzymatic glucose sensing	[59]

Ji and co-workers [34] synthesized reduced graphene oxide/Ni (rGO/Ni) nanocomposites with different morphologies using a simple method. In this approach, a mixture of nickel chloride (NiCl_2) and graphene oxide (GO) was reduced with hydrazine hydrate at $100\text{ }^\circ\text{C}$ for 3 h under N_2 atmosphere. SEM and TEM images clearly showed that Ni nanoparticles are densely and uniformly distributed on the surfaces of rGO sheets with an average size of 2–4 nm (**Figure 3.1**).

The catalytic activity of the resulting rGO/Ni nanocomposites was investigated for the reduction of p-nitrophenol by NaBH_4 . It was found that the nanocomposites exhibit higher catalytic activity compared with the unsupported Ni nanoparticles [34].

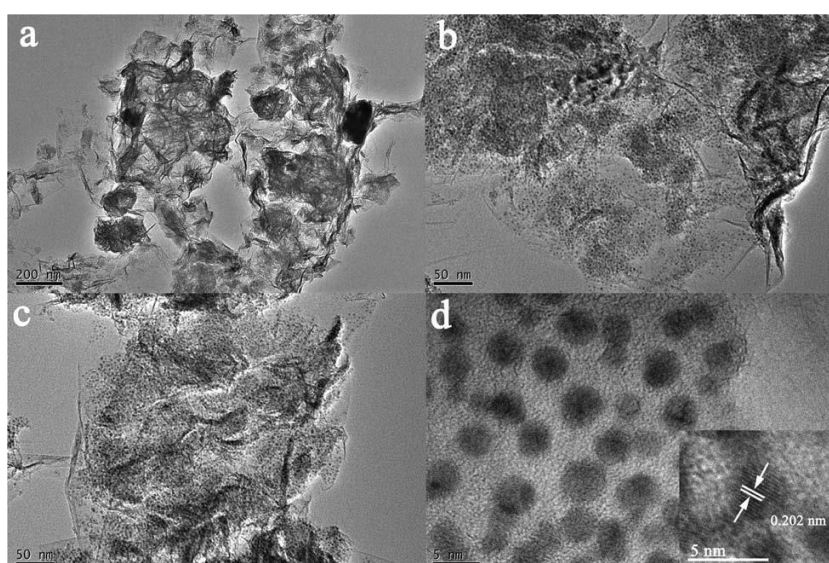


Figure 3.1: Typical (a)–(c) TEM and (d) HRTEM images of the rGO/Ni nanocomposites [34].

Yang et al. [42] have used a simple solvothermal route starting with graphite oxide to prepare rGO-NiO composites. Nickel nitrate $[\text{Ni}(\text{NO}_3)_2 \cdot 6\text{H}_2\text{O}]$ mixed with GO was dispersed in DMF and then heated at $180\text{ }^\circ\text{C}$ for 12 h in an autoclave. The dried RGO-Ni(OH)₂ composites were calcined at $250\text{ }^\circ\text{C}$ for 4 h in air to obtain the final black coloured product, the rGO-NiO composites. The authors found that the electrochemical performance of the composites could be affected by the mass ratio between rGO and NiO and that rGO sheets were uniformly covered with NiO nanoparticles to form a three-dimensional network structure (flower), the same as the pure NiO, but with thicker petals (**Figure 3.2**). When it was published the

composite exhibited one of the highest specific capacitance of $576 \text{ F} \cdot \text{g}^{-1}$ at $1 \text{ A} \cdot \text{g}^{-1}$, compared with pure NiO ($240 \text{ F} \cdot \text{g}^{-1}$) and pure rGO ($98 \text{ F} \cdot \text{g}^{-1}$) [42].

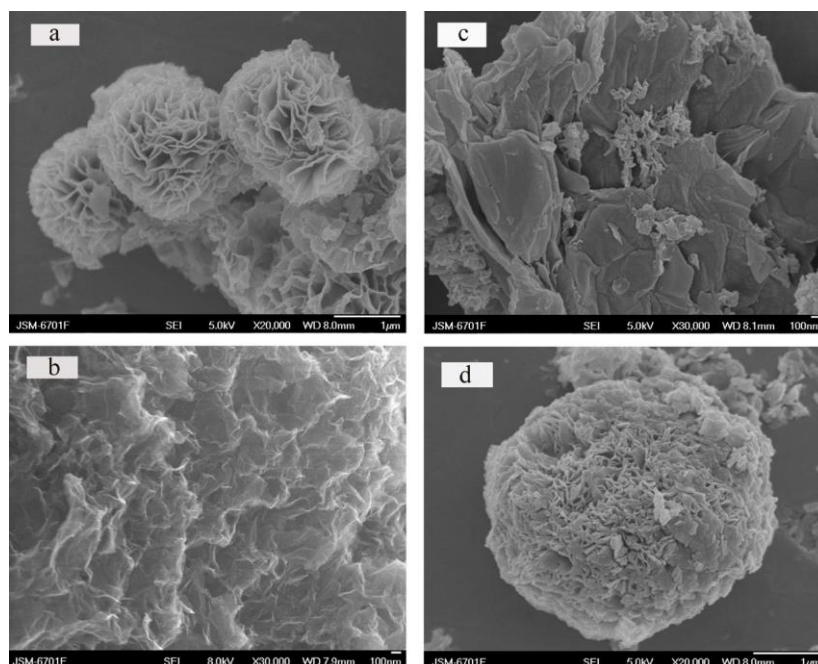


Figure (3.2): FESEM images of pure NiO (a) pure rGO, and (b) rGO–NiO composites with different mass ratios of NiO to rGO up to 79:21 (c) and 63.8:36.2 (d) [42].

Zhu et al. [43] have prepared a rGO/NiO composite by homogeneous co-precipitation and subsequent annealing.

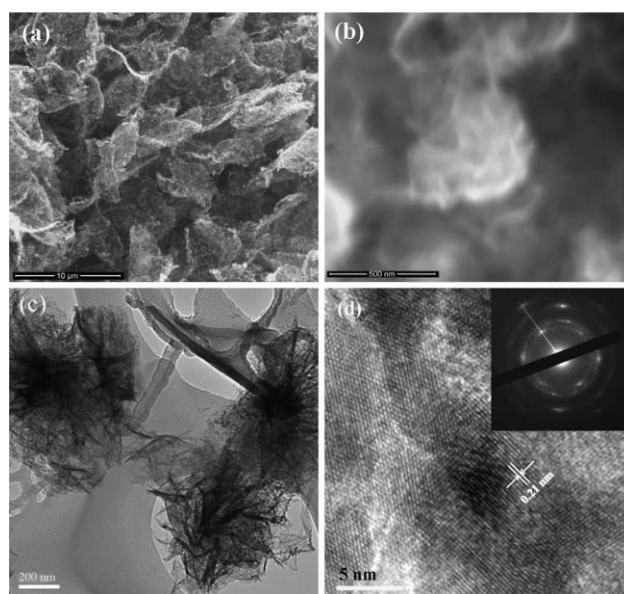


Figure 3.3: SEM and TEM images of the rGO/NiO [43].

Urea and NiCl_2 solutions were slowly and sequentially added to graphene oxide and heated at 90°C for 1.5 h. The mixture was cooled down to room temperature and hydrazine hydrate was added to the mixture and refluxed at 100°C for 24 h in an oil bath so that both graphene oxide and nickel oxide were reduced. The as-prepared product was annealed at 400°C for 3 h under nitrogen atmosphere in order to obtain rGO/NiO composite. Detailed characterizations showed that NiO particles have a nanosheet-based microsphere structure and are anchored uniformly on the surface of reduced graphene oxide platelets **Figure 3.3**. The rGO/NiO-based supercapacitors exhibit high specific capacitance of about $670 \text{ F} \cdot \text{g}^{-1}$ at $1 \text{ A} \cdot \text{g}^{-1}$ and an enhanced rate capability for electrochemical supercapacitors [43].

Sahoo et al. [54] have demonstrated a simplistic *in situ* one-step reduction approach for the synthesis of rGO/Pt–Ni nanocatalysts with different atomic ratios of Pt and Ni, without using any capping agent. The nanocatalysts were synthesized by a one-step chemical reduction method in the absence of capping agents.

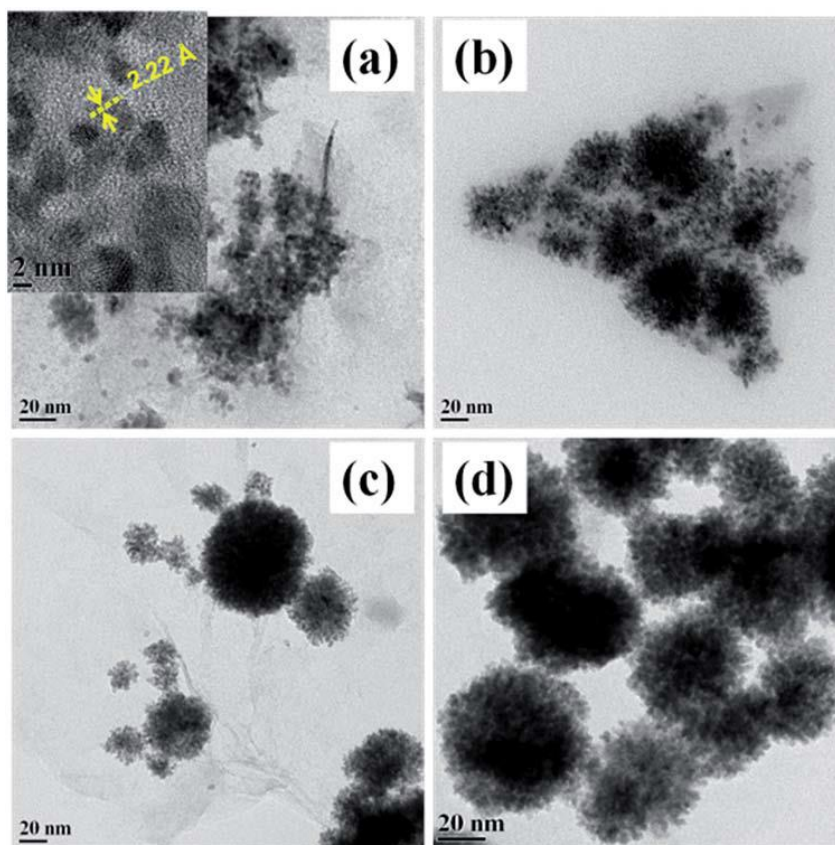


Figure (3.4): TEM images of rGO/Pt–Ni nanocatalysts at Pt–Ni different atomic ratios of (a), 25:75 (b) 33:67, (c) 50:50 and (d) bare Pt–Ni. Inset (a) shows a HRTEM image of the RGO/Pt–Ni nanocatalyst with an atomic ratio 25:75 [54].

The required amounts of $\text{H}_2\text{PtCl}_6 \cdot 6\text{H}_2\text{O}$ and $\text{Ni}(\text{NO}_3)_2 \cdot 6\text{H}_2\text{O}$ were dissolved in ethylene glycol (EG). This salt solution was added to the suspension of GO. Consequently, hydrazine hydrate and NaOH (made with EG) were added, and this mixture was kept in an ultrasonic bath for 10 min. Then, this mixture was heated at 110°C for 3 h under a N_2 atmosphere. The rGO/Pt–Ni nanocatalysts have different Pt–Ni atomic ratios as shown in **Figure 3.4**, each consisting of highly interconnected/aggregated crystallites with an average mean particle diameter of approximately 3–4 nm. The results indicate that the rGO/Pt–Ni nanocatalysts display a superparamagnetic nature at room temperature for all compositions. Furthermore, the catalytic activities of the rGO/Pt–Ni nanocatalysts were investigated by analyzing the reduction of p-nitrophenol, and the reduction rate was found to depend on the Pt to Ni ratio [54].

Liu et al. [57] have synthesized Pt/Ni-G hybrids by a chemical reduction method. Graphene oxide (GO) was dispersed in Tannin (TA) aqueous solution under sonication. Then, H_2PtCl_6 and NiSO_4 were added to the TA-GO solution under nitrogen atmosphere. Then, $\text{N}_2\text{H}_4 \cdot \text{H}_2\text{O}$ and KOH solutions were injected into the mixture. The solution turned black immediately and was kept under stirring. Finally, the product was isolated, washed with ethanol and deionized water for purification purposes [57]. TEM imaging showed that spherical nanoparticles were homogeneously dispersed on the surfaces of rGO. The size of the nanoparticles was in the range of 12–19 nm, with a mean size of 15.4 nm (**Figure 3.5**).

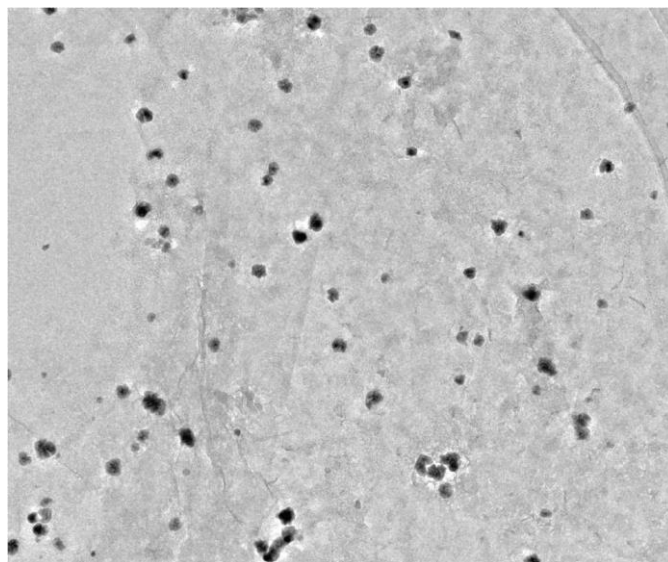


Figure 3.5: TEM image and size distribution of Pt/Ni NPs decorated on graphene sheets [57].

The Pt/Ni-G hybrids exhibited an excellent catalytic activity for the reduction of aromatic nitro compounds, and could be easily separated from the reaction mixture by applying an external magnetic field [57].

In the following section, I will describe our results on the preparation, characterization and application of reduced graphene oxide/Ni NPs nanocomposite.

3.3. Reduced graphene oxide decorated with Ni NPs (rGO/Ni NPs)

In this work, we describe an environmentally friendly, one-pot strategy toward rapid preparation of rGO-Ni NPs. The formation of rGO-Ni NPs is accomplished by directly heating a mixture of GO and $\text{NiCl}_2 \cdot 6\text{H}_2\text{O}$ aqueous solution at 100°C for 24 h under stirring without the extra introduction of any reducing agent. The central idea of this approach is that GO serves as a reducing agent for the formation of Ni NPs while GO can be converted into rGO at the same time. GO nanosheets were first produced from natural graphite powder by an improved Hummers and Offeman method [60] described in the **Experimental Part** (§ 2). A homogeneous yellow brown suspension of GO sheets (1 mg/mL) in water was achieved by ultrasonication for 3 h. Then, 5 mL of $\text{NiCl}_2 \cdot 6\text{H}_2\text{O}$ aqueous solution (0.079 M) was added to (1 mg/mL) homogeneous water suspension of GO nanosheets. The mixture was kept under stirring for 24 h at 100°C . The resulting black precipitate was separated from the aqueous supernatant by centrifugation at 14 000 rpm for 30 min. After washing thoroughly with Milli-Q water and absolute ethanol to remove any impurities, the precipitate was dried in an oven at 50°C for 24 h to yield rGO/Ni NPs (**Figure 3.6**).

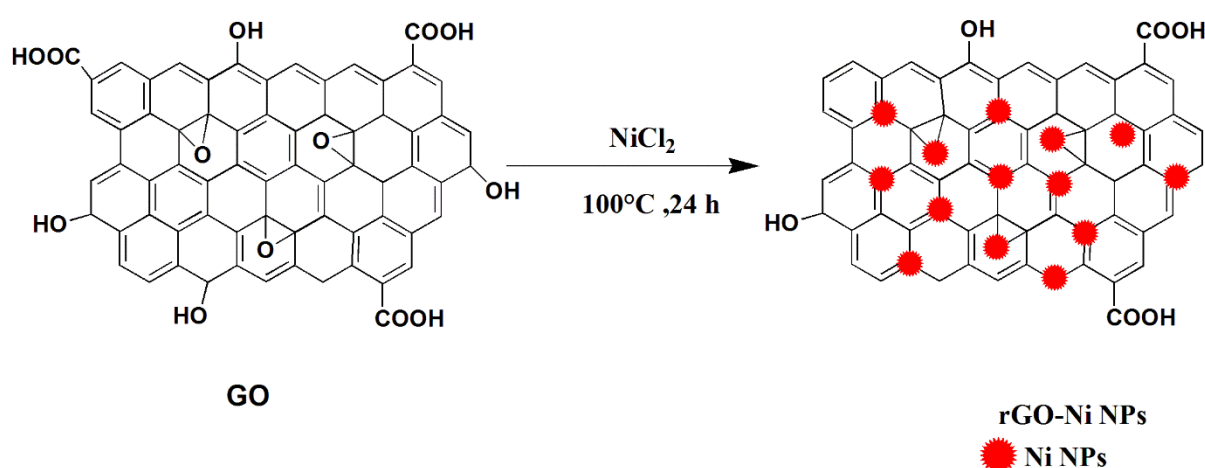


Figure 3.6: Schematic diagram for synthesis of rGO/Ni NPs.

The success of the reaction was confirmed by UV-Vis absorption spectra (**Figure 3.7**). The UV-Vis spectra show clearly that the absorption peak red-shifted from 228 to 262 nm upon

reaction with NiCl₂ at 100°C for 24 h; the 228 nm peak is due to the $\pi \rightarrow \pi^*$ transition of C=C bonds in sp² region (**Figure 3.7**). The result suggests that the GO nanosheets have been reduced and that the electronic conjugation within the GO nanosheets was restored upon reaction with NiCl₂ at 100°C.

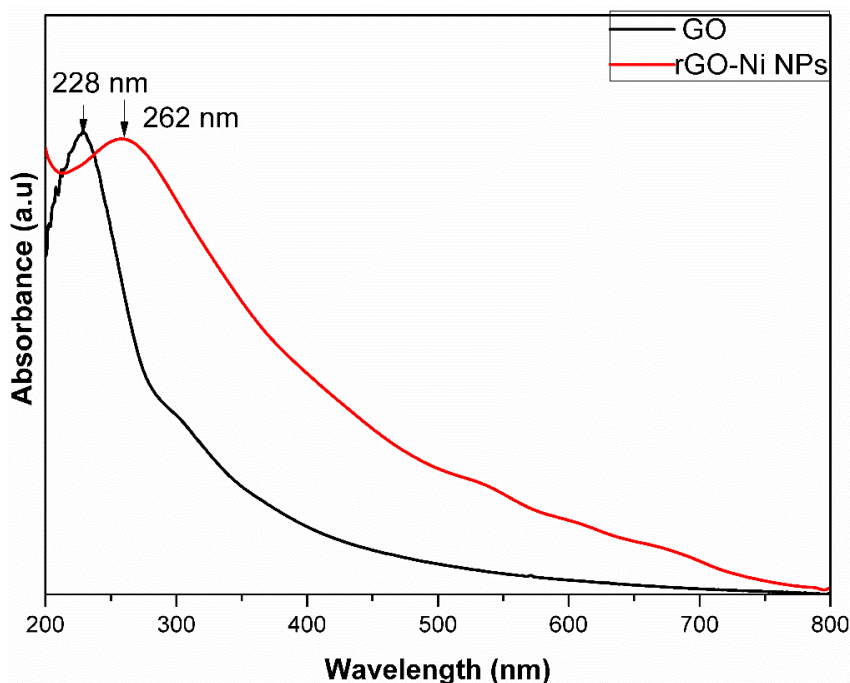


Figure 3.7: UV-Vis absorption spectra of GO before (black) and after (red) reduction with NiCl₂ at 100°C for 24 h.

X-ray photoelectron spectroscopy (XPS) analysis gives further information on the chemical transformations between GO and nickel nanoparticles. **Figure 3.8** depicts the survey XPS spectra of GO and rGO-Ni NPs. We can recognize in both GO and rGO-Ni NPs two peaks due to C_{1s} and O_{1s}. The C/O ratio is higher in rGO-Ni NPs, suggesting that the sp² network has been restored during the process [61, 62] (& **Table 3.2**). Moreover, a new peak due to Ni_{2p3/2} appeared in the XPS survey of rGO-Ni NPs, which indicates that Ni NPs have been anchored on the graphene sheets [46, 49].

The C_{1s} high resolution spectrum of GO consists of three components that correspond to C–C (285 eV), C–O (287 eV), and C=O (288.4 eV) clearly indicates a considerable degree of oxidation (**Figure 3.9**).

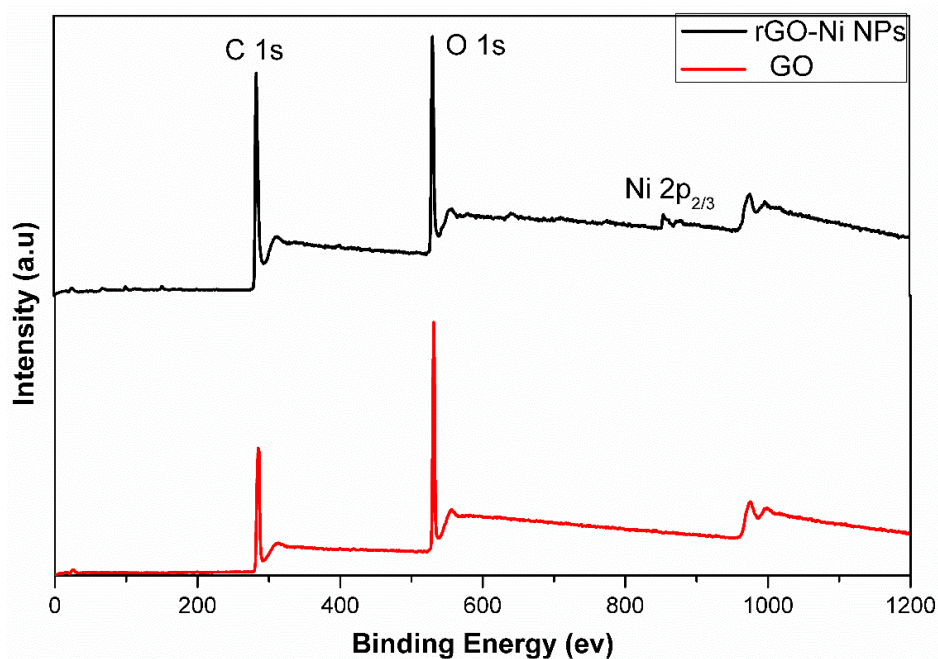


Figure 3.8: XPS survey spectra GO and rGO-Ni NPs.

In contrast, the XPS high resolution C_{1s} spectrum of rGO-Ni NPs comprises a major peak due to C=C (283.6 eV), and smaller peaks assigned to C-C/C-H (285.6 eV), C=O (287.8 eV) and HO-C=O (290 eV). The bands due to C=O and C-O bonds distinctly decrease and C=C peak has been restored during the process; this suggests a considerable deoxygenation after chemical reduction in the presence of nickel chloride [49, 50].

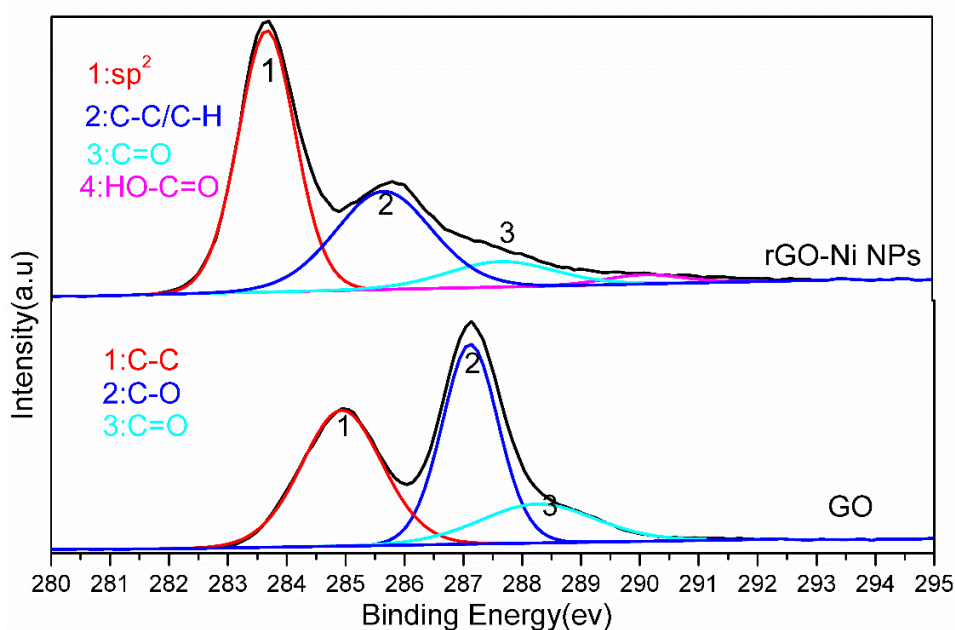


Figure 3.9: High resolution C_{1s} XPS spectra of GO and rGO-Ni NPs.

The Ni_{2p} XPS spectrum exhibits two main peaks at 855.1 and 873 eV, corresponding to Ni_{2p_{3/2}} and Ni_{2p_{1/2}}, respectively with a spin-energy separation of 18 eV [49] (**Figure 3.10**). The peaks at 855.1 eV and 573 eV correspond to that of the Ni(OH)₂ phase and also the peak at 859.4 eV corresponds to that of Ni(OH)₂ [46, 50, 63].

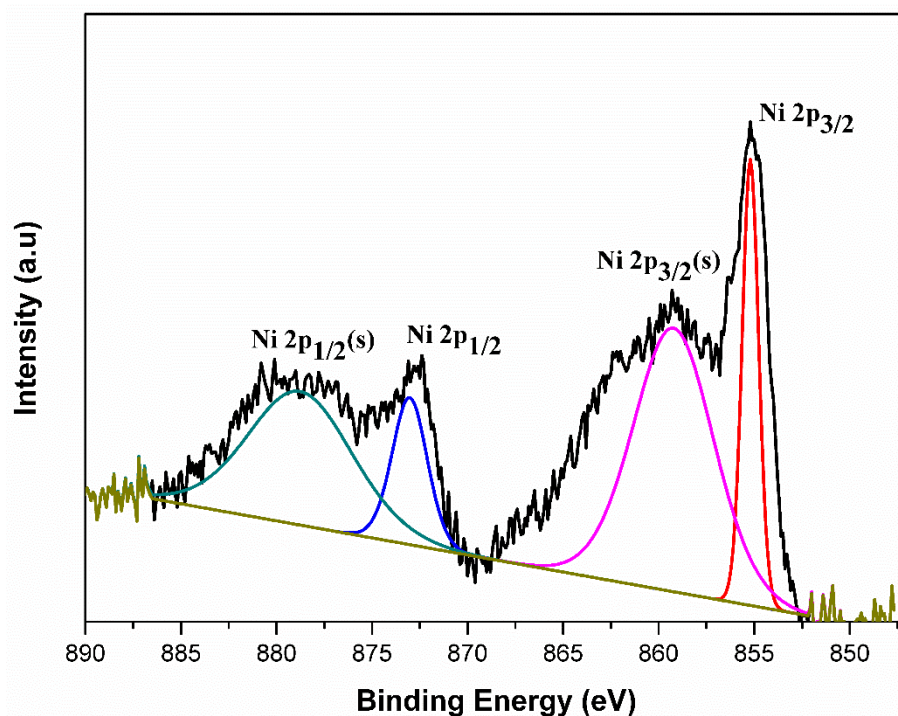


Figure 3.10: High resolution XPS spectra of Ni 2p rGO-Ni NPs.

The weight percentage of each element was analyzed by CasaXPS software (**Table 3.2**).

Table 3.2: Weight percentage of each element in GO, rGO-Ni NPs.

Material	Weight percentage	Ratio C/O
GO	C1s=71.31 O1s=28.69	2.4
rGO	C1s =77.01 O1s =22.14 Ni 2p =0.85	3.47

The weight percentage of C_{1s} increases and that of O_{1s} decreases after the reaction of GO with nickel chloride at 100°C for 24 h. The ratio of carbon to oxygen (C/O) increases from 2.4 for

GO to 3.47 for rGO-Ni NPs, which means that GO has been reduced by chemical reaction with nickel chloride.

Raman spectroscopy is a non-destructive technique adopted for the investigation of the layer, structure, doping and disorder of graphene-based materials. The presence of rGO in the rGO-Ni NPs composite is further confirmed by Raman spectroscopy as shown in **Figure 3.11**. The ratio of G band ($\sim 1565\text{ cm}^{-1}$) corresponding to the in-plane bond-stretching motion of the pairs of Csp^2 atoms (the E_{2g} phonons) and the D band ($\sim 1314\text{ cm}^{-1}$) originating from the breathing modes of rings or κ -point phonons of A_{1g} symmetry is usually used to semi-quantitatively determine the reduction extent [44, 46]. The G band is shifted from 1600 cm^{-1} in GO to 1565 cm^{-1} in rGO/Ni NPs, close to the value of the pristine graphite, confirming the reduction of GO [34, 64]. The slight increase of the $I_{\text{D}}/I_{\text{G}}$ ratio in rGO/Ni NPs (0.9 vs. 0.72 for GO) suggests a decrease in the size and an increase in the number of the sp^2 domains upon reduction by nickel chloride. This indicates that GO is significantly reduced and forms a high level of disordered structure during its chemical reduction in the presence nickel chloride [42]. The second scattering Raman mode, namely the 2D band at 2915 cm^{-1} , whose shape and position depend strongly on the structure of graphene, is usually used to identify the number of graphene layers (<10 layers) [64]. However, this peak becomes broader and without any shift, suggesting randomly aggregated graphene layers in the obtained hybrid.

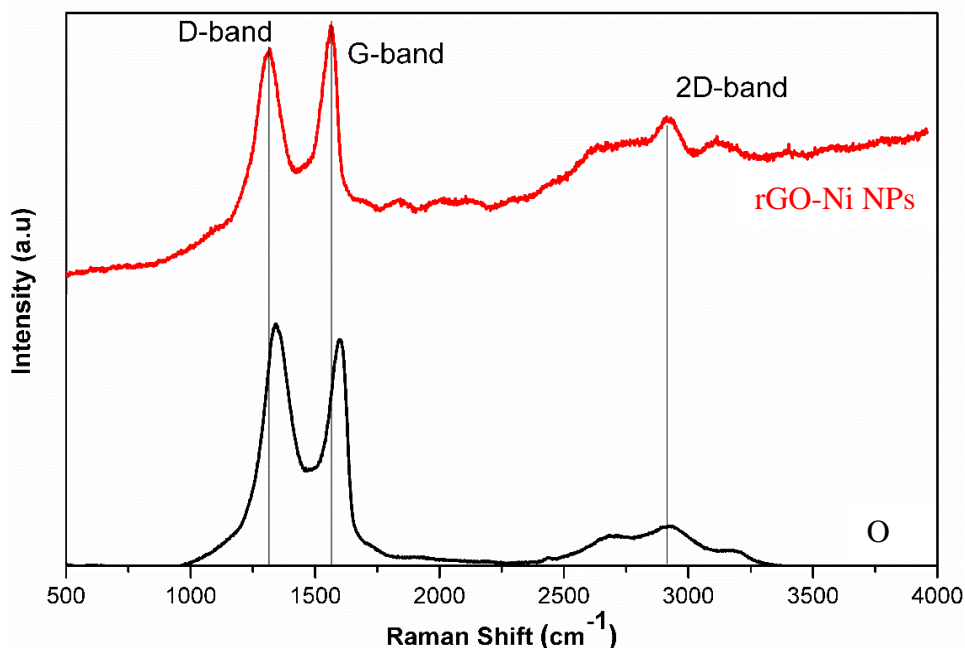


Figure 3.11: Raman spectra of GO and rGO-Ni NPs.

The conversion of oxygen-containing functional groups (carboxyl, epoxide and hydroxyl groups) on the surface of GO after the chemical reduction process are characterized by FT-IR spectra (**Figure 3.12**).

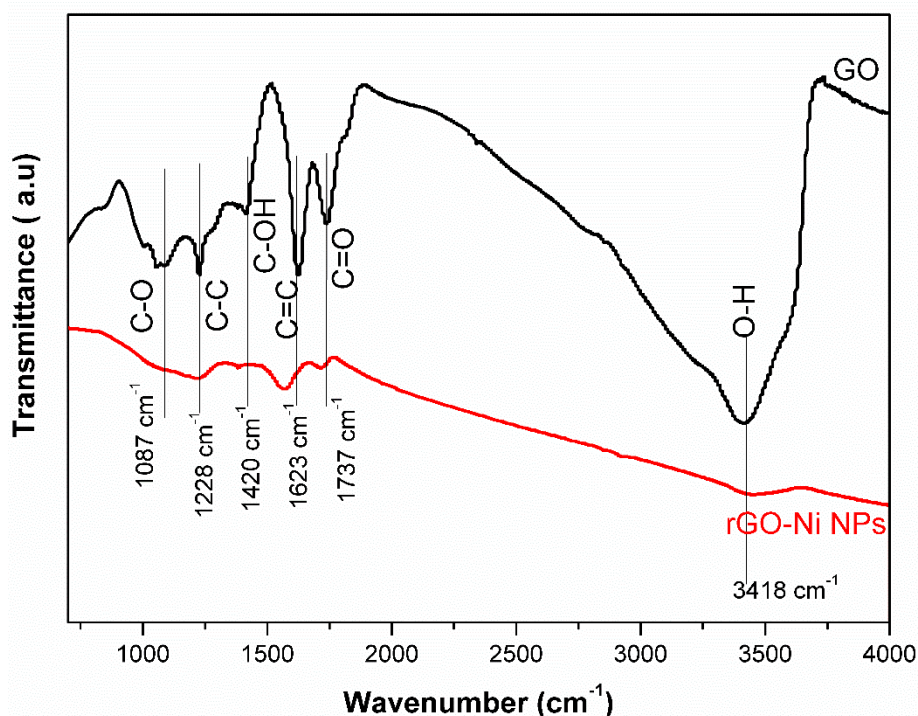


Figure 3.12: FTIR spectra of the as-prepared GO and rGO-Ni NPs.

The FTIR spectra of GO and the reduction product showed remarkable differences. For GO, a strong and broad absorption band at 3418 cm^{-1} ascribed to O–H stretching vibrations, and the C=O stretching of COOH groups (1737 cm^{-1}) situated at the edges of GO sheets are observed. The absorption at 1420 cm^{-1} may be due to tertiary C–OH groups. The absorption band at 1080 cm^{-1} is attributed to stretching vibrations of C–O groups, while the band at 1623 cm^{-1} is assigned to C=C stretching vibrations as part of the ring breathing mode in the GO skeleton. The band at 1228 cm^{-1} is attributed to the stretching vibration of C–C [47, 48]. By contrast, for the rGO-Ni NPs, the O–H band is decreased, while the skeletal C=C vibration band at 1623 cm^{-1} is shifted to 1587 cm^{-1} , and the C–C band at 1228 cm^{-1} shifts to 1233 cm^{-1} . Moreover, the C=O band at 1737 cm^{-1} decreases and shifts to 1717 cm^{-1} , and the C–OH and C–O bands of GO disappear also, indicating the reduction of GO to rGO during the chemical reaction with nickel chloride at 100°C [50].

The as-prepared composite was characterized using FESEM, TEM and X-ray energy dispersive spectroscopy (EDX) (**Figure 3.13**). In FESEM images, aggregated and crumpled rGO sheets were observed with no clear evidence for the presence of Ni nanoparticles.

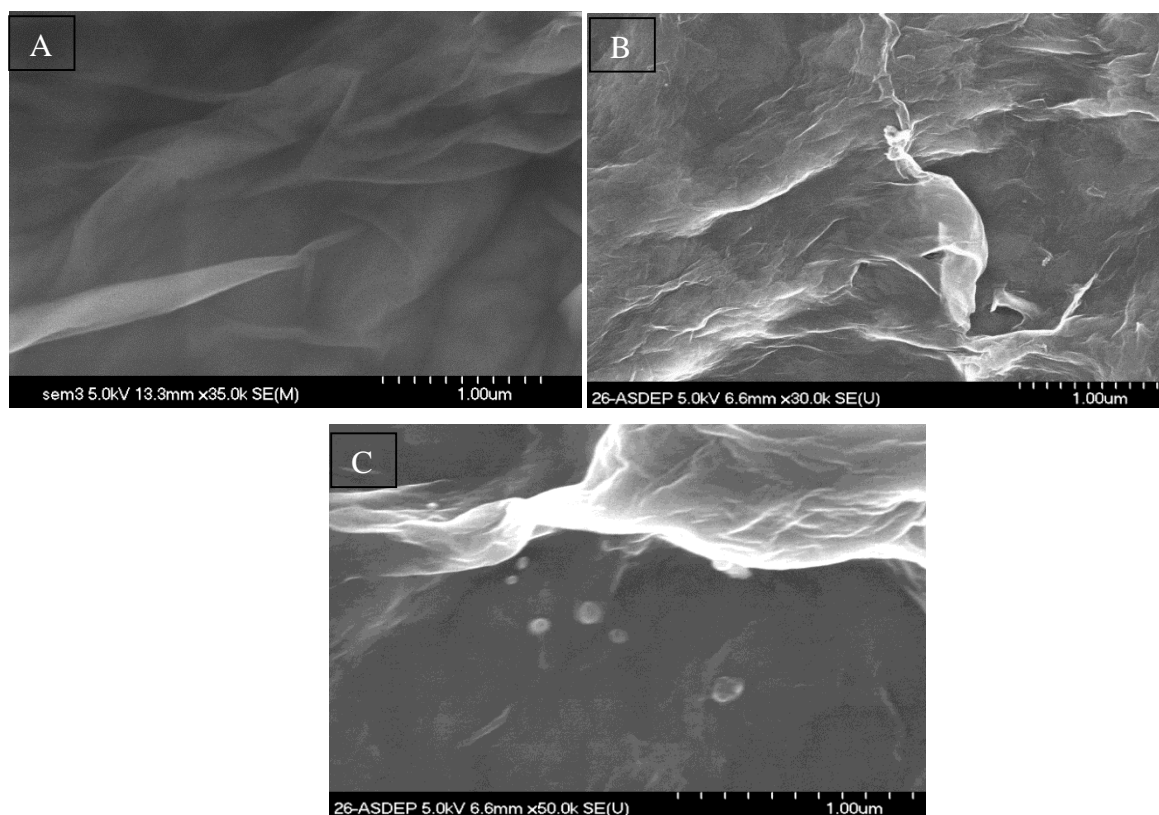


Figure 3.13: SEM images of GO (A) and rGO-Ni NPs (B, C).

We further used FEI Tecnai Osiris to analyze the rGO-Ni NPs composite. FEI Tecnai Osiris is an analytical TEM instrument optimised for high speed and high sensitivity Energy-Dispersive X-ray spectroscopy (EDX) measurements in STEM mode. **Figure 3.14** displays a STEM-HAADF image of the rGO/Ni NPs composite at an accelerating voltage of 200 kV as well as the Energy Dispersive X-Ray (EDX) spectrum recorded on it, which shows the presence of only nickel, carbon and oxygen. The copper originates from the copper grid used for dropping the sample.

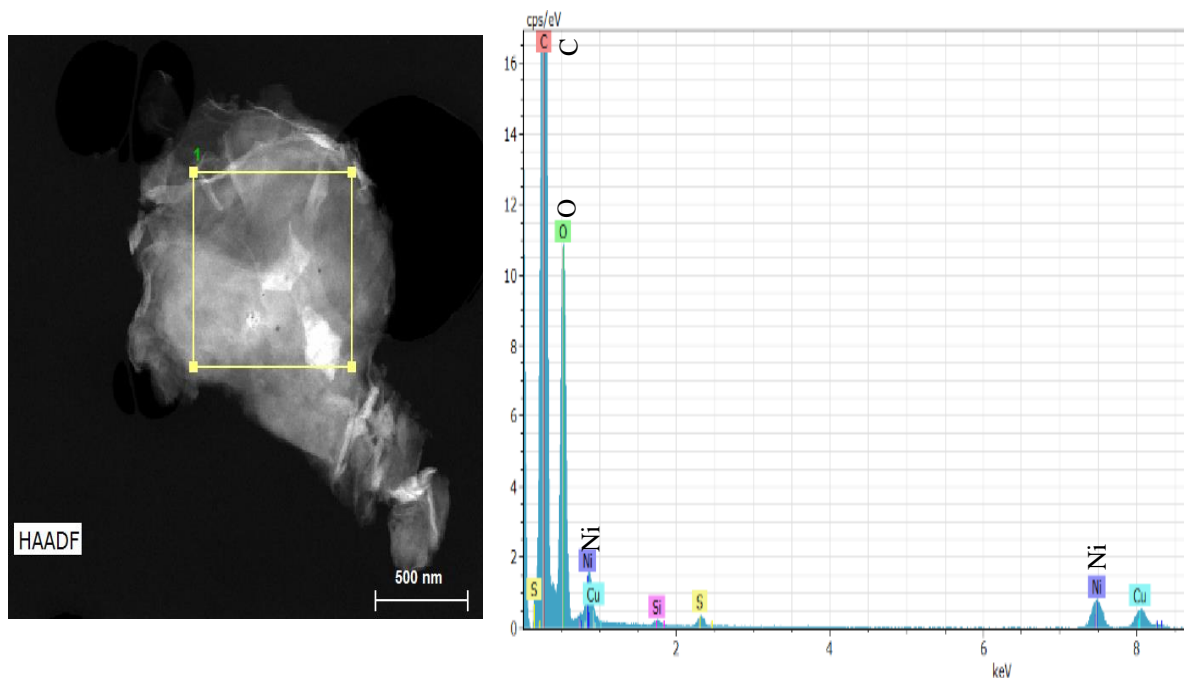


Figure 3.14: STEM, Super-X EDX at 200kV of rGO-Ni NPs.

Table 3.3: Elemental concentration of rGO-Ni NPs.

Element	C	O	Ni	Si
Mass %	80.3	16.6	2.4	0.3

Table 3.3 shows the concentration of the elements present in the sample. Ni is clearly detected. EDX mappings were also performed to further investigate the structure of rGO/Ni NPs composite. **Figure 3.15** depicts the elemental maps of carbon, oxygen and nickel of the composite, with the corresponding overlay image in **Figure 3.14**. These elemental maps indicate that the graphene is homogeneously coated on the Ni NPs [45, 49, 50].

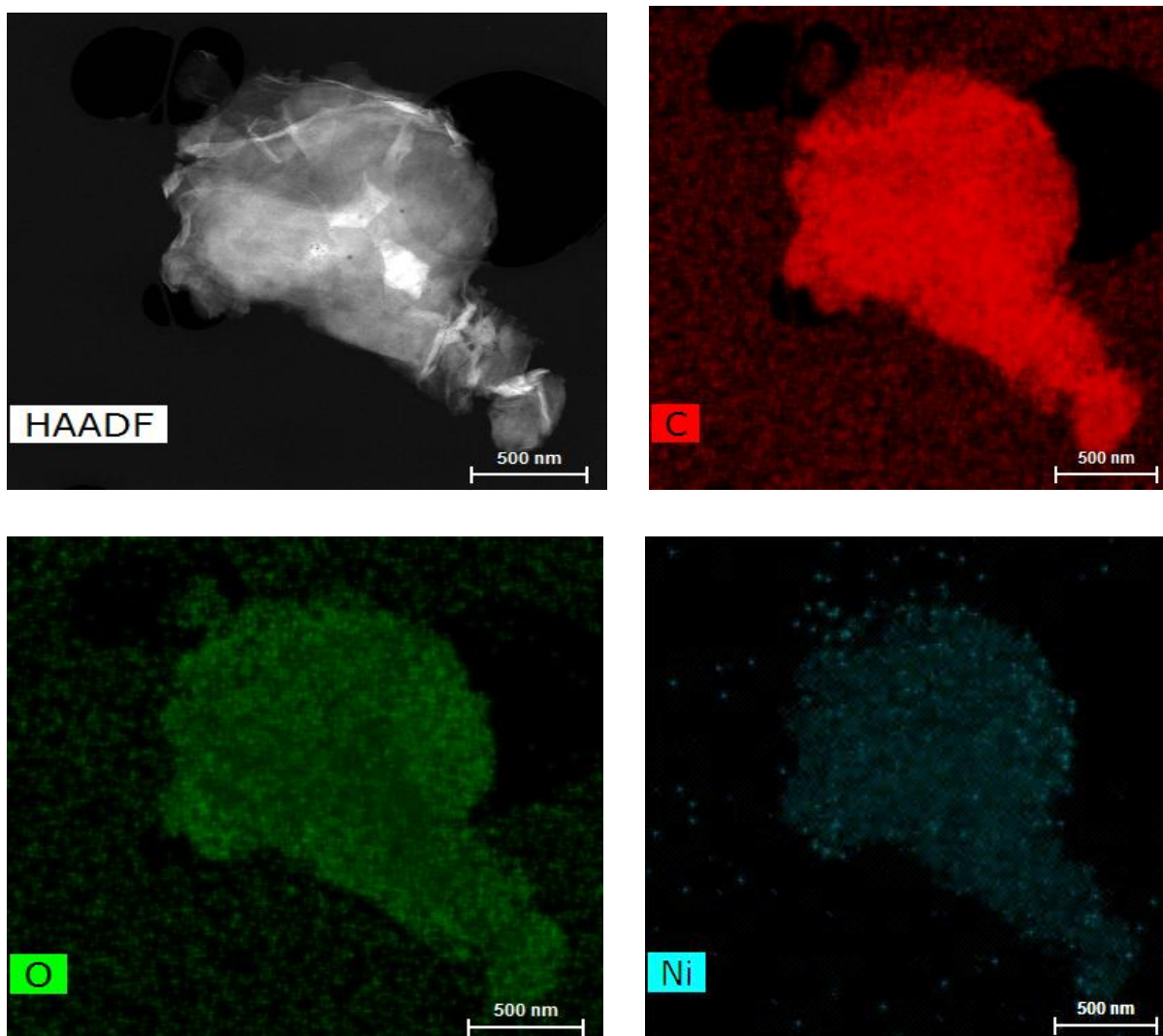


Figure (3.15): elemental maps of carbon, oxygen and nickel of the rGO-Ni NPs.

Figure (3.16), Figure (3.17) and Table (3.3) for the same sample deposited on different Si wafer.

Table 3.4: Elemental composition of rGO-Ni NPs

Element	C	O	Ni	Si
Mass %	86.4	9.6	3.5	0.4

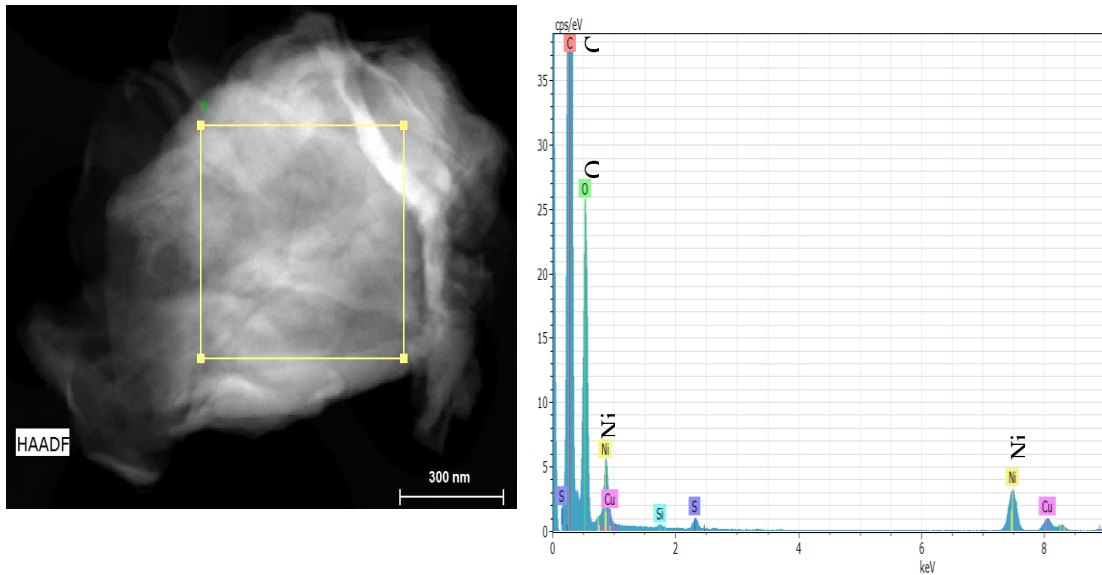


Figure 3.16: STEM, Super-X EDX at 200kV of rGO-Ni NPs.

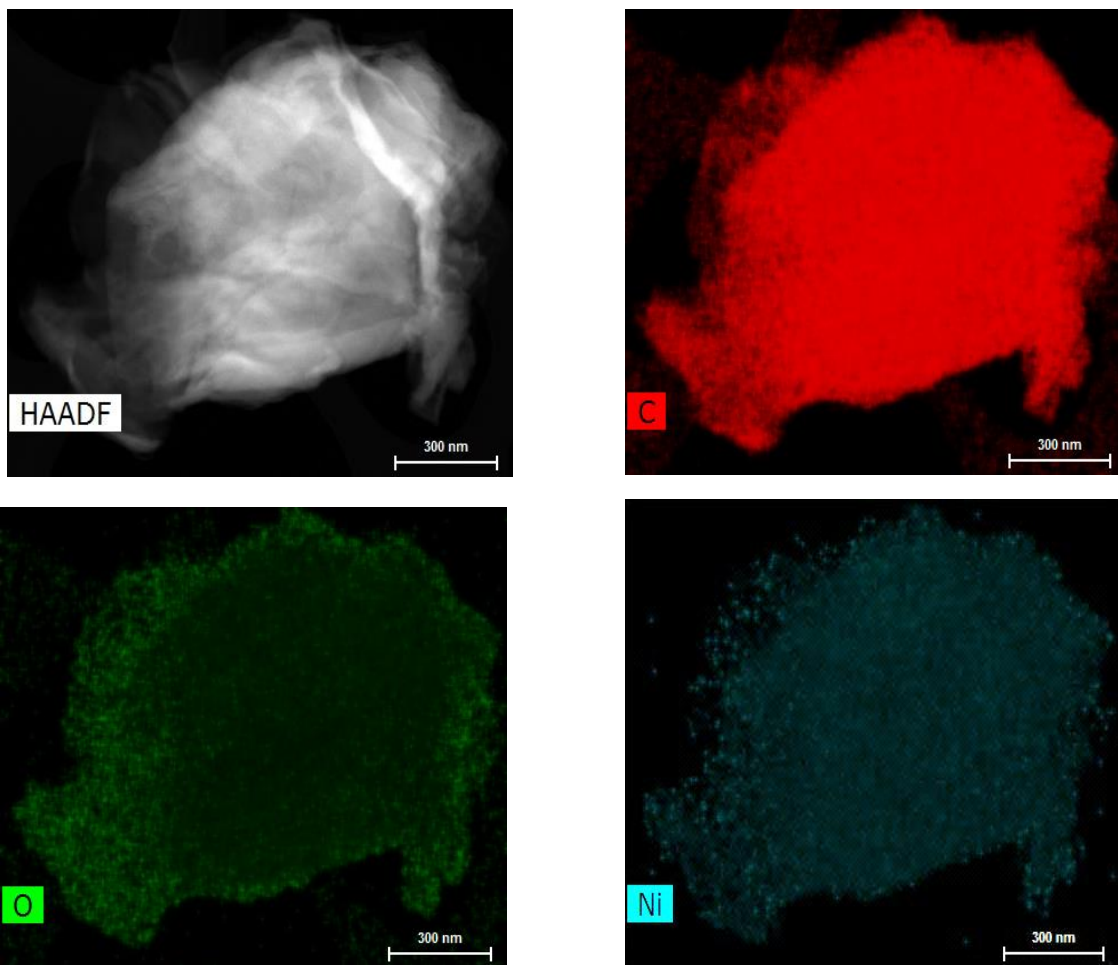


Figure 3.17: Elemental maps of carbon, oxygen and nickel of the rGO-Ni NPs.

These analysis indicate that Ni NPs are present on the graphene sheets at an average concentration of 2.9 %.

3.4. Catalytic reduction of 4-nitrophenol

The catalytic ability of the rGO-Ni NPs nanocomposite was investigated for the reduction of 4-nitrophenol (4-NP) with NaBH₄ as a model system at room temperature. Typically, after having prepared 0.1 mM of 4-NP and 0.1 M NaBH₄ solutions, a mixture of 3 ml of 4-NP and 0.5 ml NaBH₄ freshly prepared. Upon addition of NaBH₄ to 4-NP solution, the colour changed from light yellow to yellow-green because nitrophenol was converted to nitrophenolate anion. After addition of 100 µl of the catalyst rGO-Ni NPs (0.5 mg.ml⁻¹) aqueous solution to the mixture at room temperature, the yellow-green colour disappeared. The course of this reaction was monitored by UV-Vis spectroscopy.

Recycling experiments were also conducted in order to study the catalytic stability and activity. Similar to the above reduction process, a given amount of the as-prepared rGO-Ni NPs (0.5 mg.ml⁻¹) was used to catalyse 0.1 mM 4-NP mixture with 0.1 M NaBH₄. At the end of the reaction, the catalyst was separated by centrifugation at 4000 rpm for 5 min, and the supernatant was analysed using UV-Vis spectroscopy. The same procedure was repeated at least ten times in order to explore the reusability and activity of the nanocatalyst.

3.4.1. Reduction of 4-nitrophenol to 4-aminophenol by rGO-Ni NPs

The original absorption peak of p-nitrophenol at 317 nm shifts to 400 nm immediately upon the addition of freshly prepared NaBH₄ solution **Figure (3.18)**, corresponding to the colour change from light yellow to yellow-green due to the formation of p-nitrophenolate ions [65-68] as shown in. In the absence of catalyst rGO-Ni NPs, the peak due to 4-nitrophenolate ion at 400 nm remains unaltered even after a couple of days as reported in the literature [34, 69].

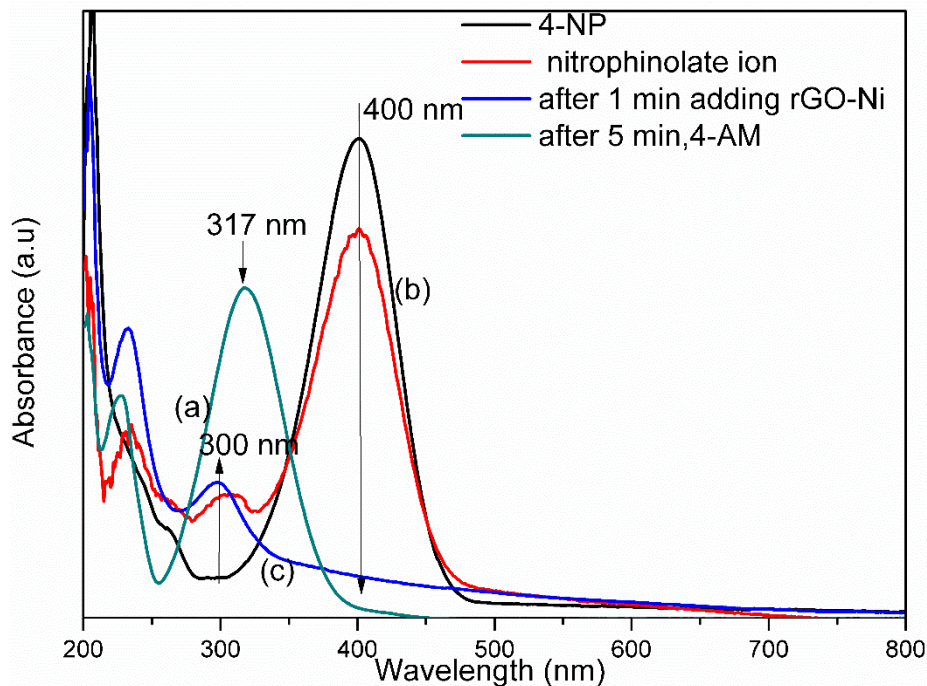


Figure 3.18: UV-visible spectra of 4-NP (a), nitrophenolate ion before (b) and after addition 100 μl , rGO-Ni NPs ($0.5 \text{ mg}\cdot\text{ml}^{-1}$) (c).

The intensity of the absorption peak at 400 nm gradually decreases as the reaction proceeds, indicating the reduction of the $-\text{NO}_2$ group of 4-nitrophenol to $-\text{NH}_2$ group (**Figure 3.19**) [69], and finally disappears at its completion after 5 min at room temperature. Meanwhile, a new peak appears of the absorption of 4-AP after 1 min to 317 nm and shift at 300 nm, revealing the reduction of 4-NP to 4-AP was completed. This phenomenon indicates that the reduction of 4-NP to 4-AP is successfully catalysed by the rGO-Ni NPs nanocatalyst.

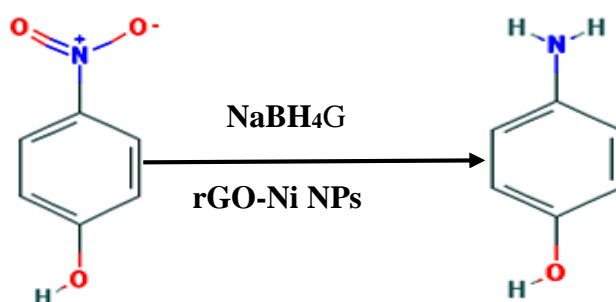


Figure 3.19: Schematic illustration of the reduction of 4-nitrophenol by NaBH_4 using rGO-Ni NPs nanocomposite as a catalyst.

As in the case of rGO/Ag nanocomposite, we can consider that the shorter time for the reduction of 4-NP to 4-AP by using rGO-Ni NPs nanocomposites is attributable to the

following factor: rGO sheets have high adsorption ability toward p-nitrophenol via π - π stacking interactions [34]. This provides a high concentration of p-nitrophenol near the Ni nanoparticles on rGO, leading to an efficient contact between them [70]; the electron transfer from the graphene to Ni nanoparticles increases the local electron concentration, facilitating the uptake of electrons by 4-NP molecules [18].

The reusability of the nanocatalyst is represented in **Figure 3.20**. It shows that the catalytic activity of the rGO-Ni NPs nanocatalyst is not altered even after ten successive catalytic cycle's rGO-Ni NPs. This means that the catalytic of rGO-Ni NPs has a good stability and activity.

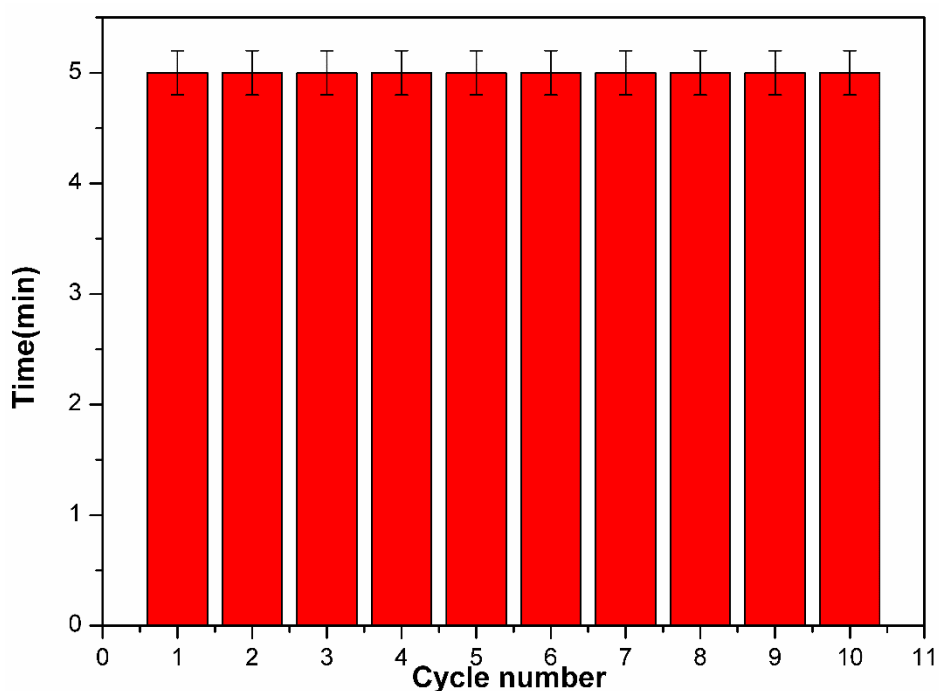


Figure 3.20: The catalytic performance of rGO-Ni NPs within ten cycles.

3.5. Conclusion

In summary, a facile method to synthesize a novel nanocomposite rGO-Ni NPs was developed using a green and facile chemical reduction. In this technique, nickel chloride has been successfully used for the reduction of graphene oxide and deposition of Ni nanoparticles on graphene sheets. FTIR, XPS and UV-vis indicate that the conjugated graphene network (sp^2 carbon) is re-established after the chemical reduction of GO and a high fraction of the oxygen

compounds is removed. The Ni NPs are well dispersed on the surface of graphene by this easy reduction method with an average concentration of 2.9 %.

The reduction of 4-NP to 4-AP by NaBH_4 was used as a model reaction to investigate the catalytic property of the rGO-Ni NPs. The nanocomposite exhibited remarkably improved catalytic activity for the reduction of 4-nitrophenol to 4-aminophenol. Moreover, we have demonstrated that the nanocomposite catalyst can be reused for ten cycles without any apparent loss of its catalytic activity. The developed nanocatalyst synthesis protocol is simple, fast, efficient, non-toxic, and low-cost to produce unique nanocomposite. Finally, we believe that this promising hybrid nanocomposite will have potential applications in many other fields especially in environmental control and biomedical applications.

3.6. References

- [1] Mas-Balleste R, Gomez-Navarro C, Gomez-Herrero J, Zamora F. 2D materials: to graphene and beyond. *Nanoscale*. 2011;3(1):20-30.
- [2] Wolf EL. *Applications of Graphene: An Overview*: Springer; 2014.
- [3] Lü M, Li J, Yang X, Zhang C, Yang J, Hu H, et al. Applications of graphene-based materials in environmental protection and detection. *Chinese Science Bulletin*. 2013;58(22):2698-710.
- [4] Zhao X, Liu L, Li X, Zeng J, Jia X, Liu P. Biocompatible graphene oxide nanoparticle-based drug delivery platform for tumor microenvironment-responsive triggered release of doxorubicin. *Langmuir*. 2014;30(34):10419-29.
- [5] Kuila T, Bose S, Mishra AK, Khanra P, Kim NH, Lee JH. Chemical functionalization of graphene and its applications. *Progress in Materials Science*. 2012;57(7):1061-105.
- [6] Neto AC, Guinea F, Peres N, Novoselov KS, Geim AK. The electronic properties of graphene. *Reviews of Modern Physics*. 2009;81(1):109.
- [7] Dreyer DR, Park S, Bielawski CW, Ruoff RS. The chemistry of graphene oxide. *Chemical Society Reviews*. 2010;39(1):228-40.
- [8] Georgakilas V. *Functionalization of graphene*: John Wiley & Sons; 2014.
- [9] Georgakilas V, Otyepka M, Bourlinos AB, Chandra V, Kim N, Kemp KC, et al. Functionalization of graphene: covalent and non-covalent approaches, derivatives and applications. *Chemical Reviews*. 2012;112(11):6156-214.
- [10] Park S, Ruoff RS. Chemical methods for the production of graphenes. *Nature Nanotechnology*. 2009;4(4):217-24.
- [11] Chua CK, Pumera M. Chemical reduction of graphene oxide: a synthetic chemistry viewpoint. *Chemical Society Reviews*. 2014;43(1):291-312.
- [12] Eigler S, Hirsch A. Chemistry with graphene and graphene oxide—challenges for synthetic chemists. *Angewandte Chemie International Edition*. 2014;53(30):7720-38.
- [13] Pei S, Cheng H-M. The reduction of graphene oxide. *Carbon*. 2012;50(9):3210-28.
- [14] Yamada Y, Suzuki Y, Yasuda H, Uchizawa S, Hirose-Takai K, Sato Y, et al. Functionalized graphene sheets coordinating metal cations. *Carbon*. 2014;75:81-94.

- [15] Wintterlin J, Bocquet M-L. Graphene on metal surfaces. *Surface Science*. 2009;603(10):1841-52.
- [16] Li Q, Mahmood N, Zhu J, Hou Y, Sun S. Graphene and its composites with nanoparticles for electrochemical energy applications. *Nano Today*. 2014;9(5):668-83.
- [17] Mitra S, Banerjee S, Datta A, Chakravorty D. Graphene composites: The materials for the future. *arXiv preprint arXiv:12071995*. 2012.
- [18] Du Y, Chen H, Chen R, Xu N. Synthesis of p-aminophenol from p-nitrophenol over nano-sized nickel catalysts. *Applied Catalysis A: General*. 2004;277(1):259-64.
- [19] Liu H, Deng J, Li W. Synthesis of nickel nanoparticles supported on boehmite for selective hydrogenation of p-nitrophenol and p-chloronitrobenzene. *Catalysis Letters*. 2010;137(3-4):261-6.
- [20] Millan WM, Smit MA. Study of electrocatalysts for oxygen reduction based on electroconducting polymer and nickel. *Journal of Applied Polymer Science*. 2009;112(5):2959-67.
- [21] LaGrow AP, Ingham B, Cheong S, Williams GVM, Dotzler C, Toney MF, et al. Synthesis, Alignment, and Magnetic Properties of Monodisperse Nickel Nanocubes. *Journal of the American Chemical Society*. 2012;134(2):855-8.
- [22] Li X, Dhanabalan A, Wang C. Enhanced electrochemical performance of porous NiO–Ni nanocomposite anode for lithium ion batteries. *Journal of Power Sources*. 2011;196(22):9625-30.
- [23] Sadiq IM, Mohammad AM, El-Shakre ME, El-Deab MS. Electrocatalytic activity of nickel oxide nanoparticles-modified electrodes: Optimization of the loading level and operating pH towards the oxygen evolution reaction. *International Journal of Hydrogen Energy*. 2012;37(1):68-77.
- [24] Inoue H, Namba Y, Higuchi E. Preparation and characterization of Ni-based positive electrodes for use in aqueous electrochemical capacitors. *Journal of Power Sources*. 2010;195(18):6239-44.
- [25] Neiva EG, Bergamini MF, Oliveira MM, Marcolino LH, Zarbin AJ. PVP-capped nickel nanoparticles: Synthesis, characterization and utilization as a glycerol electrosensor. *Sensors and Actuators B: Chemical*. 2014;196:574-81.

- [26] Wehrens-Dijksma M, Notten P. Electrochemical Quartz Microbalance characterization of Ni (OH) 2-based thin film electrodes. *Electrochimica acta*. 2006;51(18):3609-21.
- [27] Kiani M, Mousavi M, Ghasemi S. Size effect investigation on battery performance: Comparison between micro-and nano-particles of β -Ni (OH) 2 as nickel battery cathode material. *Journal of Power Sources*. 2010;195(17):5794-800.
- [28] Zhu J, Chen S, Zhou H, Wang X. Fabrication of a low defect density graphene-nickel hydroxide nanosheet hybrid with enhanced electrochemical performance. *Nano Research*. 2012;5(1):11-9.
- [29] Fang D-L, Chen Z-D, Liu X, Wu Z-F, Zheng C-H. Homogeneous growth of nano-sized β -Ni (OH) 2 on reduced graphene oxide for high-performance supercapacitors. *Electrochimica Acta*. 2012;81:321-9.
- [30] Zhu X, Jiao Q, Zhang C, Zuo X, Xiao X, Liang Y, et al. Amperometric nonenzymatic determination of glucose based on a glassy carbon electrode modified with nickel (II) oxides and graphene. *Microchimica Acta*. 2013;180(5-6):477-83.
- [31] Wu Z-S, Zhou G, Yin L-C, Ren W, Li F, Cheng H-M. Graphene/metal oxide composite electrode materials for energy storage. *Nano Energy*. 2012;1(1):107-31.
- [32] Chen G, Wang F, Liu F, Zhang X. One-pot preparation of Ni-graphene hybrids with enhanced catalytic performance. *Applied Surface Science*. 2014;316:568-74.
- [33] Kottegoda IRM, Idris NH, Lu L, Wang J-Z, Liu H-K. Synthesis and characterization of graphene–nickel oxide nanostructures for fast charge–discharge application. *Electrochimica Acta*. 2011;56(16):5815-22.
- [34] Ji Z, Shen X, Zhu G, Zhou H, Yuan A. Reduced graphene oxide/nickel nanocomposites: facile synthesis, magnetic and catalytic properties. *Journal of Materials Chemistry*. 2012;22(8):3471.
- [35] Dahal A, Batzill M. Graphene-nickel interfaces: a review. *Nanoscale*. 2014;6(5):2548-62.
- [36] Gaboardi M, Bliersbach A, Bertoni G, Aramini M, Vlahopoulou G, Pontiroli D, et al. Decoration of graphene with nickel nanoparticles: study of the interaction with hydrogen. *Journal of Materials Chemistry A*. 2014;2(4):1039-46.

- [37] Gao W, Tjiu WW, Wei J, Liu T. Highly sensitive nonenzymatic glucose and H₂O₂ sensor based on Ni(OH)₂/electroreduced graphene oxide--multiwalled carbon nanotube film modified glass carbon electrode. *Talanta*. 2014;120:484-90.
- [38] Lee JW, Ahn T, Soundararajan D, Ko JM, Kim J-D. Non-aqueous approach to the preparation of reduced graphene oxide/ α -Ni (OH)₂ hybrid composites and their high capacitance behavior. *Chemical Communications*. 2011;47(22):6305-7.
- [39] Wang H, Casalongue HS, Liang Y, Dai H. Ni (OH)₂ nanoplates grown on graphene as advanced electrochemical pseudocapacitor materials. *Journal of the American Chemical Society*. 2010;132(21):7472-7.
- [40] Sun Z, Lu X. A solid-state reaction route to anchoring Ni (OH)₂ nanoparticles on reduced graphene oxide sheets for supercapacitors. *Industrial & Engineering Chemistry Research*. 2012;51(30):9973-9.
- [41] Lv W, Sun F, Tang D-M, Fang H-T, Liu C, Yang Q-H, et al. A sandwich structure of graphene and nickel oxide with excellent supercapacitive performance. *Journal of Materials Chemistry*. 2011;21(25):9014.
- [42] Yang Y-Y, Hu Z-A, Zhang Z-Y, Zhang F-H, Zhang Y-J, Liang P-J, et al. Reduced graphene oxide–nickel oxide composites with high electrochemical capacitive performance. *Materials Chemistry and Physics*. 2012;133(1):363-8.
- [43] Zhu X, Dai H, Hu J, Ding L, Jiang L. Reduced graphene oxide–nickel oxide composite as high performance electrode materials for supercapacitors. *Journal of Power Sources*. 2012;203:243-9.
- [44] Zhu X-J, Hu J, Dai H-L, Ding L, Jiang L. Reduced graphene oxide and nanosheet-based nickel oxide microsphere composite as an anode material for lithium ion battery. *Electrochimica Acta*. 2012;64:23-8.
- [45] Kumary VA, Nancy TM, Divya J, Sreevalsan K. Nonenzymatic glucose sensor: glassy carbon electrode modified with graphene-nickel/nickel oxide composite. *International Journal of Electrochemical Science*. 2013;8:2220-8.
- [46] Liu JW, Yang T, Ma LY, Chen XW, Wang JH. Nickel nanoparticle decorated graphene for highly selective isolation of polyhistidine-tagged proteins. *Nanotechnology*. 2013;24(50):505704.

- [47] Liu S-Q, Xiao B, Feng L-R, Zhou S-S, Chen Z-G, Liu C-B, et al. Graphene oxide enhances the Fenton-like photocatalytic activity of nickel ferrite for degradation of dyes under visible light irradiation. *Carbon*. 2013;64:197-206.
- [48] Ren L, Hui KS, Hui KN. Self-assembled free-standing three-dimensional nickel nanoparticle/graphene aerogel for direct ethanol fuel cells. *Journal of Materials Chemistry A*. 2013;1(18):5689.
- [49] Min S, Zhao C, Chen G, Qian X. One-pot hydrothermal synthesis of reduced graphene oxide/Ni(OH)₂ films on nickel foam for high performance supercapacitors. *Electrochimica Acta*. 2014;115:155-64.
- [50] Yang Y, Zhang F, Wang H, Yao Q, Chen X, Lu Z-H. Catalytic Hydrolysis of Ammonia Borane by Cobalt Nickel Nanoparticles Supported on Reduced Graphene Oxide for Hydrogen Generation. *Journal of Nanomaterials*. 2014;2014:1-9.
- [51] Zheng C-h, Liu X, Chen Z-d, Wu Z-f, Fang D-l. Excellent supercapacitive performance of a reduced graphene oxide/Ni(OH)₂ composite synthesized by a facile hydrothermal route. *Journal of Central South University*. 2014;21(7):2596-603.
- [52] Wu Z, Huang XL, Wang ZL, Xu JJ, Wang HG, Zhang XB. Electrostatic induced stretch growth of homogeneous beta-Ni(OH)₂ on graphene with enhanced high-rate cycling for supercapacitors. *Scientific Reports*. 2014;4:3669.
- [53] Wu J, Dou S, Shen A, Wang X, Ma Z, Ouyang C, et al. One-step hydrothermal synthesis of NiCo₂S₄-rGO as an efficient electrocatalyst for the oxygen reduction reaction. *Journal of Materials Chemistry A*. 2014;2(48):20990-5.
- [54] Sahoo PK, Panigrahy B, Bahadur D. Facile synthesis of reduced graphene oxide/Pt-Ni nanocatalysts: their magnetic and catalytic properties. *RSC Advances*. 2014;4(89):48563-71.
- [55] Li S-J, Xia N, Lv X-L, Zhao M-M, Yuan B-Q, Pang H. A facile one-step electrochemical synthesis of graphene/NiO nanocomposites as efficient electrocatalyst for glucose and methanol. *Sensors and Actuators B: Chemical*. 2014;190:809-17.
- [56] Bhowmik K, Mukherjee A, Mishra MK, De G. Stable Ni nanoparticle-reduced graphene oxide composites for the reduction of highly toxic aqueous Cr(VI) at room temperature. *Langmuir*. 2014;30(11):3209-16.

- [57] Liu R, Zhao Q, Li Y, Zhang G, Zhang F, Fan X. Graphene supported Pt/Ni nanoparticles as magnetically separable nanocatalysts. *Journal of Nanomaterials*. 2013;2013. add article number
- [58] Jiang L, Zou R, Li W, Sun J, Hu X, Xue Y, et al. Ni(OH)₂/CoO/reduced graphene oxide composites with excellent electrochemical properties. *Journal of Materials Chemistry A*. 2013;1(3):478-81.
- [59] Wang Z, Hu Y, Yang W, Zhou M, Hu X. Facile one-step microwave-assisted route towards Ni nanospheres/reduced graphene oxide hybrids for non-enzymatic glucose sensing. *Sensors*. 2012;12(4):4860-9.
- [60] Fellahi O, Das MR, Coffinier Y, Szunerits S, Hadjersi T, Maamache M, et al. Silicon nanowire arrays-induced graphene oxide reduction under UV irradiation. *Nanoscale*. 2011;3(11):4662-9.
- [61] Wang Q, Li M, Szunerits S, Boukherroub R. Environmentally Friendly Reduction of Graphene Oxide Using Tyrosine for Nonenzymatic Amperometric H₂O₂ Detection. *Electroanalysis*. 2014;26(1):156-63.
- [62] Hosu IS, Wang Q, Vasilescu A, Petcu SF, Raditoiu V, Railian S, et al. Cobalt phthalocyanine tetracarboxylic acid modified reduced graphene oxide: a sensitive matrix for the electrocatalytic detection of peroxynitrite and hydrogen peroxide. *RSC Advances*. 2015;5(2):1474-84.
- [63] Zhang W, Li Y, Zeng X, Peng S. Synergetic effect of metal nickel and graphene as a cocatalyst for enhanced photocatalytic hydrogen evolution via dye sensitization. *Scientific Reports*. 2015;5.
- [64] Chen J, Duan M, Chen G. Continuous mechanical exfoliation of graphene sheets via three-roll mill. *Journal of Materials Chemistry*. 2012;22(37):19625-8.
- [65] Zeng J, Zhang Q, Chen J, Xia Y. A comparison study of the catalytic properties of Au-based nanocages, nanoboxes, and nanoparticles. *Nano Letters*. 2009;10(1):30-5.
- [66] Ji Z, Shen X, Yang J, Zhu G, Chen K. A novel reduced graphene oxide/Ag/CeO₂ ternary nanocomposite: green synthesis and catalytic properties. *Applied Catalysis B: Environmental*. 2014;144:454-61.

- [67] Gu W, Deng X, Jia X, Li J, Wang E. Functionalized graphene/Fe₃O₄ supported AuPt alloy as a magnetic, stable and recyclable catalyst for a catalytic reduction reaction. *Journal of Materials Chemistry A*. 2015;3(16):8793-9.
- [68] Yang Y, Ren Y, Sun C, Hao S. Facile route fabrication of nickel based mesoporous carbons with high catalytic performance towards 4-nitrophenol reduction. *Green Chemistry*. 2014;16(4):2273-80.
- [69] Joshi MK, Pant HR, Kim HJ, Kim JH, Kim CS. One-pot synthesis of Ag-iron oxide/reduced graphene oxide nanocomposite via hydrothermal treatment. *Colloids and Surfaces A: Physicochemical and Engineering Aspects*. 2014;446:102-8.
- [70] Li J, Liu C-y, Liu Y. Au/graphene hydrogel: synthesis, characterization and its use for catalytic reduction of 4-nitrophenol. *Journal of Materials Chemistry*. 2012;22(17):8426-30.

CHAPTER 4

Preparation, characterizations and applications of reduced graphene oxide decorated with Co_3O_4 nanoparticles (rGO- Co_3O_4) nanocomposite

4.1. Introduction

Graphene is a one atom thick sheet of sp^2 bonded carbon atoms in a honeycomb crystal lattice, which is at the cutting edge of materials science and condensed matter physics research [1, 2]. It's fascinating high conductivity, superior electron mobility, extremely high specific surface area and easy functionalization make graphene a good substrate to produce graphene-based nanocomposites [3, 4]. Especially, graphene–metal oxide nanocomposites have attracted extensive attention for their potential applications in environmental and energy-related areas. The physicochemical properties depend strongly on the number of layers and the dispersion performance of graphene sheets [5]. However, Van der Waals and π - π stacking interactions among individual graphene sheets result in their tendency to aggregate [6, 7] when graphene dispersion solutions are dried. A graphene layer interfacing with evenly distributed nanoparticles (NPs) on the surface could lead to a well-defined, novel graphene with exceptional surface area. In addition, the NPs could act as a stabilizer against the aggregation of individual graphene sheets. In a composite, graphene provides chemical functionality and compatibility to allow easy processing of metal oxides in the composite. The metal oxide component mainly provides high activity depending on its structure, size and crystallinity [8]. The resultant composite is not merely the sum of the individual components, but rather a new material with new functionalities and properties [9].

Moreover, the development of graphene-based composites provides an important milestone to improve the application performance of metal oxide nanomaterials in different fields such as energy harvesting, conversion and storage devices, photovoltaic devices, photocatalysis, etc. Therefore, considerable efforts have recently been devoted to decorating graphene with metal oxides NPs [10-12]. To date, various kinds of metal oxides have been synthesized and supported on graphene, which include TiO_2 , ZnO , SnO_2 , MnO_2 , Co_3O_4 , Fe_3O_4 , Fe_2O_3 , NiO , Cu_2O , etc. In the following context, we will briefly give an overview on the synthesis of graphene–metal oxide composites.

4.2. Decoration of cobalt oxide on graphene sheets as a model to metal oxide/graphene nanocomposites

Nanoparticles containing magnetic materials (such as iron, nickel and cobalt oxides) have potential applications in biotechnology, drug delivery and hyperthermic cancer treatment [13, 14]. This type of oxide is a magnetic p-type semiconductor with a cubic spinel crystal structure in which Co^{II} occupies the tetrahedral sites and the octahedral sites are occupied by Co^{III} [15]. Moreover, cobalt nanoparticles have long been of scientific and technological interest due to their unusual magnetic properties and industrial applications [16, 17]. Also, cobalt oxide (Co_3O_4) is a transition metal oxide with intriguing electronic, optical, electrochemical, high catalytic activity and electrocatalytic properties [18]. These properties of Co_3O_4 NPs make them promising materials for electronic devices [19], gas sensors [20], magnetic materials [21], electrochromic devices [22], electrochemical anodes for sensors [23], high temperature selective absorbers of solar radiation [24] and anode materials for rechargeable Li ion batteries [25].

However, the cobalt oxide outstanding properties are decreased or lost especially in applications of Li-ion batteries because of the large volume expansion/contraction; severe particle aggregation taking place in these metal compounds during the Li insertion/extraction processes often lead to electrode pulverization and loss of interparticle contacts, consequently resulting in large irreversible capacities and poor rate capability, limited capacity and rapid capacity fading, caused by their low conductivity and drastic volume expansion during the discharge/charge process [26, 27].

In catalysis, so far, not only non-noble metal NPs and noble metal NPs, but also their composites have been used for these applications, because of element abundance and related economic issues. Additionally, the catalytic performance of the metal NPs is highly dependent on the dispersion of the active metals. Thus, aggregation of the NPs during the catalytic process due to the high surface energies and magnetic properties is the main impediment to restraint their development [28].

To solve these problems, the scientific community focused on the preparation of low-cost catalysts with high catalytic activity and high specific surface area. For that, many various surfactants and substrates are successfully utilized to obtain catalysts with preferable disparity [29]. Graphene could be an ideal substrate for growing and anchoring metal NPs with good dispersion due to its high specific surface area and large density of free electrons.

Recently, Co₃O₄ nanomaterials combined with graphene have been fabricated using different techniques and have shown good properties for drug delivery [30, 31], energy storage [9], supercapacitors [32], heterogeneous catalysts [33], electrochemical sensors [34], Li-ion rechargeable batteries [16], and water treatment [35]. **Table 5.1** summarizes the different routes developed for the synthesis of Co₃O₄/rGO nanocomposites and their applications.

Table 4.1. Graphene/cobalt oxide composites: synthesis conditions and applications

Composite	Synthesis conditions	Size of NPs (nm)	Applications	Ref.
GO-Co ₃ O ₄	GO, Co(NO ₃) ₂ Hexanol, 140°C, 10 h	100	Decomposition of ammonium perchlorate (AP)	[36]
Co ₃ O ₄ /G	G, Co(NO ₃) ₂ , ammonia, 2 ^{step} 450°C, 2 h	10-30	Supercapacitors, lithium-ion batteries	[37]
Co ₃ O ₄ /G	GO, Co(NO ₃) ₂ , urea, microwave oven, 10 min, 2 ^{step} 320°C, 1h	3-5	Supercapacitors	[38]
Co ₃ O ₄ /N-rGO	GO, Co(OAc) ₂ , NH ₄ OH, ethanol, 10 h, 80°C, 2 ^{step} (150°C, 3h)	12-25	Heterogeneous catalysis	[39]
Co ₃ O ₄ /G	GO, CoCl ₂ , NaBH ₄ , 100°C, 3h, 2 ^{step} (200°C, 15h)	15-25	Supercapacitors, lithium-ion batteries	[40]
Co ₃ O ₄ /G	GO, Co(NO ₃) ₂ , ethylene glycol, microwave oven, 6 min	---	Supercapacitors	[17]
Co ₃ O ₄ /rGO	CoCl ₂ , urea, PVP, GO, hydrazine, 4 h, 100°C, 2 ^{step} (600°C, 3h, 300°C, 6 h)	100	Lithium-ion batteries	[16]
Co ₃ O ₄ /rGO	GO, CoCl ₂ , urea, 95°C, 8 h, 2 ^{step} 250°C, 4h	10-30	Supercapacitors	[41]
Co ₃ O ₄ /rGO	GO, Co(CH ₃ COO) ₂ , 10 h, 80°C, 2 ^{step} 150°C, 3 h	20	Supercapacitors	[42]
Co(OH) ₂ /G	GO, CoCl ₂ , Na ₂ S, 83°C, 4 h	30-60	-----	[43]
Co ₃ O ₄ /G	GO, ethylene glycol, CoCl ₂ , hydrazine, NaOH, 110°C, 3 h	3	-----	[44]
3D G/Co ₃ O ₄	3D graphene, CoCl ₂ , urea, 16 h, 120°C, 2 ^{step} 450°C, 2h	200-300	Supercapacitors, Glucose Detection	[45]
Co ₃ O ₄ /G	GO, Co(OAc) ₂ , NH ₄ OH, hydrazine, 4 h, 100°C, 2 ^{step} 400 °C, 1h	---	Catalytic activity for CO oxidation	[46]

Composite	Synthesis conditions	Size of NPs (nm)	Applications	Ref.
rGO–Co ₃ O ₄	GO, Co(OAc) ₂ , NH ₄ OH, 12 h, 180°C, 2 ^{step} cast on Pt electrode	---	Oxidation of methanol	[18]
Co ₃ O ₄ /rGO	GO, Co(NO ₃) ₂ , 2-methylimidazole, 2 ^{step} 600°C, 4h	---	Activator for peroxymonosulfate	[31]
Co ₃ O ₄ /G	oleic acid, xylene, Co(Ac) ₂ , GO, NaBH ₄ , 4 h, 150°C, 2 ^{step} 300°C, 3h	---	Oxygen evolution reaction	[33]

From **Table 4.1** one clearly sees that all the reported methods for the preparation of graphene/cobalt oxide are complex and require the use of hazard agents and high temperature to reduce graphene oxide and anchor cobalt oxide. In the first step, a mixture of graphene oxide and cobalt derivatives (cobalt acetate, cobalt nitrate, cobalt chloride) was heated up in an oil bath or Teflon-lined autoclave for hydrothermal treatment. During this process, GO was reduced to graphene nanosheets and Co²⁺ cations were transformed to Co(OH)₂ simultaneously. The resulting Co(OH)₂/rGO composite precursor was calcined at high temperature for several hours to obtain Co₃O₄/rGO composite.

The synthesized Co₃O₄/rGO nanocomposites were successfully applied for various applications like drug delivery [30, 31], energy storage [9], supercapacitors [32], heterogeneous catalysis [33], electrochemical sensors [34], Li-ion rechargeable batteries [16], and water treatment [35].

In this chapter, we report a one-step, easy, low-cost, and simple preparation method of Co₃O₄/rGO nanocomposite by reduction of graphene oxide and its decoration with cobalt oxide by using NaBH₄ as reducing agent at room temperature.

4.3. Reduced graphene oxide decorated with cobalt oxide nanoparticles (rGO-Co₃O₄ NPs).

GO nanosheets were produced from natural graphite powder by an improved Hummers and Offeman method [47]. Typically, GO dispersion (1 mg/ml) was dispersed in Milli-Q water. The mixture was sonicated for about 30 min, and cobalt chloride (CoCl₂, 40 mM) was added under shaking, then sodium borohydride (0.1 M) was added slowly to the mixture at room

temperature. The mixture was kept at room temperature for 30 min under shaking. The resulting black precipitate was separated from the aqueous supernatant by centrifugation at 14000 rpm for 30 min. After washing thoroughly with water and absolute ethanol to remove impurities, the precipitate was dried in an oven at 50°C for 24 h, hereafter named rGO-Co₃O₄ NPs as shown in **Figure (4.1)**.

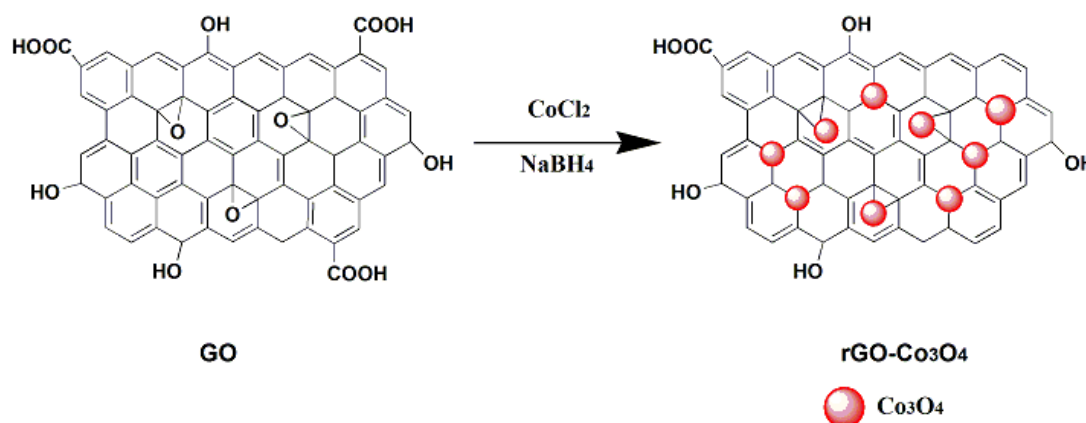


Figure 4.1: Schematic illustration of the synthesis of rGO-Co₃O₄ NPs.

4.4. Characterizations of rGO/Co₃O₄ nanocomposite

Figure (4.2) depicts the UV-vis spectra of GO, rGO and rGO-Co₃O₄ nanocomposite. The UV-vis spectrum of GO displays characteristic absorption peaks at 225 nm and a shoulder at around 300 nm due to π - π^* of aromatic carbon bonds and n - π^* transition of C=O bonds, respectively (**Figure (4.2, red trace)**). Upon GO reduction with NaBH₄ at room temperature, a red shift of the GO absorption band at 225 to 260 nm was observed, suggesting restoration of the aromatic network (**Figure 4.2, blue trace**).

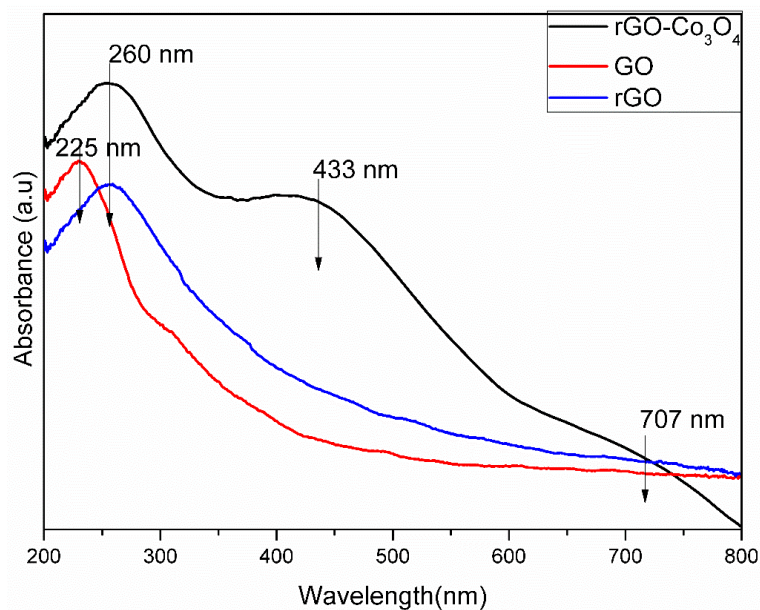


Figure 4.2: UV-Vis absorption spectra of GO before (red), rGO (blue) and rGO-Co₃O₄ nanocomposite.

NaBH₄ reduction of a mixture of GO and CoCl₂ aqueous solution induced a red-shift of the absorption band of GO from 225 to 260 nm and appearance of a new strong band at 433 nm due to Co₃O₄ NPs [48, 49] (**Figure 4.2, black trace**). The result suggests that 1- the GO nanosheets have been reduced to rGO and that the electronic conjugation within the GO nanosheets was restored upon reaction with cobalt chloride and sodium borohydride, and 2- the cobalt oxide nanoparticles have been anchored onto the graphene sheets.

X-ray photoelectron spectroscopy (XPS) analysis also confirms the formation of Co₃O₄/rGO nanocomposite. **Figure 4.3** shows the survey XPS spectra of GO and rGO-Co₃O₄ composite. We can recognize in both GO and rGO-Co₃O₄ NPs two peaks that belong to C_{1s} and O_{1s}. Moreover, new peaks belonging to Co_{2p}, Co_{3p} and Co_{3s} appear in the survey spectrum of rGO-Co₃O₄ composite, indicating that cobalt related NPs have been anchored onto the graphene sheets.

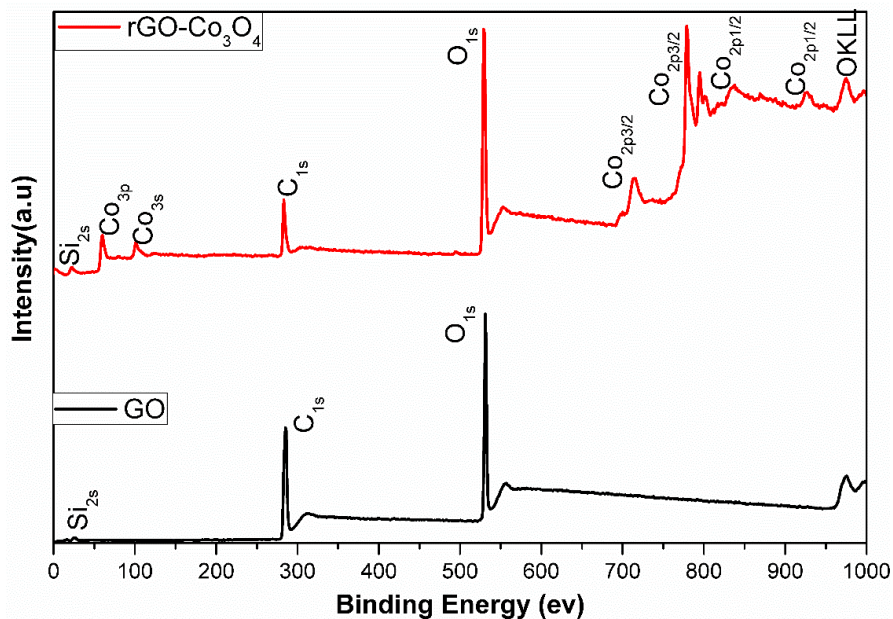


Figure 4.3: Survey (XPS) spectra of GO and rGO-Co₃O₄ nanocomposite.

Table 4.2: Weight percentage of each element in GO and rGO-Co₃O₄ nanocomposite.

Material	Weight percentage	Ratio C/O
GO	C _{1s} = 71.31 O _{1s} = 28.69	2.4
rGO-Co ₃ O ₄	C _{1s} = 51.70 O _{1s} = 38.23 Co _{2p} = 10.07	1.32

Figure 4.4 displays the C_{1s} core level XPS spectrum of GO nanosheets. It can be deconvoluted into three components with binding energies at about 284.9, 287.0 and 288.2 eV assigned to C-H/C-C, C-O and C=O species, respectively. The spectrum is dominated by the peak at 287.0 eV due to C-O, in accordance with a high oxidation degree of GO. In contrast, the C_{1s} high resolution XPS spectrum of Co₃O₄/rGO nanocomposite showed a significant decrease in the peak intensities associated with C-H/C-C, C-O and C=O groups (**Figure 4.4**).

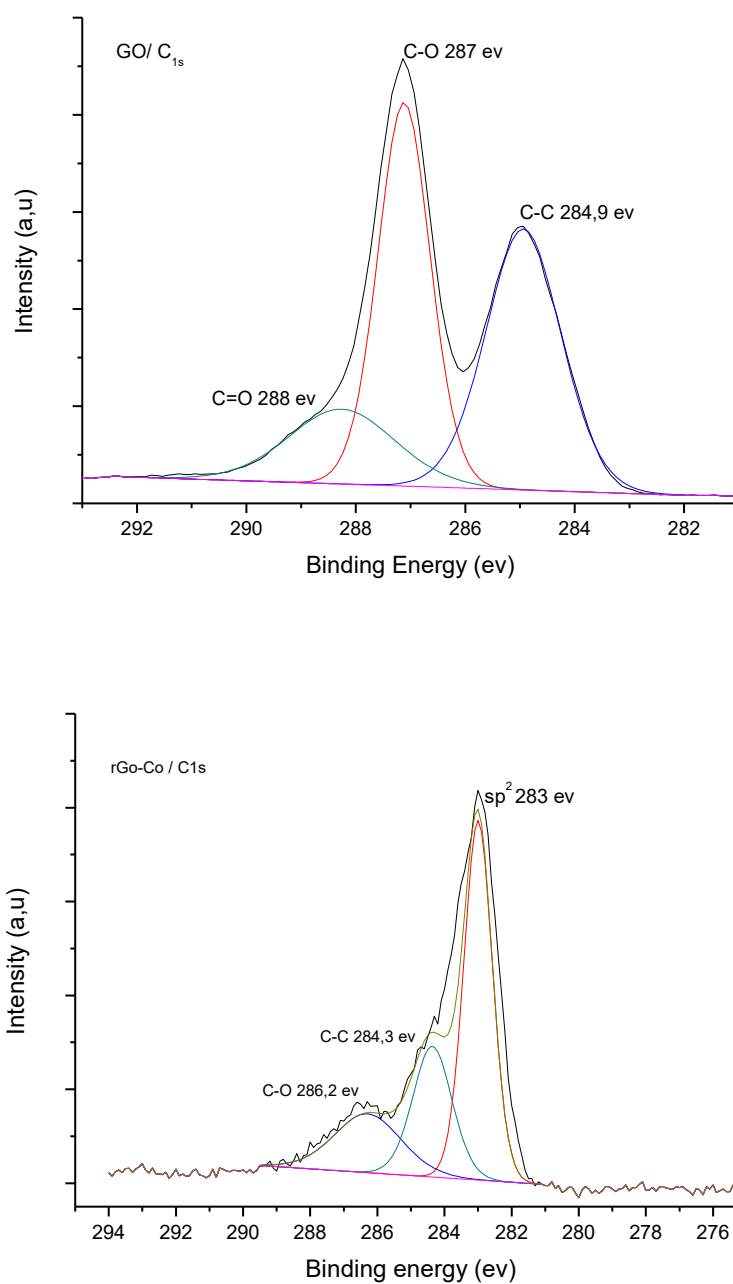


Figure 4.4: High resolution XPS spectra of C_{1s} for GO and rGO-Co₃O₄ nanocomposite.

The spectrum is dominated by a band with a binding energy at 283 eV due to sp² carbon, suggesting the restoration of the graphene network in the synthesized hybrid composite.

The high resolution Co_{2p} XPS spectrum of Co₃O₄/rGO exhibits two peaks at 780 and 795 eV, corresponding to the Co_{2p}_{1/2} and Co_{2p}_{3/2} spin-orbit peaks of Co₃O₄. The spectrum displays also two shake-up satellite peaks of the Co_{2p}_{3/2} and Co_{2p}_{1/2} located at around 784 and 801 eV with deviations from the main peaks of 4 and 7 eV, respectively. The results suggest that cobalt

exists in the form of Co_3O_4 , in good agreement with the previously reported data (Figure 4.5) [50].

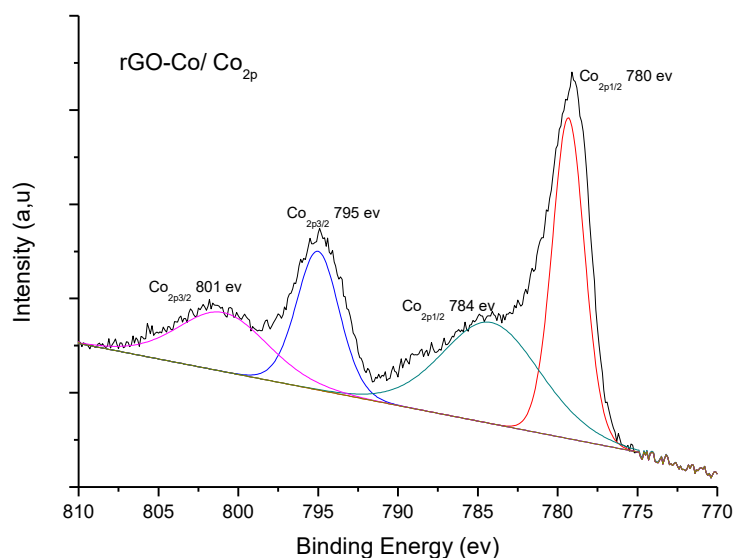


Figure 4.5: High resolution XPS spectra of Co_{2p} for rGO-NPs.

Raman spectroscopy is a powerful technique to study carbonaceous materials. **Figure 4.6** depicts the Raman spectra of Co_3O_4 NPs, prepared by CoCl_2 reduction with NaBH_4 , and rGO- Co_3O_4 hybrid. The Raman spectrum of Co_3O_4 nanoparticles displays four Raman peaks located at 486, 531, 603 and 692 cm^{-1} . They correspond to the E_g , E_g , F_{2g} , and A_{1g} modes of the crystalline Co_3O_4 . The Raman spectrum of the rGO- Co_3O_4 nanocomposite shows characteristic peaks of Co_3O_4 in the region of 400-700 cm^{-1} and characteristic peaks of the D and G bands from graphene at around 1335 and 1600 cm^{-1} , respectively. The presence of these peaks clearly indicates the existence of both rGO and Co_3O_4 in the as-prepared hybrid. Furthermore, the higher intensity of D band in the composite showed a largely disordered structure of the obtained rGO. The results confirm that crystalline cobalt oxide are anchored onto the graphene sheets [31, 46].

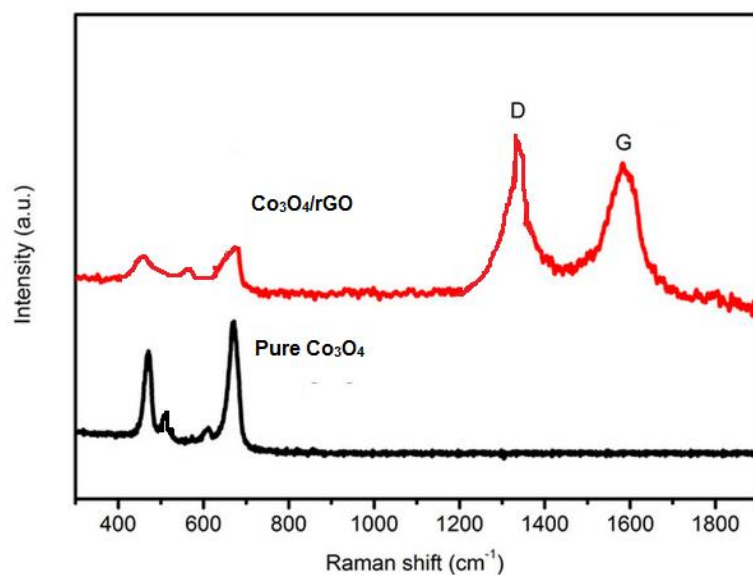


Figure 4.6: Raman spectra of Co_3O_4 NPs and rGO- Co_3O_4 nanocomposite.

The XRD pattern of rGO- Co_3O_4 displays diffraction peaks (2θ) at 31.27° , 36.84° , 38.56° , 44.8° , 59.35° , 65.23° , 74.11° , 77.34° and 78.4° which correspond to the (220), (311), (222), (400), (511), (440), (620), (533) and (622) crystalline planes of Co_3O_4 (ICDD file number 043-1003) (**Figure 4.7**) [26, 27, 31]. The crystallite size (i.e. coherent domain size) was evaluated at 5 nm using the Scherer formula for the two single peaks located at 59.35° (511) and 65.23° (440).

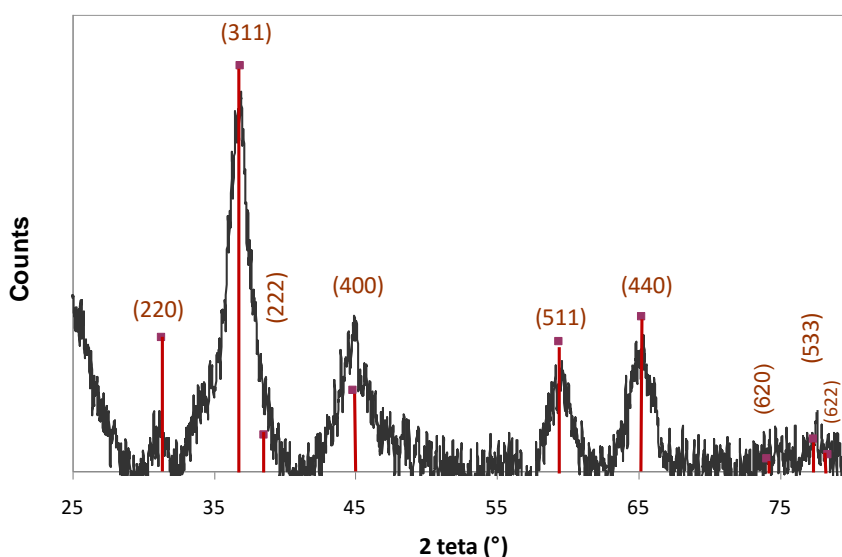


Figure 4.7: XRD pattern for the rGO- Co_3O_4 nanocomposite

The FTIR spectra of GO and rGO-Co₃O₄ showed remarkable differences (**Figure 4.8**). For GO, a strong and broad absorption at 3404 cm⁻¹ ascribed to O–H stretching vibration was observed, and the C=O stretching of COOH groups situated at the edges of GO sheets was observed at 1740 cm⁻¹. The absorption at 1422 cm⁻¹ may be due to tertiary C–OH groups. The absorption band at 1023 cm⁻¹ is attributed to stretching vibrations of C–O groups, while the band at 1623 cm⁻¹ is attributed to C=C stretching vibrations as part of the ring breathing mode in the GO skeleton [51, 52]. By contrast, for the rGO-Co₃O₄ NPs, the band O–H was shifted to 3424 cm⁻¹, while the skeletal vibration band C=C at 1623 cm⁻¹ was shifted to 1627 cm⁻¹. Moreover, the stretching band C=O at 1740 cm⁻¹ disappeared, indicating that GO was reduced to rGO during the chemical reduction with cobalt chloride and NaBH₄ [34].

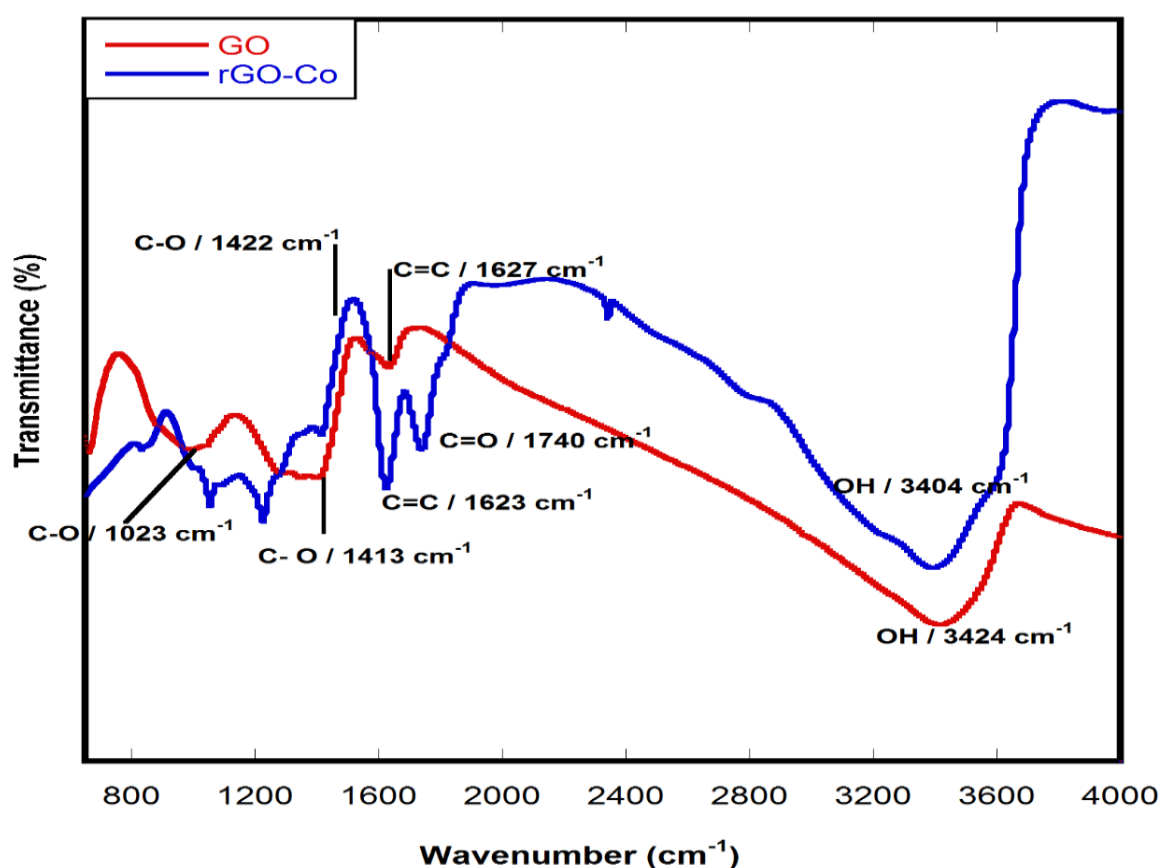


Figure 4.8: FTIR spectra of GO (red) and rGO-Co₃O₄ NPs (blue).

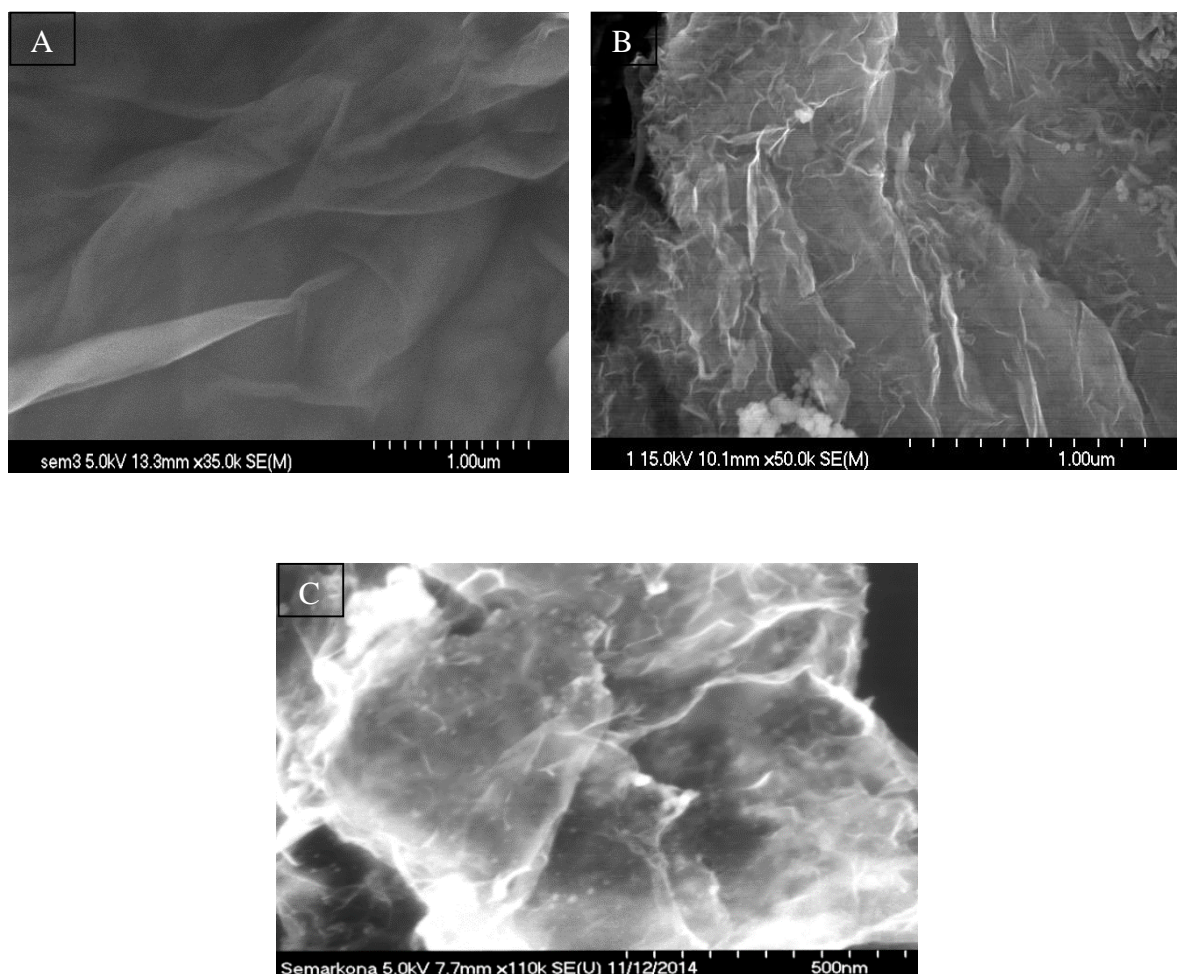


Figure 4.9: SEM images of the GO (A) and rGO-Co₃O₄ NPs (B, C).

Morphologies and microstructures of the as-prepared samples were investigated by FESEM (**Figure 4.9**). In FESEM images aggregated and crumpled sheets was observed and consisted of many graphene sheets.

The TEM images of the rGO-Co₃O₄ nanocomposite are presented in **Figure 4.10A**. They show small Co₃O₄ NPs, with a diameter in the range 1.5–2.5 nm, *i.e.* slightly smaller than that deduced from XRD spectrum (5 nm). This is opposite to what is usually observed, because the size of coherently diffracting domains derived from XRD is usually smaller than the nanoparticle size as observed by TEM [53]. This could mean that the broadening of the diffraction peaks as observed in XRD pattern is also due to the presence of micro-strains in the nanoparticles [54].

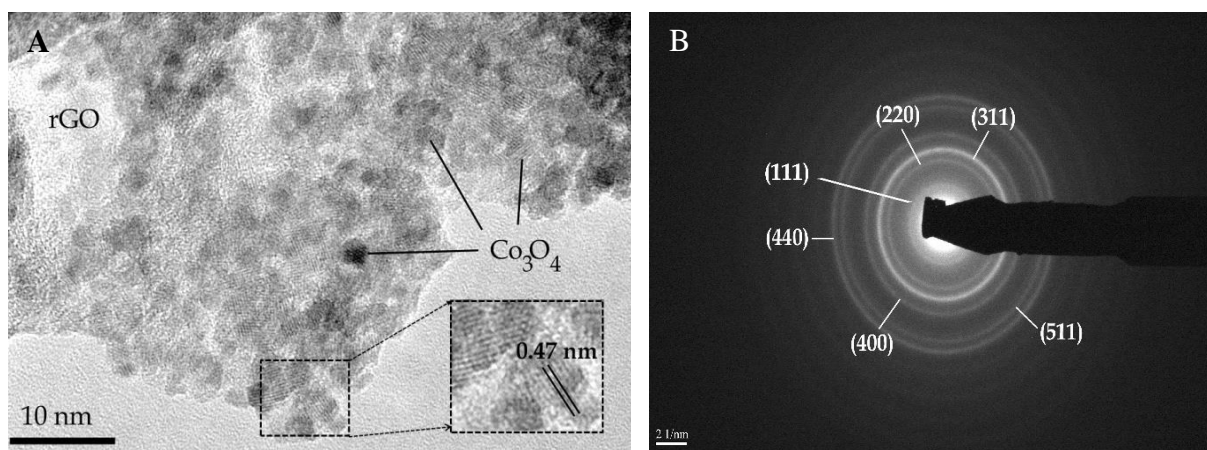


Figure 4.10: TEM images of the rGO-Co₃O₄ nanocomposite, HRTEM image of Co₃O₄ nanoparticles (Inset) lying on rGO sheets. General view and zoom on Co₃O₄ NPs (A) SAED pattern of randomly oriented Co₃O₄ NPs (B).

Figure 4.10B is a SAED pattern of the composite. It shows diffraction rings attributed to (111), (220), (311), (400), (511) and (440) planes of Co₃O₄, in agreement with XRD results. These particles anchored on the graphene sheets surface, implying a strong interaction between graphene and Co₃O₄. The inter-planar distance between adjacent planes is 0.47 nm, which corresponds to the interplanar spacing of (111) plane of Co₃O₄.

Figure 4.11 shows EDX analysis of the rGO-Co₃O₄ nanocomposite. The spectrum indicates that the as-synthesized rGO-Co₃O₄ NPs composites contain only cobalt, carbon, and oxygen, in agreement with the chemical composition of the nanocomposite. Some of the carbon signal originates from the carbon grid on which is deposited the sample for TEM observation.

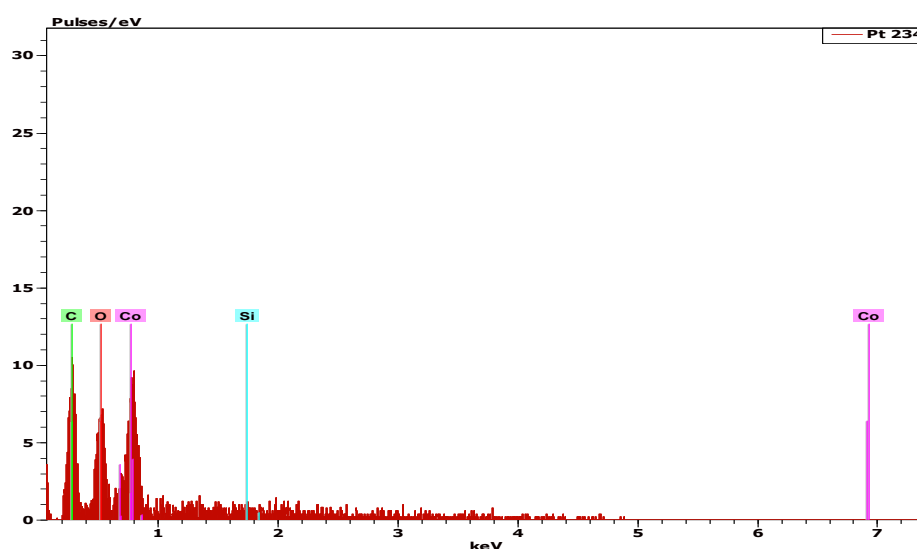
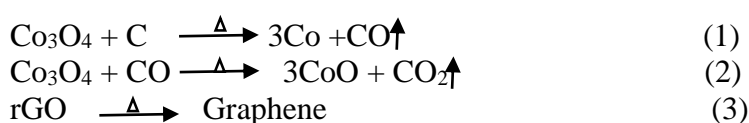


Figure 4.11: EDX analyses of the rGO-Co₃O₄ NPs.

Thermal gravimetric analysis (TGA) of rGO-Co₃O₄ nanocomposite was performed using a TGA/differential thermal analysis (DTA) analyzer. TG/DTG profiles of rGO-Co₃O₄ nanocomposite as a function of temperature at the heating rate of 10°C min⁻¹ are shown in **Figure 4.12**. The TG and DTG curves indicate that the decomposition of the nanocomposite proceeds in two main stages. The first one is the loss of H₂O at about 100°C. The second weight loss occurs between 100 and 320°C is assigned to the removal of oxygenated functional groups as CO and CO₂ from rGO [36, 55]. A total weight loss of 11.73 wt% was observed in this temperature range. The reaction may have occurred according to equations (1)–(3).



When the temperature was increased higher than 200°C, the reduction reaction of rGO-Co₃O₄ occurred following equations (1)–(3). Above 300°C, the TG and DTG curves are nearly stable without significant changes, suggesting that the composite is thermally stable.

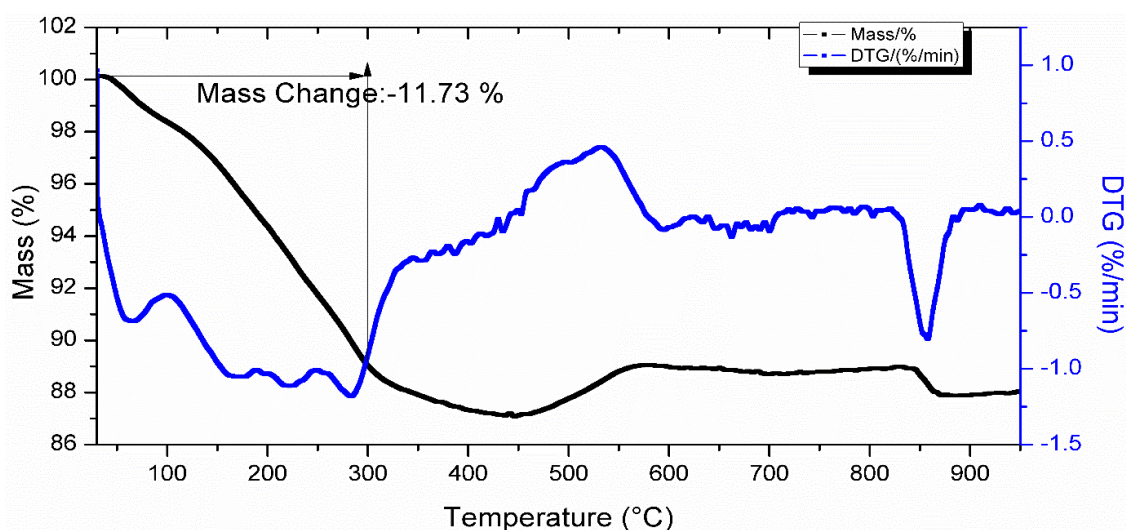


Figure 4.12: Thermogravimetric analysis (TGA) of rGO-Co₃O₄ nanocomposite.

For comparison, we have recorded the TGA/DTG curves of rGO (prepared by GO reduction using NaBH₄ at room temperature). **Figure 4.13A** reveals two well-defined steps of mass loss. The first step, which involves a 10wt % mass loss at 100°C, corresponds to the evaporation of water and volatile molecules. Between 100 and 980°C, an additional mass loss related to oxygenated groups was observed, due to pyrolysis of the carbon structure of the rGO film.

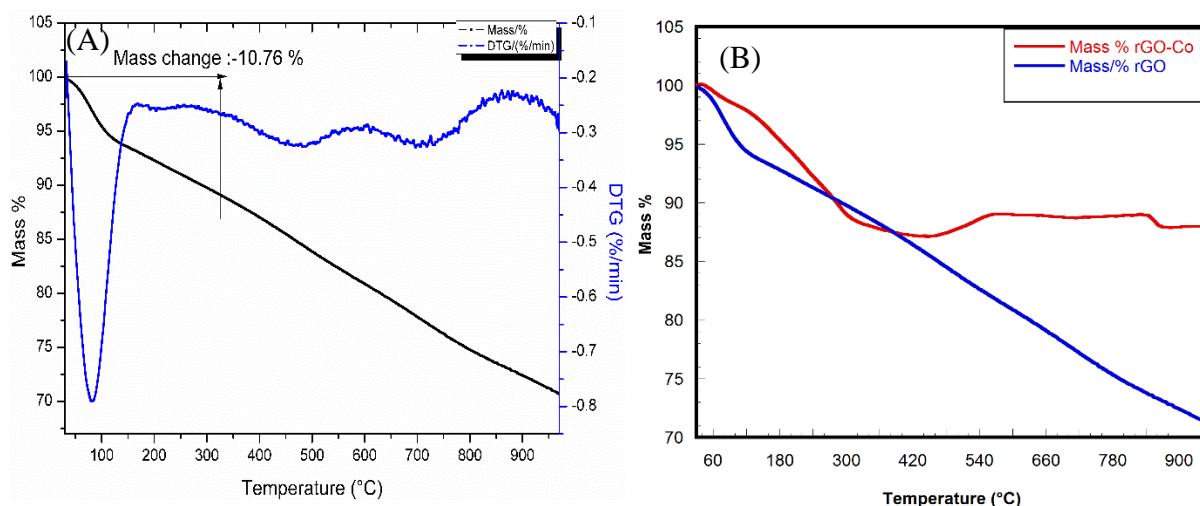


Figure 4.13: Thermogravimetric analysis (TGA) of rGO (A) and rGO-Co₃O₄ nanocomposite (B).

By comparing TG and TGD of rGO-Co₃O₄ nanocomposite with the curve of rGO (**Figure 4.13 B**), one clearly sees that higher mass loss took place in rGO films than in rGO-Co₃O₄ nanocomposite especially above 300°C. The improvement in thermal stability may be attributed to the so-called “tortuous path” effect of graphene, which delays the permeation of oxygen as well as the escape of volatile degradation products and at the same time promotes the char formation. These results demonstrate that the layered stacking graphene with cobalt oxide nanoparticles is capable of increasing the thermal stability of the composite [33, 36].

The magnetic properties of rGO-Co₃O₄ nanocomposite were investigated at different temperatures (**Figure 4.14**). The rGO-Co₃O₄ NPs hybrid exhibits typical ferromagnetic behaviour with a saturation magnetization (M_s) of 0.1 emu.g⁻¹ and a hysteresis of 115 Oe at 300 K (27°C), as shown by the magnetic hysteresis loop in **Figure 4.14A**. The coercive force increases as the temperature is decreasing, to 495 Oe at 2 K; similarly, the saturation magnetization (M_s) increased to 40 emu.g⁻¹ (**Figure 4.14B**). This saturation magnetization value facilitated the recycling of the nanocatalyst by a low energy-saving magnetic separation process.

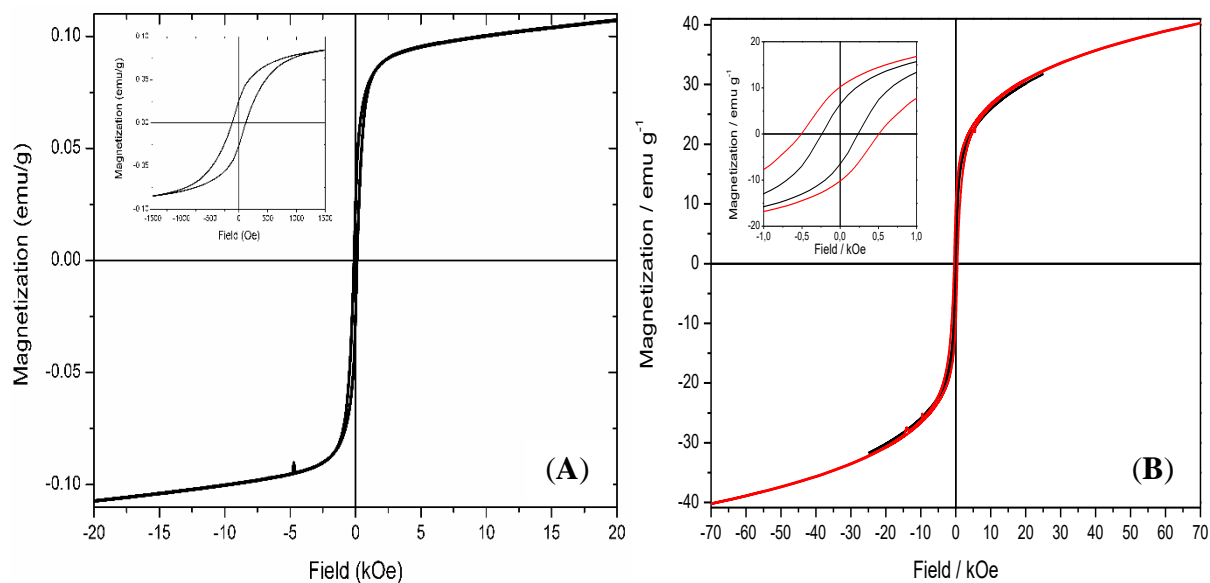


Figure 4.14: Magnetic hysteresis loop of rGO-Co₃O₄ nanocomposite at 300 K (A) and magnetic hysteresis loop at 2K (red) and 4K (dark) (B).

4.5. Applications

4.5.1. Catalytic reduction 4-nitrophenol

The catalytic activity of the rGO-Co₃O₄ nanocomposite was examined for the reduction of 4-nitrophenol (4-NP) to 4-aminophenol (4-AP) in the presence of excess NaBH₄. This catalytic reduction has been commonly used as a model reaction to evaluate the catalytic performance of metal or metal oxide nanoparticles (**Figure 4.15**).

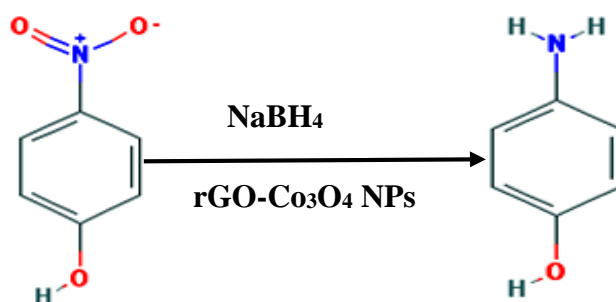


Figure 4.15: Schematic illustration of the reduction of p-nitrophenol by NaBH₄ with rGO-Co₃O₄ nanocomposite as a catalyst.

Typically, two stock aqueous solutions of 0.1 mM of 4-NP and 0.1 M NaBH₄ were prepared. Then a mixture of 3 ml of 4-NP and 0.5 ml of NaBH₄ was prepared from the stock solutions.

During this process, the color changed from light yellow to yellow-green because nitrophenol was converted to nitrophenolate anion by NaBH_4 (**Figure 4.15**). To this mixture, $100\ \mu\text{l}$ of $\text{rGO-Co}_3\text{O}_4$ nanocomposite ($0.5\ \text{mg}\cdot\text{ml}^{-1}$) catalyst was added at room temperature; the yellow-green color disappeared. The change of this reaction was monitored by UV-Vis spectroscopy.

The UV-vis absorption spectrum of 4-NP displays an absorbance peak at $317\ \text{nm}$ (**Figure 4.16**, **black curve**), which shifts to $400\ \text{nm}$ in the presence of NaBH_4 due to the formation of 4-nitrophenolate ions, corresponding to a color change from light yellow to yellow-green due to the formation of p-nitrophenolate ions [56-59] (**Figure 4.16**, **red curve**). In absence of catalyst $\text{rGO-Co}_3\text{O}_4$ NPs, the peak due to 4-nitrophenolate ion at $400\ \text{nm}$ remains unaltered even during a couple of days [60, 61]. Thus, the conversion of 4-NP to 4-AP can be followed by monitoring the decay of the characteristic absorption peak of 4-nitrophenoxide at $400\ \text{nm}$.

The intensity of the absorption peak at $400\ \text{nm}$ gradually decreases as the reaction proceeds, indicating the reduction of the $-\text{NO}_2$ group of p-nitrophenol to $-\text{NH}_2$ group (**Figure 4.16**, **blue curve**) [60], and finally disappears at its completion after 1 min. Meanwhile, a new peak appears at $300\ \text{nm}$ that gradually increases, revealing the reduction of 4-NP to 4-aminophenol (4-AP) successfully catalyzed by the multifunctional nanocatalyst.

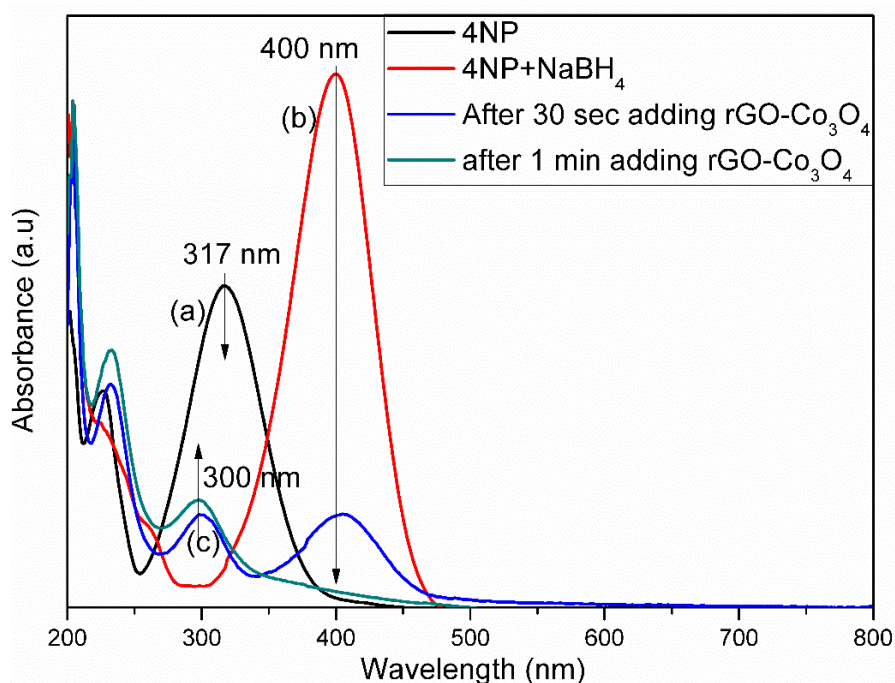


Figure 4.16: UV-visible spectra of 4-NP (a), nitrophenolate ion (b) and aminophenol (c) after adding $100\ \mu\text{l}$ of $\text{rGO-Co}_3\text{O}_4$ nanocomposite ($0.5\ \text{mg}\cdot\text{ml}^{-1}$).

The recyclability of catalysts is an important factor for a more economical process. Thus recycling catalysis experiments were conducted. Similar to the above reduction process, a given amount of the as-prepared rGO-Co₃O₄ nanocomposite (0.5 mg.ml⁻¹) was used to catalyze 4-NP (0.1 mM) reduction by NaBH₄ (0.1 M). At the end of the reaction, the catalyst was easily separated from the reaction medium using a magnet (1 Tesla) (**Figure 4.17**) and the supernatant was measured using UV-vis spectroscopy. The same procedure was repeated at least ten times in order to explore the reusability and activity of the nanocatalyst. The efficiency of the as-prepared rGO-Co₃O₄ catalyst in repeated cycles of reaction is exhibited in **Figure 4.18**. The result shows that the rGO-Co₃O₄ nanocatalyst maintains a high performance for ten cycles. This means that the catalytic of rGO-Co₃O₄ NPs has a good stability and activity.



Figure 4.17: Photograph images of the catalytic reduction of 4-NP to 4-AP using rGO-Co₃O₄ nanocomposite as catalyst and its separation at the end of the process using a magnet.

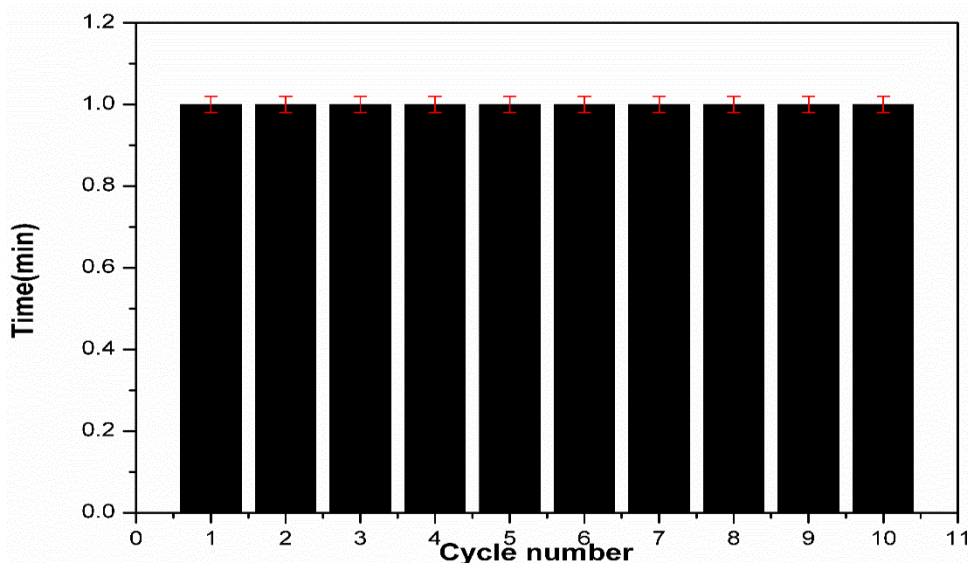


Figure 4.18: The performance of rGO-Co₃O₄ nanocomposite after ten catalytic cycles.

We can consider that the decreasing time for the reduction of 4-NP to 4-AP by using rGO-Co₃O₄ NPs nanocomposites is attributable to the following factor: rGO sheets have high adsorption ability toward p-nitrophenol *via* π - π stacking interactions [61]. This provides a high concentration of p-nitrophenol near the Co₃O₄ nanoparticles on rGO, leading to an efficient contact between them [62]; and the electron transfer from the graphene to Co₃O₄ nanoparticles increases the local electron concentration, facilitating the uptake of electrons by 4-NP molecules [63].

4.5.2. Treatment of wastewater using graphene/nanomaterials

In the environmental pollution remediation area, many graphene and magnetic graphene nanomaterials have been used as adsorbents for heavy metal ions and organic pollutants [64], while several transition metal oxide-graphene hybrids have been used for the degradation of toxic organic pollutants [65]. Hybridization of graphene with metal or metal oxide nanoparticles not only improves its pristine properties, but also introduces some specific functional groups or functional nanomaterials on the surfaces of graphene layers [66]. For instance, graphene oxide (GO) possesses several functional groups and strong acidity, exhibiting high adsorption for basic compounds and cations while reduced graphene oxide (rGO) shows hydrophobic surface and presents high adsorption capacity for chemicals through strong π - π interactions [67]. Modification of GO or rGO with metal oxides or organics can produce various nanocomposites, enhancing adsorption capacity and separation efficiency [68].

The pollutants (mainly heavy metal ions and organic dyes) in wastewater that strongly threaten human, animals and plants, GO/rGO-based composites typically show strong binding with these pollutant species, as summarized in **Table 4.3**.

Table 4.3: Adsorption capacities of heavy metal ions and organic contaminants from wastewater

Adsorbent	Adsorbate	Adsorption capacity (mg.g ⁻¹)	Condition	Ref.
2,6-Diamino pyridine-RGO	Cr(VI)	393.7	C ₀ 500 mg.L ⁻¹	[69]
PPY-GO	Cr(VI)	497.1	pH = 3.0	[70]
PANI-GO	Cr(VI)	1149.4	pH = 3.0; T 298 K	[71]
PPY/Fe ₃ O ₄	Cr(VI)	243.9	pH = 2.0 ;T 298 K	[72]
Ni-rGO	Cr(VI)	≥98%,4 min Cr =0.37 mM	pH = 2.0 ;T 298 K	[73]
PEI-GO	Cr(VI)	539.53	pH = 2.0 ;T 298 K	[74]
Fe ₃ O ₄ @mTiO ₂ @GO	Cr(VI)	117.94	pH = 2.0 ;T 303 K	[75]
Graphene sand composite	Cr(VI)	2859.38	pH = 1.5 ;T 298 K	[76]
MCGN	Cr(VI)	120	pH = 3 ;T 298 K	[77]
CCGO	Cr(VI)	67.66	pH = 3 ;T 298 K	[78]
G-nZVI ZVI(zero valent iron)	Cr(VI)	162	pH = 3 ;T 323 K	[79]
GO	Methylene blue	714	pH = 6.0; T 298 K	[80]
RGO	Methylene blue	158	T 283 K	[81]
MCGO	Methylene blue	179.6	pH =10.0	[82]
Fe ₃ O ₄ /SiO ₂ -GO	Methylene blue	97	T 298 K	[83]
EGO	Methylene blue Methyl violet Rhodamine B	17.3 2.47 1.24	pH = 10.0 pH = 6.0 pH = 6.0	[84]

Adsorbent	Adsorbate	Adsorption capacity (mg.g ⁻¹)	Condition	Ref.
Fe ₃ O ₄ -RGO	Rhodamine B Rhodamine 6G Acid blue92 Orange(II) Malachite green	~50 ~30 ~90 ~90 ~50	-----	[85]
Magnetic Fe ₂ O ₄ -RGO	Rhodamine B	22.5	pH =7.0	[86]
Fe ₃ O ₄ /RGO	Rhodamine B	296.2	pH=5.30; T 298 K	[87]
SnS ₂ /rGO	Rhodamine B	94.07	T 298 K	[88]
GO/PEI	Rhodamine B Methylene blue	131.926 334.448	T 298 K	[89]
GO/Fe ₃ O ₄	Rhodamine B Methylene blue	30.21 20.24	T 298 K	[90]
HNTs@rGO	Rhodamine B	45.4 mg.mg ⁻¹	T 298 K	[91]
(α -Fe ₂ O ₃)-PVP@ rGO	Rhodamine B	≥89.8%,120 min	T 298 K	[92]
TiO ₂ /ZnO-NH ₂ -rGO	Methyl orange (MO)	40 , ≥45%,10 min	T 298 K	[93]
rGO/Ni/MMO	Methyl orange (MO)	210.8	T 298 K	[94]
rGO-CNT-PPD	Methyl orange (MO)	294	pH=3; T 298 K	[95]

Wastewater from many industries, such as metallurgical, mining, chemical manufacturing, and battery manufacturing industries, contain many kinds of toxic heavy metal ions [75]. Chromium and its compounds are widely used in industries such as the electroplating, mining operation, leather tanning and pigment manufacturing and so on [96]. In aqueous solution Cr exists both in trivalent Cr(III) and hexavalent Cr(VI) forms. Trivalent chromium is considered as an essential micronutrient for human, plant and animal metabolism and less toxic than Cr(VI), which is extremely mobile in the environment and very toxic, carcinogenic and mutagenic to living organisms [97]. It can cause liver damage, pulmonary congestions, and severe diarrhea. Even at low concentrations, Cr(VI) can cause harm to the human body, due to bioaccumulation through the food chain. Actually, the discharge limit of Cr(VI) was restricted to be only 0.05 mg L⁻¹ by the U.S.EPA, while the discharge limit of the total Cr [Cr(VI), Cr(III) and other forms of them] is regulated to 2 mg L⁻¹ [72]. Waste matter from certain industries

often contain values higher than those and therefore, it is necessary to reduce the Cr(VI) concentration to acceptable level before discharging into the environment.

A number of technologies to remove Cr(VI) have been developed, including electro-chemical precipitation [98, 99], reverse osmosis [100, 101], ion exchange [102, 103], and adsorption [70, 72-75, 104, 105]. Among these, reverse osmosis, ion exchange, electrodialysis and electrolysis are costly technologies. Adsorption is a fast, inexpensive and widely applicable technique. Moreover, it is universal in nature as it can be applied for the removal of soluble and insoluble contaminants and biological pollutants with removal efficiency of 90-99%. For that, adsorption has become by far the most versatile and widely used technology [106].

Recent reports have shown that GO/rGO-based composites have excellent adsorption ability for aqueous heavy metals and thus can be used as promising adsorbents for water purification. Various heavy metals have been successfully treated by GO/rGO-based composites as shown in the **Table 4.3**, including Cr(VI).

Additionally, it has been reported that, if graphene oxide (GO) is modified with magnetic materials, it is possible to obtain new materials simultaneously possessing the unique properties of GO (large surface area and good mechanical properties) and magnetic properties for easy separation. For example, magnetic β -cyclodextrin/graphene oxide nanocomposites (MCGN) have been successfully used in environmental remediation as adsorbents for Cr(VI) removal from wastewater [77]. The result showed that MCGN was extremely fast for Cr-removal from wastewater with high removal efficiency within 60 min. The Cr-removal capability was more than $120 \text{ mg}\cdot\text{g}^{-1}$. The MCGN was stable and easily recovered. The adsorption isotherms were investigated, and indicate that the equilibrium adsorptions are well-described by the Langmuir isotherm mode and higher adsorption capacity was achieved for solutions with relatively low pH values [77].

On the other hand, novel $\text{Fe}_3\text{O}_4@m\text{TiO}_2@GO$ microspheres, synthesized by immobilizing a mesoporous TiO_2 shell on the surface of magnetic Fe_3O_4 nanoparticles prior to binding with GO, were applied for the removal of Cr(VI). It was shown that the sorption of the microspheres for Cr(VI) was strongly dependent on pH value and contact time.

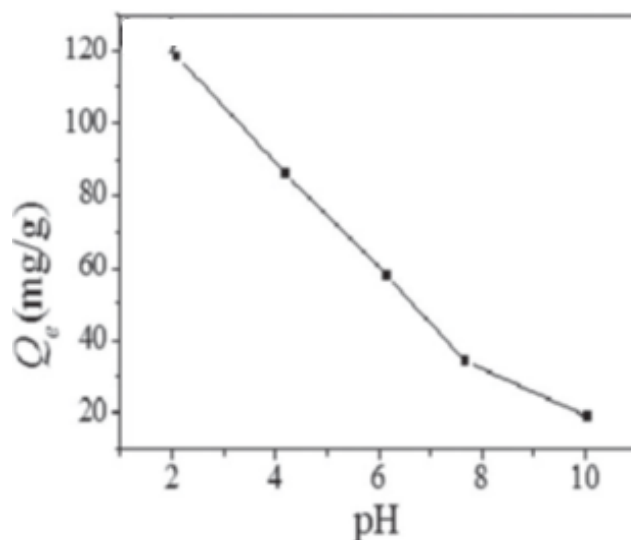


Figure 4.19: Effect of pH on the adsorption of Cr(VI) on $\text{Fe}_3\text{O}_4@\text{mTiO}_2@\text{GO}$. The concentration of $\text{Fe}_3\text{O}_4@\text{mTiO}_2@\text{GO}$ was 1.0 g L^{-1} . The initial Cr(VI) ion concentration was 100 mg L^{-1} . The contact time was 40 min. The temperature was 303 K [75].

It is known that the initial pH would govern the surface charge of the adsorbent and metal ions. It can be seen from **Figure 4.19** that the adsorbent has a maximum adsorbing capacity when the pH is 2.0. At lower pH, Cr(VI) mainly exists in the form of negatively charged HCrO_4^- and they can be absorbed by positive charges through electrostatic attraction. The adsorbent showed a good performance in adsorption during the first 40 min, and the adsorbing capacity was not enhanced obviously with increasing time. As a Cr-removal adsorbent, the maximum Cr-removal capability of microspheres was 117.94 mg g^{-1} [75].

Decorating the surface of graphene sheets with nanoparticles (NPs) is one of the recent approaches taken up by scientists all over the world. Because of this kind of electronic environment, NPs present on RGO surface are rarely oxidized to a higher oxidation state. Also, the high surface area of RGO prevents the NPs from agglomerating into larger particles [73]. Bhowmik et al. [73] reported a reduction of toxic Cr(VI) to nontoxic Cr(III) using formic acid as a reducing agent at room temperature in the presence of Ni NPs stabilized by reduced graphene oxide (Ni-RGO). In the presence of Ni-RGO the absorption bands of $\text{Cr}_2\text{O}_7^{2-}$ decrease rapidly and disappear within 4 min of reaction (**Figure 4.20**).

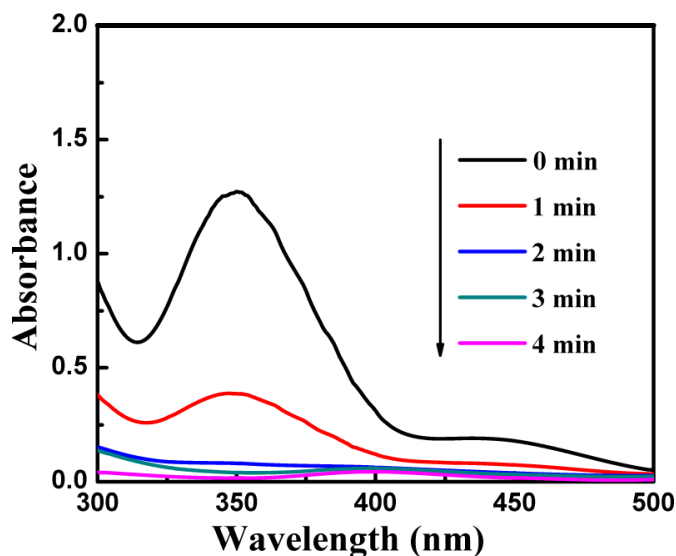


Figure 4.20: UV-visible spectral evolution with time during the reduction of $\text{Cr}_2\text{O}_7^{2-}$ by formic acid at 25°C in the presence of Ni-RGO [73].

Ni-RGO is found to be very active $\geq 98\%$ on Cr(VI) reduction at $\text{pH} = 2$ at 25°C . The authors found that Ni-RGO facilitates the formic acid-induced Cr(VI) \rightarrow Cr(III) reduction at room temperature with a very high rate constant value and can be recycled with its original activity. Ni-RGO is very cost-effective compared to Pd NPs, which are not only costly but also need high temperature to reduce Cr(VI) to Cr(III) [73].

Dubey *et al.* synthesized graphene sand composite (GSC) from sugar and sand using green chemistry approach and adsorption of Cr(VI) ions from aqueous solution was studied by batch adsorption technique under varying experimental conditions like contact time, pH, adsorbent dose, initial Cr (VI) concentration and temperature. The GSC shows very high adsorption capacity due to the large number of active sites present on the adsorbent surface as well as a variety of functional groups. Furthermore, the increase in number of Cr(VI) ions in the solution for a fixed amount of adsorbent results in a higher metal ion concentration which provides an important driving force to over-come all mass transfer resistances of the pollutant between the aqueous and solid phases, thus increasing the metal ions uptake. The adsorption capacity increases with increasing temperature in the case of the endothermic reactions. It decreases with temperature when the reaction is exothermic. The endothermic adsorption of Cr(VI) ions on the GSC appears to be an uncommon behavior.

The results clearly reveal that maximum adsorption of Cr(VI) is obtained at acidic pH, which may be due to the fact that in the aqueous solution several forms of Cr(VI) ions exist such as

chromate (CrO_4^{2-}), dichromate ($\text{Cr}_2\text{O}_7^{2-}$) and hydrogen chromate (HCrO_4^-). These forms of Cr(VI) ion are related to pH of the solution and total chromate concentration. When the pH is lower than 6.8, the dominant species are HCrO_4^- ions, while above 6.8 only CrO_4^{2-} ions are stable [76]. The optimum adsorption of Cr(VI) by the adsorbent was observed at pH 1.5. The maximum adsorption capacity of GSC for Cr(VI) was found to be 2859.38 mg/g at room temperature [76].

As a result for all the lectures, it is highly desirable to develop new adsorbent materials with high specific surface area, highly porous character, multiple adsorption sites and relatively low-cost and chemical stability in extreme conditions for high adsorption of Cr(VI) at room temperature.

Dyes are important water pollutants, which are discharged from many sources such as printing, textile, dyeing, paper and pulp, tannery and paint industries. The presence of dyes in water can cause problems to aquatic life and some dyes are toxic to human life [107]. Most dyes are dissolved and present as either cationic or anionic ions, and few are dispersive. The cationic dyes included methylene blue (MB), rhodamine B (RhB), malachite green (MG), methyl violet (MV) and rhodamine 6G (R6G), and the anionic dyes consist of methyl orange (MO) and rose Bengal [65]. One of the most difficult tasks confronted by the wastewater treatment plants of textile industries is the removal of the color of these compounds, mainly because dyes and pigments are designed to resist biodegradation, such that they remain in the environment for a long period of time [108]. Accordingly, traditional biological or chemical oxidation methods are difficult to remove them from wastewater. Simultaneously, dyes are always highly soluble in water, rendering them hard to be dealt with by precipitation or flocculation.

From an environmental point of view, the treatment and disposal of organic dyes are of great concern. Therefore, cost-effective methods are still urgently demanded to remove coloured substance from wastewater. Adsorption is an effective and classic depth processing in the field of wastewater treatment, by which a substance at the interfacial layer of the adsorbent would accumulate owing to the operation of surface forces. Adsorption has such merits as a low invest-cost, simplicity of design and operation, and no discharge of harmful substances [87]. Despite its short development history, GO/rGO-based composites have been used to treat different types of dyes (see details in **Table 4.3**). Due to ionic forms of dye molecules in water, major interaction attributed to dye adsorption on GO/rGO is cationic-anionic force. Also GO/rGO-based composites can be good adsorbents for cationic and anionic dyes through π - π stacking interactions [65]. For example, we will discuss some reports on rhodamine B (RhB)

and methyl orange (MO), two model systems of organic pollutants, removal using GO/rGO-based composites from aqueous solutions.

RhB, being a well-known water tracer fluorescent and a colorant in textiles, is highly water soluble, non-volatile, and bright reddish violet in color. However, it is a hazardous organic compound in the environment. Thus, it is considered worthwhile to develop a simple method to treat effluents containing RhB for the protection of water sources and the environment.

Bian *et al.* reported a one-pot synthesis of SnS₂/rGO nanocomposites *via in situ* reduction of graphene oxide (GO) by Sn²⁺ under hydrothermal conditions [88]. The adsorption characteristics of the SnS₂ rGO nanocomposites were examined using RhB as adsorbate in a conical flask at room temperature. The result shows that, in the initial 5 min, the concentration of RhB decreased by 90% for SnS₂/rGO nanocomposites with a maximum adsorption capacity q_{\max} of 94.07 mg/g, while only 68% and 45% for pristine rGO and SnS, respectively. However, the application is often limited due to the difficulty in removing the suspended graphene from water after the adsorption, which may increase the cost of industrial application and/or cause the treated water to be re-polluted. It is well known that magnetic separation provides a rapid and effective way for removing and recycling magnetic particles/hybrids by applying an appropriate external magnet [88].

For that matter, wide development has been made to introduce permanently anchored magnetic nanoparticles to GO or rGO nanosheets. For illustration, Geng *et al.* have synthesized RGO–Fe₃O₄ NPs by hydrothermal method. The results show that, benefiting both from the surface property of RGO and from the magnetic property of Fe₃O₄, the hybrid possesses quite a good and versatile adsorption capacity to the dyes under investigation, and can be easily and rapidly extracted from water by magnetic attraction. The adsorption performance of this hybrid has been tested on a series of dyes, such as RhB, R6G, AB92, OII, MG and NC. The result clearly shows that, the adsorption performance of the hybrid exhibits satisfactory tolerance against the variations in pH conditions/dye concentrations. Furthermore, the versatility of this RGO–Fe₃O₄ hybrid adsorbent for various dyes' adsorption and removal was further demonstrated. It was found that by simply annealing under moderate conditions, this hybrid adsorbent can be easily and efficiently regenerated for reuse without compromising its high adsorption capacity [85].

Jiao *et al.* reported on the facile preparation and dye removal efficiency of nanohybrid composed of GO/Fe₃O₄ nanoparticles. Two cationic dyes, methylene blue (MLB) and RhB, and one anionic dye, methyl blue (MB), were investigated as organic pollutants. The results

showed an impressively high removal rate for MLB, which reaches above 95% within only 30 min and the removal rate for RhB can also reach above 80%, while MB removal rate was less than 40% under the same conditions. Moreover, the magnetic properties of the nanohybrid make easy separation and adsorbent recycling as shown in **Figure 4.21** [90].

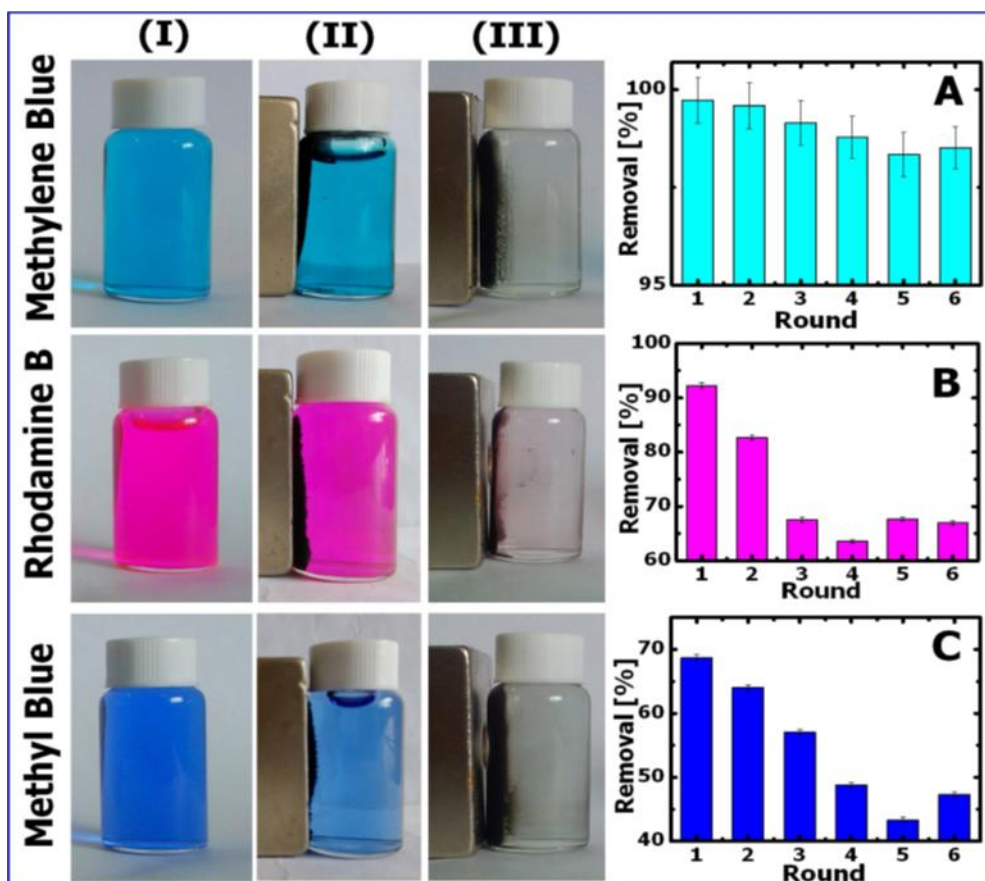


Figure 4.21: Photographs of dye solutions ($20 \text{ mg}\cdot\text{L}^{-1}$) before (I) and after (II) adding Fe_3O_4 multifaceted nanoparticles or (III) adding GO/ Fe_3O_4 nanohybrid. Percent dye removal rate was determined after 12 h adsorption with constant shaking [90].

Methyl orange (MO) is an azo dye (anionic dye) widely used in foodstuff, dyeing and printing, leather and pharmaceutical industries, as a pH indicator, research laboratories, textile, etc may result in its release to the environment through various waste streams [109]. It is also known as C.I. Acid Orange 52, C.I. 13025, helianthine B, Orange III, Gold orange, and Tropaeolin D [110]. Although MO is not highly hazardous, it can cause some harmful effects. Acute exposure to MO can cause increased heart rate, vomiting, shock, cyanosis, jaundice, quadriplegia, and tissue necrosis in humans. However, the release of MO and the products related to the

environment have caused serious pollution problems [111]. Thus, the removal of MO from wastewaters and effluents is very important because of its potential toxicity to humans and environment. For these reasons, the use of various adsorbents for removing MO is gaining increasing attention. For example, Yang *et al.* have synthesized, by calcining graphene oxide (GO)/layered double hydroxide (LDH) hybrid in nitrogen atmosphere, a magnetic hybrid nanomaterial rGO/Ni/MMO (reduced graphene oxide, zero-valent nickel, and NiAl-mixed metal oxide) [94]. This magnetic hybrid nanomaterial exhibits excellent adsorption ability toward MO in aqueous solutions. The result shows that the adsorption amount of MO increases with time, and the color has changed after the addition of the adsorbent, as shown in **Figure 4.22**. The adsorption is quite rapid in the initial 60 min, and the adsorption rate becomes slower until equilibrium is reached at about 16 h. The rGO/Ni/MMO hybrid thus prepared displays excellent adsorption ability to MO ($210.8 \text{ mg}\cdot\text{g}^{-1}$) under the following experimental conditions (MO concentration: 100 mg L^{-1} , adsorbent dosage: $1 \text{ mg}\cdot\text{mL}^{-1}$, temperature: 25°C) [94].

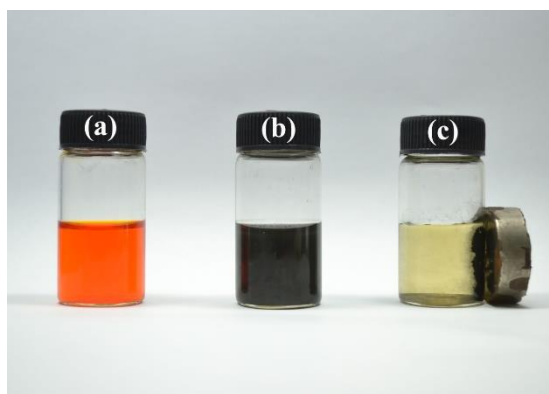


Figure 4.22: Photos showing (a) MO water solution, (b) rGO/Ni/MMO hybrid dispersed into MO aqueous solution, and (c) the MO solution turned into light yellow after adsorption and the rGO/Ni/MMO hybrid was separated by external magnetic field [94].

On the other hand, Zhang *et al.* have successfully prepared a $\text{TiO}_2/\text{ZnO-NH}_2$ -reduced graphene oxide (TZ-a-RGO) nanocomposite using a facile one-step hydrothermal method. The TZ-a-RGO was used as a catalyst to remove MO from wastewater, and the results indicated that the catalytic system TZ-a-RGO had the characteristics of fast adsorption and photodegradation simultaneously in terms of removal of MO. The removal of MO was obtained through a synergistic effect of amine-RGO adsorption and ZnO/TiO_2 photocatalysis *via* the adsorption and photocatalytic degradation experiments. The result shows that, 38% dye molecules were quickly adsorbed on the surface of TZ-a-RGO after 2 min and the solution

reached equilibrium after 10 min, at which 45% MO were adsorbed and the adsorption ability to MO was determined to be 40 mg.g⁻¹ [93].

Based on the above discussions, the most important parameters in dye adsorption technology is the initial concentration of the dye and the dose of adsorbent, and high efficiency over a wide range pH.

Finally, among all the reports, adsorption technology is one of the most effective methods for dye removal due to its low cost, high efficiency, simplicity, easy to perform, and insensitive to toxic substances. However, these conventional treatment technologies have a common drawback that they are unable to completely remove the toxic organic and inorganic pollutants from wastewater, causing secondary pollution which is economically unfeasible. For that, the magnetic adsorbent will be the best one, because it allows removal of toxic organic and inorganic pollutants (dyes, Cr (VI) ,....) and the adsorbent itself from water.

In this section, we will take benefit of the high surface area and the magnetic properties of rGO-Co₃O₄ nanocomposite for Cr(VI) removal from aqueous solutions.

4.5.3. Chromium Cr(VI) removal from aqueous solution by rGO-Co₃O₄ nanocomposite

4.5.3.1. Adsorption experiments

We prepared a stock potassium dichromate (K₂Cr₂O₇) aqueous solution (500 mg/mL) at shaking speed of 200 rpm. Simulated wastewater with different Cr concentrations (25, 50, 100, 200, 300 and 400 mg/L) were prepared by dilution of the stock K₂Cr₂O₇ standard solution with Milliq-water. The pH values of the Cr solutions were adjusted to 3 with 0.1 mol/L HCl aqueous solution [70, 72, 77, 78]. After the adsorption processes, rGO-Co₃O₄ composite was conveniently recovered by magnetic separation as shown in **Figure 4.23**. The photographs clearly indicate that after adsorption of Cr(VI) ions, the yellow color of the metal ion solution is completely lost, which suggests an almost total removal of chromium ions by the rGO-Co₃O₄. To check the effect of Cr(VI) concentration in solution on the removal capacity experiment, the as-prepared rGO-Co₃O₄ composite (2 mg) was dispersed into 2 mL of Cr(VI) solution at different Cr(VI) concentrations at pH=3 using a shaking speed of 400 rpm for 12 h. The solution was extracted by using a magnet to separate the rGO-Co₃O₄ and take the supernatant for ultraviolet analysis in order to determine the residual concentration of Cr(VI). The UV–visible analysis was performed at room temperature (25°C).

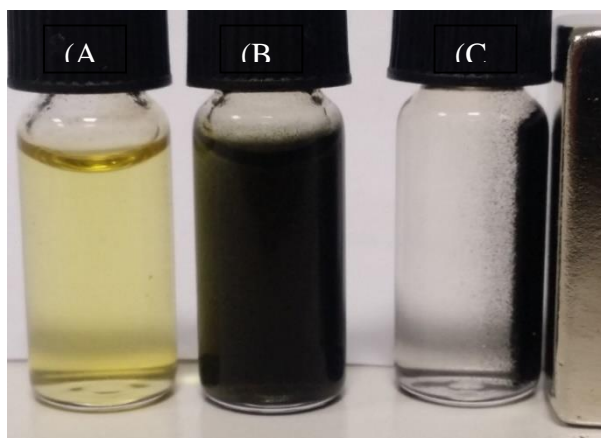


Figure 4.23: Photographs of (A) the Cr(VI) aqueous solution, (B) Cr(VI) solution with the catalyst, and (C) Cr(VI) solution adsorbed by rGO-Co₃O₄ nanocomposite after 12h .

Figure 4.24 shows the UV-vis spectrum of a Cr(VI) aqueous solution at a concentration of 50 mg/L in the range of 200–500 nm. It is clearly seen that in the presence of rGO-Co₃O₄ the absorption band of Cr₂O₇²⁻ at 348 nm shifts to 367 nm after adding the catalyst. This new peak decreases rapidly and disappears within 12 h. Also, as noted previously, the color of the solution changes from deep yellow to colorless, confirming the complete adsorption of Cr(VI) by rGO-Co₃O₄.

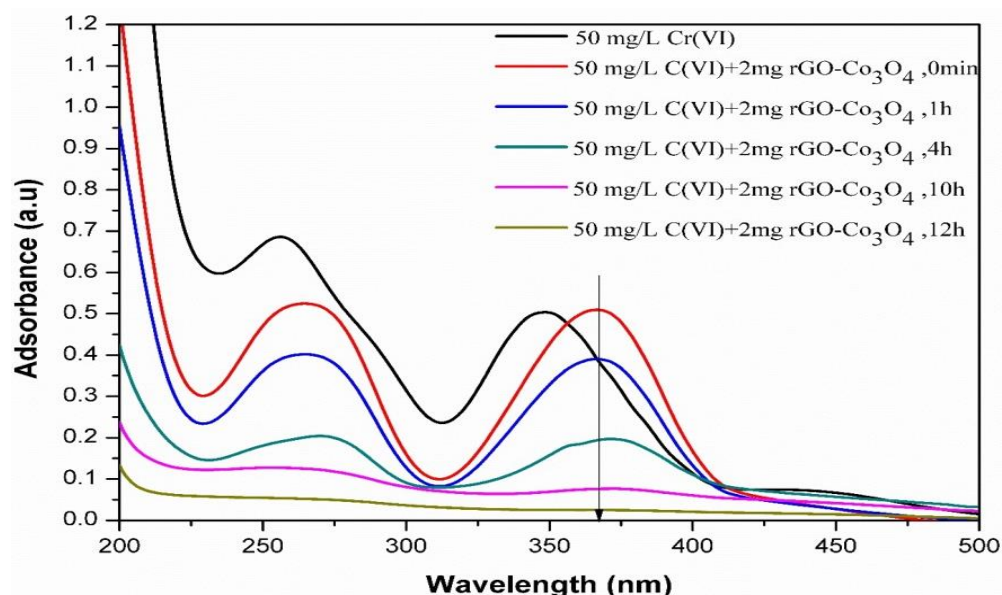


Figure 4.24: UV–visible spectral evolution with time during adsorption of Cr(VI) ions by rGO-Co₃O₄; Cr (VI) ion concentration: 50 mg/L, adsorbent dosage: 1mg/mL, temperature: 25°C, pH: 3.0.

By testing the absorbance of Cr (VI) aqueous solution with different concentrations, a linear relationship between the concentration and the absorbance was established (**Figure 4.25**).

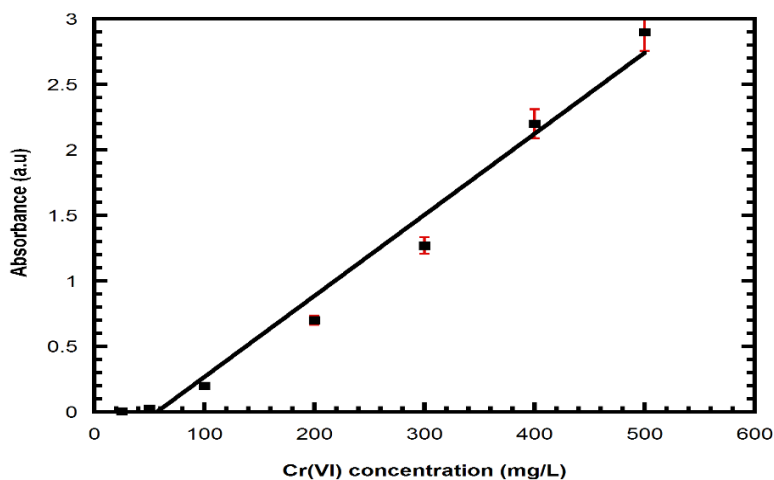


Figure (4.25): Absorbance of aqueous Cr(VI) solution as a function of aqueous Cr(VI) concentrations; adsorbent dosage: 1 mg/ml, temperature: 25°C, pH 3.0.

4.5.3.2. Adsorption isotherm

In this study, rGO-Co₃O₄ nanocomposite was used to analyse the adsorption behavior of Cr (VI), the Langmuir model was used to simulate Cr(VI) adsorption isotherm. If the adsorbent has an ideal homogeneous adsorption surface with all the adsorption sites having the same sorption energy independent of surface coverage, the Langmuir model will be fitted. The removal capacity of Cr(VI) ions is calculated by the following formula [64, 112].

$$Q = (C_0 - C_e) V/W$$

where V (L) is the initial volume of Cr(VI) solution, W (g) is the mass of the as-prepared rGO-Co₃O₄, C₀ (mg/L) is the initial concentration of Cr(VI) ions, C_e (mg/L) is the equilibrium concentration of Cr(VI) ions, Q (mg/g) is the reduction capacity.

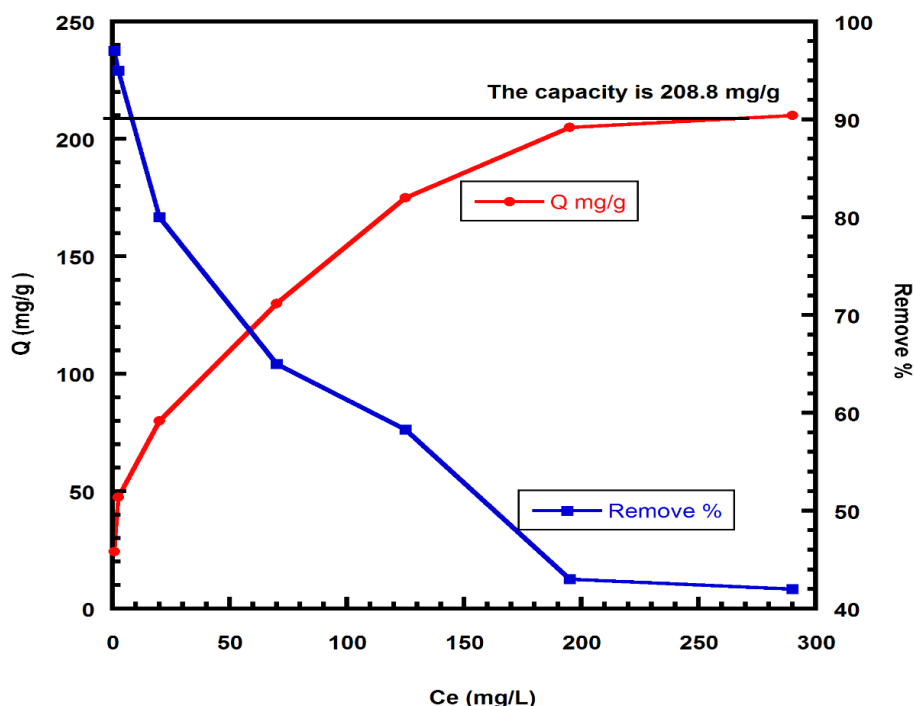


Figure 4.26: Adsorption isotherms of Cr(VI) on the rGO-Co₃O₄ at pH 3.0 (initial concentration: 25-500 mg.L⁻¹, adsorbent dosage: 1 mg/ml, pH 3.0, temperature: 25°C, contact time: 12 h).

From **Figure 4.26**, we can see that Cr(VI) ions are favorably adsorbed on the rGO-Co₃O₄ and the maximum adsorption capacity of Cr (VI) attained was 208.8 mg.g⁻¹. The adsorption capacity obtained with the rGO-Co₃O₄ is higher than that obtained with many other adsorbents, as shown in **Table 4.3**.

We calculated the removal amount of Cr(VI) ions based on a calibration curve made by UV-Vis spectrophotometer. In order to determine the concentration of Cr(VI) ions, the calibration curve was obtained from standard solutions of Cr (0.5, 1, 4, 8–300 mg/L) solution as shown in **Figure 4.27**.

The pH of the solution is one of the most important variables affecting the adsorption characteristics of ionic adsorbate. The relation between the initial pH of solution and the adsorption capacity of Cr(VI) is shown in **Figure 4.28**. It was found that a higher adsorption capacity was obtained at a lower solution pH. The effect of solution pH can be explained by the surface charge of the adsorbent and the degree of ionization of the adsorbate.

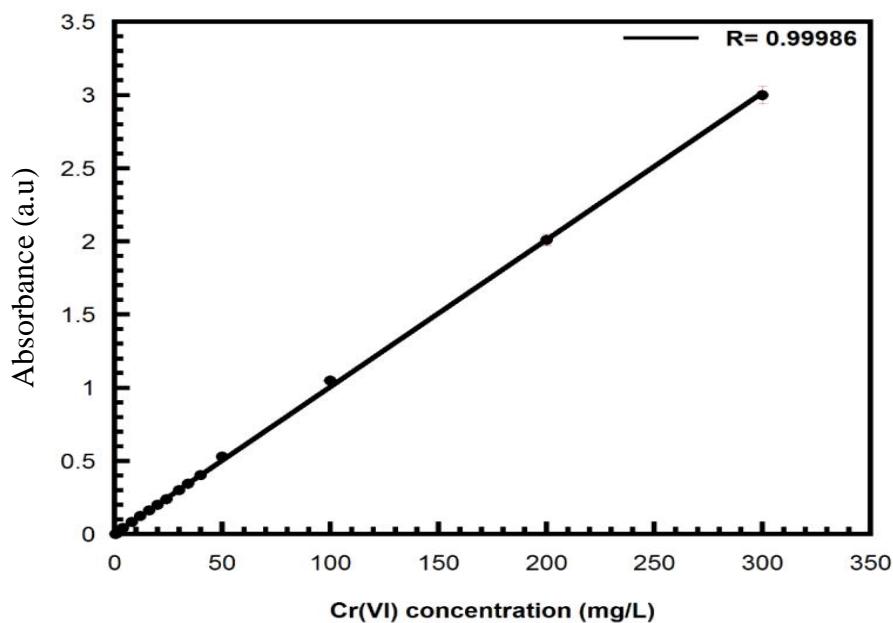


Figure 4.27: Calibration curve for Cr (VI) solution.

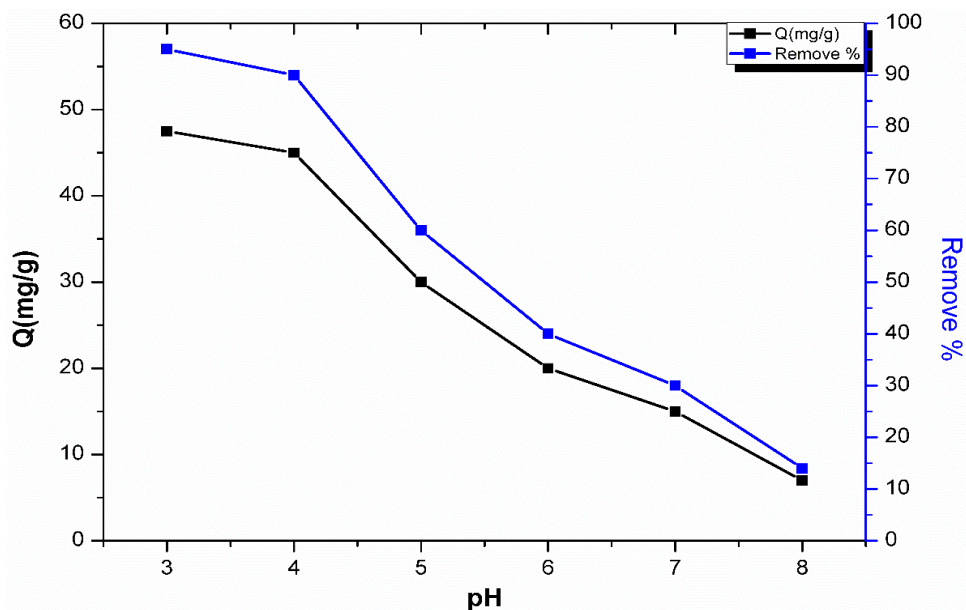
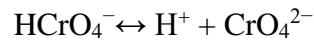


Figure 4.28: Effects of solution pH on adsorption capacity; Cr(VI) ion concentration: 50 mg/L, adsorbent dosage: 1 mg/ml, temperature: 25°C, contact time: 12 h.

Chromium occurs in different anionic forms (i.e., $\text{H}_2\text{Cr}_2\text{O}_7$, $\text{Cr}_2\text{O}_7^{2-}$, HCrO_4^- , CrO_4^{2-} and HCr_2O_7^-) in aqueous solution, depending on the solution pH and concentration [76]. The following equilibria exist in an aqueous solution:



It can be seen from **Figure 4.28** that the results clearly reveal that maximum adsorption of Cr(VI) is obtained in acidic media. This may be due to the fact that in the aqueous solution several forms of Cr(VI) ions exist such as $\text{Cr}_2\text{O}_7^{2-}$ and hydrogen chromate (HCrO_4^-), which are the dominant species in acidic media. In this case, the negatively charged HCrO_4^- can be adsorbed on the rGO- Co_3O_4 through electrostatic attraction. The reason is that as a large number of H^+ ions can neutralize the negatively charged adsorbent surface, thereby reducing hindrance to the diffusion of dichromate ions at low pH [113]. With the increase of pH, the degree of protonation of the surface decreases gradually and only chromate (CrO_4^{2-}) ions remain as stable species in alkaline media. In addition, the attachment of hydroxyl (OH^-) groups on the adsorbent surface in alkaline media can be another possible cause, which competes with the adsorption of Cr(VI) ions and leads to the decline of the removal efficiency [114]. So when the solution pH is changed, the existing form of Cr(VI) ions will influence the uptake capacity of the rGO- Co_3O_4 for Cr(VI).

The Langmuir isotherm is used to describe the equilibrium established between adsorbed metal ions on the adsorbent (Q_e) and metal ions remaining in solution (C_e) at a constant temperature. In our research, adsorption isotherms of the type Q_e vs C_e was used to verify the isotherm model. The equilibrium adsorption data were fitted with Langmuir model by the following equation:

$$Q_e = \frac{Q_{max} b C_e}{1 + b C_e} \quad \text{or} \quad \frac{C_e}{Q_e} = \frac{1}{Q_{max} b} + \frac{C_e}{Q_{max}}$$

Where C_e (mg/L) is the equilibrium concentration of Cr(VI) ions, Q_e (mg/g) is the amount of Cr(VI) ions adsorbed, Q_{max} (mg/g) is the maximum adsorption capacity of Cr(VI) ions, and b (L/mg) is the Langmuir isotherm coefficient.

A linear fit was applied to obtain the Langmuir isotherm parameters as shown in **Figure 4.29**. Taking into consideration the values of the correlation coefficient as a criterion for goodness of fit for the system, the Langmuir model shows better correlation ($R^2=0.990$), which indicates that the Langmuir equation represents the adsorption process more ideally. The Langmuir

isotherm model gives a maximum adsorption capacity of 222.22 mg. g⁻¹ for Cr(VI), which is very close to the experimental value of 208.8 mg.g⁻¹.

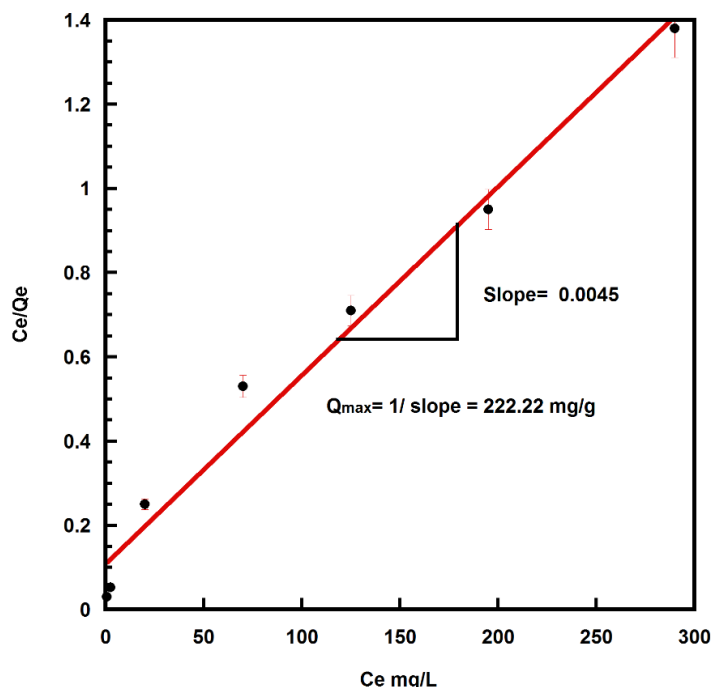


Figure 4.29: The Langmuir isotherm; Cr(VI) ion concentration: 50 mg/ L, adsorbent dosage: 1 mg/ml, temperature: 25°C, contact time: 12 h.

In conclusion, we have demonstrated that optimized rGO-Co₃O₄ composite with a high specific surface area and stable superparamagnetic properties exhibits a fast Cr(VI) removal performance with a high adsorption capacity. In addition, the equilibrium adsorption process was found to follow the Langmuir model suggesting monolayer coverage sorption of Cr(VI) on the surface of rGO-Co₃O₄. The adsorption capacity of rGO-Co₃O₄ for Cr(VI) ions was highly pH dependent, and the adsorption capacity of rGO-Co₃O₄ for Cr(VI) ions decreased with increasing solution pH. Finally, these results evidence that rGO-Co₃O₄ has a promising potential for the removal of heavy metal ions from wastewater.

4.5.4. Dye removal from aqueous solution

In order to investigate the removal ability of rGO-Co₃O₄ nanocomposite of organic dyes in aqueous solutions, we have investigated three different dyes (rhodamine B, methyl orange and Rose Bengal) at three different concentrations for each dye. For the adsorption experiments, 2

mg of rGO-Co₃O₄ nanocomposite was added to 2 mL of an aqueous solution containing RhB, MO or rose Bengal (5, 10 or 15 μM) at room temperature at pH 7.

Dye removal efficiency was calculated by measuring the dye concentration before and after adsorption using UV–Vis spectroscopy. The concentrations of the remnant dye were determined by measuring the absorbance of solutions at 554 nm (RhB), 463 nm (MO) and 550 nm (Rose Bengal), respectively (see **Figures 4.30, 4.31 and 4.32**).

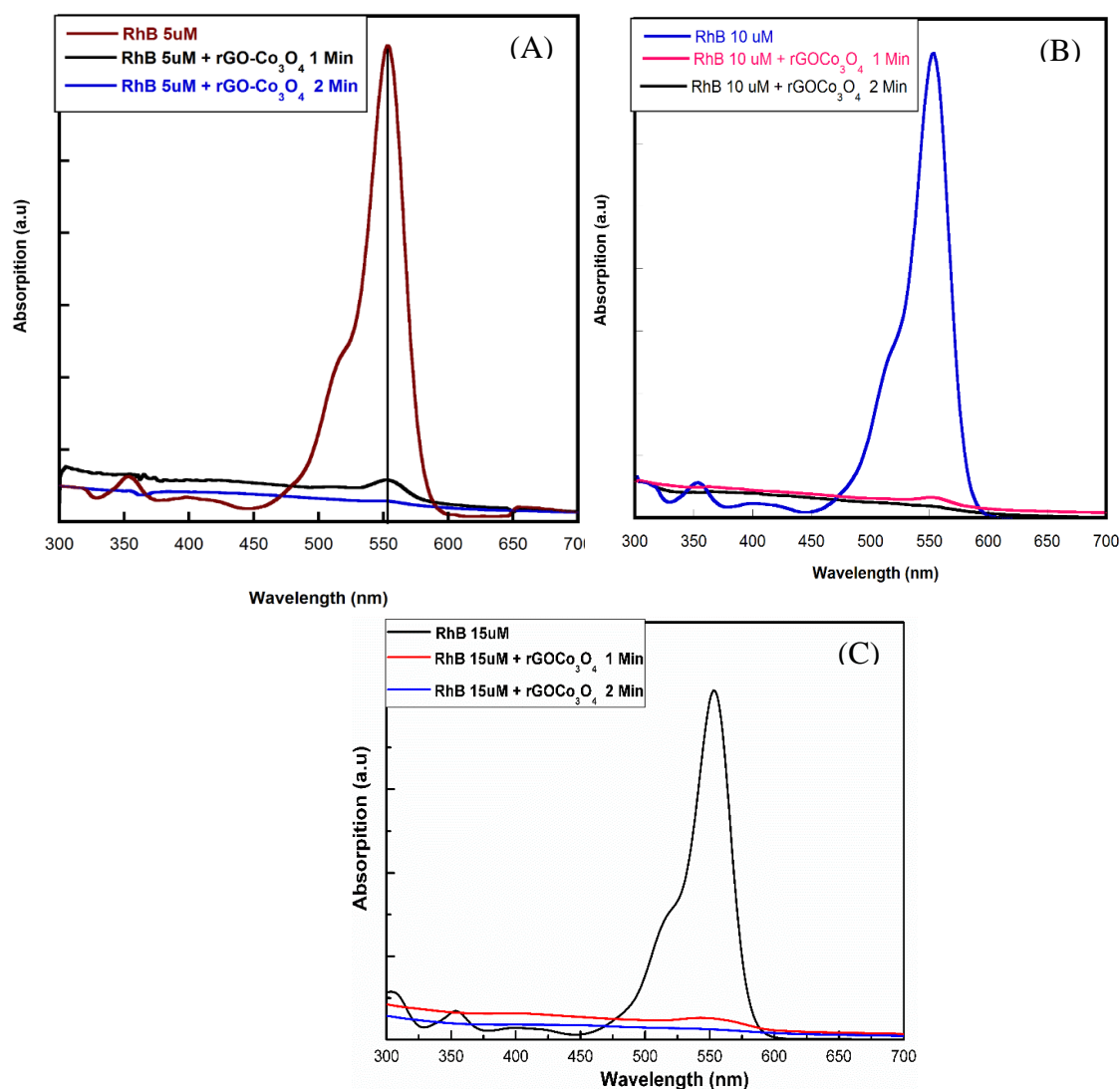


Figure 4.30: UV-Vis spectra of the original RhB solution (A) 5 μM, (B) 10 μM and (C) 15 μM before and after adsorbent treatment (1 mg/ml of rGO-Co₃O₄, 25°C).

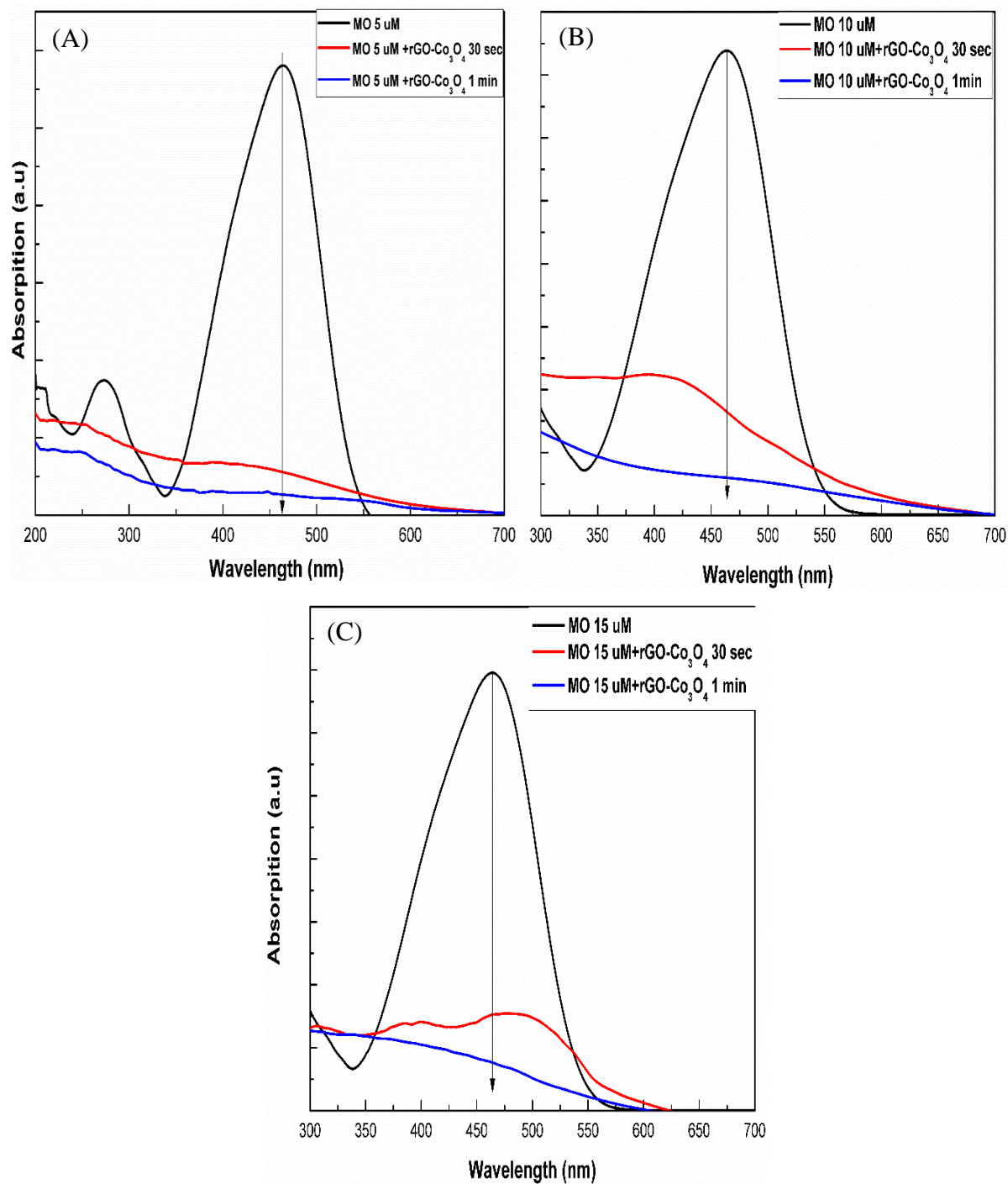


Figure 4.31: UV-Vis spectra of the original MO solution (A) 5 μM , (B) 10 μM and (C) 15 μM before and after adsorbent treatment (1 mg/ml of rGO-Co₃O₄, 25°C).

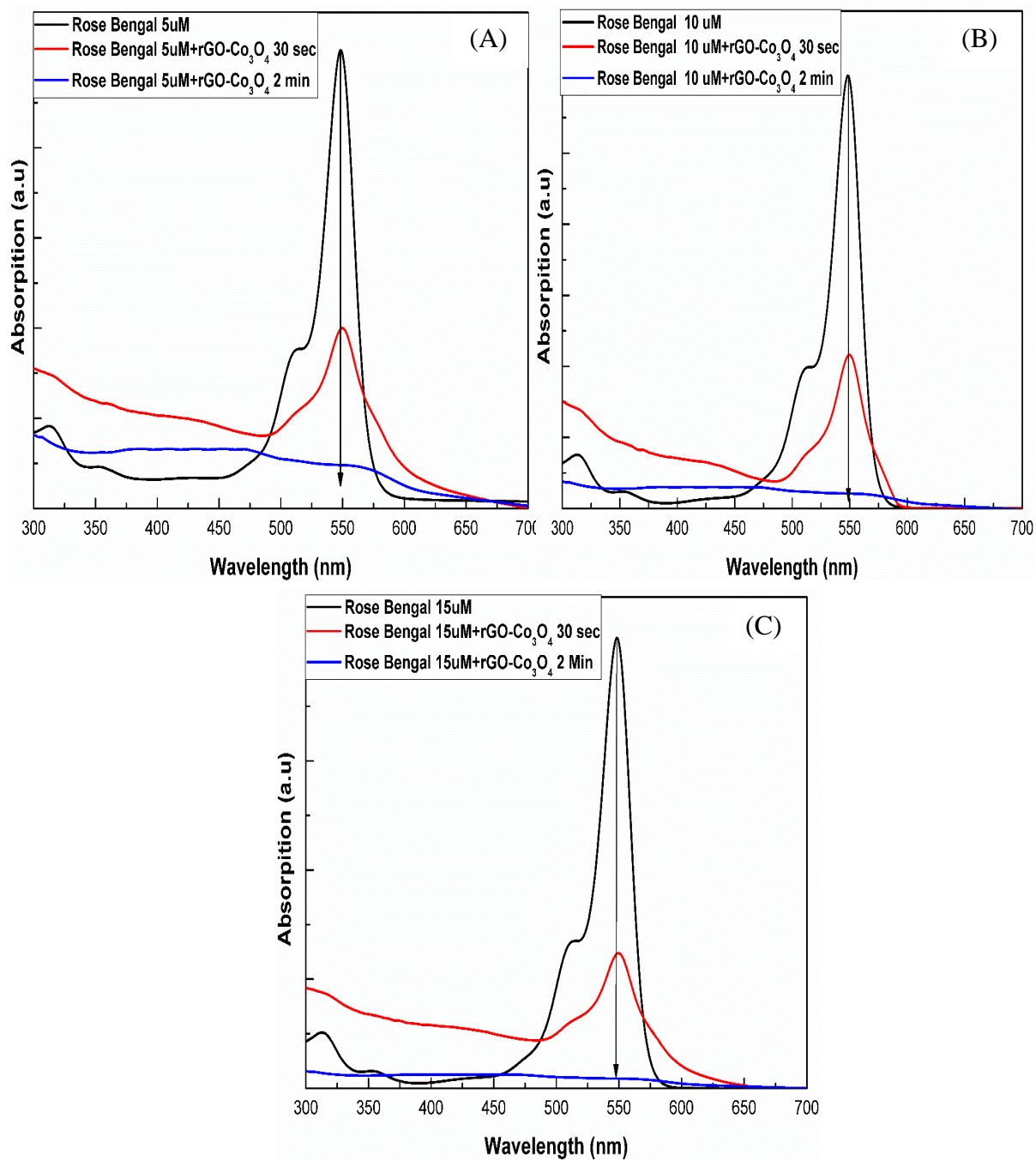


Figure 4.32: UV-Vis spectra of the original Rose Bengal solution (A) 5 μM , (B) 10 μM and (C) 15 μM before and after adsorbent treatment (1 mg/ml of rGO-Co₃O₄, 25°C).

The results indicate that rGO-Co₃O₄ nanocomposite was very efficient for dye adsorption with complete removal within 2, 1 and 2 min for RhB, MO and Rose Bengal, respectively. The performance of the rGO-Co₃O₄ nanocomposite was quite high as compared to other graphene-

based adsorbents (see **Table 4.3**) with the benefit of being easily separated by applying an external magnet.

Figure 4.33 displays photos of the adsorption process; the formation of transparent solutions upon application of an external magnet (1 Tesla) clearly indicates that the dyes have been successfully adsorbed by rGO-Co₃O₄ nanocomposite.



Figure 4.33: Photographs of (A) RhB, (B) MO and (C) Rose Bengal aqueous solutions before and after treatment with 1 mg/ml of rGO-Co₃O₄ nanocomposite. The right photos correspond to the solutions of the bottles in the centre upon application of an external magnet (1 Tesla).

4.5.4.1. Adsorption mechanism

To gain a better understanding on the important parameters that govern the adsorption process, we have applied rGO as adsorbent of RhB, MO and Rose Bengal from aqueous solution (Figure 5.34).

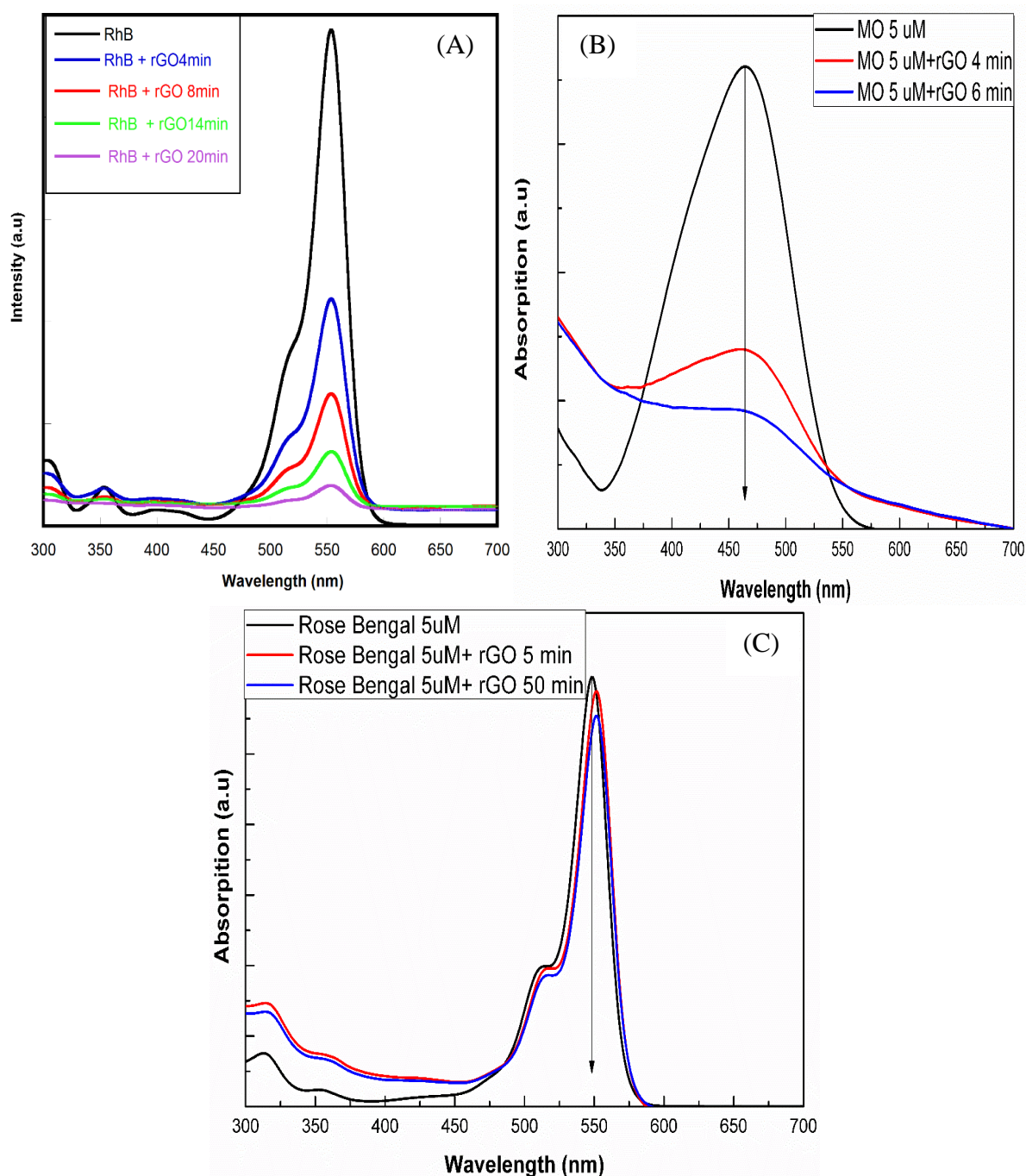


Figure 4.34: UV-Vis spectra of the original RhB (A), MO (B) and (C) Rose Bengal aqueous solutions before and after adsorbent treatment (initial concentration of dyes: 5 μM, rGO: 1mg/ml, T=25°C).

Although rGO is efficient for dye removal, the adsorption process was quite longer; it took 20 min to remove 92% of RhB and 6 min to remove 75 % of MO. However, rGO was not efficient for Rose Bengal adsorption with only 8% removal after 50 min. Interestingly, under otherwise identical experimental conditions, rGO-Co₃O₄ nanocomposite removed 96%, 91% and 92% of RhB, MO and Rose Bengal after 2, 1 and 2 min, respectively.

From these results, we can conclude that hybridization of rGO with Co₃O₄ NPs improved significantly its adsorption capacity for all investigated dyes with the big advantage of being easily separated by an external magnet.

The mechanism of dye adsorption is controlled by various factors such as the physical and/or chemical properties of the graphene. rGO nanosheets are capable of interacting with a dye molecule through π - π conjugation, H-bonding, electrostatic and hydrophobic interactions [111, 115]. Moreover, adsorption strongly depends on the pore structure and surface area as well as surface functionality of adsorbents [65]. The surface structure of graphene has a strong influence on its adsorption capability. First, the electrostatic forces between the positive charge dyes and the negative charged surfaces of rGO and these forces increasing when we introduced Co₃O₄ NPs on the graphene sheets [116] [111]. Moreover, the highly dispersion of Co₃O₄ NPs over the rGO support results in enhanced surface area and improved porosity and adsorb ability. Additionally, we would like to attribute the interaction between the hybrid and dyes to π - π conjugation through sp² carbon instead of binding at the oxygen groups that coming from the cobalt oxide [87].

The result proved that rGO-Co₃O₄ nanocomposite is an excellent dye adsorbent; it works at neutral pH and is very efficient as compared to other adsorbents as in **Table 4.3**. Moreover, the rGO-Co₃O₄ hybrid is superparamagnetic at room temperature. Therefore it can be easily and rapidly extracted from the solution through magnetic separation.

4.6. References

- [1] Novoselov KS, Jiang D, Schedin F, Booth TJ, Khotkevich VV, Morozov SV, et al. Two-dimensional atomic crystals. *Proceedings of the National Academy of Sciences of the United States of America*. 2005;102(30):10451-3.
- [2] Geim AK, Novoselov KS. The rise of graphene. *Nature materials*. 2007;6(3):183-91.
- [3] Neto AC, Guinea F, Peres N, Novoselov KS, Geim AK. The electronic properties of graphene. *Reviews of modern physics*. 2009;81(1):109.
- [4] Novoselov KS, Fal'ko VI, Colombo L, Gellert PR, Schwab MG, Kim K. A roadmap for graphene. *Nature*. 2012;490(7419):192-200.
- [5] Si Y, Samulski ET. Exfoliated graphene separated by platinum nanoparticles. *Chemistry of Materials*. 2008;20(21):6792-7.
- [6] Nethravathi C, Anumol E, Rajamathi M, Ravishankar N. Highly dispersed ultrafine Pt and PtRu nanoparticles on graphene: formation mechanism and electrocatalytic activity. *Nanoscale*. 2011;3(2):569-71.
- [7] Xu C, Wang X, Zhu J. Graphene– metal particle nanocomposites. *The Journal of Physical Chemistry C*. 2008;112(50):19841-5.
- [8] Gotoh K, Kinumoto T, Fujii E, Yamamoto A, Hashimoto H, Ohkubo T, et al. Exfoliated graphene sheets decorated with metal/metal oxide nanoparticles: simple preparation from cation exchanged graphite oxide. *Carbon*. 2011;49(4):1118-25.
- [9] Wu Z-S, Zhou G, Yin L-C, Ren W, Li F, Cheng H-M. Graphene/metal oxide composite electrode materials for energy storage. *Nano Energy*. 2012;1(1):107-31.
- [10] Bell NJ, Ng YH, Du A, Coster H, Smith SC, Amal R. Understanding the enhancement in photoelectrochemical properties of photocatalytically prepared TiO₂-reduced graphene oxide composite. *The Journal of Physical Chemistry C*. 2011;115(13):6004-9.
- [11] Huang X, Zhou X, Zhou L, Qian K, Wang Y, Liu Z, et al. A Facile One-Step Solvothermal Synthesis of SnO₂/Graphene Nanocomposite and Its Application as an Anode Material for Lithium-Ion Batteries. *Chemphyschem : a European journal of chemical physics and physical chemistry*. 2011;12(2):278-81.
- [12] Koo HY, Lee HJ, Go HA, Lee YB, Bae TS, Kim JK, et al. Graphene-Based Multifunctional Iron Oxide Nanosheets with Tunable Properties. *Chemistry-A European Journal*. 2011;17(4):1214-9.
- [13] Mandal S, Phadtare S, Sastry M. Interfacing biology with nanoparticles. *Current Applied Physics*. 2005;5(2):118-27.
- [14] LaConte L, Nitin N, Bao G. Magnetic nanoparticle probes. *Materials Today*. 2005;8(5):32-8.
- [15] Ikedo Y, Sugiyama J, Nozaki H, Itahara H, Brewer J, Ansaldo E, et al. Spatial inhomogeneity of magnetic moments in the cobalt oxide spinel Co₃O₄. *Physical Review B*. 2007;75(5):054424.
- [16] Pan L, Zhao H, Shen W, Dong X, Xu J. Surfactant-assisted synthesis of a Co₃O₄/reduced graphene oxide composite as a superior anode material for Li-ion batteries. *Journal of Materials Chemistry A*. 2013;1(24):7159.
- [17] Park S, Park S-J, Kim S. Fabrication and Capacitance of Co₃O₄-Graphene Nanocomposites Electrode Prepared by Pulse Microwave-assisted Reduction Methods. *Bulletin of the Korean Chemical Society*. 2012;33(12):4247-50.
- [18] Shahid MM, Pandikumar A, Golsheikh AM, Huang NM, Lim HN. Enhanced electrocatalytic performance of cobalt oxide nanocubes incorporating reduced graphene oxide as a modified platinum electrode for methanol oxidation. *RSC Adv*. 2014;4(107):62793-801.

- [19] Cheng C-S, Serizawa M, Sakata H, Hirayama T. Electrical conductivity of Co₃O₄ films prepared by chemical vapour deposition. *Materials chemistry and physics*. 1998;53(3):225-30.
- [20] Ando M, Kobayashi T, Iijima S, Haruta M. Optical recognition of CO and H₂ by use of gas-sensitive Au-Co₃O₄ composite films. *J Mater Chem*. 1997;7(9):1779-83.
- [21] Pirovano C, Trasatti S. The point of zero charge of Co₃O₄: Effect of the preparation procedure. *Journal of electroanalytical chemistry and interfacial electrochemistry*. 1984;180(1):171-84.
- [22] Sakamoto S, Yoshinaka M, Hirota K, Yamaguchi O. Fabrication, mechanical properties, and electrical conductivity of Co₃O₄ ceramics. *Journal of the American Ceramic Society*. 1997;80(1):267-8.
- [23] Shinde V, Mahadik S, Gujar T, Lokhande C. Supercapacitive cobalt oxide (Co₃O₄) thin films by spray pyrolysis. *Applied Surface Science*. 2006;252(20):7487-92.
- [24] Shalini K, Mane AU, Shivashankar S, Rajeswari M, Choopun S. Epitaxial growth of Co₃O₄ films by low temperature, low pressure chemical vapour deposition. *Journal of crystal growth*. 2001;231(1):242-7.
- [25] Rahman MM, Wang J-Z, Deng X-L, Li Y, Liu H-K. Hydrothermal synthesis of nanostructured Co₃O₄ materials under pulsed magnetic field and with an aging technique, and their electrochemical performance as anode for lithium-ion battery. *Electrochimica Acta*. 2009;55(2):504-10.
- [26] Garakani MA, Abouali S, Zhang B, Takagi CA, Xu Z-L, Huang J-q, et al. Cobalt Carbonate/ and Cobalt Oxide/Graphene Aerogel Composite Anodes for High Performance Li-Ion Batteries. *ACS applied materials & interfaces*. 2014;6(21):18971-80.
- [27] Li Z, Li W, Xue H, Kang W, Yang X, Sun M, et al. Facile fabrication and electrochemical properties of high-quality reduced graphene oxide/cobalt sulfide composite as anode material for lithium-ion batteries. *RSC Advances*. 2014;4(70):37180.
- [28] Ott LS, Finke RG. Transition-metal nanocluster stabilization for catalysis: a critical review of ranking methods and putative stabilizers. *Coordination Chemistry Reviews*. 2007;251(9):1075-100.
- [29] Yang Y, Zhang F, Wang H, Yao Q, Chen X, Lu Z-H. Catalytic Hydrolysis of Ammonia Borane by Cobalt Nickel Nanoparticles Supported on Reduced Graphene Oxide for Hydrogen Generation. *Journal of Nanomaterials*. 2014;2014:1-9.
- [30] Goenka S, Sant V, Sant S. Graphene-based nanomaterials for drug delivery and tissue engineering. *Journal of controlled release : official journal of the Controlled Release Society*. 2014;173:75-88.
- [31] Lin K-YA, Hsu F-K, Lee W-D. Magnetic cobalt-graphene nanocomposite derived from self-assembly of MOFs with graphene oxide as an activator for peroxydisulfate. *Journal of Materials Chemistry A*. 2015;3(18):9480-90.
- [32] Wang Q, Jiao L, Du H, Si Y, Wang Y, Yuan H. Co₃S₄ hollow nanospheres grown on graphene as advanced electrode materials for supercapacitors. *Journal of Materials Chemistry*. 2012;22(40):21387.
- [33] Zhao Y, Chen S, Sun B, Su D, Huang X, Liu H, et al. Graphene-Co₃O₄ nanocomposite as electrocatalyst with high performance for oxygen evolution reaction. *Sci Rep*. 2015;5.
- [34] Hosu IS, Wang Q, Vasilescu A, Petcu SF, Raditoiu V, Railian S, et al. Cobalt phthalocyanine tetracarboxylic acid modified reduced graphene oxide: a sensitive matrix for the electrocatalytic detection of peroxydinitrite and hydrogen peroxide. *RSC Adv*. 2015;5(2):1474-84.

- [35] Shi P, Su R, Wan F, Zhu M, Li D, Xu S. Co₃O₄ nanocrystals on graphene oxide as a synergistic catalyst for degradation of Orange II in water by advanced oxidation technology based on sulfate radicals. *Applied Catalysis B: Environmental*. 2012;123:265-72.
- [36] Xu C, Wang X, Zhu J, Yang X, Lu L. Deposition of Co₃O₄ nanoparticles onto exfoliated graphite oxide sheets. *Journal of Materials Chemistry*. 2008;18(46):5625-9.
- [37] Wu Z-S, Ren W, Wen L, Gao L, Zhao J, Chen Z, et al. Graphene anchored with Co₃O₄ nanoparticles as anode of lithium ion batteries with enhanced reversible capacity and cyclic performance. *ACS nano*. 2010;4(6):3187-94.
- [38] Yan J, Wei T, Qiao W, Shao B, Zhao Q, Zhang L, et al. Rapid microwave-assisted synthesis of graphene nanosheet/Co₃O₄ composite for supercapacitors. *Electrochimica Acta*. 2010;55(23):6973-8.
- [39] Liang Y, Li Y, Wang H, Zhou J, Wang J, Regier T, et al. Co₃O₄ nanocrystals on graphene as a synergistic catalyst for oxygen reduction reaction. *Nature materials*. 2011;10(10):780-6.
- [40] Wang B, Wang Y, Park J, Ahn H, Wang G. In situ synthesis of Co₃O₄/graphene nanocomposite material for lithium-ion batteries and supercapacitors with high capacity and supercapacitance. *Journal of Alloys and Compounds*. 2011;509(29):7778-83.
- [41] Song Z, Zhang Y, Liu W, Zhang S, Liu G, Chen H, et al. Hydrothermal synthesis and electrochemical performance of Co₃O₄/reduced graphene oxide nanosheet composites for supercapacitors. *Electrochimica Acta*. 2013;112:120-6.
- [42] Xiang C, Li M, Zhi M, Manivannan A, Wu N. A reduced graphene oxide/Co₃O₄ composite for supercapacitor electrode. *Journal of Power Sources*. 2013;226(0):65-70.
- [43] Chen S, Zhu J, Wang X. One-step synthesis of graphene–cobalt hydroxide nanocomposites and their electrochemical properties. *The Journal of Physical Chemistry C*. 2010;114(27):11829-34.
- [44] Ji Z, Shen X, Song Y, Zhu G. In situ synthesis of graphene/cobalt nanocomposites and their magnetic properties. *Materials Science and Engineering: B*. 2011;176(9):711-5.
- [45] Dong X-C, Xu H, Wang X-W, Huang Y-X, Chan-Park MB, Zhang H, et al. 3D graphene–cobalt oxide electrode for high-performance supercapacitor and enzymeless glucose detection. *ACS nano*. 2012;6(4):3206-13.
- [46] Wang X, Song L, Yang H, Xing W, Lu H, Hu Y. Cobalt oxide/graphene composite for highly efficient CO oxidation and its application in reducing the fire hazards of aliphatic polyesters. *Journal of Materials Chemistry*. 2012;22(8):3426.
- [47] Fellahi O, Das MR, Coffinier Y, Szunerits S, Hadjersi T, Maamache M, et al. Silicon nanowire arrays-induced graphene oxide reduction under UV irradiation. *Nanoscale*. 2011;3(11):4662-9.
- [48] Farhadi S, Pourzare K, Sadeghinejad S. Simple preparation of ferromagnetic Co₃O₄ nanoparticles by thermal dissociation of the [CoII(NH₃)₆](NO₃)₂ complex at low temperature. *Journal of Nanostructure in Chemistry*. 2013;3(1):1-7.
- [49] Zhang N, Shi J, Mao SS, Guo L. Co₃O₄ quantum dots: reverse micelle synthesis and visible-light-driven photocatalytic overall water splitting. *Chemical communications*. 2014;50(16):2002-4.
- [50] Kumar R, Kim H-J, Park S, Srivastava A, Oh I-K. Graphene-wrapped and cobalt oxide-intercalated hybrid for extremely durable super-capacitor with ultrahigh energy and power densities. *Carbon*. 2014;79:192-202.
- [51] Liu S-Q, Xiao B, Feng L-R, Zhou S-S, Chen Z-G, Liu C-B, et al. Graphene oxide enhances the Fenton-like photocatalytic activity of nickel ferrite for degradation of dyes under visible light irradiation. *Carbon*. 2013;64:197-206.

- [52] Ren L, Hui KS, Hui KN. Self-assembled free-standing three-dimensional nickel nanoparticle/graphene aerogel for direct ethanol fuel cells. *Journal of Materials Chemistry A*. 2013;1(18):5689.
- [53] Birkholz M. *Thin film analysis by X-ray scattering*: John Wiley & Sons; 2006.
- [54] Yogamalar R, Srinivasan R, Vinu A, Ariga K, Bose AC. X-ray peak broadening analysis in ZnO nanoparticles. *Solid State Communications*. 2009;149(43):1919-23.
- [55] Du W, Liu R, Jiang Y, Lu Q, Fan Y, Gao F. Facile synthesis of hollow Co₃O₄ boxes for high capacity supercapacitor. *Journal of Power Sources*. 2013;227(0):101-5.
- [56] Zeng J, Zhang Q, Chen J, Xia Y. A comparison study of the catalytic properties of Au-based nanocages, nanoboxes, and nanoparticles. *Nano letters*. 2009;10(1):30-5.
- [57] Ji Z, Shen X, Yang J, Zhu G, Chen K. A novel reduced graphene oxide/Ag/CeO₂ ternary nanocomposite: green synthesis and catalytic properties. *Applied Catalysis B: Environmental*. 2014;144:454-61.
- [58] Gu W, Deng X, Jia X, Li J, Wang E. Functionalized graphene/Fe₃O₄ supported AuPt alloy as a magnetic, stable and recyclable catalyst for a catalytic reduction reaction. *Journal of Materials Chemistry A*. 2015;3(16):8793-9.
- [59] Yang Y, Ren Y, Sun C, Hao S. Facile route fabrication of nickel based mesoporous carbons with high catalytic performance towards 4-nitrophenol reduction. *Green Chemistry*. 2014;16(4):2273-80.
- [60] Joshi MK, Pant HR, Kim HJ, Kim JH, Kim CS. One-pot synthesis of Ag-iron oxide/reduced graphene oxide nanocomposite via hydrothermal treatment. *Colloids and Surfaces A: Physicochemical and Engineering Aspects*. 2014;446:102-8.
- [61] Ji Z, Shen X, Zhu G, Zhou H, Yuan A. Reduced graphene oxide/nickel nanocomposites: facile synthesis, magnetic and catalytic properties. *Journal of Materials Chemistry*. 2012;22(8):3471.
- [62] Li J, Liu C-y, Liu Y. Au/graphene hydrogel: synthesis, characterization and its use for catalytic reduction of 4-nitrophenol. *Journal of Materials Chemistry*. 2012;22(17):8426-30.
- [63] Du Y, Chen H, Chen R, Xu N. Synthesis of p-aminophenol from p-nitrophenol over nano-sized nickel catalysts. *Applied Catalysis A: General*. 2004;277(1):259-64.
- [64] Lü M, Li J, Yang X, Zhang C, Yang J, Hu H, et al. Applications of graphene-based materials in environmental protection and detection. *Chinese Science Bulletin*. 2013;58(22):2698-710.
- [65] Wang S, Sun H, Ang HM, Tadé MO. Adsorptive remediation of environmental pollutants using novel graphene-based nanomaterials. *Chemical Engineering Journal*. 2013;226:336-47.
- [66] Chang H, Wu H. Graphene-based nanocomposites: preparation, functionalization, and energy and environmental applications. *Energy & Environmental Science*. 2013;6(12):3483-507.
- [67] Tu W, Zhou Y, Zou Z. Versatile Graphene-Promoting Photocatalytic Performance of Semiconductors: Basic Principles, Synthesis, Solar Energy Conversion, and Environmental Applications. *Advanced Functional Materials*. 2013;23(40):4996-5008.
- [68] Zhao G, Wen T, Chen C, Wang X. Synthesis of graphene-based nanomaterials and their application in energy-related and environmental-related areas. *RSC Advances*. 2012;2(25):9286-303.
- [69] Dinda D, Gupta A, Saha SK. Removal of toxic Cr (VI) by UV-active functionalized graphene oxide for water purification. *Journal of Materials Chemistry A*. 2013;1(37):11221-8.

- [70] Li S, Lu X, Xue Y, Lei J, Zheng T, Wang C. Fabrication of polypyrrole/graphene oxide composite nanosheets and their applications for Cr(VI) removal in aqueous solution. *PloS one*. 2012;7(8):e43328.
- [71] Zhang S, Zeng M, Xu W, Li J, Li J, Xu J, et al. Polyaniline nanorods dotted on graphene oxide nanosheets as a novel super adsorbent for Cr (VI). *Dalton Transactions*. 2013;42(22):7854-8.
- [72] Bhaumik M, Maity A, Srinivasu VV, Onyango MS. Enhanced removal of Cr(VI) from aqueous solution using polypyrrole/Fe₃O₄ magnetic nanocomposite. *Journal of hazardous materials*. 2011;190(1-3):381-90.
- [73] Bhowmik K, Mukherjee A, Mishra MK, De G. Stable Ni nanoparticle-reduced graphene oxide composites for the reduction of highly toxic aqueous Cr(VI) at room temperature. *Langmuir : the ACS journal of surfaces and colloids*. 2014;30(11):3209-16.
- [74] Chen JH, Xing HT, Guo HX, Weng W, Hu SR, Li SX, et al. Investigation on the adsorption properties of Cr(vi) ions on a novel graphene oxide (GO) based composite adsorbent. *Journal of Materials Chemistry A*. 2014;2(31):12561.
- [75] Li L, Duan H, Wang X, Luo C. Adsorption property of Cr(vi) on magnetic mesoporous titanium dioxide-graphene oxide core-shell microspheres. *New J Chem*. 2014;38(12):6008-16.
- [76] Dubey R, Bajpai J, Bajpai AK. Green synthesis of graphene sand composite (GSC) as novel adsorbent for efficient removal of Cr (VI) ions from aqueous solution. *Journal of Water Process Engineering*. 2015;5:83-94.
- [77] Fan L, Luo C, Sun M, Qiu H. Synthesis of graphene oxide decorated with magnetic cyclodextrin for fast chromium removal. *Journal of Materials Chemistry*. 2012;22(47):24577.
- [78] Li L, Fan L, Sun M, Qiu H, Li X, Duan H, et al. Adsorbent for chromium removal based on graphene oxide functionalized with magnetic cyclodextrin-chitosan. *Colloids and surfaces B, Biointerfaces*. 2013;107:76-83.
- [79] WooáLee J, BináKim S. Enhanced Cr (VI) removal using iron nanoparticle decorated graphene. *Nanoscale*. 2011;3(9):3583-5.
- [80] Yang S-T, Chen S, Chang Y, Cao A, Liu Y, Wang H. Removal of methylene blue from aqueous solution by graphene oxide. *Journal of colloid and interface science*. 2011;359(1):24-9.
- [81] Chen L, Yang J, Zeng X, Zhang L, Yuan W. Adsorption of methylene blue in water by reduced graphene oxide: Effect of functional groups. *Materials Express*. 2013;3(4):281-90.
- [82] Fan L, Luo C, Sun M, Li X, Lu F, Qiu H. Preparation of novel magnetic chitosan/graphene oxide composite as effective adsorbents toward methylene blue. *Bioresource technology*. 2012;114:703-6.
- [83] Yao Y, Miao S, Yu S, Ma LP, Sun H, Wang S. Fabrication of Fe₃O₄/SiO₂ core/shell nanoparticles attached to graphene oxide and its use as an adsorbent. *Journal of colloid and interface science*. 2012;379(1):20-6.
- [84] Ramesha G, Kumara AV, Muralidhara H, Sampath S. Graphene and graphene oxide as effective adsorbents toward anionic and cationic dyes. *Journal of colloid and interface science*. 2011;361(1):270-7.
- [85] Geng Z, Lin Y, Yu X, Shen Q, Ma L, Li Z, et al. Highly efficient dye adsorption and removal: a functional hybrid of reduced graphene oxide-Fe₃O₄ nanoparticles as an easily regenerative adsorbent. *Journal of Materials Chemistry*. 2012;22(8):3527-35.

- [86] Bai S, Shen X, Zhong X, Liu Y, Zhu G, Xu X, et al. One-pot solvothermal preparation of magnetic reduced graphene oxide-ferrite hybrids for organic dye removal. *Carbon*. 2012;50(6):2337-46.
- [87] Qin Y, Long M, Tan B, Zhou B. RhB Adsorption Performance of Magnetic Adsorbent Fe₃O₄/RGO Composite and Its Regeneration through A Fenton-like Reaction. *Nano-Micro Letters*. 2014;6(2):125-35.
- [88] Bian X, Lu X, Xue Y, Zhang C, Kong L, Wang C. A facile one-pot hydrothermal method to produce SnS₂/reduced graphene oxide with flake-on-sheet structures and their application in the removal of dyes from aqueous solution. *Journal of colloid and interface science*. 2013;406:37-43.
- [89] Guo H, Jiao T, Zhang Q, Guo W, Peng Q, Yan X. Preparation of graphene oxide-based hydrogels as efficient Dye adsorbents for wastewater treatment. *Nanoscale research letters*. 2015;10(1):1-10.
- [90] Jiao T, Liu Y, Wu Y, Zhang Q, Yan X, Gao F, et al. Facile and Scalable Preparation of Graphene Oxide-Based Magnetic Hybrids for Fast and Highly Efficient Removal of Organic Dyes. *Scientific reports*. 2015;5.
- [91] Liu Y, Jiang X, Li B, Zhang X, Liu T, Yan X, et al. Halloysite nanotubes@ reduced graphene oxide composite for removal of dyes from water and as supercapacitors. *Journal of Materials Chemistry A*. 2014;2(12):4264-9.
- [92] Liu J, Cao H, Xiong J, Cheng Z. Ferromagnetic hematite@ graphene nanocomposites for removal of rhodamine B dye molecules from water. *CrystEngComm*. 2012;14(16):5140-4.
- [93] Zhang L, Li H, Liu Y, Tian Z, Yang B, Sun Z, et al. Adsorption-photocatalytic degradation of methyl orange over a facile one-step hydrothermally synthesized TiO₂/ZnO-NH₂-RGO nanocomposite. *RSC Advances*. 2014;4(89):48703-11.
- [94] Yang Z, Ji S, Gao W, Zhang C, Ren L, Tjiu WW, et al. Magnetic nanomaterial derived from graphene oxide/layered double hydroxide hybrid for efficient removal of methyl orange from aqueous solution. *Journal of colloid and interface science*. 2013;408:25-32.
- [95] Sarkar C, Bora C, Dolui SK. Selective Dye Adsorption by pH Modulation on Amine-Functionalized Reduced Graphene Oxide-Carbon Nanotube Hybrid. *Industrial & Engineering Chemistry Research*. 2014;53(42):16148-55.
- [96] Mohan D, Pittman CU. Activated carbons and low cost adsorbents for remediation of tri- and hexavalent chromium from water. *Journal of hazardous materials*. 2006;137(2):762-811.
- [97] Mohan D, Rajput S, Singh VK, Steele PH, Pittman CU. Modeling and evaluation of chromium remediation from water using low cost bio-char, a green adsorbent. *Journal of hazardous materials*. 2011;188(1):319-33.
- [98] Uysal M, Ar I. Removal of Cr (VI) from industrial wastewaters by adsorption: Part I: determination of optimum conditions. *Journal of hazardous materials*. 2007;149(2):482-91.
- [99] Kongsricharoern N, Polprasert C. Chromium removal by a bipolar electro-chemical precipitation process. *Water Science and Technology*. 1996;34(9):109-16.
- [100] Hafez A, El-Mariharawy S. Design and performance of the two-stage/two-pass RO membrane system for chromium removal from tannery wastewater. Part 3. *Desalination*. 2004;165:141-51.
- [101] Goyal RK, Jayakumar N, Hashim M. A comparative study of experimental optimization and response surface optimization of Cr removal by emulsion ionic liquid membrane. *Journal of hazardous materials*. 2011;195:383-90.

- [102] Rengaraj S, Joo CK, Kim Y, Yi J. Kinetics of removal of chromium from water and electronic process wastewater by ion exchange resins: 1200H, 1500H and IRN97H. *Journal of hazardous materials*. 2003;102(2):257-75.
- [103] Edebali S, Pehlivan E. Evaluation of Amberlite IRA96 and Dowex 1× 8 ion-exchange resins for the removal of Cr (VI) from aqueous solution. *Chemical Engineering Journal*. 2010;161(1):161-6.
- [104] Wei S, Li D, Huang Z, Huang Y, Wang F. High-capacity adsorption of Cr(VI) from aqueous solution using a hierarchical porous carbon obtained from pig bone. *Bioresource technology*. 2013;134:407-11.
- [105] Yu W, Zhang L, Wang H, Chai L. Adsorption of Cr(VI) using synthetic poly(m-phenylenediamine). *Journal of hazardous materials*. 2013;260:789-95.
- [106] Ali I, Gupta V. Advances in water treatment by adsorption technology. *Nature protocols*. 2006;1(6):2661-7.
- [107] Ren X, Chen C, Nagatsu M, Wang X. Carbon nanotubes as adsorbents in environmental pollution management: a review. *Chemical Engineering Journal*. 2011;170(2):395-410.
- [108] Chequer FMD, de Oliveira DP, Ferraz ERA, de Oliveira GAR, Cardoso JC, Zanoni MVB. Textile dyes: dyeing process and environmental impact: INTECH Open Access Publisher; 2013.
- [109] Li L, Li X, Yan C, Guo W, Yang T, Fu J, et al. Optimization of methyl orange removal from aqueous solution by response surface methodology using spent tea leaves as adsorbent. *Frontiers of Environmental Science & Engineering*. 2014;8(4):496-502.
- [110] Index M. An encyclopedia of Chemicals, Drugs and Biologicals 12th edition., Merck and Co. INC, USA. 1996:8697.
- [111] Gong R, Ye J, Dai W, Yan X, Hu J, Hu X, et al. Adsorptive Removal of Methyl Orange and Methylene Blue from Aqueous Solution with Finger-Citron-Residue-Based Activated Carbon. *Industrial & Engineering Chemistry Research*. 2013;52(39):14297-303.
- [112] Fan L, Luo C, Sun M, Qiu H, Li X. Synthesis of magnetic beta-cyclodextrin-chitosan/graphene oxide as nanoadsorbent and its application in dye adsorption and removal. *Colloids and surfaces B, Biointerfaces*. 2013;103:601-7.
- [113] Wang S, Yang W, Chen G. Graphene-decorated porous ceramics for efficient removal of Cr (vi). *RSC Advances*. 2015;5(81):65982-90.
- [114] Zhou G, Xu X, Zhu W, Feng B, Hu J. Dispersedly embedded loading of Fe₃O₄ nanoparticles into graphene nanosheets for highly efficient and recyclable removal of heavy metal ions. *New Journal of Chemistry*. 2015;39(9):7355-62.
- [115] Lin T-Y, Chen D-H. One-step green synthesis of arginine-capped iron oxide/reduced graphene oxide nanocomposite and its use for acid dye removal. *RSC Advances*. 2014;4(56):29357-64.
- [116] Vallés C, Drummond C, Saadaoui H, Furtado CA, He M, Roubeau O, et al. Solutions of negatively charged graphene sheets and ribbons. *Journal of the American Chemical Society*. 2008;130(47):15802-4.

Chapter 5

CONCLUSION AND PERSPECTIVES

In the last years, graphene has been the most studied material, attracting the attention of the entire scientific community for its fascinating physical and chemical properties. Graphene is the “thinnest” known material with a long range π -conjugation that exhibits a high specific surface area, extraordinary electronic properties and electron transport capabilities, high mechanical strength, unprecedented pliability, remarkable optical transparency, as well as excellent thermal and electrical conductivities. There is obviously still much work to be done to understand the properties of graphene and fully develop its potential.

In **chapter 1**, we have summarized the different techniques for the synthesis of graphene and its derivatives. According to the classification of the synthetic methods of nanomaterials, graphene synthesis can be achieved using “bottom-up” and “top-down” approaches. The “bottom-up” approach involves the direct synthesis of graphene from carbon sources using chemical vapour-deposition (CVD) or epitaxial growth on SiC, solvothermal reaction, and organic synthesis. The “top-down” path uses graphite as a starting material, and includes mechanical exfoliation (the scotch tape method), liquid-phase exfoliation, chemical, thermal, photothermal or electrochemical reduction of graphene oxide (GO).

GO reduction by chemical means is one of the most commonly used techniques. Due to the toxicity and explosive properties of some of the chemical reductants explored earlier, many environmentally friendly and highly-efficient reductants have been developed and used for the reduction of GO.

Moreover, in the field of catalysis, metal nanoparticles are quite efficient, but their performance is highly dependent on their dispersion of the active metals. Thus, aggregation of the NPs during the catalytic process due to the high surface energies and magnetic properties is the main impediment to their development. To solve these problems, the scientific community focused on the preparation of low-cost catalysts with high catalytic activity and high specific surface area, and Graphene became an ideal substrate for growing and anchoring metal NPs with good dispersion due to its high specific surface area and large density of free electrons.

The work presented here and which deals with the catalytic activity of graphene/metal nanocomposites was set in this context.

We have developed novel approaches to reduce GO and decorate it with metal or metal oxide nanoparticles. The resulting rGO-based nanocomposites have been characterized by a variety of different techniques, including SEM, TEM, FTIR, Raman, UV-Vis, XPS, XRD and TGA to study their morphology, chemical composition and thermal behaviour.

First, we have produced rGO/Ag nanoparticles by an easy and environmentally friendly chemical method in a two-step process (**Chapter 2**). We have used arginine (Arg) as a reducing agent and silver nitrate as metal precursor. We have shown that, in this novel composite, Ag NPs were homogeneously dispersed on the surface of rGO/Arg. Furthermore we have demonstrated that the catalytic activity of the as-prepared rGO/Ag NPs composite is highly enhanced compared to previously developed rGO/Ag nanocomposites for the reduction of 4-nitrophenol to 4-aminophenol with a full reduction in less than 1 min at room temperature. This value is small and efficient compared with other reports which used metal (Ni, Co, Au, SiO₂, Fe₃O₄) supported Ag NPs with graphene.

In **chapter 3**, we have developed a novel approach for the synthesis of reduced graphene oxide decorated with nickel nanoparticles (rGO/Ni NPs) by a simple chemical reduction of GO with nickel chloride at 100°C for 24 h. The catalytic activity of the rGO/Ni NPs was evaluated for the reduction of 4-nitrophenol to 4-aminophenol. A full reduction of 4-nitrophenol was observed after 5 min using NaBH₄ as reducing agent at room temperature. This value is small and efficient compared with other reports which used metal (Ag,Pt) supported Ni NPs with graphene.

Chapter 4 deals with a novel, one-step, easy, low-cost, and simple method to prepare Co₃O₄/rGO nanocomposite using a mixture of GO, a cobalt salt, and NaBH₄ as reducing agent at room temperature. We have shown that the Co₃O₄/rGO nanocomposite displays a good catalytic performance for the reduction of 4-NP into 4-AM with a conversion time of 1 min. Also, Co₃O₄/rGO displayed high adsorption capacity for organic dyes. The rGO-Co₃O₄ nanocomposite removed 96%, 91% and 92% of RhB, MO and Rose Bengal after 2, 1 and 2 min, respectively. These results were fast and highly-efficient compared with other reported data. Moreover, the maximum adsorption capacity of Cr (VI) was 222.2 mg. g⁻¹, which is very close to the experimental value of 208.8 mg.g⁻¹. This value is higher (or comparable) to previously reported data. Finally, the rGO/Co₃O₄ nanocomposite has been used as a superior heterogeneous catalyst for one-pot oxidative esterification of aldehydes to methyl esters [1].

More work remains to be done to improve the properties and facilitate the practical applications of rGO composites as well as broaden their application fields in the future. The three nanocomposites could be used for nonenzymatic sensing of glucose and hydrogen peroxide (H_2O_2). Also, they could be applied as drug delivery systems by using functional rGO/metal-metal oxide nanocomposites as nanocarrier. The nanocarrier system can be synthesized by attaching drugs to rGO/metal-metal oxide nanocomposites *via* strong π - π stacking interaction, followed by encapsulation of rGO/metal-metal oxide nanocomposites with folic acid conjugated chitosan. Moreover, and because of the magnetic properties, especially (rGO- Co_3O_4), we could control the drug delivery at a specific place.

Furthermore, the rGO- Co_3O_4 nanocatalyst could be used to degrade Orange II, methylene blue (MB) or other dyes from water *via* advanced oxidation processes. They could also be good candidates as electrode materials for supercapacitors or lithium-ion batteries.

Finally, the high electrocatalytic activity of rGO/metal oxide nanocomposites for hydrogen evolution reaction is under investigation and the preliminary results are very encouraging.

Additionally to this work on photocatalysis, we have successfully synthesized ZnO nanorods by a wet chemical method and annealed under high pressure water vapor (HWA) at a pressure of 1.3 to 3.9 MPa and at 2.6 MPa. We have shown that the HWA annealed nanorods exhibited a much higher UV luminescence band compared with that induced by air annealing at the same temperature (260°C). We could demonstrate that HWA-annealing induces a less defective ZnO layer, and also generates the growth of a new thin ZnO layer of higher quality at the nanorods surface. The surface of the nanorods is therefore reconstructed [2].

[1] Jain SL, Panwar V, Al-Nafiey A, Addad A, Sieber B, Roussel P, et al. Magnetic Co_3O_4 /reduced graphene oxide nanocomposite as superior heterogeneous catalyst for one-pot oxidative esterification of aldehydes to methyl esters. RSC Advances. 2015. DOI: 10.1039/C5RA14665H.

[2] Amer Al-Nafiey , B. Sieber ,B. Gelloz , A. Addad , M.Moreau , J. Barjon, M. Girleanu, O. Ersen and R. Boukeherroub . Enhanced Ultraviolet Luminescence of ZnO Nanorods Treated by High-Pressure Water Vapor Annealing (HWA). Under review in (The Journal of Physical Chemistry C (ACS Publications)) - Manuscript ID 2015-09201y-jp).

Appendix

EXPERIMENTAL PART

1. Chemicals

All chemicals were reagent grade or higher and were used as received unless otherwise specified. Graphite powder (< 20 micron), potassium permanganate (KMnO_4), sulphuric acid (H_2SO_4), phosphoric acid (H_3PO_4), hydrogen peroxide (H_2O_2), dimethylformamide (DMF), L-arginine ($\text{C}_6\text{H}_{14}\text{N}_4\text{O}_2$), silver nitrate ($\text{AgNO}_3 \cdot 6\text{H}_2\text{O}$), nickel chloride ($\text{NiCl}_2 \cdot 6\text{H}_2\text{O}$), cobalt chloride ($\text{CoCl}_2 \cdot 6\text{H}_2\text{O}$), sodium borohydride (NaBH_4), 4-nitrophenol ($\text{C}_6\text{H}_5\text{NO}_3$), potassium dichromate ($\text{K}_2\text{Cr}_2\text{O}_7$), rhodamine B (RhB), methyl orange (MO), rose Bengal dye, ethanol, and hydrochloric acid (HCl) were purchased from Sigma-Aldrich. Silicon wafers were purchased from Siltronics.

2. Preparation of graphene oxide (GO)

The schematic of graphene oxide (GO) synthesis is depicted in **Figure 1**. GO was prepared by oxidizing graphite powder using a modified Hummer's method. The GO is heavily oxygenated with basal and edges planes mainly occupied by C=O, C-OH and COOH groups.

A 9:1 mixture of concentrated $\text{H}_2\text{SO}_4/\text{H}_3\text{PO}_4$ (90:10 mL) was added to a mixture of graphite flakes (0.75 g) and KMnO_4 (4.85 g). The reaction was then heated to 50°C and stirred for 12 h. The reaction was cooled to room temperature and poured into ice (100 mL) with slowly adding 30% H_2O_2 (0.75 mL). The solid product was separated by centrifugation. It was first washed with 30% HCl (2 times), secondly washed with 5% HCl solution (3-5 times) until the sulphate ions are removed. Then washed with distilled water repeatedly until it becomes free of chloride ions and the pH of the solution is neutral, and finally washed 3–4 times with ethanol. The material remaining after this extended multiple-wash process was coagulated with 100 mL of ether, and the resulting suspension was filtered over a PVDF membrane with a $0.45\ \mu\text{m}$ pore size. The solid GO obtained on the filter was vacuum-dried overnight at room temperature.

A homogeneous yellow brown suspension (0.5 mg/mL) of GO sheets in water was achieved by ultrasonication for 3 h.

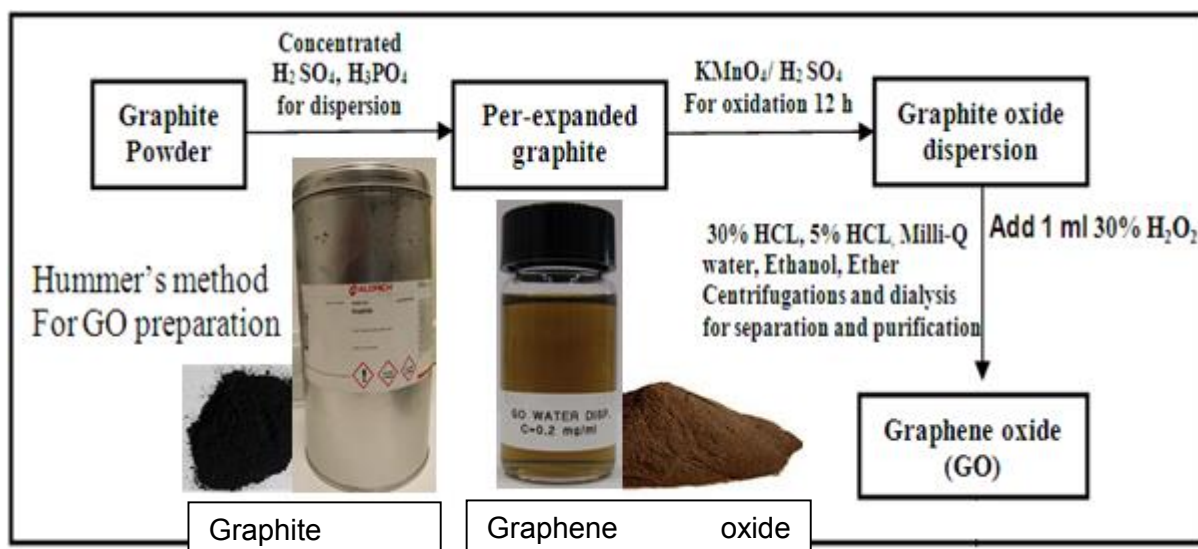


Figure 1: Schematic of synthesis graphene oxide using a modified Hummer's method.

3. Instrumentation

3.1. X-ray photoelectron spectroscopy (XPS)

X-ray photoelectron spectroscopy (XPS) is also known as electron spectroscopy for chemical analysis (ESCA). XPS is a surface characterization technique that utilizes X-rays to probe the chemical composition and electronic configuration of the elements present on the sample surface. The photoelectrons emitted from the material are collected as a function of their kinetic energy, and the number of photoelectrons collected in a defined time interval is plotted versus kinetic energy. The kinetic energy of the photoelectron depends only on its binding energy in the sample. The binding energy is given by the difference between the initial and final states after the photoelectron has left the atom. Peaks appear in the spectrum at discrete energies due to emission of electrons from states of specific binding energies in the material. The positions of the peaks identify the chemical elements in the material.

The relative concentrations of elements can be determined from the measured photoelectron intensities. The positions and shapes of the peaks in an XPS spectrum can also be analyzed in greater detail to determine the chemical state of the constituent elements in the material, including oxidation state, partial charge, and hybridization.

XPS experiments were performed on a PHI 5000 VersaProbe-Scanning ESCA Microprobe (ULVAC-PHI, Japan/USA) instrument at a base pressure below 5×10^{-9} mbar. Monochromatic

AlK α radiation was used and the X-ray beam, focused to a diameter of 100 μm , was scanned on a 250 μm \times 250 μm surface, at an operating power of 25 W (15 kV). Photoelectron survey spectra were acquired using a hemispherical analyzer at pass energy of 117.4 eV with a 0.4 eV energy step. Core-level spectra were acquired at pass energy of 23.5 eV with a 0.1 eV energy step. All spectra were acquired with 90° between X-ray source and analyzer and with the use of low energy electrons and low energy argon ions for charge neutralization. After subtraction of the Shirley-type background, the core-level spectra were decomposed into their components with mixed Gaussian-Lorentzian (30:70) shape lines using the CasaXPS software. Quantification calculations were performed using sensitivity factors supplied by PHI.

The samples for XPS analysis were prepared by casting 50 μL aqueous or ethanol suspension of GO, rGO, rGO/Ag, rGO/Ni or rGO/Co₃O₄ on a clean silicon wafer surface followed by drying in an oven at 80°C to make sure the solvent was removed.

3.2. Fourier-transform infrared (FTIR) spectroscopy

The vibrational motions of the chemically bound constituents of matter have frequencies in the infrared regime. The oscillations induced by certain vibrational modes provide a means for matter to couple with an impinging beam of infrared electromagnetic radiation and to exchange energy with it when the frequencies are in resonance. Infrared spectroscopy is based on the phenomenon of infrared absorption by molecular vibrations. When a molecule is irradiated by electromagnetic waves within the infrared frequency range, one particular frequency may match the vibrational frequency of the molecule. Consequently, the molecular vibration will be excited by infrared frequency causing the energy of molecular vibration to increase. In the meantime, the electromagnetic radiation with a specific frequency will be absorbed by the molecule because the photon energy is transferred to excite molecular vibrations.

FTIR spectra were recorded using a ThermoScientific FTIR instrument (Nicolet 8700) in the 4000-200 cm^{-1} frequency range at a spectral resolution of 4 cm^{-1} . Dried GO, rGO, rGO/Ag, rGO/Ni or rGO/Co₃O₄ (1 mg) was mixed with KBr powder (100 mg) in an agate mortar. The mixture was pressed into a pellet under 10 tons load for 2–4 min, and the spectrum was recorded immediately. Sixteen accumulative scans were collected. The signal from a pure KBr pellet was subtracted as the background.

3.3. Raman spectroscopy

Raman spectroscopy is a very important analysis technique in the field of carbon research and has historically played an important role in the structural characterization of graphitic materials.

Raman spectroscopy is a non-destructive technique that investigates the optical and electronic properties of a material. Based on the inelastic scattering of monochromatic light, it involves a laser excitation to interact with the vibrational and rotational modes of the system, resulting in a shift in the energy of the scattered photons. Frequency of the reemitted photons shifts up or down with respect to original monochromatic frequency. This is called the Raman effect. This shift or the transition provides sufficient information about rotational, vibrational and other transitions occurring in molecules. Micro-Raman spectroscopy is more commonly used for materials characterization than other Raman instruments. Micro-Raman spectroscopy is able to examine microscopic areas of materials by focusing the laser beam down to the micrometre level without much sample preparation, as long as a surface of the sample is free from contamination. An important difference between Micro-Raman and micro-FTIR spectroscopies is their spatial resolution. The spatial resolution of the Raman microscope is at least one order of magnitude higher than the FTIR microscope.

Micro-Raman spectroscopy was performed on a Horiba Jobin Yvon LabRam HR Micro-Raman system combined with either a 473 nm or a 532 nm laser diode as excitation source. The beam was focused on the sample surface through an optical objective (x100, 0.9 NA) with a lateral resolution (XY) of less than 1 μm . The scattered light was collected by the same objective in the backscattering configuration, dispersed by a 1800-mm focal length monochromator and detected by a CCD.

The samples were prepared by casting 50 μL aqueous or ethanol suspension of GO, rGO, rGO/Ag, rGO/Ni or rGO/Co₃O₄ on a clean silicon wafer surface followed by drying in an oven at 80°C to make sure the solvent was removed.

3.4. UV-Vis measurements

UV-VIS spectroscopy is a non-destructive technique useful to characterize absorption, transmission, and reflectivity of different types of compounds and provides information on the electronic bonding in a molecule. Absorption spectra were recorded using a Perkin Elmer Lambda UV-Vis 950 spectrophotometer in quartz cuvettes with an optical path of 10 mm. The wavelength range was 200–800 nm.

2 mg/mL of GO, rGO, rGO/Ag, rGO/Ni or rGO/Co₃O₄ were nicely dispersed in water or ethanol with the aid of ultrasonication and then filled into the quartz cuvettes for measurements.

3.5. Thermogravimetric analysis (TGA)

Thermogravimetric analysis or thermal gravimetric analysis (TGA) is a technique of thermal analysis in which changes in physical and chemical properties of materials are measured as a function of increasing temperature (with constant heating rate), or as a function of time (with constant temperature and/or constant mass loss). TGA consists of a sample pan that is supported by a precision balance. That pan resides in a furnace and is heated or cooled during the experiment. The mass of the sample is monitored during the experiment.

Thermogravimetric analysis (TGA) measurements were carried out in Al₂O₃ crucibles under nitrogen atmosphere at a heating rate of 10°C/min using a TA Instruments Q50 thermogravimetric analyzer.

3.6. Scanning electron microscopy (SEM)

In SEM a focused electron beam is applied, and electrons emitted from the sample are used to image the surface. Inelastic scattering interactions between the scanning beam and the specimen produce low energy secondary electrons, which can be detected with a so-called in lens detector. The resulting micrographs show a high spatial resolution, high depth of field as well as a material and orientation dependent contrast.

SEM investigations were carried out on a Hitachi S-4700 SEM FEG (field emission gun) operating with an acceleration voltage of 3 or 6 kV and two different detectors (high-efficiency In-lens SE detector, Everhart-Thornley secondary electron detector).

The samples were prepared by casting 50 µL aqueous or ethanol suspension of GO, rGO, rGO/Ag, rGO/Ni or rGO/C₃O₄ on a clean silicon wafer surface followed by drying in an oven at 80°C to make sure the solvent was removed.

3.7. Transmission electron microscopy (TEM)

In TEM, a parallel electron beam impinges onto a sample. The electrons transmitted through the material are used to create an image of the sample and to gain information on phase composition, structure and lattice defects. The image contrast comprises also information based on electron diffraction of the crystalline parts of the specimen.

TEM imaging was usually performed on a FEI Tecnai G2-F20 microscope operating at 200 kV. Samples were drop-casted from aqueous or ethanol dispersions of GO, rGO, rGO/Ag, rGO/Ni or rGO/C₃O₄ onto carbon coated TEM grids and the solvent was evaporated under gentle heating.

Some experiments were performed with a FEI Tecnai Osiris in Eindhoven (Philips Laboratory). High-angle annular dark-field imaging (HAADF) as well as Energy Dispersive X-Ray (EDX) spectra and mapping have been used specifically on rGO/Ni NPs composite. HAADF, which relies on the detection at very high angle of the incoherently scattered electrons, is highly sensitive to the atomic number of atoms in the sample. The higher the Z number, the higher the HAADF signal. An EDX spectrum records the intensity of the X-rays produced by the elements present in a sample under the action of an electron beam. EDX mapping allows the imaging of the spatial distribution of an element in the sample (monochromatic imaging).

3.8. X-Ray diffraction (XRD)

X-ray diffraction is a technique that provides detailed information about the chemical composition and crystallographic structure of the materials. It gives detailed information about the lattice parameter, lattice defects, lattice strain, chemical composition, crystallite size (in case of nanoparticles) and the type of chemical bonding.

The structural characterization of the samples was carried out on a 9 KW Rigaku Smartlab rotated anode X-ray diffractometer using Cu K α 1 (1.5406 Å) wavelength, operated in Bragg-Brentano reflection geometry.

The samples were prepared by casting 50 μ L aqueous or ethanol suspension of GO, rGO, rGO/Ag, rGO/Ni or rGO/Co₃O₄ on a clean silicon wafer surface followed by drying in an oven at 80°C to make sure the solvent was removed.